

The geochemistry of antimony in hydrothermal solutions

By

Nellie J. Olsen

A thesis

submitted to the Victoria University of Wellington

in partial fulfillment of the requirements for the

degree of Doctor of Philosophy

School of Geography, Environment and Earth Sciences

Victoria University of Wellington

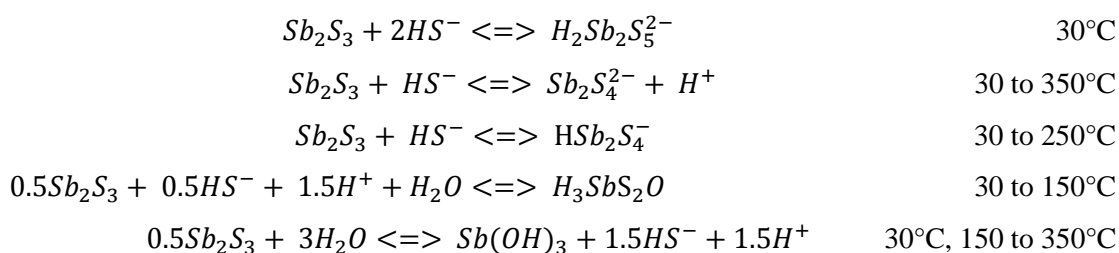
Wellington, New Zealand

November 2016

Abstract

In this thesis, 30°C stibnite solubility experiments, ambient temperature X-ray absorption spectroscopic measurements of antimony in solution, and high temperature (70 to 400°C) stibnite solubility experiments were carried out in order to determine the aqueous antimony species present in equilibrium with stibnite in hydrosulfide solutions from pH = 3.5 to 12 and reduced sulfur concentrations from 0.001 to 0.1 mol kg⁻¹. Both ambient and elevated temperature solubility studies were conducted using a flow-through apparatus containing a column of stibnite grains through which solutions were pumped. Above 100°C, solubility experiments were conducted at slightly above saturated water vapour pressure to pressures of 300 bar.

At 30°C, the stibnite solubility curve was best reproduced by a scheme of five species: Sb₂S₄²⁻, HSb₂S₄⁻, H₂Sb₂S₅²⁻, H₃SbS₂O, and Sb(OH)₃. At higher temperatures (≥ 70 °C), stibnite solubility at the conditions of the experiments was due to the following four species: Sb₂S₄²⁻, HSb₂S₄⁻, H₃SbS₂O, and Sb(OH)₃. Equilibrium constants were determined for the following five heterogeneous solubility reactions for the temperature ranges listed:



Stibnite solubility was independent of pressure at ≤ 350°C. At ~ 400°C, the solubility of stibnite was strongly dependent on pressure and decreased from Sb_{total} = 0.015 to 0.0003 mol kg⁻¹ (~2000 to 40 ppm) with a pressure decrease from 300 to 160 bars.

The Sb K-edge X-ray absorption spectroscopic (XAS) measurements of antimony in alkaline (pH = 10.9 to 12) hydrosulfide solutions gave average first shell coordination environments that were consistent with the speciation model derived from solubility experiments for strongly alkaline solutions (i.e., Sb₂S₄²⁻ and Sb(OH)₃). XAS data enable the elimination of a speciation model involving only monomeric antimony complexes at strongly alkaline pH.

Antimony speciation in near neutral to strongly alkaline pH's is dominated by dimeric antimony-sulfide complexes at 30°C and sulfide concentrations > 0.001 mol kg⁻¹. With increasing temperature, antimony speciation becomes increasingly dominated by Sb(OH)₃. For hydrothermal solutions with sulfide concentrations between 0.0001 and 0.01 mol kg⁻¹, antimony-sulfide complexes are predominant at < 100°C, whereas antimonous acid, Sb(OH)₃, is the main aqueous species at contributing to stibnite solubility at > 200°C with the speciation in the intervening temperature range

being dependent on the pH and sulfide concentration of the solution. For higher sulfide concentrations (i.e., $\sim 0.1 \text{ mol kg}^{-1}$), HSb_2S_4^- and $\text{Sb}_2\text{S}_4^{2-}$ control stibnite solubility to higher temperatures.

Acknowledgements

This PhD was supported by a Victoria University of Wellington PhD Scholarship. The research expenses and additional PhD support was provided by the Geothermal Resources Program at GNS Science. Measurements at the Australian Synchrotron were made possible by the New Zealand Synchrotron Group Limited (Projects AS132/XAS/6413 and AS142/XAS/7621) and the Royal Society of New Zealand. Additional support came from the Irene Memorial Scholarship, an extraordinarily well-targeted scholarship.

This research would have been impossible without the help and understanding of the excellent staff of the NZGAL (New Zealand Geothermal Analytical Laboratory) and the scientists and technical staff at the Wairakei Research Centre, in particular the irreplaceable Marshall Muller (a walking reference book for multiple analytical techniques), Dave Keen (a master of all electronic paraphernalia accompanying experimental apparatus), and Ed Mroczek (without whom the VBA codes would have required much more sweat and pain).

Embarking on a PhD in a foreign country based at a research institution introduces its own challenges, and these acknowledgements would be incomplete without thanking my colleagues at GNS and the community of Taupo. Thanks to the Wairakei Student Group, the Exphiles, and the Thursday Journal Club for coffee and chocolate and a university-y community away from a university. Special thanks must go to Kevin Lee, my ex-officemate of multiple years, for cat videos, wide-ranging conversations, and for putting up with pithy responses to grammatical questions. I have very much enjoyed my time in this community on the edge of a massive caldera and this is in large part due to the people I have shared it with: Renee and her zoo, St. Andrews, the members of the most flippant home group ever, the members of the least formal Frisbee club ever, the Edge Rock Wall, the (usually) Tuesday International Dinning Extravaganza, random beautiful people I have met skiing, and a few wonderful bad influences who have gotten me out on tramping, skiing, climbing, rowing, and mountain biking adventures (you know who you are). Finances in the last year have been greatly helped by the privilege of caring for multiple well-loved animal companions: so thanks to the people belonging to Phoenix, Charlie, Einstein, Moby, Remu, Urban, Afie, TK, and Pihanga, and to chickens 1, 2, and Fluffball. And finally, thanks to my parents for being who they are and letting me keep playing in the dirt.

Lastly, thanks to my two supervisors, Prof. Terry Seward and Dr. Bruce Mountain, who have provided invaluable help in formulating, accomplishing, and presenting this body of research.

Table of contents

Abstract	i
Acknowledgements	iii
Table of contents	v
List of figures	ix
List of tablesxi

Chapter (1): Antimony geochemistry in hydrothermal solutions: Research context and experimental approach.....1

1.1. Aqueous complexes in geochemistry	1
1.2. Research motivation	2
1.3. Research questions and study methods	3
1.4. References	4

Chapter (2): Stibnite solubility and antimony speciation in aqueous sulfide solutions at 30°C.....5

2.1. Introduction	5
2.1.2. <i>Previous studies of Sb(III) speciation</i>	6
2.2. Methods.....	13
2.2.1. <i>Flow-through solubility apparatus</i>	13
2.2.2. <i>Analytical methods</i>	14
2.2.3. <i>Selection of aqueous complexes and nonlinear least-squares fitting</i>	14
2.3. Results	19
2.3.1. <i>Attainment of equilibrium</i>	19
2.3.2. <i>Measured stibnite solubility curves</i>	20
2.3.3. <i>Determining equilibrium constants for antimony-sulfide complexes</i>	22
2.3.4. <i>Estimating an equilibrium constant for antimonous acid</i>	26
2.4. Discussion	29
2.4.1. <i>Comparison of Sb(III)-S(II) speciation model with previous studies</i>	29
2.4.2. <i>Influence of sulfide concentration on aqueous antimony speciation</i>	32
2.5. Conclusions	35
2.6. References	36

Chapter (3) X-ray absorption spectroscopy measurements of antimony-sulfide and –hydroxide complexes at stibnite saturation39

3.1. Introduction	39
3.1.2. Previous XAS studies of antimony in aqueous solutions	40
3.1.3. X-ray near edge fine structure (XANES) at the Sb K-edge.....	43
3.2. Methods	45
3.3. Results	47
3.3.2. X-ray absorption spectra of solutions containing sufficient sulfide to complex antimony	48
3.3.3. X-ray absorption spectra of solutions containing insufficient sulfide to complex antimony.....	48
3.3.4. X-ray near edge fine structure of aqueous antimony complexes.....	49
3.4. Discussion.....	51
3.4.1. Motivation for combining solubility and spectroscopic approaches.....	52
3.4.2. Antimony first coordination shells measured by EXAFS and predicted by stibnite solubility studies	51
3.4.3. Re-evaluation of previous Sb(III)-S(II) XAS studies and future research directions	54
3.5. Conclusions	56
3.6. References	56
 Chapter (4) Stibnite solubility and antimony speciation in hydrosulfide solutions from 70 to 400°C	59
4.1. Introduction	59
4.1.2. Previous studies of antimony speciation in hydrosulfide solutions at elevated temperatures	60
4.1.3. Interpretations of the change in stibnite solubility's dependence on sulfide concentration with temperature	62
4.2. Methods	63
4.2.1. High pressure-temperature flow-through reaction system solution preparation.....	63
4.2.2. Sample collection.....	65
4.2.3. Speciation of solutions and calculation of pH.....	66
4.2.4. Fitting of heterogeneous solubility constants.....	68
4.3. Results	68
4.3.1. Attainment of equilibrium.....	68
4.3.2. Pressure dependence of stibnite solubility from 100 to 350°C.....	69
4.3.3. General changes in stibnite solubility with temperature.....	70
4.3.4. Fitting of stibnite solubility from 70 to 350°C.....	72
4.3.5. Stibnite solubility at 400°C in supercritical fluids and in fluids with vapour-like densities	79

4.4. Discussion	82
4.4.1. <i>Temperature dependence of equilibrium constants for $Sb_2S_4^{2-}$, $HSb_2S_4^-$, and $Sb(OH)_3$.</i>	82
4.4.2. <i>Evidence for changes in antimony speciation at elevated temperatures from previous spectroscopic studies</i>	85
4.4.3. <i>Stibnite solubility and antimony speciation applied in natural hydrothermal fluids</i>	86
4.5. Conclusions	91
4.6. References	92
 Chapter (5): Antimony geochemistry in hydrothermal solutions: Concluding remarks	97
5.1. Summary of results.....	97
5.2. Scope of current study and avenues for future research.....	99
5.2.2. <i>Ruminations on the value of combining solubility and spectroscopic experimental techniques</i>	102
5.3. Implications for antimony transport by hydrothermal fluids in the Earth's crust	102
5.5. References	104
 Appendix (A)	107

List of figures

Figure (2.1) Schematic of the occurrence and intensity of Raman spectral features in sodium sulfide solutions	10
Figure (2.2) Flow-through experimental setup at 30°C.....	13
Figure (2.3) Schematic of possible stibnite solubility versus pH at constant sulfide (A) or versus sulfide (B) for selected monomers and dimers.....	16
Figure (2.4) Solubility of stibnite at different flow rates in solutions with constant pH and sulfide concentration	20
Figure (2.5) Stibnite solubility versus pH (A) and versus sulfide concentration (B through E)	21
Figure (2.6) Comparison of the preferred speciation model (Fit 30-G, A) and the 30°C solubility data (B) from the current study and models and solubility from previous solubility studies at ambient temperature.....	29
Figure (2.7) Distribution of Sb(III) species at 30°C from pH = 3 to 12.....	33
Figure (2.8) Calculated stibnite solubility at 30°C from pH = 3 to 12 at constant total sulfide concentrations	34
Figure (3.1) Antimony K-edge XANES and first derivative spectra for representative mineral and solution samples from the current study.....	44
Figure (3.2) The background subtracted EXAFS (A) and Fourier transforms (B)	48
Figure (3.3) Antimony K-edge energies for solid reference samples and experimental solutions...	50
Figure (3.4) Local coordination of antimony within stibnite, an antimony(III)-sulfide monomer (represented by H_3SbS_3), and an antimony(III)-sulfide dimer (represented by $\text{Sb}_2\text{S}_4^{2-}$)	53
Figure (3.5) First coordination shells of antimony(III) complexes at different sulfide concentrations	55
Figure (4.1) Previously published values of equilibrium constants for stibnite solubility in terms of $\text{Sb}(\text{OH})_3$ (Equation 4.2), $\text{Sb}_2\text{S}_4^{2-}$, and HSb_2S_4^- (Equation 4.1)	61
Figure (4.2) Diagram of the flow-through autoclave reactor	64
Figure (4.3) Stibnite solubility at different flow rates at 150°C (A) and 200°C (B)	69
Figure (4.4) Variation in stibnite solubility with pressure at constant temperature input fluid conditions for five experiments from 100 to 350°C.....	69
Figure (4.5) Measured stibnite solubility from 70 to 350°C plotted with respect to pH (<i>left</i>) and sulfide concentration (<i>right</i>).....	70
Figure (4.6) Stibnite solubility between 390 and 406°C versus input solution pH.....	80
Figure (4.7) Stibnite solubility at ~400°C versus pressure (A) and fluid density (B)	81

Figure (4.8) Stibnite solubility (A) and K_{1033} (B) between 390 and 406°C as a function of fluid density	82
Figure (4.9) Temperature dependence of logarithms of the equilibrium constants for heterogeneous stibnite solubility reactions involving $\text{Sb}(\text{OH})_3$ (A), $\text{Sb}_2\text{S}_4^{2-}$ (B), $\text{HSb}_2\text{Sb}_4^-$ (C)	84
Figure (4.10) Previously published EXAFS results for antimony in sodium sulfide solutions at elevated temperature	85
Figure (4.11) Stibnite solubility at 250°C for $\text{S}^{2-}_{\text{total}} = 0.0001, 0.001, 0.01, \text{ and } 0.1 \text{ mol kg}^{-1}$	87
Figure (4.12) Stibnite solubility and reported antimony concentrations for fluids in the Rotokawa (A) and Ngawha (B) power stations	89
Figure (4.13) Stibnite solubility and aqueous antimony speciation from pH = 4 to 9 for a 70°C fluid with ~15 ppm sulfide	91
Figure (5.1) Stibnite solubility and antimony species distribution from 300 to 80°C at pH = 8 and a sulfide concentration of 0.02 mol kg^{-1} at swvp	100
Figure (5.2) Stibnite solubility and antimony species distribution from 270 to 70°C at pH = 5.5 (A, B, and C) and at pH = 6.5 for sulfide concentrations of 0.01, 0.001, and $0.0001 \text{ mol kg}^{-1}$	103
Figure (A.1) XRD of Chinese stibnite used in experiments	107
Figure (A.2) SEM images of reacted stibnite from high temperature experiments	122

List of tables

Table (2.1) Summary of experimental studies of aqueous Sb(III) speciation at < 100°C	7
Table (2.2) Heterogeneous solubility reactions used in nonlinear fitting	17
Table (2.3) Supporting thermodynamic data at 30°C	18
Table (2.4) Non-linear least squares fits of stibnite solubility at 30°C	23
Table (2.5) Speciation models that failed to fit stibnite solubility at near neutral pH at 30°C	25
Table (2.6) Non-linear fits of stibnite solubility at 30°C including deionized water experiments ...	27
Table (2.7) Previously published values for K_{1033}	28
Table (2.8) Summary of proposed heterogeneous stibnite solubility reactions and the logarithms of the equilibrium constants at 30°C	35
Table (3.1) Summary of previous EXAFS studies of antimony speciation in solution	41
Table (3.2) Chemistry of XAS solutions in order of highest to lowest pH	45
Table (3.3) EXAFS results	47
Table (3.4) Comparison of the average first shell coordination numbers in strongly alkaline solutions measured with EXAFS with those predicted by different speciation models derived from stibnite solubility measurements (Chapter 2)	52
Table (4.1) Input fluid conditions for high temperature experiments	65
Table (4.2) Summary of supporting thermodynamic data	67
Table (4.3) Summary of heterogeneous stibnite solubility reactions	72
Table (4.4) Fits of stibnite solubility at 70 and 110°C	73
Table (4.5) Preferred fit of stibnite solubility at 150°C (150-A) and fits demonstrating misfit of speciation models including $H_2SbS_2O^-$ (150-B) and $H_2SbS_3^-$ (150-C)	75
Table (4.6) Fit of stibnite solubility at 200°C	76
Table (4.7) Fit of stibnite solubility at 250°C	77
Table (4.8) Fits of stibnite solubility at 300 and 350°C	78
Table (4.9) Experimentally derived logarithms of equilibrium constants for heterogeneous stibnite solubility reactions from 30 to 350°C	83
Table (4.10) Coefficients for fits to Equation (4.11)	83
Table (A.1) Calculation of detection limits for antimony analyses by inductively-coupled plasma- optical spectroscopy (ICP-OES) and hydride-generation atomic absorption spectroscopy (HG-AAS)	108

Table (A.2) Stibnite solubility data at 30°C.....	109
Table (A.3) Stibnite solubility data from 70 to 400°C.....	117

Chapter (1):

Antimony geochemistry in hydrothermal solutions: Research context and experimental approach

1.1. Aqueous complexes in geochemistry

The transport of elements by aqueous fluids is one of the main processes responsible for variably distributing metals within the Earth's crust. Within these fluids, metals and metalloids exist as metal-ligand complexes, in which anions or anionic molecules bind to one or more metal atoms to form a stable aqueous complex or an aqueous species. It is the stability of these complexes relative to that of possible mineral phases which determines the solubility of a given element in a given fluid. Since coordination complexes were first proposed in the late 1800s (Werner, 1893), detailed studies of the stability, stoichiometry, and geometry of metal complexes has enabled the prediction of metal solubility over a wide range of temperature, pressure, and chemical conditions.

The ability to predict metal behavior to high temperatures for different fluid chemical compositions is instrumental to understanding the formation of ore deposits from hydrothermal fluids, the behavior of metals during high-temperature industrial processes (particularly of interest for this study are mineral precipitation/dissolution reactions inside geothermal power stations), and the environmental and biological impacts of discharging high-temperature, metal-bearing solutions into the Earth's surface environment. Aqueous complexes may be studied using either solubility experiments, in which all physiochemical variables other than a metal's solubility are either carefully controlled or measured, or by a variety of other experimental methods including spectroscopy (e.g., visible/ultraviolet, Raman, and synchrotron X-ray absorption), potentiometry, and mass spectrometry as well as modern quantum chemical *ab initio* methods. Unlike solubility studies, many of these other techniques probe the geometric and/or stoichiometric characteristics of the aqueous complexes directly. The goal of experimental studies is to identify the complexes in solution (i.e., the type and number of coordinating ligands complexed with the metal atoms), to quantify the stability of those complexes, and enable geochemical modeling by the derivation of equilibrium constants.

Both the stoichiometry of complexes and thermodynamic equilibrium constants can be derived from solubility data by nonlinear regression fitting of the data with equations defined by possible combinations of aqueous species. The speciation model that is best able to reproduce the measured solubility can then be used to predict solubility outside the range of the chemical conditions of the experiments. However, depending on the system being studied, several different complexes may produce mathematically identical solubility curves and therefore speciation models may in some

situations be non-unique. Additionally, multiple different combinations of aqueous species may produce statistically indistinguishable fits given the uncertainty or scatter present in real solubility data. In contrast, spectroscopic techniques directly measure the complexes actually present in a solution at the time of analysis. Of importance to the current study, the average first shell coordination of dissolved metals in solutions can be determined by X-ray absorption spectroscopy (XAS) and these data may compliment and reinforce conclusions drawn from the solubility measurements.

Hydroxide (OH^-), sulfide (HS^-), chloride (Cl^-), and fluoride (F^-) ligands are important inorganic ligands in natural aqueous fluids within the Earth's crust. For hydroxide and sulfide ligands, reaction with metal cations can result in deprotonation of the bound ligand to form negatively charged complexes. Obtaining accurate thermodynamic data for the interactions of metal cations with each of these ligands under the conditions of natural fluids is the prerequisite being able to model the transport and precipitation of metals in natural systems. The importance of different metal-ligand complexes can be predicted using the qualitative divisions of "hard" and "soft" ligands and metals, which were referred to as, respectively, "acids" and "bases" when the terminology was proposed by Pearson (1963). Hard metals and ligands tend to be small, strongly charged, and form ionic bonds by electron transfer. In contrast, soft metals and ligands are larger ions that are likely to be more weakly charged and form covalent bonds by the sharing of electrons. In general, hard metals will preferentially form complexes with hard ligands. Likewise, soft metals will form complexes with soft ligands. Of the common inorganic ligands mentioned above, OH^- and F^- are hard bases, Cl^- is borderline between hard and soft bases, and sulfide is a soft base. The 3+ valence state of antimony (Sb^{3+} or Sb(III)) is a borderline acid and so may be expected to have significant interactions with both hard and soft ligands. Additionally, chemical bonding in aqueous solutions becomes increasingly ionic in character with increasing temperature in response to changes in the structure of water. Thus, the preference of antimony for HS^- versus OH^- ligands may be expected to change significantly over the temperature range from ambient temperatures in surface and groundwaters to elevated temperatures in hydrothermal fluids.

1.2. Research motivation

This current study combines solubility and X-ray absorption spectroscopic approaches to investigate the interaction of antimony (Sb) with hydroxide (OH^-) and sulfide (HS^-) ligands in reduced fluids from ambient temperatures to 400°C. Antimony is a trace element that is of geological interest because it can be strongly associated with precious metals, particularly gold (Au), in many hydrothermal ore deposits (Boyle and Jonasson, 1984; Dill, 1998; Goldfarb et al., 2005; Nevia et al., 2006). The element is of economic importance because it is currently used in semiconductors, batteries, metal alloys, flame retardants, and as an additive to some ceramic and glass (Filella et al., 2002), and it may have applications thin-film solar cell technology (e.g., Sinsermsuksakul et al., 2012; Suehiro et al., 2015). Finally, antimony is of environmental concern because it is toxic to aquatic and

terrestrial life and because it forms stable aqueous antimony-hydroxide complexes at ambient temperature in near neutral pH fluids, a chemical property that can make antimony soluble, and therefore mobile, in surface and groundwaters (Wilson et al., 2010). Antimony's interactions with sulfide ligands are the focus of this study because antimony-sulfide complexes are known to be present in natural hydrothermal fluids and reliable thermodynamic data for antimony-sulfide complexes necessary to model antimony chemistry in these fluids is currently unavailable.

1.3. Research questions and study methods

The purpose of the current endeavor has been to determine antimony speciation present in reducing sulfide-containing (i.e., H_2S and HS^-) solutions and to measure stibnite solubility in these solutions from ambient temperature to supercritical conditions along the liquid-vapor saturation line. Two complementary techniques have been employed to gain insight into antimony-sulfide interactions (speciation): (1) the solubility of stibnite was measured using flow-through reactors from 30 to 400°C and (2) the synchrotron X-ray absorption spectra (both XANES and EXAFS) of dissolved antimony in solutions at stibnite saturation were measured at ambient temperature. The results from these studies are presented in the following chapters and are briefly summarized below.

Chapter (2): Stibnite solubility and antimony speciation in aqueous sulfide solutions at 30°C

The results of 30°C stibnite solubility studies conducted using a flow-through experimental setup are presented in this chapter. Experimental fluids contained sulfide concentrations from 0.008 to 0.1 mol kg⁻¹ $\text{S}^{2-}_{\text{total}}$ and the pH was varied from pH = 4 to 12. In addition, previous studies of antimony speciation in hydrosulfide solutions using batch solubility experiments, potentiometric studies, spectroscopic measurements, ab initio calculations, and ion chromatography methods are summarized, including attempts to determine antimony speciation in fluids from hot springs. The computational approach used to determine complex stoichiometries from solubility data is also developed.

Chapter (3): X-ray absorption spectroscopy measurements of antimony- sulfide and-hydroxide complexes at stibnite saturation

The results from XAS measurements of the Sb K-edge from fluids equivalent to those studied in Chapter (2) are presented and the complimentary aspects and apparent discrepancies between the spectroscopic and solubility data are considered in detail.

Chapter (4): Stibnite solubility and antimony speciation in hydrosulfide solutions from 70 to 400°C

This chapter builds on the low temperature experiments presented in Chapter (2), beginning with a summary of previous high temperature studies and finishing with new high-temperature stibnite solubility experiments conducted in a flow-through autoclave reactor. Experiments were conducted

from 70 to 400°C at slightly above saturated water vapor pressure (swvp) using fluids with sulfide concentrations between 0.003 to 0.05 mol kg⁻¹ S²⁻_{total} and pH from pH = 3.5 to 8.5.

The thesis ends with concluding remarks presented after Chapter (4). Expanded background for each topic, methodologies, and references are included in each chapter. An appendix follows Chapter (5). Additionally, two manuscripts presenting the research in this thesis are in preparation for publication. The first manuscript combines Chapters (2) and (3), and the second manuscript covers the higher temperature solubility experiments.

1.4. References

- Boyle, R.W., Jonasson, I.R., 1984. The geochemistry of antimony and its use as an indicator element in geochemical prospecting. *J. Geochem. Explor.* **20**, 233-302.
- Dill, H.G., 1998. Evolution of Sb mineralisation in modern fold belts: a comparison of the Sb mineralisation in the Central Andes (Bolivia) and Western Carpathians (Slovakia). *Min. Dep.* **33**, 359-378.
- Filella, M., Belzile, N., Chen, Y.-W., 2002. Antimony in the environment: a review focused on natural waters I. Occurrence. *Earth-Science Reviews* **57**, 125-176.
- Goldfarb, R.J., Baker, T., Dubé, B., Groves, D.I., Hart, C.J.R., Gosselin, P., 2005. Distribution, character, and genesis of gold deposits in metamorphic terranes. *Econ. Geol.* **100**, 407-450.
- Nevia, A.M.R., Andras, P., Ramos, J.M.F., 2006. Antimony quartz and antimony-gold quartz veins from northern Portugal. *Goldschmidt Conference Abstracts* A442.
- Pearson, R.G., 1963. Hard and soft acids and bases. *J. Am. Chem Soc.* **85**, 3533-3539.
- Sinsermsuksakul, P., Chakraborty, R., Kim, S.B., Heald, S.M., Buonassisi, T., Gordon, R.G., 2012. Antimony-doped tin(II) sulfide thin films. *Chemistry of Materials* **24**, 4556-4562.
- Suehiro, S., Horita, K., Yuasa, M., Tanaka, T., Fujita, K., Ishiwata, Y., Shimanoe, K., Kida, T., 2015. Synthesis of copper-antimony-sulfide nanocrystals for solution-processed solar cells. *Inorganic Chemistry* **54**, 7840-7845.
- Werner, A., 1893. Beitrag zur Konstitution anorganischer Verbindungen. *Zeitschrift für anorganische Chemie* 267-330.
- Wilson, S.C., Lockwood, P.V., Ashley, P.M., Tighe, M., 2010. The chemistry and behaviour of antimony in the soil environment with comparisons to arsenic: a critical review. *Environ. Pollut.* **158**, 1169-1181.

Chapter (2):

Stibnite solubility and antimony speciation in aqueous sulfide solutions at 30°C

2.1. Introduction

Antimony is a metalloid that is widely distributed in natural fluids in trace amounts and is of environmental and regulatory concern because of its toxic and carcinogenic properties. The maximum contaminant level set by the United States Environmental Protection Agency for antimony in drinking water is 6 ppb (EPA, 2009). In unpolluted ground and surface waters, the antimony concentration is rarely > 10 ppb ($\sim 10^{-7}$ mol kg⁻¹ Sb) and usually < 1 ppb (Filella et al., 2002; Wilson and Webster-Brown, 2009). However in geothermal fluids, the antimony concentration is frequently > 10 ppb and can be as high as ~ 1000 ppb (Smith, 1987; Wilson et al., 2007; Landrum et al., 2009; Wilson et al., 2012; Hannington et al., 2016). In natural waters, antimony occurs as complexes with chloride (Cl⁻), hydroxide (OH⁻), and sulfide or thio (HS⁻) ligands. Antimony complexed with organic ligands may also contribute a significant portion of the dissolved antimony in natural settings where the concentrations of the organic ligands are at mol kg⁻¹ concentrations (Tella and Pokrovski, 2009). Antimony(III)-chloride complexes are limited to acidic, strongly saline conditions (Belevantsev et al., 1998a; Pokrovski et al., 2006). The neutral antimony(III)-hydroxide complex, Sb(OH)₃ (i.e., antimonous acid) is the stable antimony(III)-hydroxide complex in all but the most acidic or alkaline fluids from ambient to near supercritical conditions (Zakaznova-Herzog and Seward, 2006). However at ambient temperatures, when moderate concentrations of sulfide are present (> 0.0001 mol kg⁻¹ S_{total}²⁻), stibnite solubility due to Sb(OH)₃ is limited to only a few tens of ppb except at moderately to strongly alkaline pH. In such reducing, sulfidic natural waters, antimony also forms stable complexes with sulfide ligands, and these antimony-sulfide complexes can enhance stibnite solubility by multiple orders of magnitude above that due to Sb(OH)₃ alone.

Despite numerous, previous experimental and theoretical studies, there is still appreciable disagreement concerning the stoichiometry and stability of antimony(III)-sulfide species at ambient conditions (see Table 2.1 and associated references). The aim of this current study was therefore to determine the stoichiometry and stability of antimony(III)-sulfide and -hydroxide-sulfide complexes in aqueous solutions at 30°C by measuring the solubility of stibnite over a range of pH and total reduced sulfur concentration. The solubility data have been complemented by X-ray absorption spectroscopic measurements of antimony(III) coordination in solutions equilibrated with stibnite.

Since the 1950s, the speciation of antimony and the solubility of stibnite (Sb_2S_3) in the presence of reduced sulfur has been studied using a variety of methods. Most solubility studies indicate the presence of an antimony-sulfide dimer, while many spectroscopy studies fail to find evidence for a dimer and, along with chromatography studies, have been interpreted in terms of antimony-sulfide monomers. As summarised in Table (2.1), multiple stoichiometries for antimony and sulfide atoms in antimony-sulfide complexes have been proposed in the $\text{Sb(III)-S(II)-H}_2\text{O}$ system. Additionally, a solubility study in which both sulfide ($\text{H}_2\text{S}+\text{HS}^-$) and elemental sulfur (S^0) were present introduced the possibility of a mixed valence Sb(III,V) dimers (Helz, 2002), which then prompted theoretical calculations of the stability of such mixed valence complexes and use of these complexes to interpret spectroscopic data (Tossell, 2003a; Planer-Friedrich and Scheinost, 2011). The unresolved contradictions in antimony(III) speciation displayed in Table (2.1) and the possibility of complicated changes in speciation during oxidation, have highlighted the need for further study of antimony in the $\text{Sb(III)-S(II)-H}_2\text{O}$ system.

To determine the solubility of stibnite and the speciation of Sb(III) in the presence of sulfide, solubility experiments have been conducted using natural stibnite in a flow-through apparatus at 30°C over the pH range from pH = 4 to 12 and with sulfide concentrations from 0.008 to $0.1 \text{ mol kg}^{-1} \text{ S}^{2-}_{\text{total}}$. From the dependence of stibnite solubility on sulfide concentration and pH, the stoichiometries of possible complexes were constrained. The speciation model which best fitted the data was chosen using nonlinear least squares regression fitting of the solubility data. The average first shell coordination environment around antimony derived from X-ray absorption spectroscopy measurements, which are described in Chapter (3), proved useful in selecting the solubility model in alkaline solutions with low sulfide concentrations. The equilibrium constants presented here can be used to predict stibnite solubility and Sb(III) speciation at ambient temperatures at reducing conditions in which the sulfide concentration is $> \sim 0.005 \text{ mol kg}^{-1} \text{ S}^{2-}_{\text{total}}$. In the presence of sufficient concentrations of sulfide, it was found that dissolved antimony forms negatively charged antimony-sulfide dimers in circumneutral and alkaline fluids. These dimers transition to Sb(OH)_3 , and possibly mixed-ligand antimony monomers, as the sulfide concentration decreases.

2.1.2. Previous studies of Sb(III) speciation

Antimony complexation in the $\text{Sb(III)-S(II)-H}_2\text{O}$ system at ambient temperature has been studied using a variety of methods, including batch solubility experiments (Babko and Lisetskaya, 1956; Arnston et al., 1966; Learned, 1966; Kolpakova, 1982; Krupp, 1988; Akinifiyev et al., 1994; Belevantsev et al., 1998b; Shikina and Zotov, 1999), potentiometric and spectroscopic measurements (Shestitko and Demina, 1971; Wood, 1989; Gushchina et al., 2000; Mosselmans et al., 2000; Sherman et al., 2000; Planer-Friedrich and Scheinost, 2011), *ab initio* calculations (Tossell, 1994, 2003a, b), and ion chromatography techniques (Planer-Friedrich and Scheinost, 2011; Planer-Friedrich and Wilson, 2012). Antimony-sulfide complexes have also been detected in natural solutions using ion

Table (2.1) Summary of experimental studies of aqueous Sb(III)-S(II) speciation at < 100°C.

Species	pH	S (mol kg ⁻¹) ^a	S:Sb ratio	Method	Reference
SbS ₂ ⁻ , SbS ₃ ³⁻ , Sb ₂ S ₅ ⁴⁻	alkaline	0.005 - 3 Na ₂ S		solubility and phase equilibrium	Fiala and Konopik (1950)
SbS ₂ ⁻ , SbS ₃ ³⁻	0.6 - 12.3	0.005 - 0.1		solubility ^b	Akeret (1953)
SbS ₂ ⁻	(a) 8-9	(a) 0.04	1.5 - 200	solubility ^b	Babko and Lisetskaya (1956)
Sb(OH) ₂ ⁻	(b) 10-11	(b) no added sulfide			
Sb ₄ S ₇ ²⁻	alkaline	Na ₂ S	4 - 5	solubility	Armston et al. (1966)
SbS ₃ ³⁻ , Sb ₄ S ₇ ²⁻ , Sb ₂ S ₅ ⁴⁻	alkaline	0.25-2.5 Na ₂ S with 0-0.12 Sb ₂ S ₃	4 - 60	potentiometry	Shestiko and Demina (1971)
H ₂ Sb ₂ S ₄ , HSb ₂ S ₄ ⁻ , Sb ₂ S ₄ ²⁻	3 - 9	0.0001 - 0.006	0.5 - 10 ⁴	solubility and reinterpretation of Akeret (1953), Babko and Lisetskaya (1956)	Kolpakova (1971, 1982)
H ₂ Sb ₂ S ₄ , HSb ₂ S ₄ ⁻ , Sb ₂ S ₄ ²⁻	3 - 12	0.0002 - 0.13, most ~0.01	10 - 10 ⁶	solubility	Krupp (1988)
H ₂ Sb ₂ S ₄ , HSb ₂ S ₄ ⁻ , Sb ₂ S ₄ ²⁻ , Sb(OH) ₃				recalc. of published data with newdata for water and H ₂ S. Does not include Krupp (1988)	Spycher and Reed (1989)
Sb ₂ S ₄ ²⁻ or Sb ₄ S ₇ ²⁻ SbS ₂ ⁻ or SbS ₃ ³⁻	alkaline	(a) 0.95 Na ₂ S + 0.1 Sb (b) 0.95 Na ₂ S + 0.005-0.05 Sb	10 - 200	Raman	Wood (1989)
HSbS ₃ ²⁻ , H ₂ Sb ₂ S ₄ , SbS ₂ ²⁻				gas phase quantum chemical calculations	Tossell (1994)
Sb ₂ S ₄ ²⁻ , minor SbS ₂ ⁻	alkaline	0.914	1 - 150	Raman, observed similar spectral features as Wood (1989)	Guschina et al. (2000)
First shell CN 3-4 S atoms	8 - 13	0.01 - 1	3 - 150	EXAFS ^c	Mosselmans et al. (2000)
First shell CN 4-5 S atoms				EXAFS ^{c, d}	Sherman et al. (2000)
HSb(III), V ₂ S ₅ ⁻ , Sb(V) ₂ S ₆ ²⁻	7.6 - 10	0.0002 - 0.1	2 - 50	solubility and UV-vis ^e	Helz et al. (2002)
First shell CN 3-4 S atoms	alkaline	(a) 0.1 - 0.2	(a) 10 - 20	EXAFS ^{d,f}	Planer-Friedrich and Scheinost (2011)
First shell CN 2 S + 1 O atoms		(b) 0.02	(b) 2		

^a The sulfur concentration is the amount of free sulfur, if reported, or total sulfur including that complexed with antimony if only the starting solution composition was available.

^b amorphous Sb-sulfide used

^c range in first shell coordination numbers rounded to nearest whole number derived from fits of EXAFS spectra

^d polysulfides and Sb(V) possibly present based upon solution preparation methods

^e most experiments in Sb(III)-S(II)-S(0)-O-H system, solution equilibrated with elemental sulfur (S⁰)

^f anoxic and oxic sample preparation methods used in study. Results from anoxic samples reported in the table

chromatography combined with mass spectrometry (Planer-Friedrich and Scheinost, 2011; Planer-Friedrich and Wilson, 2012; Ullrich et al., 2013). Various authors have also periodically collected previously published equilibrium constants, critically evaluated them, and produced compilations of thermodynamic data (Spycher and Reed, 1989; Akinifiyev et al., 1994; Zotov et al., 2003; Filella and May, 2005; Obolensky et al., 2007). The models for antimony-sulfide speciation proposed in the experimental studies are summarised in Table (2.1).

Solubility studies

Several of the earlier studies measured stibnite solubility in alkaline sodium sulfide (Na_2S) solutions (Arnston et al., 1966; Learned, 1966), while other studies have considered stibnite or amorphous antimony-sulfide solubility over a wider range of sulfide and pH conditions (Babko and Lisetskaya, 1956; Kolpakova, 1982; Krupp, 1988). Solubility experiments conducted in Na_2S solutions indicated that stibnite solubility increases with increasing sulfide content at least up to 250°C in alkaline solutions (Arnston et al., 1966; Learned, 1966). These data require aqueous antimony complexes containing a stoichiometric ratio of S:Sb that is greater than 1.5:1 under the high pH conditions ($> \text{pH } 11$) and generally high sulfide concentrations (0.05 to $3 \text{ mol kg}^{-1} \text{ S}_{\text{total}}$) of the Na_2S solutions. The various studies interpreted their results in terms of $\text{Sb}_2\text{S}_4^{2-}$, $\text{Sb}_4\text{S}_7^{2-}$, SbS_2^- , or a mixture of these species.

Other solubility studies have investigated antimony complexation over a wider range of sulfide and pH conditions. Babko and Lisetskaya (1956) determined when oversaturation of antimony sulfide occurred, as indicated by the formation of colloidal suspensions, for relatively high pH solutions with and without added sulfide. Due to this experimental approach, the authors were probably measuring the solubility of an amorphous phase; however the solubilities measured are not dissimilar from later, more carefully controlled studies that indicated the presence of antimony-sulfide species. Kolpakova (1971, 1982) conducted stibnite solubility experiments at moderate to low pH from 25 to 95°C and re-evaluated earlier studies to argue for the protonated dimer, HSb_2S_4^- , predominating over a wide range of pH. Krupp (1988) studied stibnite solubility from $\text{pH} = 3$ to 12 and 25 to 350°C with the majority of his experiments conducted using solutions with $0.01 \text{ mol kg}^{-1} \text{ S}^{2-}_{\text{total}}$. Additional solutions with 0.0003 to $0.13 \text{ mol kg}^{-1} \text{ S}^{2-}_{\text{total}}$ were used by Krupp to determine the relationship between sulfide and stibnite solubility.

At 25° C, Krupp proposed the same speciation model as Kolpakova (1971, 1982) with $\text{H}_2\text{Sb}_2\text{S}_4$ dominant at $< \text{pH } 4$, HSb_2S_4^- dominant from $\text{pH} \sim 4$ to ~ 9 , and $\text{Sb}_2\text{S}_4^{2-}$ dominant at $> \text{pH } 9.5$. At temperatures $> \sim 120^\circ\text{C}$, stibnite became more soluble with decreasing sulfide concentration when the sulfide concentration was $< \sim 0.01 \text{ mol kg}^{-1} \text{ S}^{2-}_{\text{total}}$. Krupp interpreted this change as due to hydroxide ligands replacing the non-bridging sulfurs in $\text{H}_x\text{Sb}_2\text{S}_4^{x-2}$ to form a mixed hydrosulfide dimer (i.e., $\text{Sb}_2\text{S}_2(\text{OH})_2$). More recent studies that investigated stibnite and Sb(III)-oxide (senarmonite and valentinite) solubility at elevated temperatures and at lower sulfide concentrations than those used by Krupp (1987) have rejected the mixed species $\text{Sb}_2\text{S}_2(\text{OH})_2$ in favour of increasing stability of $\text{Sb}(\text{OH})_3$ with increasing temperature (Akinifiyev et al., 1994; Shikina and Zotov, 1999; Zotov et al., 2003).

Potentiometric studies

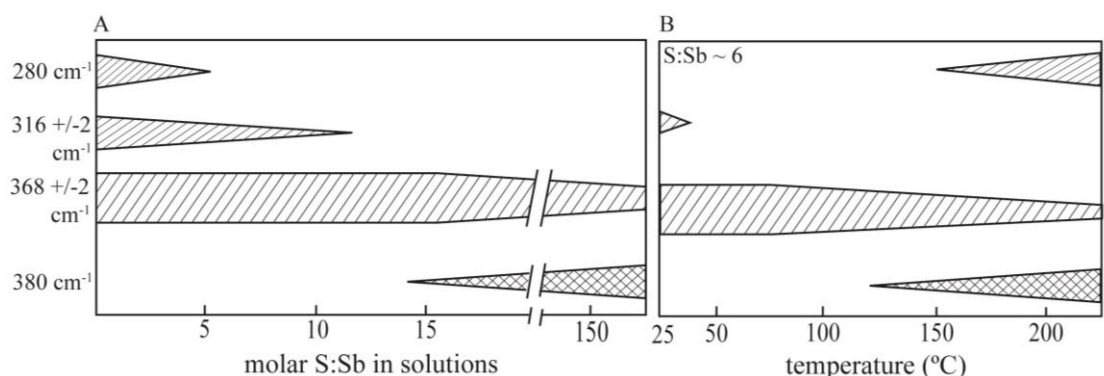
Shestitko and Demina (1971) investigated the stoichiometry of antimony complexes using an Sb electrode immersed in sodium sulfide solutions with sulfide concentrations from ~ 0.25 to ~ 2.5 mol kg⁻¹. Their results indicated a change in the slope of the electrode potential's dependence on the sulfide concentration as the sulfide concentration increased. The authors interpreted this slope change as a transition from multiple polynuclear antimony species with a high number of coordinating sulfurs (13 to 18) to a single antimony species with three coordinating sulfurs. The existence of a polynuclear species with ten or more sulfur atoms is unique to this study and may be an artifact of the method. No effort was made in the study to account for the impact of complexed sulfur on free sulfide activity or changes in activity coefficients in concentrated alkaline solutions.

Raman spectroscopy

Raman spectroscopy can identify spectral features of individual species but cannot assign these features to the unique species without additional constraints from measurements of standards or estimates of vibrational spectra from theoretical calculations. The high concentrations of antimony in solution (> 0.005 mol kg⁻¹) required for Raman spectroscopy require high pH solutions for 25°C experiments. As a result, Raman measurements are most comparable to the solubility studies conducted in Na₂S solutions or at high pH. Raman spectroscopic measurements of antimony sulfide complexes were conducted by Wood (1989) and Gushchina et al. (2000) for similar solutions of high sulfide concentrations (~ 0.9 mol kg⁻¹) and antimony concentrations up to ~ 0.1 mol kg⁻¹. Solutions in both studies were prepared by dilution of a Sb(III)-Na₂S solution with a solution of similar Na₂S concentration such that antimony was progressively diluted at a constant Na₂S concentration. Wood (1989) found four spectral features attributable to antimony species: a broad, weak band at 314 cm⁻¹; a somewhat more intense band at 369 cm⁻¹; a prominent shoulder near 350 cm⁻¹; and a shoulder at 380 cm⁻¹. The number of distinguishable features increased with increasing antimony concentration. Using predicted vibrational frequencies for a variety of species and measured vibrational frequencies for antimony solids and the SbS₄⁻ ion, the spectra were interpreted as representing a dimer (Sb₂S₄²⁻ or Sb₄S₇²⁻) that decomposed to a bent pyramidal species (SbS₂⁻ or SbS₃³⁻) upon dilution.

Gushchina et al. (2000) observed three spectral features similar to those found by Wood (1989): weak peak at ~ 318 cm⁻¹; an intense peak at ~ 366 cm⁻¹; and a shoulder at 380 cm⁻¹. They also found an additional small peak at 280 cm⁻¹ in their solutions that had the highest antimony concentration relative to the sulfide concentration. This solution had seven times more Sb than the most concentrated solution of Wood (1989) and thus a lower molar S:Sb. The observed changes in intensity for these four peaks with respect to S:Sb ratio are shown schematically in Figure (2.1). They did not observe a shoulder at ~ 350 cm⁻¹ on the main peak at ~ 370 cm⁻¹. The spectra for two less concentrated solutions were measured up to 250°C at 25-50°C intervals. With increasing temperature, the peaks at 280 cm⁻¹ and 380 cm⁻¹ became more pronounced, particularly $\geq 175^\circ\text{C}$, while all other peaks diminished. As concluded earlier by Wood (1989), Gushchina et al. (2000) resolved that no

Figure (2.1) Schematic of the occurrence and intensity of Raman spectral features in sodium sulfide solutions. Features observed by Gushchina et al. (2000) and Wood (1989) with (A) increasing S:Sb ratio in solution and (B) increasing temperature for a solution with S:Sb 6:1.



single species could account for all of the observed peaks shown qualitatively in Figure (2.1), and consequently postulated that more than one antimony species was present.

X-ray absorption spectroscopy (XAS)

The extended X-ray absorption fine structure (EXAFS) portion of the XAS spectra probes the average atomic environment around the target element and provides information on the number of neighboring atoms and their distance from the targeted element. EXAFS cannot distinguish between a mixed-ligand sulfide-hydroxide species (e.g., $\text{Sb}_2\text{S}_4(\text{OH})_2$) and mixture of species with sulfide and hydroxide ligands (e.g., $\text{H}_2\text{Sb}_2\text{S}_4$ and $\text{Sb}(\text{OH})_3$). Similar to Raman spectroscopy, EXAFS studies have been limited to antimony concentrations $\geq 0.001 \text{ mol kg}^{-1}$. Sherman et al. (2000) measured Sb K-edge spectra in Na_2S solutions without the exclusion of atmospheric oxygen during sample preparation. At ambient temperatures, the fitting of their spectra showed coordination numbers of ~ 4 sulfur atoms and Sb-S distances of 2.33 to 2.36 Å, which is consistent with an antimony(V)-sulfide complex such as $\text{Sb}(\text{V})\text{S}_4^{3-}$. This suggests that antimony(III)-sulfide complexes, or thioantimonites, may be easily oxidised to antimony(V)-sulfide complexes, or thioantimonates, in the presence of oxygen. Later studies summarised in Table (2.1) in which oxygen was apparently excluded found spectra consistent with an Sb(III) atom surrounded by three sulfurs, although some fits revealed first coordination shells that were intermediate between antimony(III)- and antimony(V)-sulfide species (Mosselmans et al., 2000; Planer-Friedrich and Scheinost, 2011). Oxygen atoms were found within the first coordination shell of antimony when the molar ratio of S:Sb in solution was $\leq 2:1$ (Planer-Friedrich and Scheinost, 2011) and when low sulfide solutions were measured at temperatures above 150°C (Mosselmans et al., 2000).

Ab initio

Tossell (1994) calculated the gas-phase minimum energy geometries and Raman vibrational spectra for a number of antimony-sulfide monomers and oligomers, including $\text{H}_x\text{SbS}_3^{x-3}$, $\text{H}_x\text{Sb}_2\text{S}_4^{x-2}$, and $\text{H}_4\text{Sb}_2\text{S}_5$, and for one mixed-ligand complex, $\text{Sb}_2\text{S}_2(\text{OH})_2$. In addition, the author estimated the effect of the interaction of one water with SH^- and the previously mentioned Sb(III) monomers. The

calculations produced estimates for Sb-S distances, gas-phase vibrational frequencies, hydrated distances, the binding energy of H₂O complexes, Born hydration energies, and gas-phase and solution phase proton affinities. In the gas phase, the transition from a fully protonated monomer, H₃SbS₃, to a fully protonated dimer, H₂Sb₂S₄, was favourable but the progression to neutral trimer, H₃Sb₃S₆, was not. The exchange of SH ligands for OH⁻ ligands in an Sb(III) dimer was favoured only above 300°C.

Tossell later re-evaluated and expanded his calculations from 1994 to include oxidation energetics for Sb(III) and mixed-valence Sb(III,V) dimers (Tossell, 2003a), and UV-vis absorbances for Sb(III) and Sb(V) monomers and dimers (Tossell, 2003b). Gas-phase calculations in Tossell (2003a) included geometries, Raman active vibrational frequencies, and energies for singly and doubly deprotonated Sb(III), Sb(V), and Sb(III, V) dimers (i.e., Sb₂S₄²⁻, HSb₂S₄⁻, Sb₂S₅²⁻, and Sb₂S₆²⁻). Combining these calculations with estimates of hydration energies, the author produced energetics for the oxidation of Sb(III) dimers to Sb(III,V) and Sb(V) dimers by either polysulfide (modelled as S₄H⁻) or elemental sulfur (modelled as S₈) in solution. In terms of aqueous phase energetics, the oxidation of an Sb(III) dimer to a mixed Sb(III, V) dimer was favoured but the next step to an Sb(V) dimer was not. In addition, this oxidation reaction was most favoured when the dimers were doubly rather than singly deprotonated. However, these estimates of aqueous phase energetics were very sensitive to the estimation of hydration energies and are much less accurate than the gas-phase calculations. In one of the complementary papers, these calculations were extended to include estimates of absorbances in the UV-vis wavelengths and estimated pK_a's for Sb monomers (Tossell, 2003b). The reported estimates of pK_a's for HSbS₄⁻ and HSbS₃²⁻ were 5.4 and 9.1, respectively. Thus, the author predicted that the last deprotonation step to a fully-deprotonated species, would occur at pH = 5.4 for an Sb(V)-sulfide monomer and at pH = 9.1 for an Sb(III)-sulfide monomer.

Ion Chromatography

Ion chromatography (IC) separates aqueous species based upon their retention within a reactive column. When linked with an elemental analysis technique such as mass spectrometry (MS), the combined techniques can determine the relative abundance of, and Sb:S ratio within, individual complexes. Within the last five years, IC-ICP-MS has begun to be applied to antimony-sulfide speciation in synthetic and geothermal fluids, as detailed in the following.

In synthetic Sb(III)-S(II) aqueous solutions, five antimony species have been detected: Sb(OH)₃ (as SbO₃³⁻ in the conditions of the reactive column), Sb(OH)₆⁻, two Sb(V)-sulfide species, and an unknown antimony species (Planer-Friedrich and Scheinost, 2011; Planer-Friedrich and Wilson, 2012). The two Sb(V)-sulfide species had S:Sb ratio of 3:1 and 4:1, which are referred to as trithioantimonate and tetrathioantimonate, respectively. Trithioantimonite, e.g., H_xSbS₃^{x-3}, was not detected by IC-ICP-MS even when a species with this S:Sb ratio was found in nearly identical solutions using X-ray absorption spectroscopy (Planer-Friedrich and Scheinost, 2011). This is in line with two recent ion chromatography studies that failed to directly detect trithioarsenite (H_xAsS₃^{x-3}) in prepared trithioarsenite standards and in reducing geothermal fluids where thioarsenites would be expected (Planer-Friedrich et al., 2010; Keller et al., 2014). With IC-ICP-MS, Planer-Friedrich et al.

(2010) detected arsenite (AsO_3^{3-}) instead of trithioarsenite ($\text{H}_x\text{AsS}_3^{x-3}$) in synthetic solutions in which $\text{H}_x\text{AsS}_3^{x-3}$ was identified by the same study with X-ray absorption spectroscopy. Keller et al. (2014) noted that samples that should have had $\text{H}_x\text{AsS}_3^{x-3}$ instead had a split arsenite peak when trithioarsenite standards and fluids from the hot springs of the Geysir geothermal area (Iceland) were measured by Ion chromatography–hydride generation–atomic fluorescence spectrometry (IC-HG-AFS), which suggests that trithioarsenite was changed to arsenite during the analytical process. Both studies attributed the failure to directly detect thioarsenites to differences in the ligand exchange rates of arsenite and arsenate. The exchange rate for OH^- ligands in arsenite is on the order of milliseconds, but that for OH^- in arsenate is on the order of days (Okumura et al., 1995). Assuming that the exchange rates for SH^- ligands behave similarly, the SH^- ligands in $\text{As}(\text{HS})_3$ will be rapidly replaced by OH^- when a sample is diluted by the alkaline eluent that is used in a chromatographic column, and as a result will be measured as $\text{As}(\text{OH})_3$. Accurate speciation of antimony IC-ICP-MS may be limited by a similar instability of antimony-sulfide complexes when diluted by alkaline eluents.

An additional difficulty to the direct measurement of antimony species in solution is the instability of $\text{Sb}(\text{III})$ species during storage, which was noted as part of LC-ICP-MS studies. In synthetic $\text{Sb}(\text{III})$ - $\text{S}(\text{II})$ samples prepared or analysed under oxic conditions, tetrathioantimonate, e.g., SbS_4^{3-} , was observed instead of the expected $\text{Sb}(\text{III})$ -sulfide complex with three sulfurs when the molar $\text{S}:\text{Sb}$ ratio in solution was greater than five (Planer-Friedrich and Scheinost, 2011). During storage or upon the addition of an oxidant, there may be a step-wise transformation from $\text{Sb}(\text{HS})_3$ to SbS_4^{3-} to $\text{Sb}(\text{OH})_3$ and finally to $\text{Sb}(\text{OH})_6^-$. Certain conditions of storage, namely freezing, refrigeration and the exclusion of light, can slow but not entirely stop this oxidation (Planer-Friedrich and Wilson, 2012). Under similar laboratory conditions, antimony-sulfide species appear more sensitive to oxidation than equivalent arsenic species. Thus, due to their instability during storage or in the conditions within a chromatographic column, the ability to infer the presence, absence, or thermodynamic stability of antimony(III)-sulfide species using ion chromatography approaches may be limited.

Within natural hot springs, antimony-sulfide species have been detected by LC-ICP-MS in fluids collected from springs in the U.S.A. (Yellowstone) and in New Zealand (Waiotapu and Orakei-Korako). At Yellowstone, the abundance of $\text{Sb}(\text{V})$ complexed with three or four sulfur atoms increased with pH and sulfide content and contributed up to 30% of the dissolved antimony present (Planer-Friedrich and Scheinost, 2011). Antimony-sulfide species were not detected at Steamboat Springs, CO or at Steamboat Springs, NV by the same study, possibly due to competition with arsenic for the available sulfide. Recently, Ullrich et al. (2013) detected arsenite, arsenate, antimonite and a selection of thioarsenates and thioantimonates in hot spring waters in New Zealand using IC-ICP-MS. At Waiotapu, antimonite (SbO_3^{3-}) was the major species (~ 60%) detected in a slightly acidic sulfidic hot spring, in addition to lesser amounts of antimonate, trithioantimonate, and, in one study, tetrathioantimonate (Planer-Friedrich and Wilson, 2012; Ullrich et al., 2013). With increased distance from the geothermal source, the amount of antimonate increased while all thioantimonates eventually

disappeared when dissolved sulfide became undetectable (Ullrich et al., 2013). In contrast, fluids from Orakei-Korako, an alkaline hot spring with lower sulfide concentrations, had higher dissolved total antimony but a lower proportion of Sb(V)-sulfide species (Planer-Friedrich and Wilson, 2012).

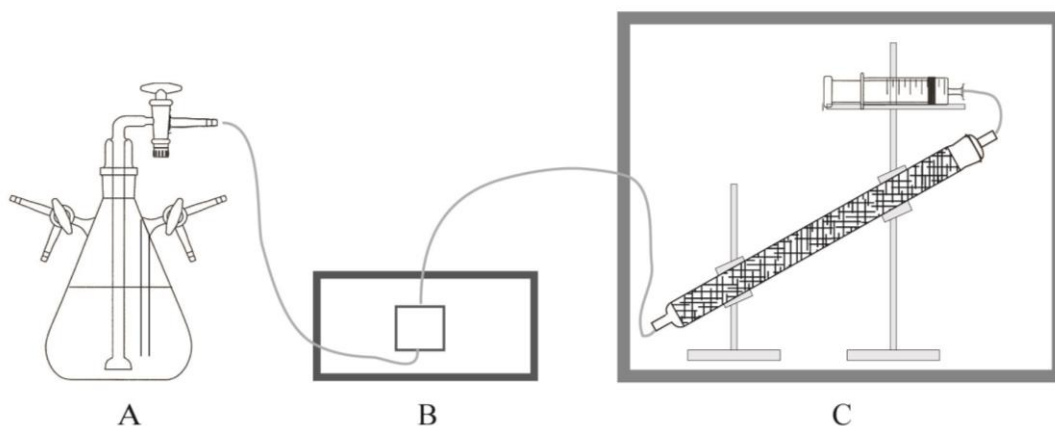
The high concentrations of antimony measured in reducing fluids discharging from sulfidic hot springs into the earth's surface environment, as summarised above, demonstrate that antimony's behaviour in these types of fluids is critical to how antimony is distributed within the Earth's crust. Because the speciation of antimony in natural systems has proved difficult to study directly, the current and previous experimental studies provide much needed insight into how stibnite solubility and aqueous speciation respond to changes in sulfide concentration and pH. In this Chapter, measurements of stibnite solubility at 30°C and antimony speciation models derived from that data are presented. The 30°C speciation models developed in this Chapter will also serve as the starting point for interpreting the high temperature data presented in Chapter (4).

2.2. Methods

2.2.1. Flow-through solubility apparatus

The flow-through apparatus shown schematically in Figure (2.2) was used to conduct solubility experiments. The apparatus consisted of (a) a 2 l glass flask in which solutions were prepared, (b) a Teflon-lined HPLC pump with sapphire pistons that transferred solution at a constant flow rate from the flask through the reactive column, and (c) a 30 cm long glass column containing stibnite that was mounted in an oven which was maintained at constant temperature. Finally, solution samples were collected in a gas-tight syringe from the column outlet located in the oven. The stibnite was natural stibnite from Wuning County in the Jianxi Province, China (XRD pattern in Figure A.1), and was crushed, cleaned with deionised water, and sieved to achieve a grain size of 0.5 to 1 mm prior to use in the column. Three thermocouples measured the temperature inside the oven at the inlet, mid-point, and outlet of the glass column. The reported temperature is the average of these three values

Figure (2.2) Flow-through experimental setup at 30°C. A sulfide solution is first made in a 2 l flask (A) then pumped with an HPLC pump (B) through a glass column containing crushed stibnite in an oven (C) before being collected in a syringe for periodic sampling.



with an estimated uncertainty of 0.4°C.

For each experiment, a deoxygenated sulfide solution was first prepared in a 2 l flask. A sufficient amount of NaOH was added to 1.5 to 1.75 l of 18.3 M Ω deionised water to adjust the pH. This solution was then deoxygenated by bubbling high purity nitrogen (BOC 99.999%) through the solution while the flask sat in an ultrasonic bath for a minimum of 30 minutes. After deoxygenation, sulfide was added by bubbling a H₂S/N₂ gas mixture through the solution until the solution was saturated with respect to the H₂S/N₂ gas mixture (1% H₂S, 5% H₂S, 10% H₂S, 20% H₂S, 50% H₂S, and 98% H₂S gas mixtures were used). The flask was then connected directly to an HPLC pump, and all lines up to the stibnite column were purged with the deoxygenated solution prior to commencement of each experiment. To maintain a constant sulfide concentration, the appropriate H₂S/N₂ gas mixture was bubbled through the headspace of the flask during an experiment.

2.2.2. Analytical methods

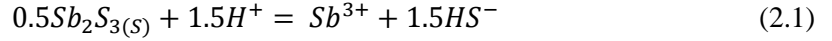
Solution pH was measured with a Metrohm pH meter (with temperature probe) which was calibrated against standard buffer solutions daily. The concentrations of reduced sulfur were determined by idiometric back titration. The antimony concentration was measured by inductively-coupled plasma-optical emission spectroscopy (ICP-OES) for concentrations greater than 50 to 100 ppb ($\sim 4 \times 10^{-7}$ to 8×10^{-7} mol kg⁻¹) and by hydride-generation atomic absorption spectroscopy (HG-AAS) for lower concentrations. In preparation for ICP-OES samples, a 1 mol kg⁻¹ NaOH solution was added to the sample for a final concentration of 0.08 mol kg⁻¹ NaOH in the samples to prevent the precipitation of antimony in the presence of sulfide. The ICP-OES detection limit was 10 ppb ($\sim 1 \times 10^{-7}$ mol kg⁻¹) with an estimated uncertainty of $\sim 20\%$ at the detection limit. For HG-AAS, the detection limit and estimated uncertainty were 0.3 ppb ($\sim 3 \times 10^{-9}$ mol kg⁻¹) and $\sim 20\%$, respectively (Table A.1). Generation of volatile antimony hydrides from Sb(III) for HG-AAS requires a sample matrix of 10% (v/v) HCl. Thus, samples to be analyzed by HG-AAS were diluted with an HCl solution to achieve the desired final HCl concentration and then bubbled with nitrogen to remove dissolved sulfide and prevent antimony loss. Potassium iodide was added to HG-AAS samples prior to analysis to assure that all antimony was reduced to Sb(III). The matrices of the antimony standards were matched to the samples for both analysis techniques.

2.2.3. Selection of aqueous complexes and non-linear least squares fitting

The stoichiometry of the dominant complexes in solution determines the dependence of stibnite solubility on changes in solution pH and sulfide concentration. These relationships were used to select the possible species present, as explained in the following, and equilibrium constants for the selected species were determined using a non-linear least squares fitting procedure to fit the measurements of stibnite solubility.

Development of solubility curves and selection of complexes

Stibnite solubility as Sb^{3+} in the absence of complexation can be represented by the following equation when reduced sulfur occurs as HS^-



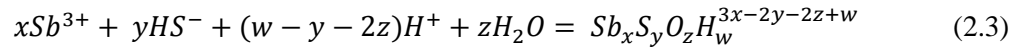
The solubility product for this reaction is

$$K_{sp} = a_{Sb^{3+}} \cdot a_{HS^-}^{1.5} \cdot a_{H^+}^{-1.5} \quad (2.2)$$

where a_i is the activity of an aqueous species. If complexing by aqueous sulfide and/or OH^- occurs, then the complexes that form can be represented by the general stoichiometry



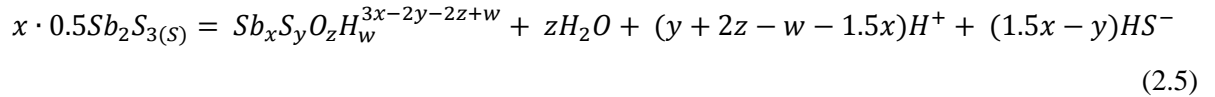
in which x , y , z , and w are variables that represent the coefficients of the constituent atoms in the complex. The general equation for the formation of the complexes takes the form of



Equation (2.3) can be solved for Sb^{3+} to give

$$Sb^{3+} = \frac{1}{x}Sb_xS_yO_zH_w^{3x-2y-2z+w} - \frac{y}{x}HS^- + \frac{y+2z-w}{x}H^+ + \frac{z}{x}H_2O \quad (2.4)$$

which can be substituted into (2.1) to give a general equation for the solubility of stibnite as sulfide-hydroxide complexes



Defining the activity of water and the pure mineral stibnite as unity, the equilibrium constant for Equation (2.5) then becomes,

$$K_{xyzw} = a_{Sb_xS_yO_zH_w^{3x-2y-2z+w}} \cdot a_{HS^-}^{1.5x-y} \cdot a_{H^+}^{y+2z-w-1.5x} \quad (2.6)$$

Taking the logarithm of this expression and solving for the activity of the antimony complex,

$$\log a_{Sb_xS_yO_zH_w^{3x-2y-2z+w}} = \log K_{xyzw} + (y - 1.5x) \cdot \log a_{HS^-} + (y + 2z - w - 1.5x) \cdot pH \quad (2.7)$$

From Equation (2.7), the relationship between the activity of a complex and changes in the activity of HS^- (a_{HS^-}) and pH can be derived

$$\left(\frac{\partial \log a_{Sb_xS_yO_zH_w^{3x-2y-2z+w}}}{\partial \log a_{HS^-}} \right)_{P,T,pH} = y - 1.5x \quad (2.8)$$

$$\left(\frac{\partial \log a_{Sb_xS_yO_zH_w^{3x-2y-2z+w}}}{\partial pH} \right)_{P,T,a_{HS^-}} = y + 2z - w - 1.5x \quad (2.9)$$

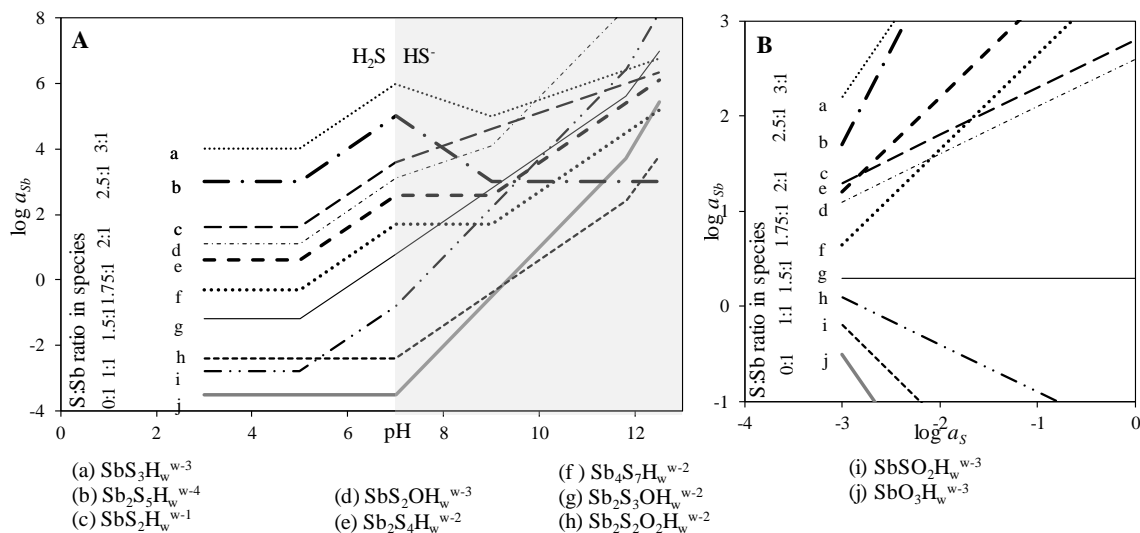
The same approach can be used to derive a general reaction and equilibrium constant written in terms of H_2S^0 . For the relationship of solubility and pH, this produces

$$\left(\frac{\partial \log a_{Sb_xS_yO_zH_w^{3x-2y-2z+w}}}{\partial pH} \right)_{P,T,a_{H_2S}} = 2y + 2z - w - 3x \quad (2.10)$$

The relationship of solubility and $\log a_{H_2S}$ is the same as that for $\log a_{HS^-}$ expressed in Equation (2.8).

The slopes of experimental solubility curves with respect to pH or sulfide concentration are compared to ideal slopes calculated from Equations (2.8), (2.9), and (2.10) to select the complex or

Figure (2.3) Schematic of possible stibnite solubility versus pH curves at constant sulfide (A) or versus sulfide (B) for selected monomers and dimers. Curves are arranged in order of S:Sb ratio. Curves in (A) were calculated using Equations (2.9) and (2.10) in, respectively, the predominance regions of HS^- and H_2S . Curves in (B) used Equation (2.8). The curves for complexes with two or more HS^- ligands were calculated such that the first deprotonation occurs at $\text{pH} = 5$ and the second at $\text{pH} = 9$. The first deprotonation of an OH^- ligand is estimated to occur at $\text{pH} = 11.8$. In (A), the field where dissolved sulfide is predominantly HS^- is shaded.



complexes that may be present. In Figure (2.3), ideal solubility versus pH (2.3A) and $\log a_{\text{HS}^-}$ (2.3B) curves are plotted showing the changes in slope associated with progressive deprotonation of HS^- and OH^- ligands.

The plots were constructed assuming that the first and second deprotonations of HS^- ligands bound to Sb(III) occur at $\text{pH} \approx 5$ and ≈ 9 , respectively, as suggested by previous solubility studies (Krupp, 1988), and assuming that the OH^- ligands in mixed-ligand antimony species did not deprotonate until $\text{pH} \approx 12$, as is the case for OH^- ligands in $\text{Sb}(\text{OH})_3$ (Zakaznova-Herzog and Seward, 2006). At $\text{pH} \leq 7$, the slope of the solubility curve is equal to the negative of the complex charge (i.e., Equation 2.10). Above $\text{pH} \geq 7$, different ionic charges and complex stoichiometries produce various slopes. The relationship of stibnite solubility to the activity of total reduced sulfur (i.e., $\text{HS}^- + \text{H}_2\text{S}^0$) is independent of pH and the protonation state and is thus constant across the pH region for a given complex (Figure 2.3B). In this study, subscripts are used to indicate the relevant antimony complex, aqueous species or reaction when activities (a), concentrations as molality (m), activity coefficients (γ) or equilibrium constants (K) are included in text or equations. Equilibrium constants expressing stibnite solubility in terms of different antimony species (i.e Equation 2.6) are written in terms of a_{HS^-} and a_{H^+} and balanced in terms of moles of the antimony complex. The stibnite solubility reactions for each the aqueous antimony species considered in speciation models used in non-linear fitting are listed in Table (2.2).

Table (2.2) Heterogeneous solubility reactions used in the nonlinear least squares fitting.

K_{xyzw}	Aqueous antimony species	Reaction
antimony-hydroxide complexes		
K_{1033}	$\text{Sb}(\text{OH})_3$	$0.5\text{Sb}_2\text{S}_3 + 3\text{H}_2\text{O} = \text{Sb}(\text{OH})_3 + 1.5\text{HS}^- + 1.5\text{H}^+$
K_{1032}	H_2SbO_3^-	$0.5\text{Sb}_2\text{S}_3 + 3\text{H}_2\text{O} = \text{H}_2\text{SbO}_3^- + 1.5\text{HS}^- + 2.5\text{H}^+$
antimony-sulfide complexes		
K_{1300}	SbS_3^{3-}	$0.5\text{Sb}_2\text{S}_3 + 1.5\text{HS}^- = \text{SbS}_3^{3-} + 1.5\text{H}^+$
K_{1301}	HSbS_3^{2-}	$0.5\text{Sb}_2\text{S}_3 + 1.5\text{HS}^- = \text{HSbS}_3^{2-} + 0.5\text{H}^+$
K_{1302}	H_2SbS_3^-	$0.5\text{Sb}_2\text{S}_3 + 1.5\text{HS}^- + 0.5\text{H}^+ = \text{H}_2\text{SbS}_3^-$
K_{1303}	H_3SbS_3	$0.5\text{Sb}_2\text{S}_3 + 1.5\text{HS}^- + 1.5\text{H}^+ = \text{H}_3\text{SbS}_3 + 1.5\text{HS}^-$
K_{2400}	$\text{Sb}_2\text{S}_4^{2-}$	$\text{Sb}_2\text{S}_3 + \text{HS}^- = \text{Sb}_2\text{S}_4^{2-} + \text{H}^+$
K_{2401}	HSb_2S_4^-	$\text{Sb}_2\text{S}_3 + \text{HS}^- = \text{HSb}_2\text{S}_4^{2-}$
K_{2402}	$\text{H}_2\text{Sb}_2\text{S}_4$	$\text{Sb}_2\text{S}_3 + \text{HS}^- + \text{H}^+ = \text{H}_2\text{Sb}_2\text{S}_4$
K_{2502}	$\text{H}_2\text{Sb}_2\text{S}_5^{2-}$	$\text{Sb}_2\text{S}_3 + 2\text{HS}^- = \text{H}_2\text{Sb}_2\text{S}_5^{2-}$
antimony-hydroxide-sulfide (mixed-ligand) complexes		
K_{1211}	$\text{HSbS}_2\text{O}^{2-}$	$0.5\text{Sb}_2\text{S}_3 + 0.5\text{HS}^- + \text{H}_2\text{O} = \text{HSbS}_2\text{O}^{2-} + 1.5\text{H}^+$
K_{1212}	$\text{H}_2\text{SbS}_2\text{O}^-$	$0.5\text{Sb}_2\text{S}_3 + 0.5\text{HS}^- + \text{H}_2\text{O} = \text{H}_2\text{SbS}_2\text{O}^- + 0.5\text{H}^+$
K_{1213}	$\text{H}_3\text{SbS}_2\text{O}$	$0.5\text{Sb}_2\text{S}_3 + 0.5\text{HS}^- + \text{H}_2\text{O} + 0.5\text{H}^+ = \text{H}_3\text{SbS}_2\text{O}$
K_{1122}	$\text{H}_2\text{SbSO}_2^-$	$0.5\text{Sb}_2\text{S}_3 + 2\text{H}_2\text{O} = \text{H}_2\text{SbSO}_2^- + 0.5\text{HS}^- + 1.5\text{H}^+$
K_{1123}	H_3SbSO_2	$0.5\text{Sb}_2\text{S}_3 + 2\text{H}_2\text{O} = \text{H}_3\text{SbSO}_2 + 0.5\text{HS}^- + 0.5\text{H}^+$

Speciation of solutions and the non-linear fitting procedure

Non-linear least squares fitting of experimental solubilities with selected complexes was performed using the DataFitX software (Oakdale Engineering, 2000) after initial derivation of a_{HS^-} from the measured sulfide concentrations. The fitting procedure fits the following equation:

$$m_{\text{Sb}_{\text{total}}} = \sum^{xyzw} x \cdot m_{\text{Sb}_x\text{S}_y\text{O}_z\text{H}_w^{3x-2y-2z+w}} = \sum^{xyzw} x \cdot a_{\text{Sb}_x\text{S}_y\text{O}_z\text{H}_w^{3x-2y-2z+w}} \cdot \gamma_{\text{Sb}_x\text{S}_y\text{O}_z\text{H}_w^{3x-2y-2z+w}}^{-1} \quad (2.11)$$

which is equivalent to

$$m_{\text{Sb}_{\text{total}}} = \sum^{xyzw} x \cdot K_{wxyz} \cdot a_{\text{HS}^-}^{-y-1.5x} \cdot a_{\text{H}^+}^{1.5x+w-y-2z} \cdot \gamma_{\text{Sb}_x\text{S}_y\text{O}_z\text{H}_w^{3x-2y-2z+w}}^{-1} \quad (2.12)$$

Note that the K_{wxyz} used in Equation (2.12) and defined by Equation (2.6) is for a reaction in terms of moles of a given antimony complex. This is in contrast to equations (2.1) and (2.4), which are written in terms of moles of antimony. The inputs to the fitting procedure for each individual experiment were the antimony concentration ($\text{mol kg}^{-1} \text{Sb}_{\text{total}}$), the measured pH as a_{H^+} , and the calculated a_{HS^-} and ionic strength, as detailed in the following section.

The activities of the aqueous species OH^- , H^+ , HS^- , H_2S° , NaHS° , NaOH° , and Na^+ were calculated using reaction and mass balance constraints. The following independent reactions define the equilibrium relationships between these species:



Table (2.3) Supporting thermodynamic data at 30°C. Logarithms of the equilibrium constants used in fluid speciation calculations and values for the parameters in Equation (2.23).

Eqn No.	Reaction	25°C	30°C	Reference
2.17	$H_2O \rightleftharpoons H^+ + OH^-$	-14.00	-13.84	a
2.18	$H_2S^o \rightleftharpoons H^+ + HS^-$	-6.98	-6.91	b
2.19	$NaOH^o \rightleftharpoons Na^+ + OH^-$	0.72	0.67	c
2.20	$NaHS^o \rightleftharpoons Na^+ + HS^-$	1.18	1.14	d
Debye-Hückel Parameters				
2.23	A	0.5164	0.5148	e
2.23	B	3.25E+07	3.26E+07	e
2.23	B-dot	0.041	0.041	f

a. Marshall and Franck (1981)

b. Suleimenov and Seward (1997)

c. Ho and Palmer (1996)

d. Ho et al. (1994), by analogy with NaCl^o

e. Helgeson and Kirkham (1974)

f. Helgeson (1969)



For these reactions, following equilibrium constants can be written

$$K_w = a_{H^+} \cdot a_{OH^-} \cdot a_{H_2O}^{-1} \quad (2.17)$$

$$K_{H_2S} = a_{H^+} \cdot m_{SH^-} \cdot \gamma_{SH^-} \cdot m_{H_2S^o}^{-1} \cdot \gamma_{H_2S^o}^{-1} \quad (2.18)$$

$$K_{NaOH} = m_{Na^+} \cdot \gamma_{Na^+} \cdot m_{OH^-} \cdot \gamma_{OH^-} \cdot m_{NaOH^o}^{-1} \cdot \gamma_{NaOH^o}^{-1} \quad (2.19)$$

$$K_{NaSH} = m_{Na^+} \cdot \gamma_{Na^+} \cdot m_{SH^-} \cdot \gamma_{SH^-} \cdot m_{NaHS^o}^{-1} \cdot \gamma_{NaHS^o}^{-1} \quad (2.20)$$

Additionally, the Na and S species are constrained by the following two mass balance equations

$$m_{Na_{total}} = m_{NaSH^o} + m_{Na^+} + m_{NaOH^o} \quad (2.21)$$

$$\begin{aligned} m_{S_{total}} &= m_{H_2S^o} + m_{SH^-} + m_{NaHS^o} + \sum^{xyzw} y \cdot m_{Sb_xS_yO_zH_w} \\ &= m_{H_2S^o} + m_{SH^-} + m_{NaHS^o} + m_{S_{complexed}} \end{aligned} \quad (2.22)$$

The concentration of sulfur complexed with antimony was unknown prior to determination of the antimony species present. For all experiments with pH < 10.4, the concentration of sulfide was much greater than that of antimony and thus $m_{S_{complexed}}$ was negligible. When the concentration of antimony was $\geq 1\%$ S_{total} , $m_{S_{complexed}}$ was likely to be greater than the relative standard deviation of titration measurements ($\sim 3\%$). For such experiments, the total sulfide concentration was corrected for the simultaneous titration of $m_{S_{complexed}}$ using the appropriate complex for the Sb(III) speciation model being tested. The resulting total free sulfide concentration, or $m_{S_{free}}$, was used to derive a_{HS^-} .

The ionic strengths for experimental solutions varied between $\sim 1 \times 10^{-4}$ and 0.2 mol kg^{-1} but were $< 0.02 \text{ mol kg}^{-1}$ for the majority of experiments. The activity of water and the activity coefficients for NaOH^o, NaHS^o, and neutral Sb complexes were set to unity. Activity coefficients for Na⁺, HS⁻, H⁺,

OH⁻, and aqueous antimony ions were calculated using an extended Debye-Hückel equation (Helgeson, 1969)

$$-\log \gamma_i = \frac{Az_i^2 \sqrt{I}}{1 + B\tilde{a}_i \sqrt{I}} + \dot{B} \cdot I \quad (2.23)$$

where A , B , and \dot{B} (or B-dot) are temperature dependent constants calculated from polynomial fits of data in Helgeson (1969) and Helgeson and Kirkham (1974), z is the ion charge, I is the ionic strength, and \tilde{a} is the ion size parameter (in cm), which was set to 4×10^{-8} , 3.5×10^{-8} , 9×10^{-8} , and 4.5×10^{-8} for Na⁺, OH⁻/HS⁻, H⁺, and antimony complexes, respectively (Kielland, 1937). For the 30°C experiments, values of 0.5148, 3.26×10^{-7} , and 0.041 were used for parameters A , B , and \dot{B} , respectively. The ionic strength, I , is defined as

$$I = \frac{1}{2} \sum m_i \cdot z_i^2 \quad (2.24a)$$

For the solutions in these experiments, this was implemented as

$$I = \frac{1}{2} (m_{H^+} + m_{OH^-} + m_{Na^+} + m_{HS^-} + \sum^{xyzw} m_{Sb_x S_y O_z H_w} \cdot (3x - 2y - 2z + w)^2) \quad (2.24b)$$

The thermodynamic data used for speciation calculations and for the non-linear least squares regression fitting are given in Table (2.3). The ion product for water (Equation 2.17) was taken from Marshall and Franck (1981). The first ionization constant for H₂S° (Equation 2.18) was selected from Suleimenov and Seward (1997). The dissociation constant for NaOH° (Equation 2.19) was from Ho and Palmer (1996). The dissociation constant for NaHS° (Equation 2.20) was assumed to be the same as that for NaCl°, for which the measurements of Ho et al. (1994) were used.

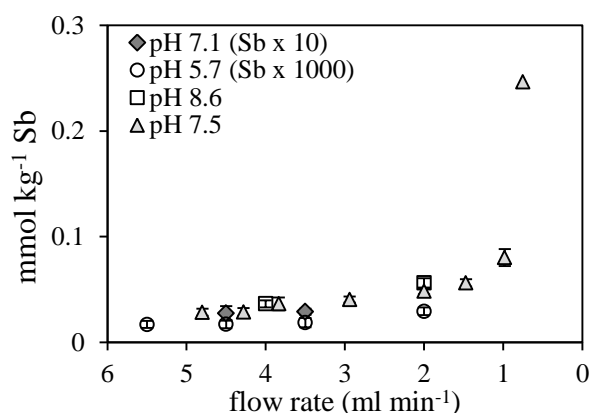
After determination of an initial value for K_{xyzw} , a_{HS^-} and I were re-calculated to include the effect of sulfide complexed with antimony on m_{Sfree} and the effect of charged antimony species on ionic strength. The resulting a_{HS^-} and ionic strengths were used in the fitting procedure with mol kg⁻¹ Sb_{total} and the measured pH to produce new estimates for K_{xyzw} . This process was repeated until the K_{xyzw} values for successive iterations converged. Fits converged within ≤ 10 iterations. The equilibrium constants for these reactions are distinguished by subscripts indicating the antimony species, i.e., K_{xyzw} , as defined for Equation (2.6) and listed in Table (2.2).

2.3. Results

2.3.1. Attainment of equilibrium

The attainment of equilibrium with stibnite in the flow-through apparatus was tested by measuring stibnite solubility at different flow rates in solutions with constant pH and sulfide concentration. Constant antimony concentrations at variable flow rates are considered to represent equilibrium conditions. As shown in Figure (2.4), antimony concentrations were constant within error for flow rates between 3.5 ml min⁻¹ and 5.5 ml min⁻¹ in tests conducted with the HPLC pump. For a single preliminary experiment conducted with a diaphragm pump but with the same column at 50°C, stibnite solubility was constant between 1 and 8 ml min⁻¹ and decreased above ~ 10 ml min⁻¹ flow rate

Figure (2.4) Solubility of stibnite at different flow rates in solutions with constant pH and sulfide concentration. Sulfide concentrations for different solutions were between 0.02 and 0.1 mol kg⁻¹ S²⁻_{total}. The increase of stibnite solubility flow rates < 2 ml min⁻¹ may be attributed to slight oxidation of the solution while passing through the tubing between flask and column, especially for those with higher sulfide contents. Antimony concentrations are constant within error for flow rates between 3.5 ml min⁻¹ and 5.5 ml min⁻¹.



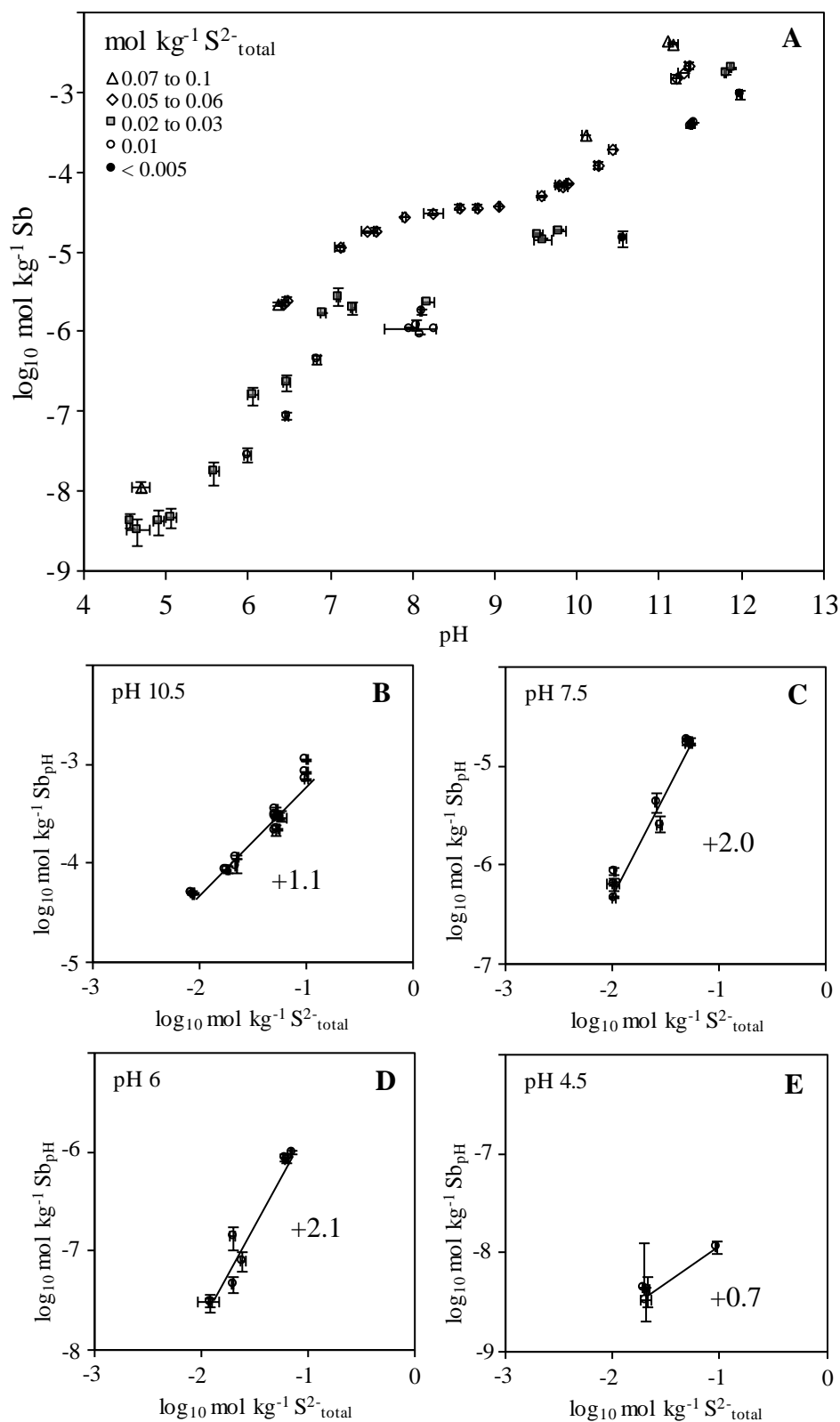
(results not shown). For most solutions tested, especially for those with higher sulfide contents, the solubility of stibnite increased at flow rates < 2 ml min⁻¹. This behaviour may be attributed to slight oxidation of the solution while passing through the Teflon tubing between flask and column, as evidenced by yellowing of some solutions in the Teflon tubing during extremely slow flow rates (0.01 ml min⁻¹) when the residence time in the Teflon tubing was > ~ 6 hours. The yellowing was due to the formation of polysulfide species. A 4.5 ml min⁻¹ flow rate was used for all subsequent experiments included in the development of the speciation model.

2.3.2. Measured stibnite solubility curves

Stibnite solubility measurements are presented in Figure (2.5), and complete results are tabulated in Table (A.2) in Appendix (A). The measured stibnite solubility at different sulfide contents is plotted versus pH in Figure (2.5A). Stibnite solubility decreased from hundreds of ppm (~ 10^{-3.5} mol kg⁻¹) to less than 1 ppb (~ 10^{-8.5} mol kg⁻¹) as pH decreased from 12 to 4. The measured stibnite solubility has been projected to a constant pH in Figures (2.5B, C, D, and E). These plots show that stibnite solubility increased with increasing sulfide content for the entire pH range studied. The increase is greatest between pH = 5 and 8 (Figures 2.5C and 2.5D). At pH = 4.5, the slope of stibnite solubility slope versus sulfide content was slightly > +0.5 (Figure 2.5E). For the data shown in these four plots, the sulfide concentration was high enough that the amount of sulfide complexed with antimony did not change the solubility-sulfide concentration relationship within the error of the sulfide measurements.

The slope of the stibnite solubility curve with respect to pH (i.e., the Sb/pH slope), as shown in Figure (2.5A), changes at pH = 9.5, at pH = 7, possibly at pH = 6.5, and at pH = 5. These slope changes indicate a change in the dominant reaction controlling stibnite solubility. The dominant dissolved sulfide species changes from H₂S° to HS⁻ at pH > 7 at 30°C, and this speciation change will result in a change in the stibnite solubility curve regardless of a change in antimony speciation. Thus,

Figure (2.5) Stibnite solubility versus pH (A) and versus sulfide concentration (B through E). For the sulfide plots, the measured solubility has been projected to a constant pH (pH shown in plots) using a slope of $Sb/pH = +1$ for (B) and (D), a slope of $Sb/pH = +0.5$ for (C), and zero slope for (E). A linear least squares fits and their slopes are shown for (B) through (E).



the solubility curve suggests the existence of three to four distinct antimony complexes: one species at $\text{pH} > 9$, one to two species at $5 < \text{pH} < 9$, and another complex at $\text{pH} < 5$. The species at low pH must be a neutral species because the solubility curve slope in Figure (2.5A) approaches a zero slope at $\text{pH} < 5$. This is because all neutral Sb(III)-S-O complexes produce stibnite solubility curves that are independent of pH when H_2S is the dominant form of dissolved sulfide, as can be shown with Equation (2.10). The dependence of stibnite solubility on sulfide activity (approximated by sulfide concentration in Figure 2.5) changed with decreasing pH from $\sim +1$ at strongly alkaline pH (Figure 2.5A), to $\sim +2$ at mildly alkaline to mildly acidic pH (Figures 2.5C and 2.5D), and finally was $\sim +0.7$ at $\text{pH} < 5$ (Figure 2.5E).

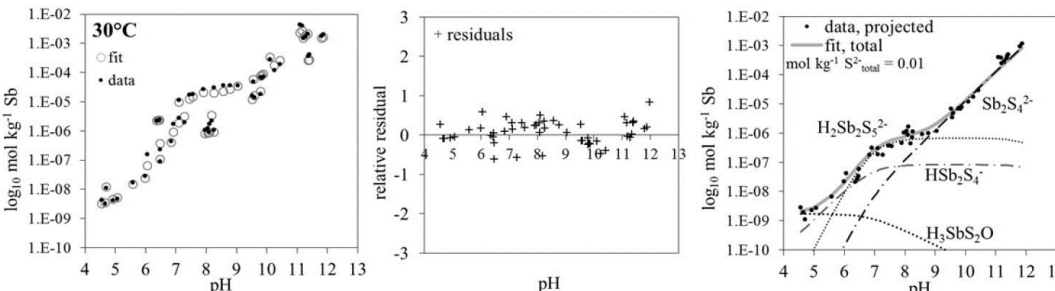
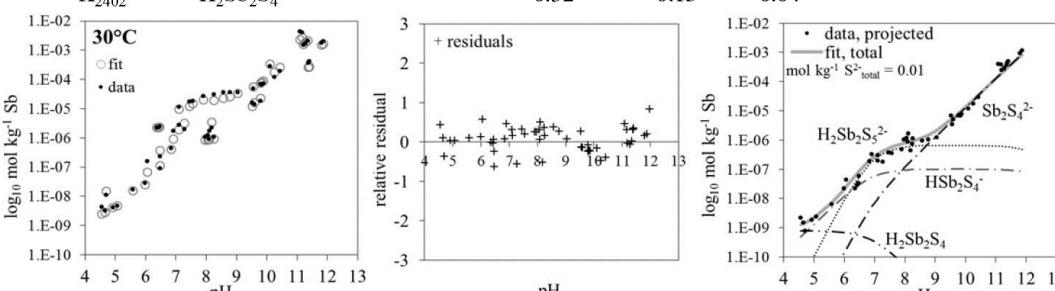
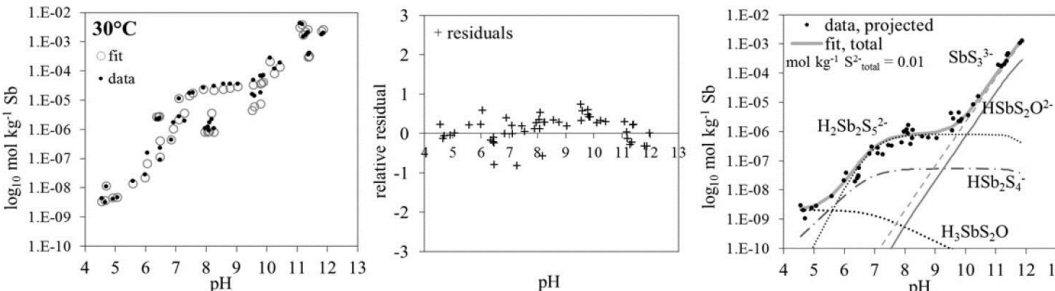
In addition to these experiments in which sulfide was added to the initial experimental solution, two experiments were conducted in which stibnite solubility was measured in deoxygenated, deionised water at $\text{pH} = 10.5$ and 12.0 (Sb90 and Sb91 in Table A.2). These experiments are plotted in Figure (2.5A) but are not included in Figure (2.5B). Figure (2.5A) shows that stibnite solubility still increased rapidly with increasing pH at low sulfide concentrations ($< 0.005 \text{ mol kg}^{-1} \text{ S}_{\text{total}}^{2-}$). The stibnite solubilities measured in these experiments (1.5×10^{-5} and $9.3 \times 10^{-4} \text{ mol kg}^{-1} \text{ Sb}_{\text{total}}$) were greater than that which could be accounted for by the antimony-sulfide complexes present at higher sulfide concentrations. These results were used to estimate the heterogeneous equilibrium constants for the stibnite solubility reactions due to neutral and singly deprotonated antimonous acid (i.e., $\text{Sb}(\text{OH})_3$ and H_2SbO_3^-) and to investigate the possibility of partially deprotonated mixed-ligand monomers at alkaline pH.

2.3.3. Determining equilibrium constants for antimony-sulfide complexes

Complexes to be included in speciation models must satisfy both the pH and sulfide solubility relationships observed. The aqueous antimony species considered and the form of the reaction used for obtaining equilibrium constants for each of these species are compiled in Table (2.2). The preferred speciation model (Fit 30-A) is presented in Table (2.4) and its accompanying plots. These three plots display the fit of the measured solubilities, the relative residuals versus pH, and the distribution of species at $0.01 \text{ mol kg}^{-1} \text{ S}_{\text{total}}^{2-}$. Fit (30-A) includes a fully deprotonated $\text{Sb}_2\text{S}_4^{2-}$ dimer at high pH, two partially protonated dimers in the near neutral region ($\text{H}_2\text{Sb}_2\text{S}_5^{2-}$ and HSb_2S_4^-), and a fully protonated, mixed ligand monomer ($\text{H}_3\text{SbS}_2\text{O}$) at low pH. Fit (30-A) is the preferred fit because of its good fit statistics, its consistency with first shell EXAFS results (Chapter 3), and its agreement with the high temperature data that is best fit with $\text{Sb}_2\text{S}_4^{2-}$ and HSb_2S_4^- (Chapter 4). Fit (30-A) also has chemically reasonable deprotonation states for the sulfide ligand as suggested by *ab initio* calculations (Tossell, 2003b)

Included with Fit (30-A) in Table (2.4) are several other fits having similar statistics that were considered but that did not produce the best fit to the data. The first of these fits, Fit (30-B), is identical to Fit (30-A) except for the neutral species. The choice of the neutral species was determined by the $+0.7$ slope of stibnite solubility curve with respect to sulfide concentration at $\text{pH} = 4.5$ (Figure

Table (2.4) Non-linear least squares fits of stibnite solubility at 30°C. The plots accompanying each fit show the fit of the measured solubilities at variable sulfide concentrations (*left*), the relative residuals of the fit (*middle*), and the distribution of species at 0.01 mol kg⁻¹ S²⁻_{total} with the data projected to that sulfide concentration (*right*). K is the derived equilibrium constant for the stated reaction (see Table 2.2), σ is one standard deviation, p is Prob(t) for the null hypothesis that $K = 0$, R^2 is the proportion of the variation in the data that is explained by the fit, and N is the number of data points.

Fit	Reaction	Aqueous antimony species	K	σ	p^a	R^{2b}	pH range	N
30-A	K ₂₄₀₀	Sb ₂ S ₄ ²⁻	4.7E-14	4.E-15	1.3E-16	0.91	4.5 to 12	51
	K ₂₅₀₂	H ₂ Sb ₂ S ₅ ²⁻	2.8E-03	3.E-04	2.3E-14			
	K ₂₄₀₁	HSb ₂ S ₄ ⁻	4.2E-06	1.9E-06	0.03			
	K ₁₂₁₃	H ₃ SbS ₂ O	4.8E-05	1.8E-05	0.01			
								
30-B	K ₂₄₀₀	Sb ₂ S ₄ ²⁻	4.7E-14	4.E-15	3.3E-16	0.90	4.5 to 12	51
	K ₂₅₀₂	H ₂ Sb ₂ S ₅ ²⁻	2.7E-03	3.E-04	1.1E-13			
	K ₂₄₀₁	HSb ₂ S ₄ ⁻	5.1E-06	1.9E-06	0.01			
	K ₂₄₀₂	H ₂ Sb ₂ S ₄	0.32	0.15	0.04			
								
30-C	K ₁₃₀₀	SbS ₃ ³⁻	3.2E-19	7.E-20	4.7E-05	0.86	4.5 to 12	51
	K ₁₂₁₁	HSbS ₂ O ²⁻	1.5E-20	4.E-21	6.2E-04			
	K ₂₅₀₂	H ₂ Sb ₂ S ₅ ²⁻	3.3E-03	3.E-04	3.1E-14			
	K ₂₄₀₁	HSb ₂ S ₄ ⁻	2.7E-06	2.4E-06	0.26			
	K ₁₂₁₃	H ₃ SbS ₂ O	5.8E-05	2.2E-05	0.01			
								

^a p is Prob(t) for the null hypothesis that $K = 0$, i.e. values of p approaching 1 indicate that a species can be removed without changing the fit.

^b R^2 is the ratio of variation in the data explained by the fit to the total variation in the data, i.e. $R^2 = \frac{\sum_{i=1}^N (\hat{y}_i - \bar{y})^2}{\sum_{i=1}^N (y_i - \bar{y})^2}$

where y_i is the i^{th} data point, \bar{y} is the mean of N data points, and \hat{y}_i is the fit of the i^{th} data point.

2.5E). Given this slope, the moderately acidic region was best fit by the presence of a species with a +1 slope (i.e., HSb_2S_4^-) and a species with a +0.5 slope (i.e., $\text{H}_3\text{SbS}_2\text{O}$). However, a speciation model using $\text{H}_2\text{Sb}_2\text{S}_4$ and HSb_2S_4^- (Fit 30-B) could fit the data nearly as well given the limited amount of data at this pH. Fit (30-A), which included $\text{H}_3\text{SbS}_2\text{O}$ and HSb_2S_4^- , was the preferred fit because HSb_2S_4^- is integral to fits of the higher temperature solubility data and because monomeric rather than dimeric species are expected to be stable at the low antimony concentrations (i.e., $< 10^{-8} \text{ mol kg}^{-1} \text{ Sb}$) that define stibnite solubility at $\text{pH} < 5$. Neutral antimony complexes that produce slopes of stibnite solubility versus sulfide activity that are $> +1$ (e.g., H_3SbS_3 or $\text{H}_4\text{Sb}_2\text{S}_5$) or < 0 (e.g., H_3SbSO_2 and $\text{Sb}(\text{OH})_3$) were inconsistent with the observed sulfide dependence at $\text{pH} = 4.5$.

An increase in sulfide concentration produced an increase of equal magnitude in the stibnite solubility at moderate to strongly alkaline pH and 0.01 to $0.1 \text{ mol kg}^{-1} \text{ S}^{2-}_{\text{total}}$. This sulfide dependence could be fit with a speciation modeling containing either $\text{Sb}_2\text{S}_4^{2-}$ or a combination of monomers. As described in the introduction, X-ray absorption spectroscopic measurements fail to detect Sb-Sb distances in sodium sulfide solutions and may thus be interpreted to suggest the presence of antimony-sulfide monomers. Therefore, the possibility of antimony-sulfide monomers at alkaline pH was considered. The last fit in Table (2.4), Fit (30-C), is one in which the alkaline region was fit with two monomers, SbS_3^{3-} and $\text{HSbS}_2\text{O}^{2-}$, instead of $\text{Sb}_2\text{S}_4^{2-}$. These two monomers have Sb-S solubility curves with, respectively, +1.5 and +0.5 slopes that when combined could approximate the +1 slope of the experimental data shown in Figure (2.5B).

Fit (30-C) had good fit statistics, but this fit was rejected because it contradicted the first shell coordination numbers for antimony that were measured by EXAFS for solutions between pH 10.9 and 11.7 with $\geq 0.02 \text{ mol kg}^{-1} \text{ S}^{2-}_{\text{total}}$. The speciation model from Fit (30-C) for alkaline pH (i.e., SbS_3^{3-} and $\text{HSbS}_2\text{O}^{2-}$) predicted oxygen atoms in the first coordination shell of antimony at moderate sulfide concentrations but none were detected from the EXAFS at these conditions. In contrast, the speciation model from Fit (30-A) for alkaline pH (i.e., $\text{Sb}_2\text{S}_4^{2-}$, $\text{Sb}(\text{OH})_3$, and H_2SbO_3^-) predicted average first shell coordination numbers that were consistent with EXAFS results. The details of EXAFS measurements are discussed in Chapter (3).

The choice of $\text{Sb}_2\text{S}_4^{2-}$ was further tested by performing non-linear least squares fits using only the data from pH 10 to pH 12 (fit not shown). The value for the equilibrium constant for $\text{Sb}_2\text{S}_4^{2-}$ (K_{2400}) from this fit (4.3×10^{-14}) was within error of the fits conducted using the complete data set. The larger oligomer $\text{Sb}_4\text{S}_7^{2-}$ produces a solubility curve that is identical to that of $\text{Sb}_2\text{S}_4^{2-}$, as can be calculated using Equations (2.8) and (2.9). The smaller dimer was selected because *ab initio* calculations suggest that the transition from antimony dimers to larger oligomers is energetically unfavorable (Tossell, 1994). Including the fully deprotonated monomer, SbS_3^{3-} , produced a fit of the same quality as Fit (30-C). In this fit, the high p value for SbS_3^{3-} and large standard deviation of its equilibrium constant suggest that this species does not make a significant contribution to the dissolved antimony at the experimental sulfide concentrations. Therefore, the fully deprotonated dimer $\text{Sb}_2\text{S}_4^{2-}$ was judged to be

Table (2.5) Speciation models that failed to fit stibnite solubility at near neutral pH at 30°C. The plots accompanying each fit show the fit of the measured solubilities at variable sulfide concentrations (*left*), the relative residuals of the fit (*middle*), and the distribution of species at 0.01 mol kg⁻¹ S₂²⁻ total with the data projected to that sulfide concentration (*right*). K is the derived equilibrium constant for the stated reaction (see Table 2.2), σ is the standard deviation, p is Prob(t) for the null hypothesis that $K = 0$, R^2 is the proportion of the variation in the data that is explained by the fit, and N is the number of data points.

Fit	Reaction	Aqueous antimony species	K	σ	p^a	R^{2b}	pH range	N
30-D	K ₂₄₀₀	Sb ₂ S ₄ ²⁻	5.7E-14	7.E-15	5.9E-11	0.67	4.5 to 12	51
	K ₂₄₀₁	HSb ₂ S ₄ ⁻	1.3E-05	2.E-06	1.5E-08			
<div><div><p>30°C</p><p>log₁₀ mol kg⁻¹ Sb</p><p>○ fit • data</p></div><div><p>+ residuals</p><p>relative residual</p></div><div><p>log₁₀ mol kg⁻¹ Sb</p><p>• data, projected — fit, total mol kg⁻¹ S₂²⁻total = 0.01</p><p>Sb₂S₄²⁻ HSb₂S₄⁻</p></div></div>								
30-E	K ₂₄₀₀	Sb ₂ S ₄ ²⁻	4.3E-14	7.E-15	7.8E-08	0.71	4.5 to 12	51
	K ₁₂₁₂	H ₂ SbS ₂ O ⁻	9.4E-10	1.5E-10	1.9E-07			
	K ₁₂₁₃	H ₃ SbS ₂ O	2.3E-05	2.2E-05	0.32			
<div><div><p>30°C</p><p>log₁₀ mol kg⁻¹ Sb</p><p>○ fit • data</p></div><div><p>+ residuals</p><p>relative residual</p></div><div><p>log₁₀ mol kg⁻¹ Sb</p><p>• data, projected — fit, total mol kg⁻¹ S₂²⁻total = 0.01</p><p>Sb₂S₄²⁻ H₂SbS₂O⁻ H₃SbS₂O</p></div></div>								
30-F	K ₂₄₀₀	Sb ₂ S ₄ ²⁻	2.6E-14	1.E-14	0.008	0.70	4.5 to 12	51
	K ₁₃₀₁	HSbS ₃ ²⁻	4.4E-08	1.0E-08	6.2E-05			
	K ₁₃₀₂	H ₂ SbS ₃ ⁻	3.2E-01	1.0E-01	0.003			
	K ₁₂₁₃	H ₃ SbS ₂ O	1.5E-05	3.1E-05	0.63			
<div><div><p>30°C</p><p>log₁₀ mol kg⁻¹ Sb</p><p>○ fit • data</p></div><div><p>+ residuals</p><p>relative residual</p></div><div><p>log₁₀ mol kg⁻¹ Sb</p><p>• data, projected — fit, total mol kg⁻¹ S₂²⁻total = 0.01</p><p>Sb₂S₄²⁻ HSbS₃²⁻ H₂SbS₃⁻ H₃SbS₂O</p></div></div>								

^a p is Prob(t) for the null hypothesis that $K = 0$, i.e. values of p approaching 1 indicate that a species can be removed without changing the fit.

^b R^2 is the ratio of variation in the data explained by the fit to the total variation in the data, i.e. $R^2 = \frac{\sum_{i=1}^N (\hat{y}_i - \bar{y})^2}{\sum_{i=1}^N (y_i - \bar{y})^2}$

where y_i is the i^{th} data point, \bar{y} is the mean of N data points, and \hat{y}_i is the fit of the i^{th} data point.

the only significant antimony-sulfide species at $\text{pH} > 9$ at stibnite saturation and sulfide concentrations $> 0.01 \text{ mol kg}^{-1} \text{ S}^{2-}_{\text{total}}$.

Fit (30-A) included the species $\text{H}_2\text{Sb}_2\text{S}_5^{2-}$, which has not been proposed previously for the Sb(III)-S(II)- H_2O system. The fully deprotonated form of this species, $\text{Sb}_2\text{S}_5^{4-}$, was put forward by two early studies of antimony speciation in strongly alkaline solutions (Fiala and Konopik, 1950; Shestitko and Demina, 1971), but protonated forms of this Sb-S stoichiometry have not been documented. Fits that did not include $\text{H}_2\text{Sb}_2\text{S}_5^{2-}$ were not able to fit the solubility data. Examples of such fits are shown in Table (2.5). Attempts to fit the near neutral solubility data using only HSb_2S_4^- species (Fit 30-D) produced poor fits with values for $R^2 = 0.70$ because HSb_2S_4^- was unable to reproduce stibnite solubility in the near neutral pH region. The $\text{H}_2\text{Sb}_2\text{S}_5^{2-}$ moiety is the only species (monomer or dimer) that produces a Sb-pH solubility curve that changes from a +2 slope below to a zero slope at $\text{pH} > \text{pK}_a$ of H_2S . This curve shape was required to fit the experimental data between $\text{pH} = 6$ and 9.

Various combinations of monomers, including $\text{H}_x\text{SbS}_2\text{O}^{x-3}$ species (Fit 30-E) and $\text{H}_x\text{SbS}_3^{x-3}$ species (Fit 30-F), were also unable to fit the experimental data. The presence of $\text{H}_2\text{Sb}_2\text{S}_5^{2-}$ between $\text{pH} = 6$ and 9 was also consistent with the greater dependence of stibnite solubility on sulfide activity observed at near neutral pH. As is shown in Figures (2.5C) and (2.5D), the slope describing the dependence of stibnite solubility on sulfide concentration curve is $\sim +2$ immediately above and below the pK_a of H_2S (i.e., at $\text{pH} = 6.5$ and 7.5). Antimony-sulfide complexes in the series $\text{H}_x\text{Sb}_2\text{S}_5^{x-4}$ are the only monomeric or dimeric complexes that produce a stibnite solubility versus sulfide activity curve with a slope of +2 (see Figure 2.3B). Antimony-sulfide monomers ($\text{H}_x\text{SbS}_3^{x-3}$) also produce a Sb/S curve with a slope $> +1$, but they are unable to reproduce stibnite solubility versus pH (Sb/pH) curve, as is shown in Fit (30-F).

2.3.4. Estimating an equilibrium constant for antimonous acid

The stibnite solubilities in two deionised water experiments conducted at strongly alkaline pH were greater than what could be accounted for by the antimony-sulfide complexes which were determined from the experiments conducted at higher sulfide concentration. This suggests that additional aqueous antimony species must be present at low sulfide concentrations ($< 0.005 \text{ mol kg}^{-1} \text{ S}^{2-}_{\text{total}}$). EXAFS measurements of the solution from one of these two deionised water experiments found that the first coordination shell of dissolved antimony at $\text{pH} = 12$ and a sulfide concentration of $\sim 0.001 \text{ mol kg}^{-1} \text{ S}^{2-}_{\text{total}}$ contained more oxygen than sulfur atoms. Therefore, stibnite solubility and EXAFS measurements require that, in addition to $\text{Sb}_2\text{S}_4^{2-}$, antimony-hydroxide and possibly mixed-ligand species are present at high pH and low sulfide concentrations.

A fit was conducted in which the solubility data from the two deionized water experiments were combined with the solubility data at higher sulfide concentrations so that provisional values for the equilibrium constants for $\text{Sb}(\text{OH})_3$ (i.e., K_{1033}) and H_2SbO_3^- (i.e., K_{1032}) could be determined. In the fitting procedure, K_{1032} was defined as a parameter dependent on K_{1033} using the pK_a of $\text{Sb}(\text{OH})_3$ at 30°C . Thus, the addition of the two species $\text{Sb}(\text{OH})_3$ and H_2SbO_3^- to the speciation model only added

Table (2.6) Non-linear fits of stibnite solubility at 30°C including deionized water experiments. The plots accompanying each fit show the fit of the measured solubilities at variable sulfide concentrations (*left*), the relative residuals of the fit (*middle*), and the distribution of species at 0.01 mol kg⁻¹ S²⁻_{total} with the data projected to that sulfide concentration (*right*). K is the derived equilibrium constant for the stated reaction (see Table 2.2), σ is the standard deviation, p is Prob(t) for the null hypothesis that $K = 0$, R^2 is the proportion of the variation in the data that is explained by the fit, and N is the number of data points. Equations for R^2 and p with Tables (2.4) and (2.5).

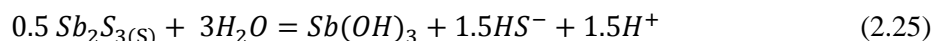
Fit	Reaction	Aqueous antimony species	K	σ	p^a	R^{2b}	pH range	N
30-G	K ₂₄₀₀	Sb ₂ S ₄ ²⁻	4.7E-14	4.E-15	2.2E-16	0.90	4.5 to 12	53
	K ₂₅₀₂	H ₂ Sb ₂ S ₅ ²⁻	2.8E-03	2.6E-04	5.3E-14			
	K ₂₄₀₁	HSb ₂ S ₄ ⁻	4.2E-06	2.0E-06	3.9E-02			
	K ₁₂₁₃	H ₃ SbS ₂ O	4.8E-05	1.9E-05	1.2E-02			
	K ₁₀₃₃	Sb(OH) ₃	3.1E-27	8.E-28	5.6E-04			
	K ₁₀₃₂	H ₂ SbO ₃ ⁻	5.2E-39	dependent on K ₁₀₃₃				
<p>30°C ○ fit • data</p> <p>+ residuals</p> <p>data, projected — fit, total mol kg⁻¹ S²⁻_{total} = 0.01</p> <p>Sb₂S₄²⁻ H₂Sb₂S₅²⁻ HSb₂S₄⁻ Sb(OH)₃ H₃SbS₂O H₂SbO₃⁻</p>								
30-H	K ₂₄₀₀	Sb ₂ S ₄ ²⁻	3.6E-14	5.E-15	7.4E-09	0.90	4.5 to 12	53
	K ₂₅₀₂	H ₂ Sb ₂ S ₅ ²⁻	2.9E-03	3.E-04	3.9E-14			
	K ₂₄₀₁	HSb ₂ S ₄ ⁻	3.8E-06	2.0E-06	0.07			
	K ₁₂₁₃	H ₃ SbS ₂ O	5.1E-05	1.9E-05	0.01			
	K ₁₂₁₁	HSbS ₂ O ²⁻	1.2E-20	3.E-21	7.1E-04			
<p>30°C ○ fit • data</p> <p>+ residuals</p> <p>data, projected — fit, total mol kg⁻¹ S²⁻_{total} = 0.01</p> <p>Sb₂S₄²⁻ H₂Sb₂S₅²⁻ HSb₂S₄⁻ HSbS₂O²⁻ H₃SbS₂O</p>								
30-I	K ₂₄₀₀	Sb ₂ S ₄ ²⁻	4.6E-14	4.E-15	7.5E-17	0.92	4.5 to 12	53
	K ₂₅₀₂	H ₂ Sb ₂ S ₅ ²⁻	2.8E-03	2.E-04	0.00			
	K ₂₄₀₁	HSb ₂ S ₄ ⁻	4.1E-06	1.9E-06	3.1E-02			
	K ₁₂₁₃	H ₃ SbS ₂ O	4.9E-05	1.7E-05	0.008			
	K ₁₁₂₂	H ₂ SbSO ₂ ⁻	1.8E-23	4.E-24	1.2E-05			
<p>30°C ○ fit • data</p> <p>+ residuals</p> <p>data, projected — fit, total mol kg⁻¹ S²⁻_{total} = 0.01</p> <p>Sb₂S₄²⁻ H₂Sb₂S₅²⁻ HSb₂S₄⁻ H₂SbSO₂⁻ H₃SbS₂O</p>								

Table (2.7) Previously published values for K_{1033} . The thermodynamic data for H_2S and H_2O presented in this has been used to modify the published reaction when it was in a format other than that used in the current study.

K_{1033} at (a) 25 or (b) 30°C	Reference
2.8×10^{-27}	(a) Spycher and Reed (1981), <i>derived from Popova et al. (1975)</i>
3.4×10^{-28}	(a) Akinifiev et al. (1994), <i>based upon Popova et al. (1975) with additional experimental data at 350 °C</i>
6.6×10^{-29}	(b) Shikina and Zotov (1999), <i>extrapolated from 200-350°C data</i>
3.1×10^{-27}	(a) Filella and May (2003), <i>recalculation of literature data</i>
3.1×10^{-27}	(b) current study, Fit (30-G)

one variable, K_{1033} , to the fit equation. The estimated values for K_{1033} and K_{1032} enabled prediction of the distribution of antimony species over the range of sulfide concentrations found in natural fluids. In addition, fits were conducted using the two mixed-ligand monomers ($HSbS_2O_2^-$ and $H_2SbSO_2^-$) likely to be present at strongly alkaline pH based upon the slope of the solubility versus pH curve and on the deprotonation state of OH^- and HS^- ligands (bound to Sb^{3+}) in $Sb(OH)_3$ (Zakaznova-Herzog and Seward, 2006) and antimony-sulfide complexes (determined in this study). The results of these fits are presented in Table (2.6). EXAFS measurements assisted in comparing the speciation models of these three fits.

Fit (30-G) is the fit in which stibnite solubility at alkaline pH and low sulfide concentrations was due to antimonous acid ($Sb(OH)_3$ and $H_2SbO_3^-$). The equilibrium constant for $Sb(OH)_3$ from this fit was 3.1×10^{-27} , which is comparable to previously published values that are listed in Table (2.7). Stibnite dissolves to form neutral antimonous acid according to the following reaction



Most of the previously published values for reaction (2.25) at ambient temperatures (i.e., Spycher and Reed, 1989; Filella and May, 2003) have been derived by evaluation and recalculation of literature data that can be traced back to a single experimental study (Popova et al., 1975). More recent experimental work has been carried out at 200 to 350°C, but the values for K_{1033} at 25°C derived by extrapolation of these higher temperature data are 1 to 2 orders of magnitude lower than that estimated in the current study and other reported estimates, which are similar to the current study (Table 2.7).

Additionally, Fit (30-G) predicted average numbers of first shell sulfur and oxygen atoms that were consistent with the results of all of the solutions measured by EXAFS. In contrast, fits using $HSbS_2O_2^-$ instead of $Sb(OH)_3$ predicted average coordination shells that were inconsistent with EXAFS measurements. Specifically, a speciation model with $HSbS_2O_2^-$ resulted in oxygen ligands in the coordination shell where none were observed by EXAFS (Fit 30-H). A speciation model including $H_2SbSO_2^-$ (Fit 30-I) resulted in fit statistics equivalent to Fit (30-G) and a similar predicted first coordination shell. However, this mixed-ligand monomer was not present in the best fits of the high temperature data, whereas $Sb(OH)_3$ was an integral part of the speciation models from $\geq 150^\circ C$ (Chapter 4). Therefore, Fit (30-G), which is an extension of Fit (30-A) with $Sb(OH)_3$, and $H_2SbO_3^-$ at high pH and low sulfide concentrations, is considered the best fit to the current experimental data and

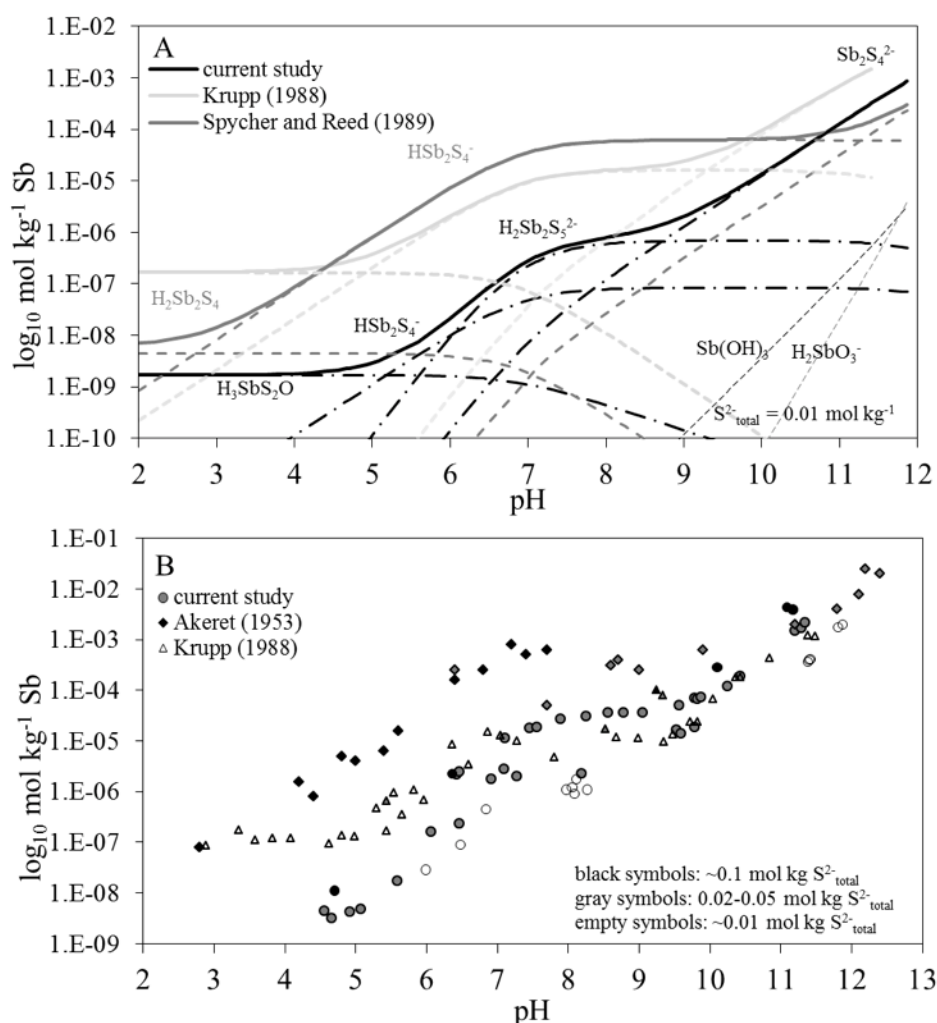
provides a reliable estimate of K_{1033} 3.1×10^{-27} at 30°C at 1 bar. In the following discussion, the equilibrium constants from Fit (30-G) have been used to construct speciation diagrams for total sulfide concentrations of 0.01, 0.001, and 0.0001 mol kg⁻¹.

2.4. Discussion

2.4.1. Comparison of Sb(III)-S(II) speciation model with previous studies

The speciation model for antimony(III) complexes presented here is different from those in previous solubility studies in terms of the solubilities measured and the species proposed at $\text{pH} \leq 9$. Figure (2.6A) compares the speciation model presented in the current study with those from the experimental study of Krupp (1988) and from the literature data re-evaluation of Spycher and Reed (1989). Spycher and Reed (1989) relied heavily on data from Akeret (1953) for their calculations of 25°C equilibrium constants. Figure (2.6B) shows the solubility data for stibnite, or amorphous Sb_2S_3

Figure (2.6) Comparison of the preferred speciation model (Fit 30-G, A) and the 30°C solubility data (B) from the current study with models and solubility data from previous studies at ambient temperature. The models in (A) are plotted at $\text{S}^{2-}_{\text{total}} = 0.01 \text{ mol kg}^{-1}$. Previous studies include the batch-solubility studies of Akeret (1953) and Krupp (1988), and literature review study of Spycher and Reed (1989).



in the case of Akeret (1953), from which these models were derived. The symbol shade (i.e., black, gray, or white/empty) indicates the sulfide concentration ranges (S_{total}^{2-}) used in the experimental studies: $\sim 0.1 \text{ mol kg}^{-1}$, $0.02 \text{ to } 0.05 \text{ mol kg}^{-1}$, and $\sim 0.01 \text{ mol kg}^{-1}$. As can be seen from both subplots, all three datasets have a similar shaped solubility curves, however speciation models of Krupp (1988) and of Spycher and Reed (1989) are 1.5 to 2 orders of magnitude higher than the current study between pH ~ 4.5 and 8.5 .

The current study, as well as those of Kolpakova (1971, 1982), Krupp (1988), Spycher and Reed (1989), have all concluded that the dimer $\text{Sb}_2\text{S}_4^{2-}$ is sufficient to account for Sb_2S_3 solubility in alkaline solutions with moderate sulfide concentrations. The solubility curves presented in Figure (2.6) are similar at pH ≥ 10 and support the conclusion that $\text{Sb}_2\text{S}_4^{2-}$ is the dominant antimony-sulfide species in alkaline solutions across a wide range of sulfide concentrations. The antimony-sulfide monomers, SbS_2^- and SbS_3^{3-} , that have been invoked by some studies (Fiala and Konopik, 1950; Babko and Lisetskaya, 1956; Shestitko and Demina, 1971; Wood, 1989) could not account for the stibnite solubilities measured in this study.

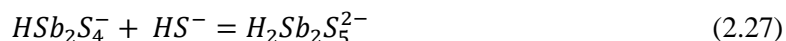
In acidic solutions, fully protonated species are expected for antimony-sulfide and antimony-hydroxide complexes at pH ≤ 5 to 6 according to *ab initio* calculations and comparison with the arsenic-sulfide aqueous complexes. The first deprotonation of $\text{H}_2\text{Sb}_2\text{S}_4$ was predicted to occur at pH ~ 5 using correlations between calculated aqueous deprotonation free energies for antimony-sulfide complexes and for sulfur and arsenic hydroxide complexes with experimentally known pK's (Tossell, 2003a). It should be noted as well that antimony(V)-sulfide complexes are expected to deprotonate at a significantly lower pH. The same *ab initio* approach as was used for $\text{H}_2\text{Sb}_2\text{S}_4$ predicts that Sb(V)-sulfide dimers will become singly deprotonated at pH ~ 2 and Sb(V) monomers will become fully deprotonated by pH $= 6$ (Tossell, 2003a, b).

One can also estimate the pH at which SH^- ligands in antimony(III)-sulfide monomers and dimers will deprotonate by considering the thioarsenite ($\text{As}(\text{HS})_3$) system. This is accomplished by assuming that the pH difference between the first deprotonation of an OH^- ligand in $\text{Sb}(\text{OH})_3$ and a HS^- ligand in a neutral monomeric antimony(III)-sulfide complex is similar to that measured for OH^- and HS^- ligands in $\text{As}(\text{OH})_3$ and $\text{As}(\text{HS})_3$. With increasing pH at 25°C , $\text{As}(\text{HS})_3$ progressively deprotonates at pH $= 3.8$, 6.5 , and 9.3 to eventually form AsS_3^{3-} at elevated pH (Zakaznova-Herzog and Seward, 2012). The first deprotonation of $\text{As}(\text{OH})_3$ occurs at pH $= 9.25$ at 25°C (Zakaznova-Herzog et al., 2006). Therefore, there is a difference of ~ 5.5 pH units between the first deprotonation of a HS^- ligand in $\text{As}(\text{HS})_3$ (at pH $= 3.8$) and of an OH^- ligand in $\text{As}(\text{OH})_3$ (at pH $= 9.3$). Applying this difference to the antimony system results in an estimated first deprotonation of antimony(III)-sulfide and antimony(III)-sulfide-hydroxide (i.e., $\text{Sb}((\text{HS})_{3-x}(\text{OH})_x)$ complexes at pH ~ 6 (i.e., $11.8 - 5.5 = 6.3$). The OH^- ligands in mixed-ligand antimony complexes will remain fully protonated over approximately the same pH range as the OH^- ligands in $\text{Sb}(\text{OH})_3$, i.e., from pH $= 1.4$ to 11.8 at 25°C (Zakaznova-Herzog and Seward, 2006). Thus, a change in the slope of the solubility curve between

pH 5 and 6 is consistent the deprotonation of an HS⁻ ligand in antimony(III)-sulfide complex or an antimony(III)-sulfide-hydroxide complex.

Identification of the correct Sb-S-O stoichiometry for the equilibrium complex at pH ≤ 5 requires experiments at different sulfide concentrations. Such experiments are limited in the current and previous experiments. The experiments of Akeret (1953) were conducted at one sulfide content at pH < 7, and thus offer no assistance. Krupp (1988) had four experiments over a range of 0.004 to 0.02 mol kg⁻¹ S²⁻_{total} near pH 5.5. These experiments were consistent with the +1 sulfide dependence expected for HSb₂S₄⁻ and H₂Sb₂S₄, but the data were scattered (the R² of the best fit line used in selecting H₂Sb₂S₄ was ~ 0.4) and, at pH ~ 5.5, are in the pH region dominated by HSb₂S₄⁻ and not by a neutral species. Although the species H₂Sb₂S₄ is consistent with dimers found at higher pH, dimers are expected to become increasingly less stable at the antimony concentrations (< 1x10⁻⁸) set by stibnite solubility at acidic pH. In the current study, H₃SbS₂O was selected because it best reproduced the stibnite solubilities measured at pH ~ 4.5. The choice of H₃SbS₂O or H₂Sb₂S₄ does not change the speciation model at higher pH.

The shape of the stibnite solubility curve between pH = 5 to 9 cannot be fit by the addition of variable protonation states of antimony-sulfide or -hydroxide monomers (i.e., Fits (30-D) through (30-F) in Table (2.5)), but may be fit with partially deprotonated dimers. This portion of the solubility curve was assigned to HSb₂S₄⁻ by Krupp (1988) and Kolpakova (1971, 1982) based upon their own experimental data and to the same species by Spycher and Reed (1989) using data from Akeret (1953) and others. In the current model, an additional species, H₂Sb₂S₅²⁻, is included to improve the fit in the circumneutral pH region. This species could be formed by the addition of an HS⁻ ligand to HSb₂S₄⁻, as represented by the following reaction.



The reaction could involve the replacement of one of the bridging sulfur atoms in HSb₂S₄⁻ with an HS⁻ ligand to form two corner-sharing SbS₃ tetrahedra connected by a single bridging sulfur atom. If this is the case, H₂Sb₂S₅²⁻ could be considered an intermediate between dimers with two bridging sulfur atoms (i.e., HSb₂S₄⁻ and Sb₂S₄²⁻) and a partially protonated Sb-sulfide monomer such as HSbS₃²⁻ or H₂SbS₃⁻, both of which would be favored by higher sulfide contents. The geometry of the H₂Sb₂S₅²⁻ complex is unknown and was not included by Tossell (1994, 2003a) in his *ab initio* calculations. Tossell (1994) considered the similar fully protonated moiety (H₄Sb₂S₅) and described it as a corner-sharing dimer but did not present geometric parameters for the species. By analogy with the SbS₃ sites in stibnite and the structure of Sb₂S₄, two distorted tetrahedral SbS₃ units could be connected by a corner-sharing sulfur atom in H₂Sb₂S₅²⁻.

The largest proportional differences between the current and previous studies occur in this intermediate pH range, and there are several possible explanations for this discrepancy. The solubility experiments of Akeret (1989), which were used to produce the Spycher and Reed (1989) solubility model, were collected using an amorphous antimony-sulfide solid, which would be expected to have higher solubility than crystalline stibnite used in the current study. In general, the experimental data of

Krupp (1988) lie between those of the current stibnite solubility study and the data of Akeret (1953), who used amorphous Sb_2S_3 . Stibnite solubility also increases in the presence of more oxidized forms of sulfur. The stibnite solubility measured by Helz et al. (2002) in a batch solubility study in which S^0 was present at slightly or below saturation with elemental sulfur was similar to the solubility measured by Akeret (1953). Either oxidation or changes in the equilibrium solid phase could also have been issues during the ~ 2 months duration of the 25°C batch solubility experiments conducted by Krupp (1988).

The exponential-like increase of antimony concentration at extremely low flow rates that was noted in Figure (2.4) suggests that stibnite solubility is strongly sensitive to slight changes in oxidation state, which would be difficult to control in long-term batch experiments. The short duration of flow-through solubility experiments (i.e., this current study), enabled by the high mineral-to-fluid reaction ratios achieved in this type of solubility experiment, minimizes the effect of trace amounts of oxygen. In this study, extreme care was taken during the preparation of the experimental solutions to assure a reducing, sulfide solution, and no evidence of oxidation in the reservoir flask (Figure 2.2) was noted during any of the experiments. Additionally, the XAS results presented in the following Chapter (3) are consistent with 3-coordinated Sb(III) rather than 4-coordinated Sb(V) being present in the experimental solutions.

2.4.2. Influence of sulfide concentration on aqueous antimony speciation

Most of the experiments conducted in this study had sulfide concentrations from $\text{S}^{2-}_{\text{total}} = 0.02$ to 0.05 mol kg^{-1} , which is above the typical sulfide concentrations found in reducing groundwaters or other fluids present in the Earth's crust. The aqueous antimony speciation in fluids with sulfide concentrations more typical of natural fluids at near ambient temperature can be predicted using the equilibrium constants calculated in this study. Figure (2.7) shows the distribution of aqueous antimony species at stibnite saturation as calculated using the speciation model from Fit (30-G) for three sulfide contents: $\text{S}^{2-}_{\text{total}} = 0.01, 0.001, \text{ and } 0.0001 \text{ mol kg}^{-1}$. At the highest of these sulfide concentrations (Figure 2.7A), the distribution of antimony species is similar to the Fit (30-A), with antimony-sulfide dimers predominating at $\text{pH} > 5$. At the moderate sulfide concentration ($0.001 \text{ mol kg}^{-1}$, Figure 2.7B), $\text{H}_2\text{Sb}_2\text{S}_5^{2-}$ is no longer a dominant aqueous species at any pH. Instead with decreasing pH, $\text{Sb}_2\text{S}_4^{2-}$ transitions directly to HSb_2S_4^- as pH decreases to $\text{pH} \sim 8$.

The neutral antimonous acid, $\text{Sb}(\text{OH})_3$, becomes increasingly important in acidic and alkaline fluids as the sulfide concentration decreases. Antimonous acid is $< 1\%$ of the total dissolved antimony at $\text{pH} = 12$ when high concentrations of sulfide are present ($\text{S}^{2-}_{\text{total}} = 0.01 \text{ mol kg}^{-1}$, Figure (2.7A)). With an order of magnitude lower sulfide concentration ($\text{S}^{2-}_{\text{total}} = 0.001 \text{ mol kg}^{-1}$), $\text{Sb}(\text{OH})_3$ and H_2SbO_3^- contribute at least 30 % of the dissolved antimony at $\text{pH} > 11$ and the percentage of $\text{Sb}(\text{OH})_3$ approaches 1 % at $\text{pH} < 6$ (Figure 2.7B). With a further decrease of sulfide concentration to $\text{S}^{2-}_{\text{total}} = 0.0001 \text{ kg}^{-1}$, $\text{Sb}(\text{OH})_3$ is the predominant species from $\text{pH} 7.5$ to 11.8 (Figure 2.7C). At this low sulfide concentration, antimony-sulfide dimers contribute $< 10\%$ of the total dissolved antimony when $\text{pH} <$

Figure (2.7) The distribution of Sb(III) species at 30°C from pH = 3 to 12. The relative abundances of antimony species at stibnite saturation are plotted for total sulfide concentrations of 0.01 mol kg⁻¹ (A), 0.001 mol kg⁻¹ (B), and 0.0001 mol kg⁻¹ (C) using the speciation model and equilibrium constants from Fit (30-G). The plots demonstrate the diminishing importance of antimony-sulfide species with decreasing sulfide concentration. Solution chemistry is identical to that used for Figure (2.8).

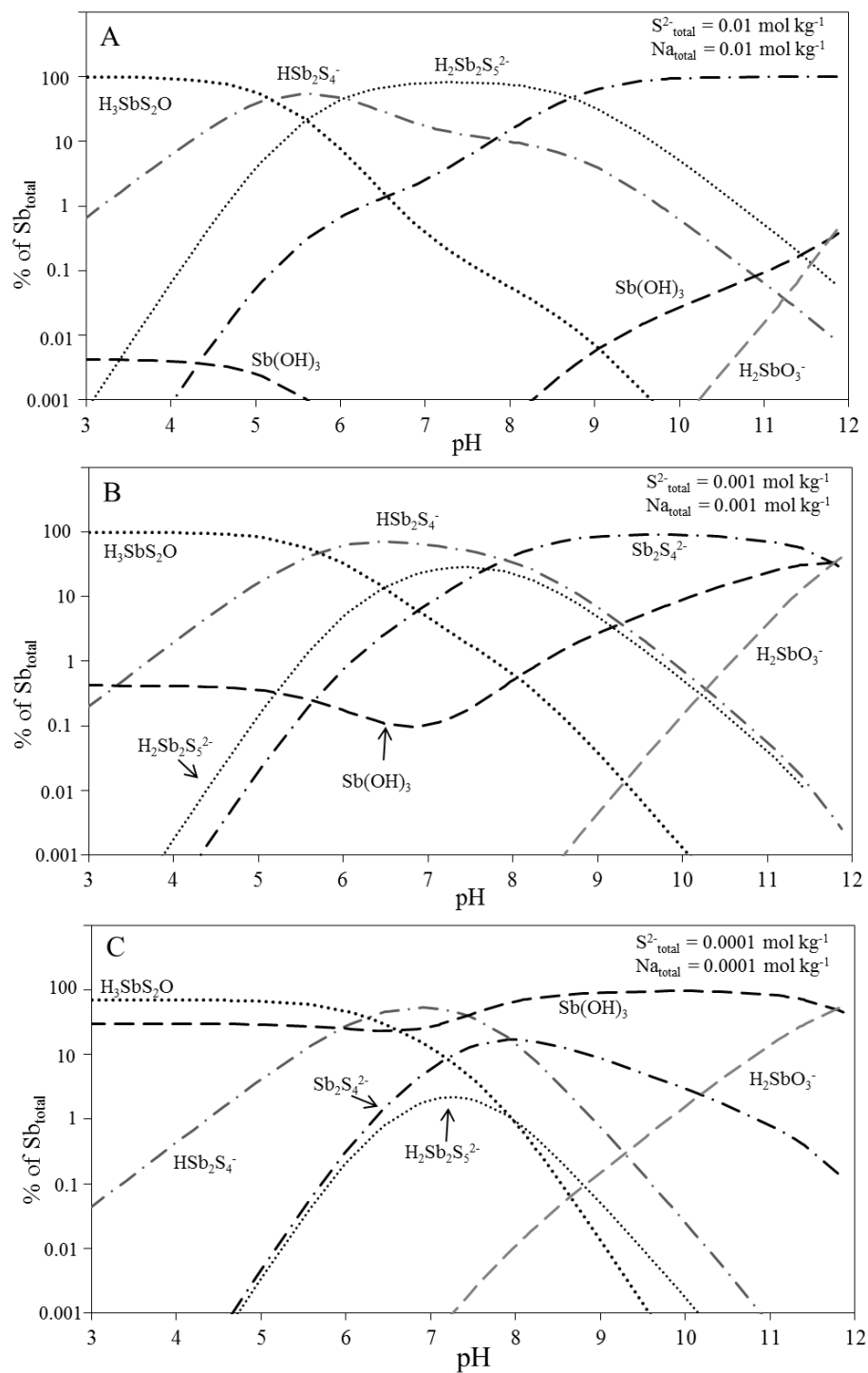
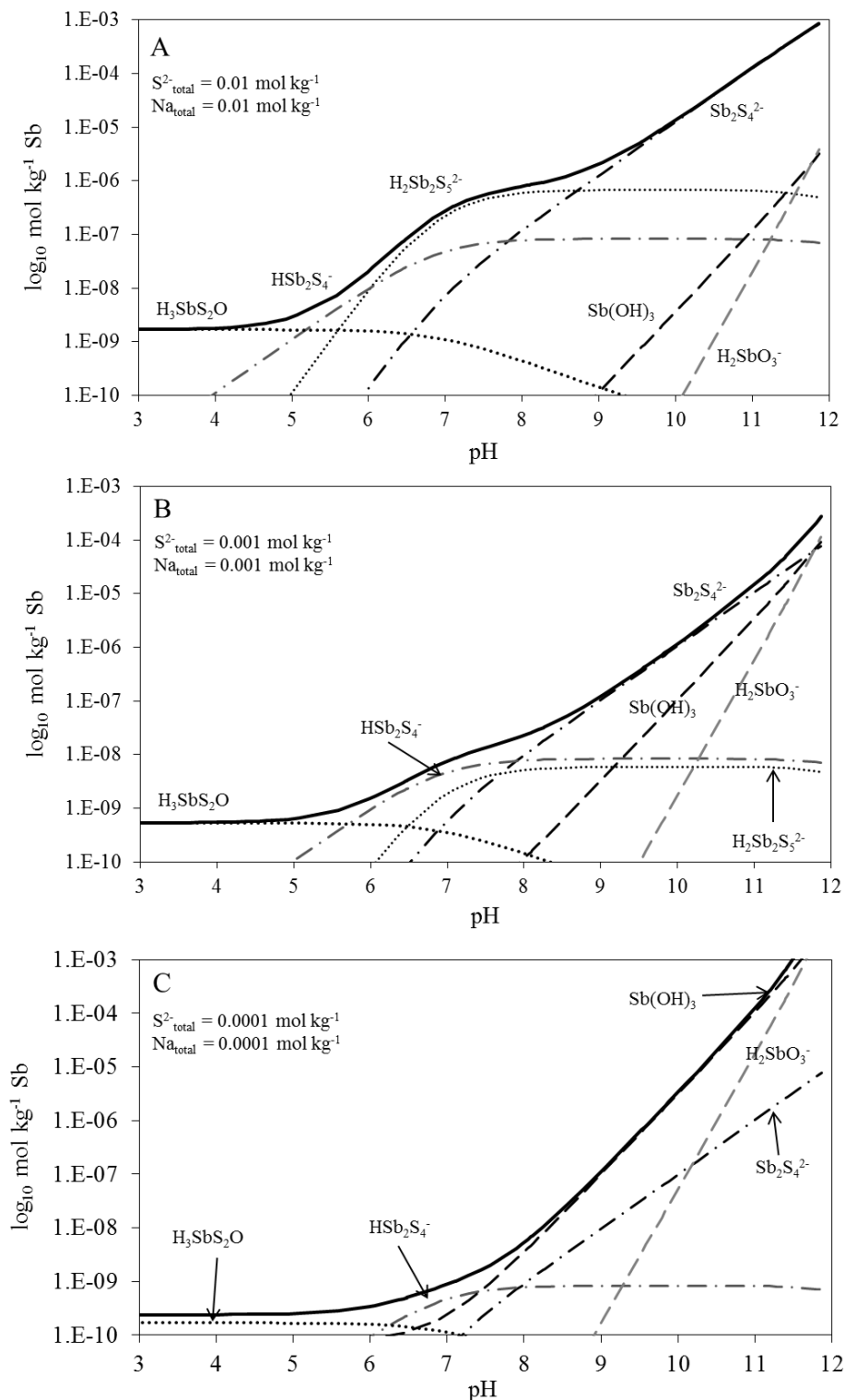


Figure (2.8) Calculated stibnite solubility at 30°C from pH = 3 to 12 at different total sulfide concentrations. Plots were constructed using the speciation model and equilibrium constants from Fit (30-G), and they demonstrate the change in the shape of the solubility curve as Sb(OH)_3 becomes predominant. Solution chemistry is identical to that used for Figure (2.7).



5.5 or $\text{pH} > 9$. The partially protonated dimer HSb_2S_4^- is the only antimony-sulfide species that still controls stibnite solubility, but it only does so over a small pH range from approximately $\text{pH} = 6.4$ to 7.5.

The shape of the stibnite solubility curve with respect to pH also changes as the dominant complexing ligand changes from sulfide (HS^-) to hydroxide (OH^-). This is demonstrated in Figure (2.8), which shows stibnite solubility from $\text{pH} = 3$ to 11 for the same three sulfide concentrations as those used in Figure (2.7). At and above $\text{S}^{2-}_{\text{total}} = 0.001 \text{ mol kg}^{-1}$, antimony-sulfide dimers control stibnite solubility in reducing fluids with pH from circumneutral to alkaline (Figures 2.7A and 2.7B). The partially protonated dimers result in a plateau in the stibnite solubility curve just above neutral pH. The prominence of this feature diminishes as the sulfide concentration decreases and $\text{Sb}(\text{OH})_3$ becomes more predominant. At the lowest sulfide concentration ($\text{S}^{2-}_{\text{total}} = 0.0001 \text{ mol kg}^{-1}$), the contribution of $\text{HSb}_2\text{S}_4^{2-}$ is barely noticeable in the overall solubility curve (Figure 2.8C). When $\text{Sb}(\text{OH})_3$ controls stibnite solubility, it is constant at $\text{pH} < 7$ but then increases rapidly with increasing pH at $\text{pH} > 7$ such that at $\text{pH} \geq 10.2$ stibnite solubility is greater in a solution containing $0.0001 \text{ mol kg}^{-1} \text{S}^{2-}_{\text{total}}$ than in one containing $0.01 \text{ mol kg}^{-1} \text{S}^{2-}_{\text{total}}$.

2.5. Conclusions

The conclusions from this study are:

- 1) Antimony speciation in alkaline solutions with sulfide concentrations of 0.01 to $0.1 \text{ mol kg}^{-1} \text{S}^{2-}_{\text{total}}$ is dominated entirely by $\text{Sb}_2\text{S}_4^{2-}$. This conclusion is supported both by stibnite solubility experiments and EXAFS measurements of antimony's first coordination shell.
- 2) Antimony speciation at stibnite saturation at 30°C in solutions with moderate sulfide concentrations is best represented by a speciation model including $\text{Sb}_2\text{S}_4^{2-}$, $\text{H}_2\text{Sb}_2\text{S}_5^{2-}$, HSb_2S_4^- , and $\text{H}_3\text{SbS}_2\text{O}$ (Fit 30-A).
- 3) At low sulfide concentrations ($\text{S}^{2-}_{\text{total}} \leq 0.001 \text{ mol kg}^{-1}$), the presence of Sb(III)-hydroxide complexes was confirmed both by solubility and EXAFS experiments at strongly alkaline pH. The equilibrium constant representing the contribution of $\text{Sb}(\text{OH})_3$ to stibnite solubility that was estimated in the current study is consistent with literature (Fit 30-G).

As the stable antimony sulfide over a wide range fluid conditions and temperatures, stibnite

Table (2.8) Summary of proposed heterogeneous stibnite solubility reactions and the logarithms of their equilibrium constants at 30°C .

Reaction	$\log_{10}K$	\pm	σ
$\text{K}_{2400} \quad \text{Sb}_2\text{S}_{3(s)} + \text{HS}^- = \text{Sb}_2\text{S}_4^{2-}$	-13.33	\pm	0.03
$\text{K}_{2502} \quad \text{Sb}_2\text{S}_{3(s)} + 2\text{HS}^- = \text{H}_2\text{Sb}_2\text{S}_5^{2-}$	-2.56	\pm	0.04
$\text{K}_{2401} \quad \text{Sb}_2\text{S}_{3(s)} + \text{HS}^- = \text{HSb}_2\text{S}_4^-$	-5.4	\pm	0.2
$\text{K}_{1213} \quad 0.5\text{Sb}_2\text{S}_{3(s)} + 0.5\text{HS}^- + \text{H}_2\text{O} = \text{H}_3\text{SbS}_2\text{O}$	-4.32	\pm	0.02
$\text{K}_{1033} \quad 0.5\text{Sb}_2\text{S}_{3(s)} + 3\text{H}_2\text{O} = \text{Sb}(\text{OH})_3 + 1.5\text{HS}^- + 1.5\text{H}^+$	-26.5	\pm	0.1

solubility is a basis for understanding antimony behavior in natural fluids. This study found that a scheme of four species (i.e., Fit 30-A) was required to fit the stibnite solubility measured for reducing solutions from pH 4 to 12 containing $\geq 0.01 \text{ mol kg}^{-1} \text{ S}^{2-}_{\text{total}}$ at 30°C: $\text{Sb}_2\text{S}_4^{2-}$ at pH > 9, HSb_2S_4^- and $\text{H}_2\text{Sb}_2\text{S}_5^{2-}$ at pH = 9 to 5, and $\text{H}_3\text{SbS}_2\text{O}$ at pH < 5. In alkaline fluids when the sulfide concentration was low ($\leq 0.001 \text{ mol kg}^{-1} \text{ S}^{2-}_{\text{total}}$), antimonous acid species were necessary to fit the measured stibnite solubility (Fit 30-G). The change in the dominant complexing ligand from sulfide to hydroxide makes the shape of the stibnite solubility curve change drastically (Figure 2.8). Table (2.8) summarizes the relevant heterogeneous equilibria describing stibnite dissolution in aqueous sulfide solutions at 30°C together with the derived equilibrium constants.

Further solubility experiments at low sulfide contents ($\leq 0.001 \text{ mol kg}^{-1} \text{ S}^{2-}_{\text{total}}$) or ultraviolet spectroscopic measurements will be needed to define the species present during the transition of antimony complexation with sulfide ligands to complexation with hydroxide ligands. Rigorous determination of the equilibrium constant for stibnite solubility in terms of $\text{Sb}(\text{OH})_3$, including the possibility of $\text{H}_2\text{SbS}_2\text{O}^-$ or $\text{H}_2\text{SbSO}_2^-$ or other possible intermediates, could be accomplished with solubility experiments at a strongly alkaline pH and sulfide concentrations from approximately 10^{-5} to $10^{-2} \text{ mol kg}^{-1} \text{ S}^{2-}_{\text{total}}$. These types of experiments were not performed in this study because the current endeavor was focused on the stability and stoichiometry of antimony-sulfide complexes

2.6. References

- Akeret, R., 1953. Ueber die Löslichkeit von Antimon(3)sulfid. Dissertation (PhD thesis) ETH, Zurich, p. 77.
- Akinifiyev, N.N., Zotov, A.V., Shikina, N.D., 1994. Experimental studies and self-consistent thermodynamic data in the Sb(III)-S(II)-O-H system. *Geochem. Internat.* **31**, 27-40.
- Arnston, R.H., Dickson, F.W., Tunnel, G., 1966. Stibnite (Sb_2S_3) solubility in sodium sulfide solutions. *Science* **153**, 1673-1674.
- Babko, A.K., Lisetskaya, G.S., 1956. Equilibrium in reactions of formation of thiosalts of tin, antimony, and arsenic in solution. *Russian Journal of Inorganic Chemistry* **1**, 969-980.
- Belevantsev, V.I., Gushchina, L.I., Obolenskii, A.A., 1998a. Antimony in hydrothermal solutions: analysis and generalization of data on antimony(III) chloride complexes. *Geochem. Internat.* **36**.
- Belevantsev, V.I., Gushchina, L.I., Obolenskii, A.A., 1998b. Solubility of stibnite, $\text{Sb}_2\text{S}_3(\text{cr})$: A revision of proposed interpretations and refinements. *Geochem. Internat.* **36**, 58-64.
- Oakdale Engineering, 2000. DataFitX for Windows Version 2.0: Programmer's Manual, Oakdale, Pennsylvania, USA
- EPA, 2009. National Primary Drinking Water Regulations. EPA 816-F-09-004
- Fiala, R., Konopik, N., 1950. Über das Dreistoffsystem $\text{Na}_2\text{S}-\text{Sb}_2\text{S}_3-\text{H}_2\text{O}$. II. Die auftretenden Bodenkörper und ihre Löslichkeit. *Monatshefte für Chemie* **81**, 505-519.
- Filella, M., Belzile, N., Chen, Y.-W., 2002. Antimony in the environment: a review focused on natural waters I. Occurrence. *Earth-Science Reviews* **57**, 125-176.
- Filella, M., May, P.M., 2003. Computer simulation of the low-molecular-weight inorganic species distribution of antimony(III) and antimony(V) in natural waters. *Geochim. Cosmochim. Acta* **67**, 4013-4031.
- Filella, M., May, P.M., 2005. Critical appraisal of available thermodynamic data for the complexation of antimony(III) and antimony(V) by low molecular mass organic ligands. *J Environ Monit* **7**, 1226-1237.

- Gushchina, L.V., Borovikov, A.A., Shebanin, A.P., 2000. Formation of antimony(III) complexes in alkali sulfide solutions at high temperatures: An experimental Raman spectroscopic study. *Geochem. Internat.* **38**, 510-513.
- Hannington, M.D., Harðardóttir, V., Garbe-Schönberg, D., Brown, K.L., 2016. Gold enrichment in active geothermal systems by acculating colloidal suspensions. *Nature Geoscience*.
- Helgeson, H.C., 1969. Thermodynamics of hydrothermal systems at elevated temperatures and pressures. *American Journal of Science* **267**, 729-804.
- Helgeson, H.C., Kirkham, D.H., 1974. Theoretical prediction of the thermodynamic behavior of aqueous electrolytes at high pressures and temperatures: II. Debye-Huckel parameters for activity coefficients and relative partial molal properties. *American Journal of Science* **274**, 1199-1261.
- Helz, G.R., Valerio, Melissa S., Capps, Nathan E., 2002. Antimony speciation in alkaline sulfide solutions: Role of zerovalent sulfur. *Environ. Sci. Technol.* **36**, 943-948.
- Ho, P.C., Palmer, D.A., 1996. Ion association of dilute aqueous sodium hydroxide solutions to 600°C and 300 MPa by conductance measurements. *Journal of Solution Chemistry* **25**, 711-729.
- Ho, P.C., Palmer, D.A., Mesmer, R.E., 1994. Electrical conductivity measurements of aqueous sodium chloride solutions to 600°C and 300 MPa. *Journal of Solution Chemistry* **23**, 997-1018.
- Keller, N.S., Stefansson, A., Sigfusson, B., 2014. Determination of arsenic speciation in sulfidic waters by Ion Chromatography Hydride-Generation Atomic Fluorescence Spectrometry (IC-HG-AFS). *Talanta* **128**, 466-472.
- Kielland, J., 1937. Individual activity coefficients of ions in aqueous solutions. *J. Am. Chem. Soc.* **59**, 1675-1678.
- Kolpakova, N.N., 1971. On the speciation of antimony (III) in sulfide solutions (in Russian), *Geochemistry of Hydrothermal Ore Deposition*, Nauka, Moscow, pp. 197-209.
- Kolpakova, N.N., 1982. Laboratory and field studies of ionic equilibria in the $\text{Sb}_2\text{S}_3\text{-H}_2\text{O-H}_2\text{S}$ system. *Geochem. Internat.* **19**, 46-54.
- Krupp, R.E., 1988. Solubility of stibnite in hydrogen sulfide solutions, speciation, and equilibrium constants, from 25 to 350°C. *Geochim. Cosmochim. Acta* **52**, 3005-3015.
- Krupp, R.E., Seward, T. M., 1987. The Rotokawa geothermal system, New Zealand: An active epithermal gold-depositing environment. *Econ. Geol.* **82**, 1109-1129.
- Landrum, J.T., Bennett, P.C., Engel, A.S., Alsina, M.A., Pastén, P.A., Milliken, K., 2009. Partitioning geochemistry of arsenic and antimony, El Tatio Geyser Field, Chile. *Appl. Geochem.* **24**, 664-676.
- Learned, R.E., 1966. The solubilities of quartz, quartz-cinnabar and cinnabar-stibnite in sodium sulfide solutions and their implications for ore genesis, Department of Geology. University of California, Riverside, Riverside, California.
- Marshall, W.L., Franck, E.U., 1981. Ion product of water substance, 0-1000°C, 1-10,000 bars. New international formulation and its background. *Journal of Physical Reference Data* **10**, 295-304.
- Mosselmans, J.F.W., Helz, G.R., Patrick, R.A.D., Charnock, J.M., Vaughan, D.J., 2000. A study of speciation of Sb in bisulfide solutions by X-ray absorption spectroscopy. *Appl. Geochem.* **15**, 879-889.
- Obolensky, A., Gushchina, L., Borisenko, A., Borovikov, A., Pavlova, G., 2007. Antimony in hydrothermal processes: solubility, conditions of transfer, and metal-bearing capacity of solutions. *Russian Geology and Geophysics* **48**, 992-1001.
- Okumura, A., Matsumiya, Y., Yamamoto, K., Ueno, R., Suzuki, M., Yamabe, S., 1995. Kinetics of oxygen exchange between arsenic acid and solvent water. *Bulletin of the Chemical Society of Japan* **68**, 1839-1849.
- Planer-Friedrich, B., Scheinost, A.C., 2011. Formation and structural characterization of thioantimony species and their natural occurrence in geothermal waters. *Environ. Sci. Technol.* **45**, 6855-6863.
- Planer-Friedrich, B., Suess, E., Scheinost, A.C., Wallschläger, D., 2010. Arsenic speciation in sulfidic waters: Reconciling contradictory spectroscopic and chromatographic evidence. *Anal. Chem.* **82**, 10228-10235.
- Planer-Friedrich, B., Wilson, N., 2012. The stability of tetrathioantimonate in the presence of oxygen, light, high temperature and arsenic. *Chem. Geol.* **322-323**, 1-10.

- Pokrovski, G., Borisova, A., Roux, J., Hazemann, J., Petdang, A., Tella, M., Testemale, D., 2006. Antimony speciation in saline hydrothermal fluids: A combined X-ray absorption fine structure spectroscopy and solubility study. *Geochim. Cosmochim. Acta* **70**, 4196-4214.
- Popova, M.Y., Khodakovskiy, I.L., Ozerova, N.A., 1975. Measurement of the thermodynamic parameters of antimony hydroxo complexes and hydrofluoride complexes up to 200°C (in Russian). *Geokhimiya* **6**, 835-843.
- Sherman, D.M., Ragnarsdottir, K.V., Oelkers, E.H., 2000. Antimony transport in hydrothermal solutions: an EXAFS study of antimony(V) complexation in alkaline sulfide and sulfide-chloride brines at temperatures from 25°C to 300°C at P_{sat} . *Chem. Geol.* **167**, 161-167.
- Shestitko, V.S., Demina, O.P., 1971. Potentiometric determination of the composition of the sulfide anions of antimony. *Russian Journal of Inorganic Chemistry* **16**, 1679-1680.
- Shikina, N.D., Zotov, A.V., 1999. Solubility of stibnite (Sb_2S_3) in water and hydrogen sulfide solutions at temperature of 200-300°C under-vapor saturated conditions and a pressure of 500 bars. *Geochem. Internat.* **37**, 82-86.
- Smith, C.L., Ficklin, W. H., Thompson, J. M., 1987. Concentrations of arsenic, antimony, and boron in steam and steam condensate at the Geysers, California. *J. Volcanol. Geotherm. Res.* **32**, 329-341.
- Spycher, N.F., Reed, M.H., 1989. As(III) and Sb(III) sulfide complexes: An evaluation of stoichiometry and stability from existing experimental data. *Geochim. Cosmochim. Acta* **53**, 2185-2194.
- Suleimenov, O.M., Seward, T.M., 1997. A spectrophotometric study of hydrogen sulphide ionisation in aqueous solutions to 350°C. *Geochim. Cosmochim. Acta* **61**, 5187-5198.
- Tella, M., Pokrovski, G.S., 2009. Antimony(III) complexing with O-bearing organic ligands in aqueous solution: An X-ray absorption fine structure spectroscopy and solubility study. *Geochim. Cosmochim. Acta* **73**, 268-290.
- Tossell, J.A., 1994. The speciation of antimony in sulfidic solutions: A theoretical study. *Geochim. Cosmochim. Acta* **58**, 5093-5104.
- Tossell, J.A., 2003a. Calculation of the energetics for the oxidation of Sb(III) sulfides by elemental S and polysulfides in aqueous solution. *Geochim. Cosmochim. Acta* **67**, 3347-3354.
- Tossell, J.A., 2003b. Calculation of the visible-UV absorption spectra of hydrogen sulfide, bisulfide, polysulfides, and As and Sb sulfides, in aqueous solution. *Geochem. Trans.* **4**, 28-33.
- Ullrich, M.K., Pope, J.G., Seward, T.M., Wilson, N., Planer-Friedrich, B., 2013. Sulfur redox chemistry governs diurnal antimony and arsenic cycles at Champagne Pool, Waiotapu, New Zealand. *J. Volcanol. Geotherm. Res.* **262**, 164-177.
- Wilson, N., Webster-Brown, J., 2009. The fate of antimony in a major lowland river system, the Waikato River, New Zealand. *Appl. Geochem.* **24**, 2283-2292.
- Wilson, N., Webster-Brown, J., Brown, K., 2007. Controls on stibnite precipitation at two New Zealand geothermal power stations. *Geothermics* **36**, 330-347.
- Wilson, N., Webster-Brown, J., Brown, K., 2012. The behaviour of antimony released from surface geothermal features in New Zealand. *J. Volcanol. Geotherm. Res.* **247-248**, 158-167.
- Wood, S.A., 1989. Raman spectroscopic determination of the speciation of ore metals in hydrothermal solutions: I. Speciation of antimony in alkaline sulfide solutions at 25°C. *Geochim. Cosmochim. Acta* **53**, 237-244.
- Zakaznova-Herzog, V.P., Seward, T., 2006. Antimonous acid protonation/deprotonation equilibria in hydrothermal solutions to 300°C. *Geochim. Cosmochim. Acta* **70**, 2298-2310.
- Zakaznova-Herzog, V.P., Seward, T.M., 2012. A spectrophotometric study of the formation and deprotonation of thioarsenite species in aqueous solution at 22°C. *Geochim. Cosmochim. Acta* **83**, 48-60.
- Zakaznova-Herzog, V.P., Seward, T.M., Suleimenov, O.M., 2006. Arsenous acid ionisation in aqueous solutions from 25 to 300°C. *Geochim. Cosmochim. Acta* **70**, 1928-1938.
- Zotov, A.V., Shikina, N.D., Akinfiyev, N.N., 2003. Thermodynamic properties of the Sb(III) hydroxide complex $\text{Sb}(\text{OH})_{3(\text{aq})}$ at hydrothermal conditions. *Geochim. Cosmochim. Acta* **67**, 1821-1836.

Chapter (3):

X-ray absorption spectroscopy measurements of antimony-sulfide and -hydroxide complexes at stibnite saturation

3.1. Introduction

X-ray absorption spectroscopy (XAS) and stibnite (Sb_2S_3) solubility measurements are two independent methods of investigating antimony-sulfide complexes in aqueous solutions that have produced apparently conflicting interpretations of antimony-sulfide speciation at alkaline pH. Specifically, XAS experiments have been interpreted in terms of antimony-sulfide monomers (Mosselmans et al., 2000; Planer-Friedrich and Scheinost, 2011), whereas solubility experiments indicate that dimers such as $\text{Sb}_2\text{S}_4^{2-}$ and HSb_2S_4^- control stibnite solubility (Arnston et al., 1966; Kolpakova, 1971, 1982; Krupp, 1988). In Chapter (2), stibnite solubilities at alkaline pH at 30°C were interpreted in terms of antimony-sulfide dimers at $\text{S}^{2-}_{\text{total}} \geq 0.001 \text{ mol kg}^{-1}$ with antimony-hydroxide monomers (i.e., $\text{Sb}(\text{OH})_3$ and H_2SbO_3^-) predominating at $\text{S}^{2-}_{\text{total}} \leq 0.0001 \text{ mol kg}^{-1}$. The current chapter presents XAS measurements of antimony(III) in solutions of pH = 10.9 to 12 that are comparable to the solutions used in the solubility experiments, and it addresses the apparent discrepancy between the two techniques.

X-ray absorption spectroscopy is an *in situ* method for solids and liquid samples that directly probes the local coordination environment of a targeted element (i.e., antimony in this study) by exciting core level electrons with tunable X-ray radiation to produce an absorption edge that is sensitive to the bonding environment of the targeted element. The extended X-ray fine structure (EXAFS) portion of XAS spectra spans from ~ 80 to ~ 800 eV above this absorption edge and provides information about the identity of, distance to, and number of atoms within several ångströms (Å) of the excited atom. Thus, EXAFS can identify the atoms in the first, and possibly also second, coordination shells of aqueous complexes. The other portion of the XAS spectra, X-ray near edge structure (XANES), extends from ~ 20 eV below to ~ 60 eV above the absorption edge and is sensitive to the electronic structure of the excited atom, particularly its valence and bonding geometry. In contrast to XAS experiments, solubility studies indirectly determine the stoichiometry of the dominant aqueous complex (or complexes) by measuring changes in solubility as a result of changes in relevant physiochemical fluid variables, such as pH and ligand concentrations. Although XAS and

solubility experiments are, in theory, both acceptable methods for identifying the antimony complexes present in solution, they have thus far produced apparently inconsistent models for antimony speciation in similar alkaline sulfide solutions.

The current and previous antimony sulfide solubility studies find that antimony-sulfide dimers dominate Sb(III) speciation at alkaline pH, whereas previous XAS studies of very similar solutions have been interpreted in terms of antimony sulfide monomers. As presented Chapter (2), Sb(III) occurs as the fully deprotonated dimer $\text{Sb}_2\text{S}_4^{2-}$ at $\text{pH} > 9$ in ambient temperature solutions with sufficient sulfide concentrations. In solutions with low sulfide concentrations, antimonous acid species (i.e., $\text{Sb}(\text{OH})_3$ and H_2SbO_3^-) can account for the observed solubilities. In alkaline Na_2S solutions, XAS studies have failed to detect the antimony-antimony interactions in antimony complexes that would be expected if antimony dimers were present, and thus previous XAS results can be used to support the presence of antimony sulfide monomers (Mosselmans et al., 2000; Sherman et al., 2000; Planer-Friedrich and Scheinost, 2011). Planer-Friedrich and Scheinost (2011) detected 1 to 2 oxygen atoms in antimony's first coordination shell in solutions in which the molar concentration of sulfide approached the antimony concentration. This observation is consistent with either a mixed ligand antimony oxy-sulfide complex or a mixture of sulfide-antimony complexes and antimonous acid. A further complication is that some of the published Sb K-edge XAS data refer to Sb(V) and/or partially oxidised Sb(III)/(V)-containing solutions.

To gain insight into the Sb(III) speciation in aqueous sulfide solutions, XAS measurements were conducted on solutions obtained by equilibrating stibnite with strongly alkaline ($\text{pH} = 10.9$ to 12.0) sodium sulfide solutions containing varying concentrations of total reduced sulfide ($\text{H}_2\text{S}^\circ + \text{HS}^-$) at 30°C . The solutions studied by XAS included both solutions in which the sulfide concentration was much greater than the antimony concentrations and solutions in which Sb-O interactions were expected due to the low sulfide concentration. The solutions studied were produced concomitantly with the solubility experiments described in the previous chapter, and so are directly comparable to the thermodynamic model developed in Chapter (2). In this chapter, attempts are made to resolve the differences between Sb(III) speciation models predicted by XAS measurements (antimony-sulfide monomers) and derived from solubility experiments (antimony-sulfide dimers) and to define the limitations of XAS studies in detecting antimony species present in solutions.

3.1.2. Previous XAS studies of antimony in aqueous solutions

Three previous X-ray absorption spectroscopy studies of aqueous antimony-sulfide speciation in sodium sulfide solutions have been published (Mosselmans et al., 2000; Sherman et al., 2000; Planer-Friedrich and Scheinost, 2011). Ambient temperature measurements included solutions having $\text{pH} = 8$ to 13 that contained 0.001 to $1 \text{ mol kg}^{-1} \text{ S}^{2-}_{\text{total}}$. Sherman et al. (2000) and Mosselmans et al. (2000) also report a few data up to 300°C . The changes in the antimony coordination environment detected at these higher temperature measurements are not discussed further in this chapter but are

Table (3.1) Summary of previous EXAFS studies of antimony speciation in solution.

T(°C)	Sb (mol kg ⁻¹)	Solution components	S:Sb ratio	First shell distances (Å)			Ligands in first shell	Reference
Hydroxide and chloride complexes								
25 - 250	0.04-0.1	2-3 mol kg ⁻¹ HCl	na	-	2.38-2.42	-	3 Cl	<i>a</i>
30 - 400	0.01-0.3	DI water	na	1.96-1.97	-	-	3 O	<i>b</i>
		2.3 mol kg ⁻¹ NaCl, 0.1 mol kg ⁻¹ HCl		1.97	2.37-2.47	-	2.5 Cl + 0.5 O	
		3.5 mol kg ⁻¹ HCl		-	2.39-2.43	-	3 Cl	
20-60	0.003-0.02	Sb ₂ O ₃ in DI water	na	1.96-1.98	-	-	3-4 O	<i>c</i>
Sulfide complexes				Sb-O	Sb-S	Sb-Sb		
25 - 300	0.05-0.1	0.2-0.1 mol kg ⁻¹ NaHS, ± 1 mol kg ⁻¹ NaCl	4:1, 12:1	-	2.34	-	4 S	<i>d</i>
-193 - 200	0.001-0.1	0.1-2.5 mol kg ⁻¹ NaHS, ± 0.02 mol kg ⁻¹ CO ₃ ²⁻ , ± elemental sulfur	3:1 to 150:1	-	2.0-2.43	~4.15 ^h	3 - 4 S	<i>e</i>
-258	0.01	0.02 to 0.2 mol kg ⁻¹ NaHS reduced sample preparation oxidising sample preparation	2:1, 10:1, 20:1					<i>f</i>
				2.05	2.40-2.41	-	2 S + 1 O, 3 - 4 S	
				1.96	2.33-2.40	5.64 ⁱ	3 S + 2 O, 4 S	

a Oelkers et al. (1998)

b Pokrovski et al. (2006)

c Tella and Pokrovski (2009)

d Sherman et al. (2000), only fits from 25 and 35°C reported. Up to 0.6 oxygen atoms in first coordination shell beginning at 200°C

e Mosselmans et al. (2000), only fits from -193 and 25°C tabulated. Evidence for 1 oxygen at 200°C

f Planer-Friedrich and Scheinost (2011)

g Chloride not found in first shell in solution containing NaCl

h Evidence of Sb-Sb interaction but insufficient data to fit

i Sb-Sb observed in solution with 2 S:1 Sb molar concentration ratio

considered with this study's high temperature solubility experiments in Chapter (4). The ambient temperature EXAFS results from these and several other XAS studies of antimony in solution are summarised briefly in Table (3.1). To achieve the high antimony concentrations (> ~ 0.001 mol kg⁻¹ Sb) required for EXAFS, XAS measurements of Sb in aqueous solution are generally limited to alkaline pH's. The first shell Sb-O distances were typically between 1.95 and 2.0 Å, while the distances for less electronegative ligands, including Cl⁻ and HS⁻, varied between 2.33 and 2.42 Å.

In the sodium sulfide solutions, the antimony species detected by XAS are influenced by how the redox-sensitive solutions were prepared. Sherman et al. (2000) measured XAS Sb K-edge spectra on solutions containing 0.2 to 1 mol kg⁻¹ S_{total} that were buffered using NaCl or NaOH to strongly alkaline (pH 12 to 13) or extremely acidic (pH < 2) conditions. Although the solutions were prepared from Sb(III) and S(II) reagents, laboratory procedures to control oxygen (i.e., de-oxygenation of solutions or preparation in a glove box) were not used. The solutions became light yellow to green in colour, indicating the probable formation of polysulfides due to oxidation. For this reason, and due to the fitted coordination numbers (~ 4) and generally shorter Sb-S distances (2.33 - 2.34 Å), the authors interpreted the spectra in terms of a four-coordinated Sb(V) species (thioantimonates, e.g., SbS₄³⁻).

Thus, the results from Sherman (2000) are not directly comparable to the Sb(III)-S(II) system considered in the current study.

Mosselmans et al. (2000) and Planer-Friedrich and Scheinost (2011) applied more stringent methods than Sherman et al. (2000) to avoid oxidation (by atmospheric oxygen) when preparing their antimony sulfide solutions and found first coordination shells consistent with tetrahedral Sb(III)S₃ in many of their solutions. Mosselmans et al. (2000) prepared alkaline (pH 8 to 14) sodium sulfide (NaHS) solutions by reacting N₂-purged NaOH-NaHS solutions with stibnite and, in some cases, with Na₂(CO₃)²⁻ and/or elemental sulfur. The EXAFS results from solutions containing Na₂(CO₃)²⁻ or elemental sulfur suggested a 4-coordinated Sb(V)-sulfide species, similar to results from Sherman et al. (2000). Other solutions contained 3-coordinated Sb(III) sulfide species or possibly a mixture of Sb(V)- and Sb(III)-sulfide complexes. In addition, the formation of polysulfide species by the reaction of elemental sulfur with HS⁻ cannot be excluded, and these polysulfide species would also form stable moieties with Sb(III) and/or Sb(V).

Planer-Friedrich and Scheinost (2011) studied the effects on antimony sulfide speciation of oxygenated vs. deoxygenated sample preparation and of the aqueous sulfide concentration relative to that of antimony using both XAS and separation of antimony species by liquid chromatography (IC) prior to elemental analysis by inductively coupled plasma-mass spectrometry (ICP-MS). Their samples consisted of complementary suites of 0.01 mol kg⁻¹ Sb(III) solutions that were prepared under reducing (i.e., prepared and sealed in a glovebox) and oxidising conditions (i.e., sealed with exposure to atmospheric oxygen) and in which the molar sulfide concentration was two to twenty times greater than that of antimony.

In the solutions from the reduced sample suite analysed by Planer-Friedrich and Scheinost (2011), antimony was surrounded by ~3.5 neighbouring atoms within 3 Å. The identity of the atoms changed with sulfide concentration. When the sulfide concentration was greater than ten times that of antimony (i.e., mol kg⁻¹ S²⁻_{total} ≥ 10 x mol kg⁻¹ Sb), the first coordination shell contained 3.4 to 3.7 sulfur atoms at ~2.4 Å. In contrast, when the sulfide concentration was only two times that of the antimony concentration (i.e., mol kg⁻¹ S²⁻_{total} = 2 x mol kg⁻¹ Sb), the first coordination shell contained ~2 sulfur atoms at ~2.4 Å and an oxygen atom at 2.05 Å. For the samples prepared under more oxidising conditions, the occurrence of sulfur and oxygen within the first shell was similar; however the total number of first shell scattering atoms was higher (~4) and the Sb-S distance was smaller (~2.34 Å). The authors interpreted these changes as evidence of oxidation of Sb(III) to Sb(V) during sample preparation under oxidising conditions. For both Mosselmans et al. (2000) and Planer-Friedrich and Scheinost (2011), the majority of the sodium sulfide solutions that were prepared with the exclusion of atmospheric oxygen (i.e., complete preparation in an glove box) and without elemental sulfur additions had first coordination shells containing < 4 sulfur atoms at 2.34 to 2.41 Å.

In addition to these XAS studies of antimony in hydrosulfide solutions, there have been a limited number of XAS studies of Sb speciation in aqueous solutions containing chloride (Oelkers et

al., 1998; Pokrovski et al., 2006) and various organic ligands (Tella and Pokrovski, 2009). These studies provide examples of the range of Sb-O distances possible under different conditions and the shape of the Sb XANES associated with different ligands and geometries. The EXAFS study of Oelkers et al. (1998) demonstrated that antimony forms 3-coordinated chloride complexes from 25 to 260°C in strongly saline acidic fluids ($\text{HCl} \geq 2.3 \text{ mol kg}^{-1}$). Pokrovski et al. (2006) considered antimony complexation up to 400°C in pure water, moderately acidic NaCl-HCl solutions, and strongly acidic HCl solutions. A 3-coordinated Sb-O species, consistent with antimonous acid, $\text{Sb}(\text{OH})_3$, was dominant in pure water and was a major species in NaCl-HCl solutions. The Sb-O distance was $1.97 \pm 0.01 \text{ \AA}$, regardless of temperature or chloride concentration.

Complexing of antimony with chloride ligands occurred in both the HCl and NaCl-HCl solutions, and the results were interpreted in terms of SbCl_2^+ , SbCl_3 , $\text{SbCl}(\text{OH})_2$, and $\text{SbCl}(\text{OH})_3^-$ based on average coordination numbers from EXAFS, linear combination fitting (LCF) of the XANES, and solubility measurements. In addition to analysis of the EXAFS, Tella and Pokrovski (2009) used solid reference materials to interpret the Sb XANES of solutions containing Sb(III) and various organic ligands. They found that antimony occurred as antimonous acid species or as bidentate Sb-organic ligand complexes, depending on the type and location of functional groups in the organic ligands present.

3.1.3. X-ray near edge fine structure (XANES) at the Sb K-edge

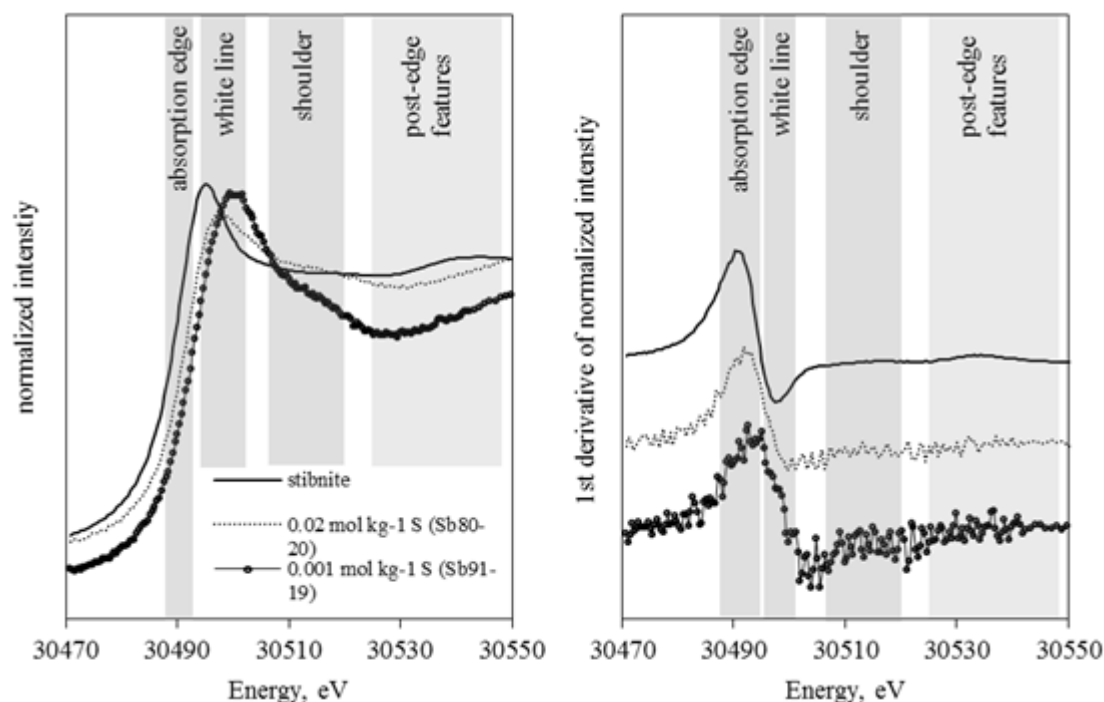
In the XAS Sb K-edge solutions discussed above, interpretation of the Sb speciation has largely been limited to the EXAFS portion of the XAS spectrum. The XANES portion of Sb K-edge X-ray absorption spectra is rarely considered in XAS studies of antimony in solution and has never been used to quantitatively study the complexation of antimony in aqueous hydrosulfide solutions. Sherman et al. (2000) did not report the Sb K-edge positions of the Sb sulfide complexes in their solutions. Mosselmans et al. (2000) and Planer-Friedrich and Scheinost (2011) did report edge energy positions for their samples but found that the edge positions of solutions interpreted in terms of Sb(III) and Sb(V) sulfide complexes overlapped and were in general between those of Sb(III) in stibnite and Sb(V) in oxides. Fortunately, there are a number of recent quantitative XANES investigations of Sb valence and bonding environment (Sb-O versus Sb-S bonds) in minerals, synthetic phases, and of Sb adsorbed onto various iron oxide phases (Scheinost et al., 2006; Kirsch et al., 2008; Fawcett et al., 2009; Varrica et al., 2013). As described in the following, these data can provide useful insights into how the features of the Sb K-edge XANES change with changes in antimony valence state and coordination environments.

An increase in atomic valence results in a slight increase in the energy position of the absorption edge. For the Sb K-edge, the edge position is 3 to 5 eV higher in Sb(V)-oxides than in Sb(III)-S and Sb(III)-O solids (e.g. Scheinost et al., 2006; Kirsch et al., 2008; Fawcett et al., 2009; Guo et al., 2014; Hockmann et al., 2014). The absorption edge position is usually defined for XANES

spectra as the maximum of the first derivative of the energy spectra, and is located at 30491 eV for Sb(0), ~ 30,492 to 30,493 eV for Sb(III), and ~ 30,495 to 30,498 eV for Sb(V). The edge position and several other features of the XANES spectra are shown for stibnite and two solutions in Figure (3.1). Increases in the edge position have been used to infer valence in adsorbed complexes in Sb-contaminated soils (Takaoka et al., 2005; Mitsunobu et al., 2006; Mitsunobu et al., 2011; Hockmann et al., 2014). Features in the XANES spectra after the edge, including the height of the white line and the presence of a post-edge shoulder, are sensitive to the coordination geometry (e.g. Ebitani et al., 1992; Tella and Pokrovski, 2009; Beauchemin et al., 2012). Together with EXAFS analysis, these features have been used to confirm antimony's coordination environment and/or valence by comparison to reference spectra (Ebitani et al., 1992; Ackermann et al., 2009; Beauchemin et al., 2012; Varrica et al., 2013; Mills et al., 2014) or to calculated theoretical spectra (Yiwata et al., 2001; Lu et al., 2002).

Interpretation of the Sb K-edge XANES is more challenging than lower energy edges because of significant spectral broadening that is caused by the short corehole lifetime of the Sb 1s electrons and poor monochromator resolution at the energy of the Sb K-edge (Krause and Oliver, 1979). The broad Sb K-edge spectra may cause the absorption edges of Sb(III) and Sb(V) to be indistinguishable, especially for samples with low antimony concentrations. The absorption edge in antimony minerals with two antimony valence states is often a single wide spectral feature rather than two distinct edges, as is the case for the As K-edge in mixed-valence arsenic samples (Fawcett et al., 2009). Several

Figure (3.1) Antimony K-edge XANES and first derivative spectra for representative mineral and solution samples from the current study. Major spectral features described in text are indicated by shaded regions. Spectra have been shifted along the vertical axis for clarity. Note the high noise in the solution XANES relative to that for stibnite.



recent studies employing Sb XAS to investigate the chemistry of antimony in environmental sediment samples containing ~ 0.01 to 3 mol kg^{-1} Sb found that the XANES was inconclusive and instead used the coordination number of the first shell, typically three for Sb(III) and six for Sb(V) in solids, to determine antimony valence (Ilgen et al., 2012; Ritchie et al., 2013; Ilgen et al., 2014). Antimony XAS studies from the material science literature frequently use Sb XANES measured at the lower energy Sb LIII or LI edges, where spectral broadening is dramatically lower (e.g. Flavell et al., 1997; Matsuzawa et al., 2003; Geraldo et al., 2007). In the current study, EXAFS, XANES, and the results of the solubility experiments were considered together.

3.2. Methods

Samples for XAS measures were collected in conjunction with the 30°C stibnite solubility experiments (Chapter 2). The solution properties are summarised in Table (3.2). Samples were collected in air-tight syringes directly from a flow-through apparatus containing stibnite, and the pH, total sulfide concentration and total antimony concentration were measured, as described in the previous chapter. For XAS analysis, samples were sealed in quartz glass ampoules that had been purged with high purity nitrogen (99.999% N_2) from which any residual oxygen had been removed by reaction with copper at 450°C . The ampoules had wall thickness of 1 mm and an internal path length of 7 mm. The top closure on the ampoules had been narrowed and elongated but still allowed injection of the solution into the nitrogen purged space via a catheter directly from the gas tight syringe. The constricted portion of the ampoule permitted rapid and effective sealing of the glass ampoule with an oxy-acetylene torch.

Antimony K-edge XAS spectra were measured at ambient temperature at the XAS Beamline at the Australian Synchrotron. The beam energy was selected using a Si(311) monochromator that was calibrated relative to the Sb K-edge of Sb foil (30,491 eV). Reference solid samples were measured in transmission mode. Solution samples were measured in fluorescence mode in a 90° geometry using a 36 element germanium detector. The distance between the detector and the sample was varied for each solution so that the fluorescence signal received by the detector was within its linear range. Thus, no deadtime correction was necessary. The sample holder and beam flight path were purged with helium. The energy resolution of the beam at the Sb K-edge is approximately 1 eV.

Table (3.2) Chemistry of XAS solutions in order of highest to lowest pH

Sample	pH	$\text{mol kg}^{-1} \text{S}^{2-}_{\text{total}}$	$\text{mol kg}^{-1} \text{Sb}$	molar S:Sb
Sb91-19	12.0	0.001	0.0009	1.5:1
Sb80-20	11.7	0.019	0.0013	15:1
Sb75-20	11.4	0.009	0.0003	26:1
Sb51-24	10.9	0.097	0.0054	18:1

Multiple scans were taken for all samples to improve signal-to-noise ratio and then merged for each sample after aligning individual scans to the reference foil. The number of scans required to produce a reasonable signal varied from a minimum of two to a maximum of eighteen for solutions containing 10^{-3} and 10^{-4} mol kg⁻¹ Sb, respectively. Re-alignment of the beam was repeated at a maximum of every five scans. Initial raw data conversion was performed using the programs Average and Sakura for transmission and fluorescence scans, respectively (Kappen and Ruben, 2013; Australian Synchrotron, 2016). Data processing and analysis were conducted with Athena and Artemis within the Demeter 0.9.17 suite of programs (Ravel and Newville, 2005). Background subtraction using the AUTOBAK procedure and normalization of measured spectra to the absorption edge-step were conducted in Athena. Fitting of normalized spectra was completed in Artemis.

Fitting of EXAFS spectra involves determining the number and Sb-scatterer distances of possible coordinating atoms around the excited atom (here Sb) that best reproduce the measured EXAFS spectra. Interpretation of spectra from unknown samples is enabled by theoretical calculation of the backscattering amplitude and phase-shift functions of different scattering atoms (e.g., sulfur versus oxygen) using known crystal structures. The fit parameters are the coordination number (*CN*), the distance from the central antimony atom to backscattering atoms (*R*), the energy shift between the measured absorption edge and that used in calculations of theoretical backscattering amplitude and phase-shift functions (ΔE_0), and lastly a Debye-Waller-like factor (σ^2) that accounts for thermal and structural disorder in the Sb-backscatter distance. An additional factor, the amplitude reduction factor (S_0^2), corrects for excited electrons that do not produce EXAFS. The theoretical backscattering amplitude and phase-shift functions for Sb-S paths were calculated with FEFF6 from the tetrahedrite crystal structure (endmember Cu₁₂Sb₄S₁₃), one of the few antimony sulfide minerals containing isolated SbS₃ tetrahedra (Peterson and Miller, 1968). The backscattering amplitude and phase-shift functions for Sb-O paths were calculated from the senarmonite (Sb₂O₃, cubic) structure (Whitten et al., 2004). The structure of stibnite used in fitting solid reference samples and second shell Sb-Sb interactions in solutions were from Lundegaard et al. (2003). Fits were performed in *R*-space on the background subtracted, normalized and Fourier transformed spectra and are shown in Figure (3.2). Fits were performed at wavenumber (*k*) weightings of 1, 2, and 3 simultaneously. Further constraints used in fitting procedures are noted in Table (3.3).

The value for the scattering amplitude factor (S_0^2) to be used in the fitting of the EXAFS of the unknown solutions was determined by fitting the EXAFS spectrum from the stibnite reference sample. The scattering amplitude factor is an estimate of the proportion of electrons participating in scattering and is usually set to a value between 0.7 and 1. The stibnite EXAFS spectrum is difficult to fit because the stibnite crystallographic structure contains four unique Sb-S bond distances between 2.4 and 2.9 Å that cannot be individually distinguished in the EXAFS spectra but appear as one Sb-S distance at ~ 2.51 Å (Lundegaard et al., 2003). Attempts were made to fit the stibnite spectra with only the shortest two Sb-S distances (2.48 and 2.52 Å) with their coordination numbers set by their abundances in the

stibnite structure but this produced values for the scattering amplitude factor greater than 1 (i.e., $S_0^2 > 1$). Adding a contribution from the next shortest Sb-S path at 2.66 Å resulted in improved fits and generated S_0^2 values between 0.80 and 0.99. A value of 0.95 was used in subsequent fitting of solution EXAFS because this value is typical of values used in EXAFS studies at the Sb K-edge (Oelkers et al., 1998; Sherman et al., 2000; Millet et al., 2003; Tella and Pokrovski, 2009; Planer-Friedrich and Scheinost, 2011; Ilgen et al., 2012; Sinsermsuksakul et al., 2012; Ritchie et al., 2013; Ilgen et al., 2014).

3.3. Results

The compositions of the solutions studied are given in Table (3.2). The absorption edge energies, details of the EXAFS spectra used in fitting procedures, and the results from the fitting of the EXAFS portion of the XAS spectra are given in Table (3.3). The best fits were selected based upon the minimization of both the R factor, which indicates the misfit of the fitted model relative to the data, and the reduced χ^2 , which is the estimated uncertainty including the number of fit variables

Table (3.3) EXAFS results. Fits of EXAFS were completed in R -space at k -weights of 1, 2, and 3 simultaneously. The amplitude reduction factor (S_0^2) was set to 0.95 (see text for explanation). Error of individual fits is listed at the 95% confidence level for the fit variables to show variation in quality of fits. These fit errors do not include the uncertainty involved in the fit settings or constraints. Estimated total uncertainty for CN is $\sim 25\%$ and for R it is ~ 0.01 Å. Additional fit constraints are noted for individual fits.

Fit Settings				Fit Results										
Sample	Edge	<i>R</i> -range (Å)	<i>k</i> -range	Atom	CN	±	<i>R</i> (Å)	±	Δ <i>E</i> ₀	±	σ ²	±	Red. χ ² ^{<i>a</i>}	<i>R</i> factor ^{<i>b</i>}
Sb91-19	30493.9	1.3 to 4.5	2.5 to 13	S	1.6	0.2	2.34	0.01	8.5	set ^{<i>c</i>}	0.0030	set ^{<i>c</i>}	6.9	0.051
				O	3.0	0.2	1.97	0.01	3.2	1.9	0.0010 ^{<i>d</i>}			
				Sb	1.2	0.7	3.78	0.03	5.8	set ^{<i>c</i>}	0.0034	0.0015		
Sb80-20	30492.0	1.4 to 3	3 to 13	S	3.3	0.2	2.38	0.00	8.8	0.6	0.0037	0.0006	3.6	0.010
Sb75-20	30491.4	1.35 to 2.75	3 to 10	S	3.5	0.8	2.36	0.02	7.3	2.5	0.0046	0.0030	24.7	0.027
Sb51-24	30490.7	1.33 to 3	3 to 14.5	S	3.4	0.2	2.35	0.00	8.2	0.7	0.0022	0.0005	43.1	0.011
Stibnite	30490.7	1.4 to 4.5	3 to 13	S ^{<i>e</i>}	2.3	0.1	2.51	0.005	5.8	0.6	0.0067	0.0008	361.3	0.013
				Sb ^{<i>f</i>}	2.1	0.8	3.86	0.02	"-"	"-"	0.0142	0.0049		
Sb ₂ O ₅	30491.7	1 to 3	3 to 8.5	O	2.7	0.2	1.98	0.01	9.4	0.9	0.0049	0.0018	38.5	0.011

^a Reduced Chi-squared $\chi^2 = \frac{N_{indp\ pts}}{N_{data\ pts}} \sum_i \left(\frac{data_i - fit_i}{\epsilon_i} \right)^2 / (N_{indp\ pts} - N_{fit\ variables})$

^b R factor (mean square misfit) = $\frac{\sum_i (data_i - fit_i)^2}{\sum_i data_i^2}$

^c Insufficient independent points to fit all variables freely. ΔE_0 and in some cases σ^2 for selected fit set to average of values from best EXAFS fits (i.e. Sb80-20 and Sb51-24) or stibnite where appropriate. See text for details

^d value for σ^2 constrained to ≥ 0.001

^e average first shell in stibnite from crystallographic data: 2 S atoms at 2.52 Å

^f average second shell in stibnite from crystallographic data: 2 Sb atoms at 3.82 Å

relative to the number of independent points. As defined above, ΔE_0 is the difference between the measured and theoretical edge energies and σ^2 quantifies the amount of disorder present in the Sb-

backscatter distance. The fit parameters related to the structure of the aqueous complexes are the identity of backscattering atoms, the coordination number (CN), and the Sb-backscatterer distance (R). The fits are compared to the measured spectra in k -space and in R -space in Figure (3.2).

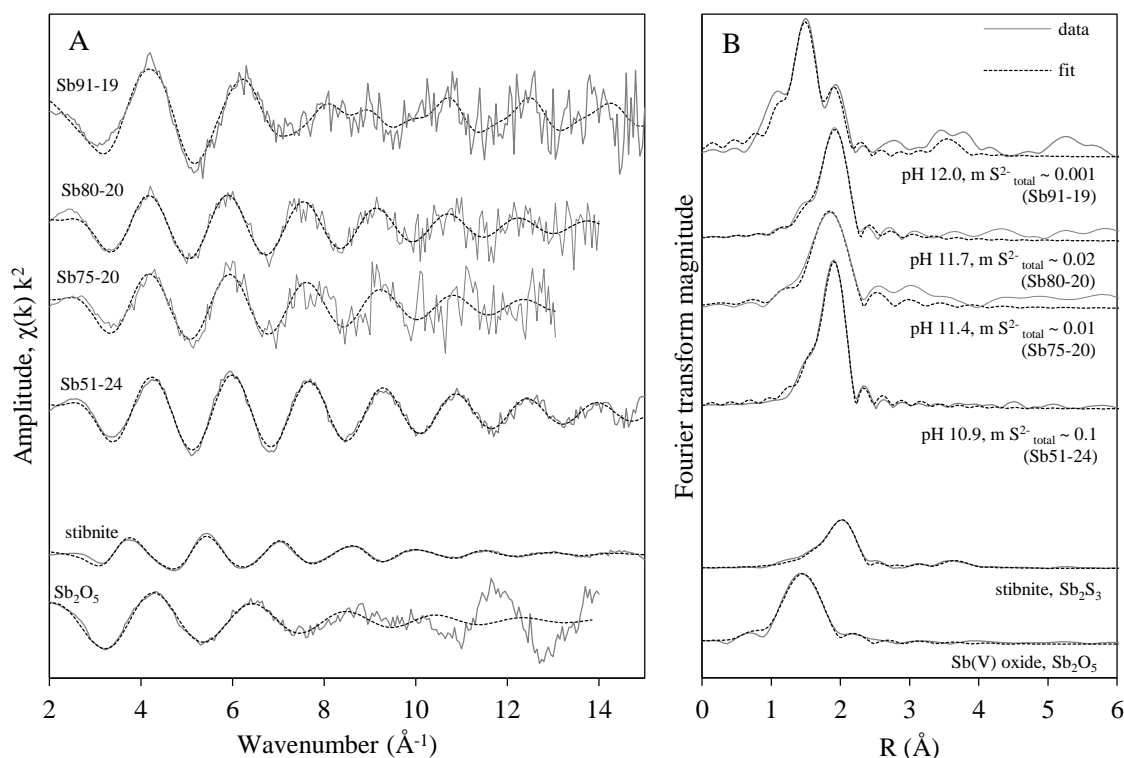
3.3.2. X-ray absorption spectra of solutions containing sufficient sulfide to complex antimony

The first coordination shell of antimony contained only sulfur atoms in solutions where the amount of sulfur present was sufficient to fully complex antimony (i.e., when $\text{mol kg}^{-1} \text{S}^{2-}_{\text{total}} \geq 3 \times \text{mol kg}^{-1} \text{Sb}$). The three solutions between $\text{pH} = 10.9$ and 11.7 (Sb51-24, Sb75-20, and Sb80-20) contained enough dissolved sulfide for $\text{Sb}_2\text{S}_4^{2-}$ to be the thermodynamically stable aqueous complex. These samples had first coordination shells with 3.3 to 3.5 sulfur atoms at distances of 2.35 to 2.38 Å. The spectra of the concentrated hydrosulfide solutions did not show evidence for longer-range Sb-Sb interactions, and therefore only the shorter Sb-O and Sb-S paths were fitted.

3.3.3. X-ray absorption spectra of solutions containing insufficient sulfide to complex antimony

The EXAFS spectra from the deionised water solubility experiment (Sb91-19), in which the concentration of sulfide was insufficient to fully complex antimony, showed that antimony is

Figure (3.2) The background subtracted EXAFS (A) and Fourier transforms (B). The EXAFS (a) are plotted at a k -weighting of 2. The R -space Fourier transforms (b) have not been corrected for phase shift. Spectra have been shifted along the vertical axes for clarity. The raw data are plotted with solid lines and the fits with dashed lines.



complexed with both hydroxide and sulfide ligands at $\text{pH} \approx 12$ and $\text{S}^{2-}_{\text{total}} \approx 0.001 \text{ mol kg}^{-1} \text{ S}^{2-}_{\text{total}}$. The Fourier transform (FT) of the EXAFS had two distinct peaks originating from the first coordination shell of antimony: an Sb-O path at $\sim 1.4 \text{ \AA}$ and an Sb-S path at $\sim 1.8 \text{ \AA}$ (distances not corrected for phase shift, see Figure (3.2)). The number of independent data points in the portion of the EXAFS spectra used to fit the first coordination shell was only slightly greater than the number of individual fit parameters, i.e., CN , R , ΔE_0 , and σ^2 for both the Sb-S and Sb-O paths, needed to fit the first coordination shell. Therefore, constraints derived from fits of the concentrated sulfide solutions were placed on the ΔE_0 and σ^2 parameters.

In fitting sample Sb91-19, the ΔE_0 and σ^2 fit parameters for the Sb-S path were set to the average of their fitted values in fits of the two best quality spectra (Sb80-20 and Sb51-24). Values of some of the fitted parameters, particularly the CN of sulfur, were sensitive to the details of the constraints used for σ^2 , but the Sb-ligand distances were not sensitive to the approach used to constrain σ^2 . The σ^2 parameter for the Sb-O path was scaled relative to the Sb-S distance, and the best fits were achieved with the value of the Sb-O σ^2 parameter at $1/3^{\text{rd}}$ to $1/5^{\text{th}}$ of the value of the Sb-S σ^2 . This approach produced first shell fits containing 2.9 to 3.1 oxygen atoms at $\sim 1.97 \text{ \AA}$ and 1.3 to 1.6 sulfur atoms at $\sim 2.34 \text{ \AA}$. Some previous Sb XAS studies have found a similar magnitude difference between the value of σ^2 for Sb-O paths and the value for less electronegative ligands (S^{2-} and Cl^-) in solutions where both types of ligands were complexing Sb(III). In Pokrovski et al. (2006; 2008) and Planer-Friedrich and Scheinost (2011), the σ^2 values for Sb-O paths were ~ 3 times less than the values for the longer Sb-Cl and Sb-S paths in solutions where both types of ligands were complexed with antimony.

The EXAFS of sample Sb91-19 also had evidence of longer-range features between 3 and 4 \AA . This is a similar distance to that at which first shell Sb-Sb interactions were fit in the stibnite EXAFS and where Sb-Sb interactions in Sb_2S_4 dimers might be expected. These features could be fit with a single Sb-Sb path at $\sim 3.8 \text{ \AA}$ or with two Sb-Sb paths at different distances, one at $\sim 3.8 \text{ \AA}$ and a second at $\sim 4.0 \text{ \AA}$. The fit of the first shell distances remained the same whether one or two Sb were considered. The number of antimony atoms in the first coordination shell could in principle be varied from ~ 1 to ~ 3 , depending on how the σ^2 parameter for the shell was constrained. However, constraining the σ^2 of the Sb-Sb path to be greater than the σ^2 of the shorter Sb-S path produced a coordination number that is consistent with an Sb_2S_4 dimer. This is considered a reasonable constraint because a longer path would be expected to be more “disordered” than a shorter path. This fit is presented in Table (3.3) and was used to plot the fit in Figure (3.2).

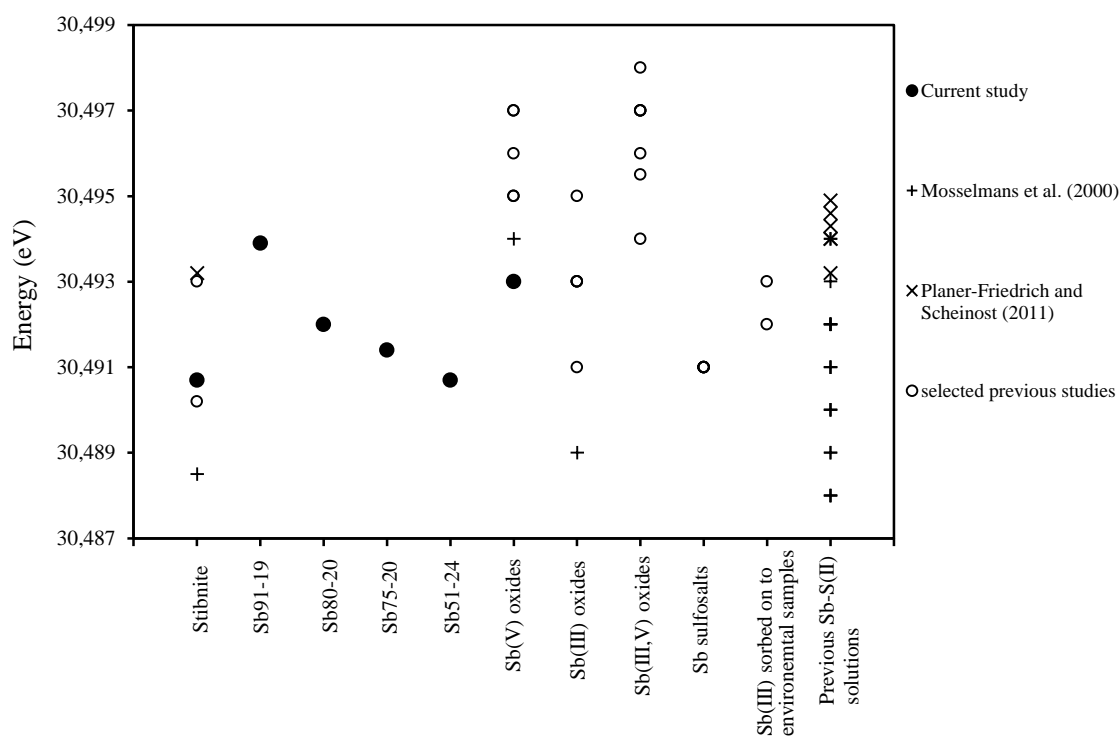
3.3.4. X-ray near edge fine structure of aqueous antimony complexes

The energy positions of the absorption edges for antimony solutions and the reference solid phases (stibnite and synthetic Sb_2O_5) are listed in Table (3.3) and are graphically compared to

absorption edges reported by previous authors for antimony hydrosulfide solutions and a range antimony minerals and solid phases Figure (3.3). The absorption edge energies for antimony dissolved in the sulfide solutions varied between 30,490.7 and 30,493.9 eV. These edge positions are generally higher than that of the antimony(III) bound to sulfide in stibnite but not as high as those usually measured for Sb(V) reference solids (30,495 – 30,497 eV). The measured Sb K-edge position for stibnite was within 0.5 eV of that reported for stibnite in the Sb K-edge XANES summary paper by Fawcett et al. (2009), slightly above that for the reference Sb metal foil (30,491 eV), and similar to Sb(III) oxides (~ 30492 eV). However, the absorption edge position for Sb in the Sb(V) oxide, Sb₂O₅, measured in this study was ~3 eV lower than what is expected for Sb(V). Two previous XAS studies have found that commercial Sb₂O₅ can contain a significant proportion (up to ~ 50%) of a Sb(III) impurity (Scheinost et al., 2006; Beauchemin et al., 2012). Because of these previous observations and the fact that the stibnite Sb edge position was correct, the nominally Sb₂O₅ sample was probably contaminated with an Sb(III) component and the edge position that was measured in this study is not believed to be representative of an Sb(V) edge. The Sb(V) edge positions found in previous studies were therefore used instead in the evaluation of antimony valence in the experimental solutions.

The Sb K-edge XANES edge energies of most of the solutions measured in this study are between energies that can be definitively attributed to Sb(III) (i.e., ≤ 30,492 eV) and energies that can be definitively attributed to Sb(V) (i.e., ≥ 30,495 eV). Therefore, antimony(III) complexes cannot be

Figure (3.3) Antimony K-edge energies for solid reference samples and experimental solutions. For reference, the current study is compared to values from previous studies of antimony in aqueous sulfide solutions (Mosselmans et al., 2000; Planer-Friedrich and Scheinost, 2011) and in minerals and environmental matrices (Scheinost et al., 2006; Kirsch et al., 2008; Ackermann et al., 2009; Fawcett et al., 2009; Guo et al., 2014; Hockmann et al., 2014)



identified nor antimony(V) complexes excluded using the XANES spectra alone. The observed Sb-S distances and coordination numbers for the solutions with high sulfide concentrations are more similar to those expected for Sb(III)-S complexes (i.e., ~ 3 sulfur atoms at 2.37 - 2.41 Å) in comparison to those for Sb(V)-sulfide complexes (4 to 4.2 sulfur atoms at ≤ 2.34 Å). In addition, the fit associated with the highest numbers of coordinated sulfurs (i.e., ~ 3.5) had the poorest fit statistics. The XAS study by Sherman et al. (2000) which measured the EXAFS spectra of Sb(V)-sulfide complexes did not report Sb K-edge positions, and so direct comparison to the XANES of Sb(V) in a hydrosulfide solution is not possible. Although the presence of Sb(V) or mixed-valence Sb(III,V) species cannot be definitively excluded for all of the solutions in the current study, the XANES and EXAFS measurements of the solutions presented in Table (3.3) and Figure (3.2) are consistent with Sb(III) interactions with sulfide and hydroxide ligands.

3.4. Discussion

3.4.1. *Motivation for combining solubility and spectroscopic approaches*

This current research combined the techniques of flow-through solubility experiments with XAS measurements to study antimony interactions with sulfide ligands in reducing aqueous solutions. This approach was taken in an attempt to overcome the inherent limitations of each technique. The solubility approach can only provide information about aqueous speciation at saturation (i.e. stibnite in this study), and the approach is further limited by the possibility that numerous possible combinations of different aqueous complexes may be able to produce speciation models that are statistically indistinguishable (but not necessary equally chemically reasonable). An example of this inherent difficulty in interpreting solubility experiments is the multiple fits in Chapter (2) with R^2 values close to 0.9. In contrast, spectroscopic techniques, including XAS, directly provide information about the complexes present in a solution and can be used to study solutions with analyte concentrations below that needed to reach saturation for the conditions of the experiment (i.e. ligand activity, pH, temperature, and pressure). However, the information derived from a spectroscopic experiment is often limited to one or several very specific characteristics of the aqueous complex or complexes. Identifying unique complexes from this information may not be possible without additional assumptions or constraints. For XAS at the Sb K-edge, measured spectra can provide average first shell coordination numbers (i.e. the number of scatterers) and antimony valence, but data interpretation can be made difficult by the presence of mixed-ligand complexes, mixtures of single-ligand complexes, or complexes with multiple Sb-ligand distances within the first coordination shell. Additionally, some spectroscopic techniques, including XAS and Raman spectroscopy for antimony, are limited to elemental concentrations several orders of magnitude higher than concentrations that would be of interest in applied environmental or geological problems.

3.4.2. Antimony first shell coordination measured by EXAFS and predicted by stibnite solubility studies

The number of sulfur and oxygen atoms in antimony's first coordination shell predicted by the several solubility models is compared to the average coordination shell measured by EXAFS in Table (3.4). The EXAFS results for antimony coordination in strongly alkaline solutions were taken from Table (3.3). The average coordination shells at stibnite saturation that were predicted by four different 30°C speciation models, i.e., Fits (30-C), (30-G), (30-H), and (30-I), are also presented. The predicted coordination shells were calculated from the species distribution for the pH and sulfide concentrations of XAS samples using the equilibrium constants presented in Table (2.4) for Fit (30-C) and Table (2.6) for the three remaining fits. Fit (30-C) is the speciation model that included only monomers (i.e. SbS_3^{3-} and HSbS_2O^-) at strongly alkaline pH, while Fits (30-G), (30-H), and (30-I) had $\text{Sb}_2\text{S}_4^{2-}$ and either $\text{Sb}(\text{OH})_3 + \text{H}_2\text{SbO}_3^-$ or a mixed-ligand monomer. Thus, the data presented in Table (3.4) can be used to evaluate which speciation models derived from stibnite solubility measurements are consistent with the XAS measurements.

Both SbS_3^{3-} and $\text{Sb}_2\text{S}_4^{2-}$ have three sulfur atoms in antimony's first coordination shell. The structures of $\text{Sb}_2\text{S}_4^{2-}$ and $\text{H}_x\text{SbS}_3^{x-3}$, as represented by H_3SbS_3 , are shown in Figure (3.4). The structure of stibnite (Sb_2S_3), also shown in Figure (3.4), contains a tetrahedral SbS_3 site (the outer antimony atoms in the diagram) and a square pyramid SbS_5 site. In contrast, both aqueous species consists of "tetrahedral" $\text{Sb}(\text{III})\text{S}_3$ units with a lone pair of electrons at one apex. In $\text{H}_x\text{Sb}_2\text{S}_4^{x-2}$, two of the sulfur atoms are shared with another antimony atom producing two connected SbS_3 units that face in opposite directions. Each antimony atom in $\text{Sb}_2\text{S}_4^{2-}$ will have a single first shell antimony atom located at 3 to 4 Å. Both SbS_3^{3-} and $\text{Sb}_2\text{S}_4^{2-}$ contain three sulfur atoms at ~ 2.4 Å in the first coordination shell

Table (3.4) Comparison of average first shell coordination numbers in strongly alkaline solutions measured by EXAFS and those predicted by speciation models derived from stibnite solubility measurements (Chapter 2).

Sample	pH	mol kg ⁻¹ S ²⁻ _{total}	EXAFS		Solubility							
			S	O	Fit (30-C) ^a		Fit (30-G) ^b		Fit (30-H) ^b		Fit (30-I) ^b	
					S	O	S	O	S	O	S	O
Sb51-24	10.9	0.097	3.4	n.d.	2.9	0.2	3.0	0.0	2.9	0.1	3.0	0.0
Sb75-20	11.4	0.009	3.7	n.d.	2.2	0.8	3.0	0.0	2.5	0.5	2.9	0.1
Sb80-20	11.7	0.019	3.3	n.d.	2.4	0.6	3.0	0.0	2.5	0.5	3.0	0.0
Sb91-19	12.0	0.001	1.6	3.1	2.0	1.0	0.6	2.4	2.1	0.9	1.1	1.9

Complexes included in fits and tables in Chapter (2) with fit statistics:

Fit (30-C): $\text{SbS}_3^{3-} + \text{HSbS}_2\text{O}^{2-} + \text{H}_2\text{Sb}_2\text{S}_5^{2-} + \text{HSb}_2\text{S}_4^- + \text{H}_3\text{SbS}_2\text{O}$ (Table 2.4)

Fit (30-G): $\text{Sb}_2\text{S}_4^{2-} + \text{H}_2\text{Sb}_2\text{S}_5^{2-} + \text{HSb}_2\text{S}_4^- + \text{H}_3\text{SbS}_2\text{O} + \text{Sb}(\text{OH})_3 + \text{H}_2\text{SbO}_3^-$ (Table 2.6)

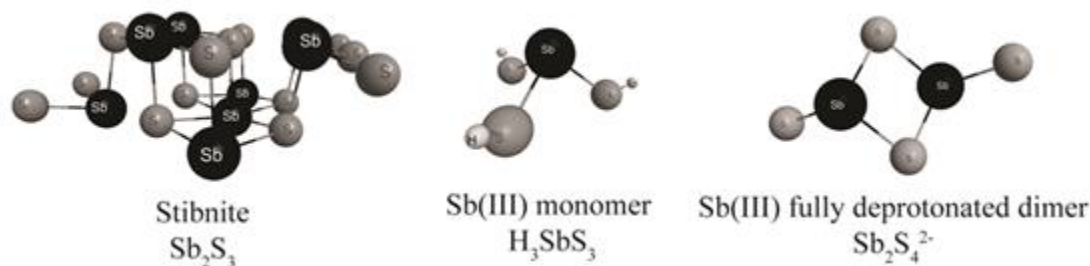
Fit (30-H): $\text{Sb}_2\text{S}_4^{2-} + \text{H}_2\text{Sb}_2\text{S}_5^{2-} + \text{HSb}_2\text{S}_4^- + \text{H}_3\text{SbS}_2\text{O} + \text{HSbS}_2\text{O}^{2-}$ (Table 2.6)

Fit (30-I): $\text{Sb}_2\text{S}_4^{2-} + \text{H}_2\text{Sb}_2\text{S}_5^{2-} + \text{HSb}_2\text{S}_4^- + \text{H}_3\text{SbS}_2\text{O} + \text{H}_2\text{SbSO}_2^-$ (Table 2.6)

^a fits conducted with added sulfide experiments (N=51)

^b fits conducted including deionised water experiments (N=53)

Figure (3.4) Local coordination of antimony within stibnite, an antimony(III)-sulfide monomer (represented with H_3SbS_3), and an antimony(III)-sulfide dimer (represented with $\text{Sb}_2\text{S}_4^{2-}$). Stibnite contains both a 5-coordinated and a 3-coordinated site. In the figure, five of the 5-coordinated sites and three of the 3-coordinated sites are represented.



(Tossell, 1994), and thus speciation models containing these two species cannot be distinguished based solely upon the number of sulfur atoms measured by EXAFS. However, SbS_3^{3-} and $\text{Sb}_2\text{S}_4^{2-}$ contain different ratios of sulfur to antimony atoms, and so, for the same experimental stibnite solubility versus sulfide concentration curve, these two speciation models will produce different average coordination shells as antimony complexation changes from sulfide to hydroxide ligands with decreasing sulfide concentration. In other words, stibnite solubility data produce criteria (i.e. predicted average first shell coordination numbers) that, when combined with EXAFS measurements, enable the presence of either SbS_3^{3-} or $\text{Sb}_2\text{S}_4^{2-}$ to be determined.

As can be seen from the predicted average coordination numbers in Table (3.4), the speciation model used in Fit (30-C) (i.e. $\text{SbS}_3^{3-} + \text{HSbS}_2\text{O}^{2-}$ at strongly alkaline pH) predicts oxygen atoms in the coordination shell where none were observed spectroscopically and a first coordination shell with more sulfur atoms than oxygen atoms when $\text{S}^{2-}_{\text{total}} = 0.001 \text{ mol kg}^{-1}$, which is opposite to the EXAFS results. In contrast, solubility-derived speciation models with $\text{Sb}_2\text{S}_4^{2-}$ at alkaline pH more closely reproduce the coordination shells found by EXAFS. In particular, the preferred speciation model (i.e. Fit 30-G) from Chapter (2) produces similar oxygen coordination numbers to the EXAFS. Therefore, the EXAFS results are consistent with $\text{Sb}_2\text{S}_4^{2-}$ but not with SbS_3^{3-} even though Sb-Sb interactions at 3 to 4 Å, which would be indicative of dimeric species, were not detected.

The failure of XAS to detect Sb-Sb interactions in antimony-sulfide complexes (i.e. in $\text{H}_x\text{Sb}_2\text{S}_4^{x-2}$) is not unique to this study. Both Mosselmans et al. (2000) and Planer-Friedrich and Scheinost (2011) did not find second shell interactions antimony sulfide solutions in which $\text{Sb}_2\text{S}_4^{2-}$ should be stable (i.e. strongly alkaline and with sulfide concentration \gg antimony concentration). Evidence in Mosselmans et al. (2000) for longer range interactions was limited to a feature at $\sim 4.1 \text{ Å}$ in a pH 8.3 solution containing carbonate and $0.1 \text{ mol kg}^{-1} \text{S}^{2-}_{\text{total}}$ that did not improve fit parameters. Planer-Friedrich and Scheinost (2011) fit a longer range feature from the EXAFS of the oxic solution with the lowest sulfide concentration with a 5.64 Å Sb-Sb path. However, this distance is greater than that expected for Sb-Sb shell in $\text{Sb}_2\text{S}_4^{2-}$. In the current study, a feature was also found in the sample with the lowest sulfide solution (Sb91-19) that could be well fit with one or two Sb-Sb distances at \sim

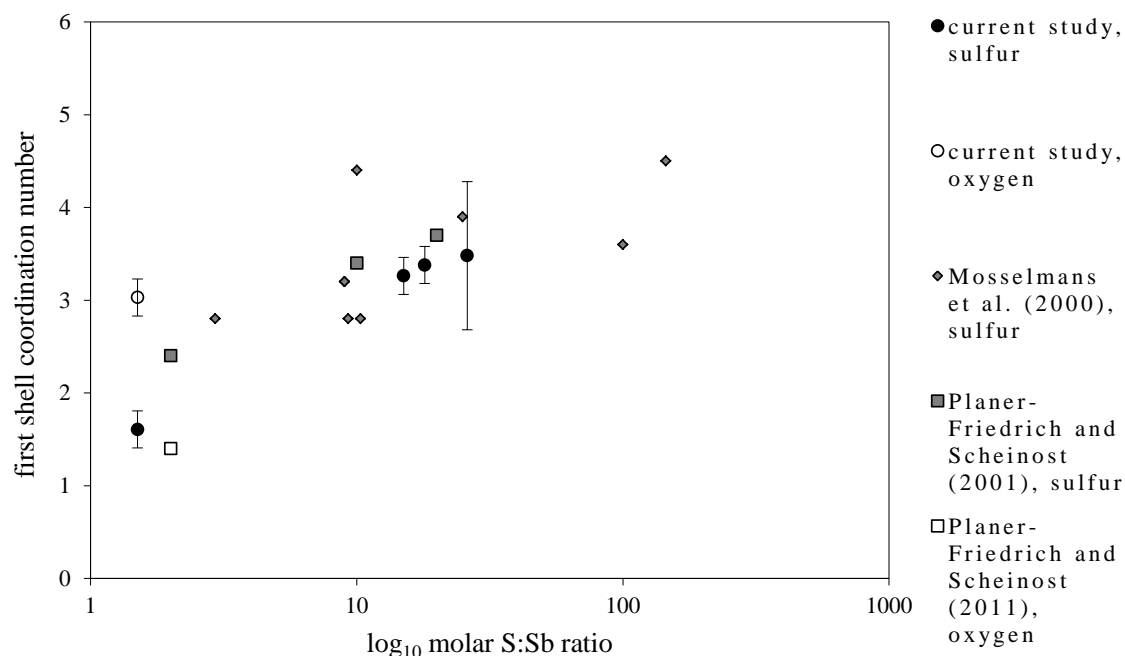
3.8 Å (results section 3.3.3. and Table (3.3)). Small features at ~ 3.8 Å similar to those in the Sb91-19 spectrum were observed in the EXAFS spectra of Sb(III) complexed with bidentate organic ligands and were interpreted in terms of several linear multiple scattering paths between Sb, O, and C (Tella and Pokrovski, 2009). This could suggest the presence of an Sb-S-O complex at the transition from antimony-sulfide to antimony-hydroxide complexes. However, such a complex is not required by solubility data and would be difficult to identify from XAS without further constraints on its structure or stoichiometry. In both Planer-Friedrich and Scheinost (2011) and the current study, Sb-Sb interactions only appear in solutions containing comparable numbers of both sulfide and hydroxide ligands, and this relationship suggests that these features could be artifacts of the Fourier transformation of noisy XAS spectra containing two significant components (Sb-O and Sb-S) rather than evidence of a dimeric species.

The amount and precision of structural and electronic information that can be gained from the XAS spectra is limited by structural disorder in the sample, which is generally greater in solutions than in mineral phases, and by spectra broadening, which is greater for high atomic number elements. Millimolar antimony concentrations (0.001 mol kg⁻¹) were close to the minimum concentrations that could produce useful XAS spectra using the facilities available in to this study. XAS analysis could identify both Sb-O and Sb-S paths at < 3 Å but was unable to resolve Sb-Sb interactions in solutions with antimony concentrations between 0.0003 and 0.005 mol kg⁻¹. However, as discussed above, XAS produced information that assisted in the interpretation of data from solubility experiments and enabled elimination of a speciation model containing SbS₃³⁻ in alkaline solutions (i.e., at pH > 9.5) in equilibrium with stibnite.

3.4.3. Re-evaluation of previous Sb(III)-S(II) XAS studies and future research directions

The XAS results of the current study are similar to those found in previous studies of Sb(III) in sodium sulfide solutions. This is demonstrated by the average first coordination shells shown graphically in Figure (3.5) in which the number of first shell sulfur atoms is plotted versus the S:Sb molar concentration ratio using the EXAFS results from the current study and the results selected from Mosselmans et al. (2000) and Planer-Friedrich and Scheinost (2011) that were the most comparable to the current study (i.e. XAS of antimony in alkaline sulfide solutions prepared without exposure to atmospheric oxygen). For Mosselmans et al. (2000), only data from sodium sulfide solutions with published antimony concentrations are plotted, and solutions with Na₂(CO)₃²⁻ and/or elemental sulfur are not included. For Planer-Friedrich and Scheinost (2011), the solutions prepared without exposure to atmospheric oxygen are plotted. Also included in Figure (3.5) are the first shell oxygen atoms for the same solutions, so that Figure (3.5) shows how the average coordination environment of antimony, as measured by EXAFS, changes from hydroxide ligands to sulfide ligands with increasing sulfide concentration.

Figure (3. 5) First coordination shells of antimony(III) complexes at different sulfide concentrations. Average coordination numbers for oxygen and sulfide ligands in around antimony alkaline sodium sulfide solutions from Sb K-edge measurements conducted in the current and two previous studies. The samples from Mosselmans et al. (2000) lacking published antimony concentrations and those containing $\text{Na}_2(\text{CO}_3)_3^{2-}$ and/or elemental sulfur are not plotted. The sulfide concentration used for the molar concentration ratio is the total sulfide in the solution, i.e., not corrected for the sulfide complexed with antimony.



In all three studies, the number of coordinating sulfur atoms was usually between 2.9 and 3.7 when there was sufficient sulfide to fully complex the dissolved antimony, whereas oxygen atoms (or a decrease in the number of sulfur atoms in the data from Mosselmans et al. (2000)) occurred in the first coordination shell when the sulfide concentration approached or was less than the antimony concentration. There is considerable scatter in some of the data from Mosselmans et al. (2000) for similar S:Sb ratios, which could have resulted from incipient oxidation during sample preparation and/or storage prior to measurement. It should be noted that in the current study, the sample with largest number of coordinating sulfur atoms (3.5 sulfurs) also had the largest uncertainties in the fit, due to the lower quality spectra derived from the lowest antimony concentration (i.e. $0.0003 \text{ mol kg}^{-1}$). For the “best” EXAFS data from the current study (i.e. Sb80-20 and Sb51-54), the number of coordinating sulfur atoms did not increase with increasing S:Sb ratio within the error of the coordination numbers and was between 3.3 and 3.4. Although the previous studies also did not detect Sb-Sb interactions in an antimony-sulfide complex, the number of sulfur and oxygen atoms in the average coordination shell and how these numbers change with the relative amount of sulfide in these studies are consistent with the current study and therefore with the presence of $\text{Sb}_2\text{S}_4^{2-}$.

Using the sulfur and oxygen ligand coordination numbers shown in Figure (3.5) as a guide, future XAS studies of antimony sulfide solutions with S:Sb ratios between 1:2 and 10:1 could be used to evaluate how well Sb K-edge EXAFS quantifies low numbers of coordinating sulfur and oxygen

atoms. Mixed-ligand species were not needed to fit the solubility in Chapter (2). However, this study had limited data at low sulfide concentrations and alkaline pH and such a species could be found by a solubility study focused on these conditions. Multiple XAS measurements at constant pH and different sulfide concentrations should spectroscopically record the entire transition from antimony-hydroxide to antimony-sulfide complexes and would be a valuable addition to studies interested in how $\text{Sb}(\text{OH})_3$ and $\text{Sb}_2\text{S}_4^{2-}$ are related at alkaline pH. Additionally, evaluating both EXAFS and XANES spectra from Sb(V)-S(II) solutions has not been done (Sherman et al.(2000) only reported EXAFS results from Sb(V) solutions). Including well-characterised Sb(V) solutions in future XAS experiments would greatly assist in quantifying an Sb(V) component in XAS spectra from antimony sulfide solutions with mixed or ambiguous oxidation states.

3.5. Conclusions

The main conclusions originating from the XAS analysis presented in this chapter are

1. The first coordination shell of antimony in alkaline sodium sulfide solutions at stibnite saturation contained 3.3 to 3.5 sulfur atoms at 2.35 to 2.38 Å when the sulfide concentration was more than ten times the antimony concentration. In solutions when the sulfide concentration was set by the dissociation of stibnite, there were 3 oxygen atoms at 1.97 Å and 1 to 2 sulfur atoms at 2.34 Å.
2. By the measurement of the average coordination environment of antimony at different sulfide concentrations, XAS measurements were able to confirm the presence of $\text{Sb}_2\text{S}_4^{2-}$ indicated by solubility studies, although XAS as unable to detect the Sb shell present in the dimer.

This study sought to use ambient temperature XAS measurements to support the antimony-sulfide speciation model derived from 30°C stibnite solubility data in Chapter (2). The speciation model derived from solubility measurements in strongly alkaline solutions included $\text{Sb}_2\text{S}_4^{2-}$ in solutions at higher sulfide concentrations and included $\text{Sb}(\text{OH})_3$, and H_2SbO_3^- in dilute sulfide solutions as the sulfide concentration decreased from 0.1 to 0.0001 mol kg⁻¹ S²⁻_{total}. The first shell coordination environments measured by XAS in four solutions were consistent with this speciation model. However, Sb-Sb interactions such those expected for $\text{Sb}_2\text{S}_4^{2-}$ were not detected, even though the solutions in this study were chosen to give the best chance of detecting such features. Without constraints provided by the solubility data that related the coordination environment to the sulfide concentration, the XAS results could be erroneously interpreted as being due to SbS_3^{3-} .

3.6. References

Ackermann, S., Giere, R., Newville, M., Majzlan, J., 2009. Antimony sinks in the weathering crust of bullets from Swiss shooting ranges. *Sci Total Environ* **407**, 1669-1682.

- Arnston, R.H., Dickson, F.W., Tunnel, G., 1966. Stibnite (Sb_2S_3) solubility in sodium sulfide solutions. *Science* **153**, 1673-1674.
- Australian Synchrotron, 2016. Data / analysis (XAS).
<http://www.synchrotron.org.au/aussyncbeamlines/x-ray-absorption-spectroscopy/data-analysis>.
- Beauchemin, S., Kwong, Y.T.J., Desbarats, A.J., MacKinnon, T., Percival, J.B., Parsons, M.B., Pandya, K., 2012. Downstream changes in antimony and arsenic speciation in sediments at a mesothermal gold deposit in British Columbia, Canada. *Appl. Geochem.* **27**, 1953-1965.
- Ebitani, K., Hattori, H., Tanaka, T., 1992. Structural consideration of antimony pentafluoride deposited on metal oxides (silica, alumina, and silica-alumina) by x-ray absorption (EXAFS/XANES) spectroscopy. *The Journal of Physical Chemistry* **96**, 5430-5434.
- Fawcett, S.E., Gordon, R.A., Jamieson, H.E., 2009. Optimizing experimental design, overcoming challenges, and gaining valuable information from the Sb K-edge XANES region. *Am. Miner.* **94**, 1377-1387.
- Flavell, W.R., Mian, M., Roberts, A.J., Howlett, J.F., Sarker, M.M., Wincott, P.L., Bilsborrow, R.L., Dorssen, G.v., 1997. EXAFS studies of $\text{SrSn}_{1-x}\text{Sb}_x\text{O}_3$ and $\text{BaPb}_{1-x}\text{Bi}_x\text{O}_3$. *Journal Material Chemistry* **7**.
- Geraldo, V., Briois, V., Scalvi, L.V.A., Santilli, C.V., 2007. EXAFS investigation on Sb incorporation effects to electrical transport in SnO_2 thin films deposited by sol-gel. *Journal of the European Ceramic Society* **27**, 4265-4268.
- Guo, X., Wu, Z., He, M., Meng, X., Jin, X., Qiu, N., Zhang, J., 2014. Adsorption of antimony onto iron oxyhydroxides: adsorption behavior and surface structure. *J Hazard Mater* **276**, 339-345.
- Hockmann, K., Lenz, M., Tandy, S., Nachtegaal, M., Janousch, M., Schulin, R., 2014. Release of antimony from contaminated soil induced by redox changes. *J Hazard Mater* **275**, 215-221.
- Ilgen, A.G., Foster, A.L., Trainor, T.P., 2012. Role of structural Fe in nontronite NAu-1 and dissolved Fe(II) in redox transformations of arsenic and antimony. *Geochim. Cosmochim. Acta* **94**, 128-145.
- Ilgen, A.G., Majs, F., Barker, A.J., Douglas, T.A., Trainor, T.P., 2014. Oxidation and mobilization of metallic antimony in aqueous systems with simulated groundwater. *Geochim. Cosmochim. Acta* **132**, 16-30.
- Kappen, P., Ruben, G., 2013. Sakura, Synchrotron Light Source Australia Pty Ltd.,
<http://www.synchrotron.org.au/aussyncbeamlines/x-ray-absorption-spectroscopy/sakura>.
- Kirsch, R., Scheinost, A.C., Rossberg, A., Banerjee, D., Charlet, L., 2008. Reduction of antimony by nano-particulate magnetite and mackinawite. *Mineral. Mag.* **72**, 185-189.
- Kolpakova, N.N., 1971. On the speciation of antimony (III) in sulfide solutions (in Russian), *Geochemistry of Hydrothermal Ore Deposition*, Nauka, Moscow, pp. 197-209.
- Kolpakova, N.N., 1982. Laboratory and field studies of ionic equilibria in the $\text{Sb}_2\text{S}_3\text{-H}_2\text{O-H}_2\text{S}$ system. *Geochem. Internat.* **19**, 46-54.
- Krause, M.O., Oliver, J.H., 1979. Natural widths of atomic K and L levels, Ka X-Ray lines and several KLL Auger lines. *Journal of Physical and Chemical Reference Data* **8**, 329-338.
- Krupp, R.E., 1988. Solubility of stibnite in hydrogen sulfide solutions, speciation, and equilibrium constants, from 25 to 350°C. *Geochim. Cosmochim. Acta* **52**, 3005-3015.
- Lu, K., Wang, Q., Li, C., Wang, Y., Chen, X., 2002. The structure, electronic states and properties in liquid Ga-Sb and In-Sb systems. *Journal of Non-Crystalline Solids* **312-314**, 34-40.
- Lundegaard, L.F., Miletich, R., Balic-Zunic, T., Makovicky, E., 2003. Equation of state and crystal structure of Sb_2S_3 between 0 and 10 GPa. *Physics and Chemistry of Minerals* **30**, 463-468.
- Matsuzawa, K., Shido, T., Iwasawa, Y., 2003. Reversible structure transformation of antimony oxides on SiO_2 relevant to selective catalytic oxidation of ethanol. *Langmuir* **19**, 2756-2762.
- Millet, J.M.M., Baca, M., Pigamo, A., Vitry, D., Ueda, W., Dubois, J.L., 2003. Study of the valence state and coordination of antimony in MoVSbO catalysts determined by XANES and EXAFS. *Applied Catalysis A: General* **244**, 359-370.
- Mills, S.J., Etschmann, B., Kampf, A.R., Poirier, G., Newville, M., 2014. Sb^{5+} and Sb^{3+} substitution in segnitite: A new sink for As and Sb in the environment and implications for acid mine drainage. *Am. Miner.* **99**, 1355-1359.
- Mitsunobu, S., Harada, T., Takahashi, Y., 2006. Comparison of antimony behavior with that of arsenic under various soil redox conditions. *Environ. Sci. Technol.* **40**, 7270-7276.

- Mitsunobu, S., Takahashi, Y., Utsunomiya, S., Marcus, M.A., Terada, Y., Iwamura, T., Sakata, M., 2011. Identification and characterization of nanosized tripuhyite in soil near Sb mine tailings. *Am. Miner.* **96**, 1171-1181.
- Mosselmans, J.F.W., Helz, G.R., Patrick, R.A.D., Charnock, J.M., Vaughan, D.J., 2000. A study of speciation of Sb in bisulfide solutions by X-ray absorption spectroscopy. *Appl. Geochem.* **15**, 879-889.
- Oelkers, E.H., Sherman, D.M., Ragnarsdottir, K.V., Collins, C., 1998. An EXAFS spectroscopic study of aqueous antimony(III)-chloride complexation at temperatures from 25 to 250°C. *Chem. Geol.* **151**, 21-27.
- Peterson, R.C., Miller, I., 1968. Crystal structure and cation distribution in freibergite and tetrahedrite. *Mineral. Mag.* **50**, 717-721.
- Planer-Friedrich, B., Scheinost, A.C., 2011. Formation and structural characterization of thioantimony species and their natural occurrence in geothermal waters. *Environ. Sci. Technol.* **45**, 6855-6863.
- Pokrovski, G., Borisova, A., Roux, J., Hazemann, J., Petdang, A., Tella, M., Testemale, D., 2006. Antimony speciation in saline hydrothermal fluids: A combined X-ray absorption fine structure spectroscopy and solubility study. *Geochim. Cosmochim. Acta* **70**, 4196-4214.
- Pokrovski, G.S., Roux, J., Hazemann, J.L., Borisova, A.Y., Gonchar, A.A., Lemesko, M.P., 2008. *In situ* X-ray absorption spectroscopy measurement of vapour-brine fractionation of antimony at hydrothermal conditions. *Mineral. Mag.* **72**, 667-681.
- Ravel, B., Newville, M., 2005. ATHENA, ARTEMIS, HEPHAESTUS: data analysis for X-ray absorption spectroscopy using IFEFFIT. *J. Synchrotron Radiat.* **12**, 537-541.
- Ritchie, V.J., Ilgen, A.G., Mueller, S.H., Trainor, T.P., Goldfarb, R.J., 2013. Mobility and chemical fate of antimony and arsenic in historic mining environments of the Kantishna Hills district, Denali National Park and Preserve, Alaska. *Chem. Geol.* **335**, 172-188.
- Scheinost, A.C., Rossberg, A., Vantelon, D., Xifra, I., Kretzschmar, R., Leuz, A.-K., Funke, H., Johnson, C.A., 2006. Quantitative antimony speciation in shooting-range soils by EXAFS spectroscopy. *Geochim. Cosmochim. Acta* **70**, 3299-3312.
- Sherman, D.M., Ragnarsdottir, K.V., Oelkers, E.H., 2000. Antimony transport in hydrothermal solutions: an EXAFS study of antimony(V) complexation in alkaline sulfide and sulfide-chloride brines at temperatures from 25°C to 300°C at P_{sat} . *Chem. Geol.* **167**, 161-167.
- Sinsermsuksakul, P., Chakraborty, R., Kim, S.B., Heald, S.M., Buonassisi, T., Gordon, R.G., 2012. Antimony-doped tin(II) sulfide thin films. *Chemistry of Materials* **24**, 4556-4562.
- Takaoka, M., Fukutani, S., Yamamoto, T., Horiuchi, M., Satta, N., Takeda, N., Oshita, K., Yoneda, M., Morisawa, S., Tanaka, T., 2005. Determination of chemical form of antimony in contaminated soil around a smelter using X-ray absorption fine structure. *Analytical Sciences* **21**, 769-773.
- Tella, M., Pokrovski, G.S., 2009. Antimony(III) complexing with O-bearing organic ligands in aqueous solution: An X-ray absorption fine structure spectroscopy and solubility study. *Geochim. Cosmochim. Acta* **73**, 268-290.
- Tossell, J.A., 1994. The speciation of antimony in sulfidic solutions: A theoretical study. *Geochim. Cosmochim. Acta* **58**, 5093-5104.
- Varrica, D., Bardelli, F., Dongarrà, G., Tamburo, E., 2013. Speciation of Sb in airborne particulate matter, vehicle brake linings, and brake pad wear residues. *Atmospheric Environment* **64**, 18-24.
- Whitten, A.E., Dittrich, B., Spackman, M.A., Turner, P., Brown, T.C., 2004. Charge density analysis of two polymorphs of antimony(III) oxide. *Dalton Transactions* **1**, 23-29.
- Yiwata, N., Harigaya, M., Tani, K., Hayakawa, K., Fujikawa, T., 2001. Sb K-edge absorption fine structure of Sb_2Te_3 . *J. Synchrotron Radiat.* **8**, 752-754.

Chapter (4):

Stibnite solubility and antimony speciation in hydrosulfide solutions from 70 to 400°C

4.1. Introduction

The antimony dissolved in reducing high temperature aqueous fluids occurs as complexes with sulfide (HS^-) or hydroxide (OH^-) ligands depending on the pH and sulfide concentration. The response of antimony sulfide solubility to changes in pH, dissolved sulfide content, and temperature will be determined by the relative stability of different antimony complexes. The stability constants for antimony(III)-sulfide and antimony(III)-hydroxide complexes presented in this Chapter can be used to evaluate antimony transport and deposition chemistry in hydrothermal systems, including as part of hydrothermal ore deposition and in fluids utilized for geothermal power generation.

Hydrothermal fluids from active geothermal systems often contain tens to hundreds of ppb Sb ($\sim 10^{-7}$ to 10^{-6} mol kg^{-1} Sb) and concentrations as high as 1- 3 ppm Sb ($\sim 10^{-5}$ mol kg^{-1} Sb) occur in some systems (Weissberg et al., 1979; Stauffer and Thompson, 1984; Simmons and Brown, 2007; Hardardottir et al., 2009; Landrum et al., 2009; Planer-Friedrich and Scheinost, 2011; Ullrich et al., 2013; Hannington et al., 2016; Simmons et al., 2016). Deposition of antimony sulfides from such fluids has produced antimony-rich deposits within and around some hot springs, including quite spectacularly at Champagne Pool, Waiotapu, New Zealand (Weissberg, 1969). Such systems are modern analogs for epithermal ore deposits, and they can serve as model systems to investigate ore deposition processes and to contrast the chemistry of antimony with that of other elements that complex with sulfide ligands to a greater or lesser degree. In particular, an improved understanding of antimony chemistry would elucidate the concurrent enrichment of antimony, arsenic and gold that is observed in some hydrothermal fluids, hydrothermal ore deposits, and hydrothermal altered rocks (e.g., Williams-Jones and Normand, 1997; Migdisov and Bychkov, 1998; Simmons and Browne, 2000). Precipitation of antimony sulfide scale, primarily as microscopic needles of stibnite, in geothermal power stations is not common but in some systems is extensive and problematic (Raymond et al., 2005; Wilson et al., 2007; Morteani et al., 2010). Thermodynamic data for antimony at the physicochemical conditions present in the power stations can be used to develop procedures to eliminate, or at least minimize, stibnite precipitation within such facilities.

The complexation of antimony(III) in hydrosulfide solutions at 30°C was investigated in Chapter (2). At ambient temperatures, antimony(III) readily complexes with HS^- ligands across the

whole pH range whenever there is sufficient free dissolved sulfide. Stibnite solubility increases with increasing pH from $\sim 10^{-9}$ mol kg⁻¹ Sb at pH = 4 to $\sim 10^{-3}$ mol kg⁻¹ Sb at pH = 12, with an intermediate region where stibnite solubility is independent of pH between pH = 7 and 9. In this Chapter, equilibrium constants for antimony(III)-sulfide and antimony-hydroxide complexes are derived from stibnite solubility experiments conducted in a flow-through reactor from 70 to 400°C at pressures slightly above saturated water vapor pressure (swvp) up to 300 bars. Experimental conditions were targeted to investigate the behaviour of antimony-sulfide complexes in hydrothermal ore solutions. Thus, fluids with pH between 3 and 9 and sulfide contents between 0.005 and 0.05 mol kg⁻¹ S²⁻_{total} were studied. This is the first study to present measurements of stibnite solubility above the critical point of water.

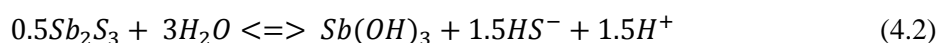
4.1.2. Previous studies of antimony speciation in hydrosulfide solutions at elevated temperatures

Solubility studies

The solubility of stibnite was first measured at elevated temperatures in conjunction with that of cinnabar (HgS) in concentrated Na₂S solutions (~ 0.1 to 0.6 mol kg⁻¹ S²⁻_{total}) from 150°C to 250°C at 100 bars by Learned (1966). In these alkaline, sulfide-rich solutions, stibnite solubility was very high ($\sim 10^{-1}$ mol kg⁻¹ Sb) and increased proportionally with the sulfide concentration. Kolpakova (1982) measured stibnite solubility in acidic to slightly alkaline 0.01 mol kg⁻¹ KCl solutions at 50 and 95°C. In the moderate sulfide concentrations ($\sim 10^{-3}$ mol kg⁻¹ S²⁻_{total}) studied by Kolpakova, the proportional relationship between stibnite solubility and sulfide concentration was maintained, even in the higher pH solutions when the dissolved antimony concentration was greater than the total un-complexed sulfide concentration. Kolpakova interpreted the results in terms of the reaction

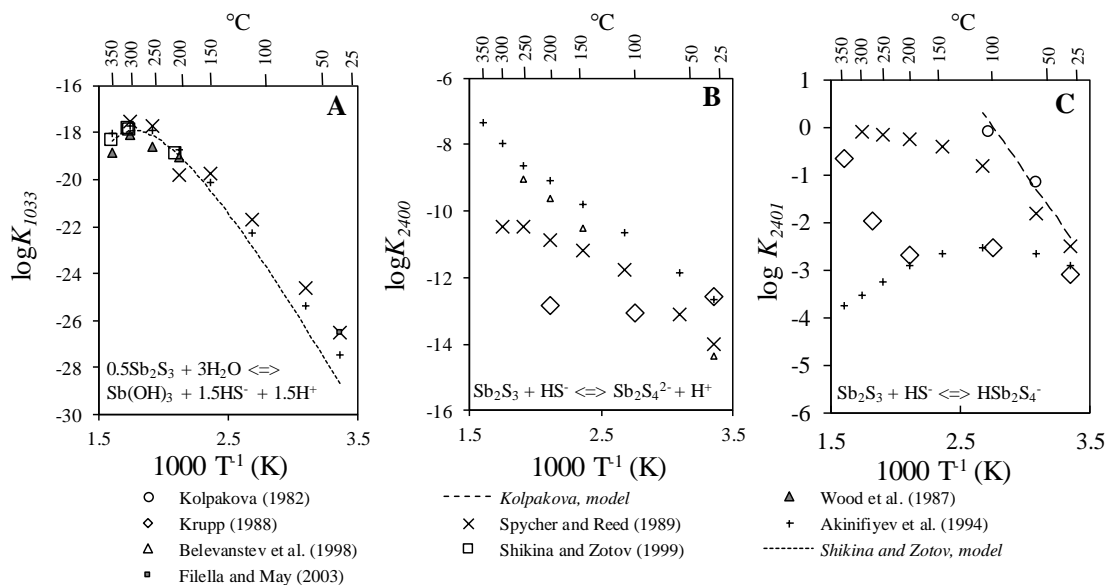


based upon previous studies at 25°C, which identified $HSb_2S_4^-$ as the dominant species in weakly alkaline pH fluids (Kolpakova, 1971). Wood et al. (1987) used antimony complexation models developed by previous researchers to interpret stibnite solubility in H₂O-NaCl-CO₂ solutions from 200 to 350°C as part of an assemblage including pyrite, pyrrhotite, magnetite, sphalerite, galena, bismuthinite, argenitite, gold, and molybdenite. Wood and co-authors attributed most of the dissolved antimony to Sb(OH)₃ due to the low sulfide content available in the pyrite-pyrrhotite-magnetite buffered system, and used their new stibnite solubility data to estimate equilibrium constants for the reaction



The stibnite solubility experiments conducted by Krupp (1988) covered a wider range of temperature (25 to 350°C), pH (2.5 to 11.5), and sulfide concentration ($10^{-2.5}$ to 10^{-1} mol kg⁻¹ S²⁻_{total}) than any previous experimental work. For the moderate sulfide content of these experiments, Krupp presented a speciation model in which the antimony-sulfide dimer, H_xSb₂S₄^{x-2}, was predominant across

Figure (4.1) Previously published values of equilibrium constants for stibnite solubility in terms of (A) $\text{Sb}(\text{OH})_3$ (Equation 4.2), (B) $\text{Sb}_2\text{S}_4^{2-}$, and (C) HSb_2S_4^- (Equation 4.1). If necessary, values have been adjusted to the form of the reaction as displayed in the figure with the K_w and/or $K_{\text{H}_2\text{S}}$ used in the reference, if available, or that consistent with this study.



the entire pH range up to 100 to 150°C. With increasing temperature, the neutral, mixed-ligand dimer $\text{Sb}_2\text{S}_2(\text{OH})_2$ became the predominant species in all but the most alkaline ($\text{pH} > \sim 9$).

Akinifiyev et al. (1994) combined new experimental data at 350°C with data from multiple previous studies from 25 to 350°C to derive a self-consistent set of thermodynamic parameters for the system $\text{Sb}(\text{III})$ - $\text{Sb}(\text{II})$ - H_2O using the Helgeson-Kirkham-Flowers (HFK) formulation (Tanger and Helgeson, 1988). This study used the same sulfide speciation model as Krupp (1988) but rejected the mixed-ligand dimer $\text{Sb}_2\text{S}_2(\text{OH})_2$ in favour of several antimony hydroxide species, primarily $\text{Sb}(\text{OH})_3$, based upon determinations of that species' thermodynamic parameters in the simpler $\text{Sb}(\text{III})$ - H_2O system. As a result, the values of the equilibrium constants for antimony-sulfide complexes from Akinifiyev et al. (1994) and Krupp (1988) are in poor agreement above 200°C. This is shown in Figure (4.1), in which published equilibrium constants values for the reactions represented by Equations (4.1) and (4.2) and stibnite solubility in terms of $\text{Sb}_2\text{S}_4^{2-}$ are compared.

Shikina and Zotov (1999) presented further stibnite solubility experiments at 200 and 300°C that supported the predominance of $\text{Sb}(\text{OH})_3$ in low-sulfide solutions at acidic to neutral pH. Zotov et al. (2003) re-evaluated the standard thermodynamic properties and HFK parameters for $\text{Sb}(\text{OH})_3$ in light of the data from Shikina and Zotov (1999) and new $\text{Sb}(\text{III})$ oxide (senarmonite (Sb_2O_3 , *crubic*) and valentinite (Sb_2O_3 , *rhombic*)) solubility experiments. For the high extremes of pH and sulfide concentration, Belevantsev et al. (1998) fitted a speciation model including $\text{Sb}_2\text{S}_4^{2-}$ and SbS_2^- to previously collected stibnite solubility data for strongly alkaline and very concentrated hydrosulfide ($\geq 0.05 \text{ S}^{2-}_{\text{total}}$) solutions. Their revised equilibrium constant for reaction (4.1) is similar to that derived from lower pH experiments when $\text{Sb}(\text{OH})_3$ is included in the complexation model (Figure 4.1).

X-ray absorption and Raman spectroscopy studies

A limited number of X-ray absorption spectroscopy (XAS) and Raman spectroscopy measurements have been conducted on antimony(III) hydrosulfide solutions above 100°C. These measurements can provide independent qualitative information about the species present in solution to compare with models derived from solubility experiments. Mosselmans et al. (2000) and Sherman et al. (2000) carried out Sb K-edge XAS in sodium sulfide solutions above 100°C. In both of these studies, evidence for the presence of complexes containing OH⁻ ligands, in the form of detectable first shell oxygen atoms and/or a decrease in the total number of first shell sulfur atoms, was found at 150 and 200°C. For some solutions, first shell sulfur atoms and first shell oxygen atoms were equally abundant by 250°C. The measurements presented in Sherman et al. (2000) were almost certainly conducted on the Sb(V)-S(II)-H₂O system due to the solution preparation procedures used, but the behaviour of Sb(III)-S(II) and Sb(III)-O(II) bonds may be qualitatively similar to that of Sb(V)-S(II) and Sb(V)-O(II) bonds. A figure summarizing the changes detected by XAS in antimony's first coordination shell with increasing temperature from 25 to 250°C is included in the Discussion.

In a Raman spectroscopy study from the same era, Gushchina et al. (2000) investigated antimony in two Na₂S solutions with different sulfide concentrations from 25 to 250°C. The spectral features found in this study were summarised in Chapter (2) and shown in Figure (2.1). With increasing temperature, two spectral features became more pronounced: a peak at 280 cm⁻¹ and a shoulder at 380 cm⁻¹. In the 25°C measurements, the spectral feature at 280 cm⁻¹ was associated with low sulfide concentrations relative to antimony concentrations (molar S:Sb < 2:1) and the feature at 380 cm⁻¹ was associated with high sulfide concentrations (molar S:Sb > 15:1). All other peaks that were prominent at 25°C diminished with increasing temperature, especially at and above 175°C. Both Raman and XAS spectroscopic studies are consistent with a significant change in antimony speciation between 100 and 200°C.

4.1.3. Interpretations of the change in stibnite solubility's dependence on sulfide concentration with temperature

Multiple studies have found that stibnite solubility increases with increasing sulfide concentration in acidic to alkaline fluids up to 100 to 150°C. Since the early 1980s, this trend has been interpreted in terms of stibnite solubility being controlled by H₂Sb₂S₄, HSb₂S₄⁻, and Sb₂S₄²⁻, but the reported values for the appropriate stibnite solubility constants vary by up to four orders of magnitude (Figure (4.1); Kolpakova, 1982; Spycher and Reed, 1989; Akinifiyev et al., 1994; Belevantsev et al., 1998; Shikina and Zotov, 1999). At temperatures > ~ 120°C, stibnite becomes more soluble with decreasing sulfide concentration in acidic solutions when the sulfide concentrations are < ~0.01 mol kg⁻¹ S²⁻_{total}. This is consistent with the detection of oxygen atoms in the first coordination shell in some high temperature EXAFS experiments (Mosselmans et al., 2000; Sherman et al., 2000).

Krupp (1988) interpreted the change in stibnite solubility as due to hydroxy ligands replacing non-bridging sulfurs forming a mixed ligand dimer (i.e., $\text{Sb}_2\text{S}_2(\text{OH})_2$). Other studies, which relied on stibnite solubility experiments conducted at lower sulfide concentrations and on thermodynamic data for $\text{Sb}(\text{OH})_3$ derived from the $\text{Sb}(\text{III})\text{-O-H}$ system, have rejected the mixed-ligand species $\text{Sb}_2\text{S}_2(\text{OH})_2$ in favor of increasing stability of $\text{Sb}(\text{OH})_3$ (Akinifiyev et al., 1994; Shikina and Zotov, 1999; Zotov et al., 2003). The stability of $\text{Sb}(\text{OH})_3$ and its contribution to stibnite solubility are quite well constrained with experimental studies from up to 350°C. However, the stoichiometry and stability of antimony-sulfide complexes at higher temperatures are less well studied. A transition from antimony-sulfide ligand interactions to antimony-hydroxide ligand interactions is expected with increasing temperature due to the increasingly “hard” character of metal-ligand interactions as the dielectric constant of water decreases. The combination of temperature, pH, and sulfide activity at which antimony complexation changes from sulfide to hydroxide ligands will be different from other elements, of particular interest are arsenic and gold, and different affinities for the sulfide and hydroxide ligands will affect the relative distribution of these three commonly associated elements (i.e., Sb, As, and Au) in hydrothermal ore deposits.

4.2. Methods

4.2.1. High pressure-temperature flow-through reaction system and solution preparation

Experiments from 70 to 400°C were conducted in a hydrothermal flow-through autoclave reactor. The flow-through approach has previously been used to conduct high-temperature metal sulfide solubility studies (e.g., Stefánsson and Seward, 2004; Tagirov et al., 2007), and a similar apparatus to the one in the current study has been used to investigate water-rock reaction (e.g., Sonney and Mountain, 2013). A diagram of the apparatus is shown in Figure (4.2). The system consisted of two piston pumps that moved fluid from a 1 l fluid reservoir through two 19.3 ml reaction vessels, the second containing stibnite, and through a backpressure regulator at the exit of the system. The reaction vessels were located in separate ovens and, in this study, the first of these vessels was used to pre-heat the solution and the second reaction vessel contained ~ 56 g of crushed and cleaned natural stibnite sieved to between 0.125 and 0.5 mm grain size. Both vessels and all connecting tubing were constructed from titanium. A titanium frit was placed at the entrance and exit of the stibnite reaction vessel to prevent movement of fine stibnite particles into the exit tubing.

The tubing sections between the ovens and between the second oven and the backpressure regulator were wrapped with heating tape to maintain a constant temperature after passage from the first vessel. The temperature of the heating tape between the stibnite reaction vessel and the backpressure regulator was maintained at 10 to 20°C above that in the oven to prevent re-precipitation of stibnite in the exit tubing for experiments up to ~ 330°C. At 350°C and in supercritical experiments,

the temperatures in the tubing and the stibnite reaction vessel were set at the same temperature to avoid stibnite precipitation due to decreasing fluid density with slight increases in temperature. In this experimental system, the pressure was constant throughout. Once the fluid reservoir was filled, the entire system was closed to oxygen and the input fluid conditions remained constant. Each experiment started at 70°C and then stibnite solubility was measured with increasing temperature up to at least 350°C. A minimum of two hours was needed to heat up the ovens and reaction vessels between temperature points. The system was allowed to fully cool to 70°C before the start of the next experiment.

The deoxygenated hydrosulfide solutions were prepared as described previously (Chapter 2). Hydrosulfide solutions with selected pH and sulfide concentrations were made by bubbling H₂S/N₂ gas mixtures through deoxygenated dilute NaOH or HCl solutions in a 2 l flask. The experimental solution was then transferred to the fluid reservoir before each experiment using the flow-through system's pumps. Prior to transferring the solutions, all tubing and lines between the preparation flask and the fluid reservoir were evacuated to exclude oxygen from the solution during transfer. The appropriate H₂S/N₂ gas mixture was slowly passed through the headspace in the flask during the transfer to maintain constant pressure and prevent degassing of H₂S from the solution. The ambient temperature pH and total sulfide content (mol kg⁻¹ S²⁻_{total}) of solutions collected directly from the fluid reservoir were measured at the beginning and end of experiments. These values are the pH and mol kg⁻¹ S_{total} values listed in Table (4.1).

After completion of all the experiments, the flow-through reaction vessel was disassembled and the reacted stibnite was inspected. No secondary mineral phases were observed and the surfaces of

Figure (4.1) Diagram of flow-through autoclave reactor. Experimental solutions are placed in the fluid reservoir under oxygen exclusion and then pumped through the vessels in Oven 1 and then Oven 2 before being collected in a syringe at the exit of the backpressure regulator. The fluid pressure is monitored at the pumps and the backpressure regulator inlet. The temperature is monitored at the entrance and exit of the reaction vessel and in the tubing leading to the backpressure regulator.

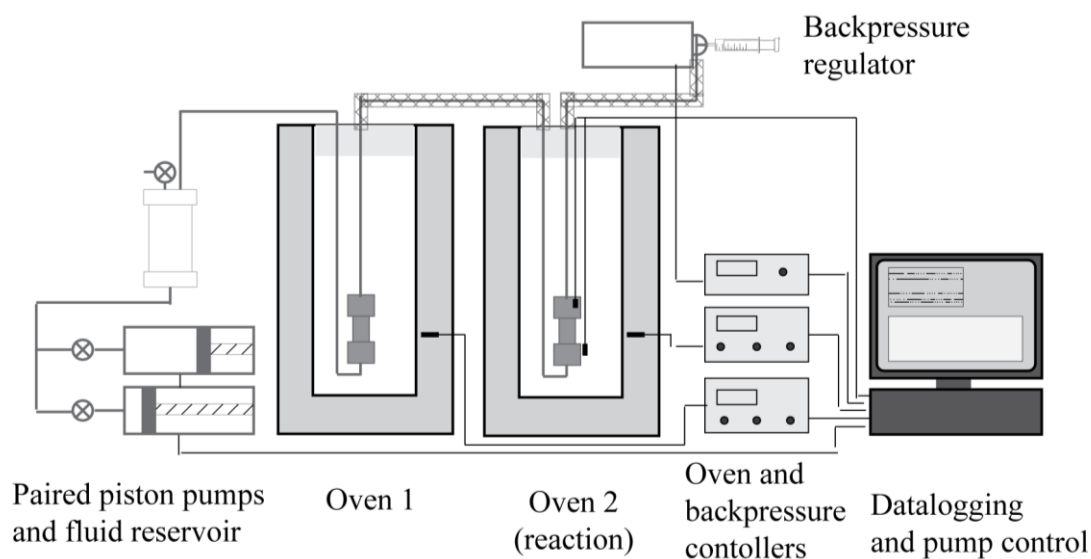


Table (4.1) Input fluid conditions for high temperature experiments.

Exp.	pH _{input}	S ²⁻ _{total} (mol kg ⁻¹)	NaOH ^a or HCl ^b (mol kg ⁻¹)	temperature range
Sb94	7.40	0.023	2.02E-02 ^a	200
Sb97	7.52	0.022	2.02E-02 ^a	150
Sb98	7.11	0.029	2.07E-02 ^a	150 - 300
Sb99	7.24	0.028	2.07E-02 ^a	100 - 350
Sb100	6.45	0.012	3.08E-03 ^a	70 - 400
Sb101	4.61	0.009	0.0	70 - 230
Sb102	3.53	0.009	2.99E-04 ^b	70 - 400
Sb103	3.57	0.028	2.84E-04 ^b	70 - 150
Sb104	5.04	0.011	5.10E-05 ^a	70 - 400
Sb105	7.15	0.003	2.00E-03 ^a	70 - 400
Sb106	5.88	0.011	9.26E-04 ^a	70 - 350
Sb107	8.55	0.010	1.04E-02 ^a	70 - 400
Sb108	8.43	0.050	5.03E-02 ^a	70 - 300
Sb109	6.41	0.024	6.74E-03 ^a	70 - 350

^a Experiments with NaOH added to the initial solution

^b Experiments with HCl added to the initial solution

None of the high temperature experiments contained both HCl and NaOH

the reacted stibnite had metallic lustre and did not shown evidence of oxidation under magnification. Scanning electron microprobe (SEM) images of stibnite grains after completion of experiments showed that the grains in the reaction vessel had embayed grain boundaries indicative of dissolution (Figure A.2). X-ray fluorescence (XRF) analyses (i.e., Sb and S concentrations) of these grains were consistent with stoichiometric stibnite. Amorphous Sb-S phases or antimony-oxide minerals, such as senarmonite, were not observed by visual inspection of the reacted grains or by SEM or XRF.

4.2.2. Sample collection

The experimental solutions were collected directly into a 50ml syringe at the exit of the backpressure regulator. For experiments up to 150°C, the solution was collected into an empty syringe. The output pH of this solution was determined at ambient temperature using a Metrohm pH meter (calibrated daily), and the total sulfide content was measured by idiometric back titration. For higher temperatures, the solution was collected into a syringe containing a measured amount of chilled NaOH solution. This was done to prevent precipitation of stibnite upon cooling and to prevent the flashing of the solution upon exiting the back pressure regulator. The amount and concentration of the NaOH solution was such that the final NaOH concentration in the sample was appropriate for direct measurement by ICP-OES (i.e., 0.08 mol kg⁻¹ NaOH). The total sulfide concentration, but not the output pH, was measured in the 200 to 400°C samples. The analysis of total antimony by ICP-OES was the same as that described in Chapter (2). The pH was measured at room temperature and is listed

as pH_{exit} in Table (A.2). In preliminary tests, the total antimony and sulfide concentrations in solutions collected in empty syringes or in collected in syringes containing a NaOH solution were the same for the 70 to 150°C experiments, indicating that collection into an alkaline solution was not needed for these more moderate temperatures.

4.2.3. Speciation of solutions and calculation of pH

The pH of the solution at the experimental temperature and pressure was calculated from the charge balance of the solution considering the following components: OH^- , H^+ , HS^- , H_2S° , $NaHS^\circ$, $NaOH^\circ$, Na^+ , Cl^- , HCl° , and the appropriate antimony species for each speciation model. These are the same components as considered in Chapter (2), with the addition of HCl° and Cl^- . The mass action and mass balance relationships for the first seven components were defined in Chapter (2) in Equations (2.13) through (2.22). The dissociation of the ion pair HCl° is given by



for which the equilibrium constant is defined as

$$K_{HCl^\circ} = m_{H^+} \cdot \gamma_{H^+} \cdot m_{Cl^-} \cdot \gamma_{Cl^-} \cdot m_{HCl^\circ}^{-1} \cdot \gamma_{HCl^\circ}^{-1} \quad (4.4)$$

Experimental solutions contained additions of HCl or NaOH but never both. Thus, the $NaCl^\circ$ ion pair was not included in calculations. The mole fractions of the total sulfide, sodium, and chloride present as HS^- , Na^+ , and Cl^- (i.e., X_{HS^-} , X_{Na^+} , and X_{Cl^-}) are given by the following equations, which are developed in Appendix (A):

$$X_{HS^-} = \frac{m_{HS^-}}{m_{S_{free}}} = \frac{1}{1 + \frac{a_{H^+} \gamma_{H^+}}{K_{H_2S}} + \frac{\gamma_{HS^-} \gamma_{Na^+} m_{Na^+}}{K_{NaHS^\circ}}} \quad (4.5)$$

$$X_{Na^+} = \frac{m_{Na^+}}{m_{Na_{total}}} = \frac{1}{1 + \frac{\gamma_{Na^+} \gamma_{HS^-} m_{HS^-}}{K_{NaSH^\circ}} + \frac{\gamma_{Na^+} K_w}{K_{NaOH^\circ} a_{H^+}}} \quad (4.6)$$

$$X_{Cl^-} = \frac{1}{1 + \frac{\gamma_{Cl^-} \gamma_{H^+} m_{H^+}}{K_{HCl^\circ}}} \quad (4.7)$$

These fractions occur in the following balance equations that were used to calculate pH for the experiments containing NaOH (Equation 4.8) or HCl (Equation 4.9):

$$0 = m_{H^+} - m_{OH^-} - m_{S_{free}} \cdot X_{HS^-} + m_{Na_{total}} \cdot X_{Na^+} + \sum^{xyzw} (3x - 2y - 2z + w) \cdot m_{Sb_x S_y O_z H_w} \quad (4.8)$$

$$0 = a_{H^+} \cdot \gamma_{H^+}^{-1} - a_{OH^-} \cdot \gamma_{OH^-}^{-1} - m_{S_{free}} \cdot X_{HS^-} - m_{Cl_{total}} \cdot X_{Cl^-} + \sum^{xyzw} (3x - 2y - 2z + w) \cdot m_{Sb_x S_y O_z H_w} \quad (4.9)$$

In these equations, w , x , y , and z are variables that define the stoichiometry of various antimony complexes as developed previously in the Methods section of Chapter (2).

The amount of sulfide complexed with antimony was taken into account in Equations (4.5) through (4.7) by using $m_{S_{free}}$ to calculate m_{HS^-} . As discussed in the text with Equation (2.22), $m_{S_{free}}$ is the amount of the total sulfide not complexed with antimony and is defined as

$$m_{S_{free}} = m_{S_{total}} - m_{S_{complexed}} = m_{H_2S^\circ} + m_{SH^-} + m_{NaSH^\circ} - \sum^{xyzw} y \cdot m_{Sb_x S_y O_z H_w} \quad (4.10)$$

Table (4.2) Summary of supporting thermodynamic data.

Reaction	70°C	150°C	250°C	350°C	400°C	Reference
$\text{H}_2\text{O} \rightleftharpoons \text{H}^+ + \text{OH}^-$	-12.813	-11.637	-11.193	-12.295	-22.497	a
$\text{H}_2\text{S}_{(\text{aq})} \rightleftharpoons \text{H}^+ + \text{HS}^-$	-6.564	-6.495	-7.163	-8.908	-18.033	b
$\text{NaOH}^\circ \rightleftharpoons \text{Na}^+ + \text{OH}^-$	0.304	-0.269	-0.916	-1.844	-5.187	c
$\text{NaSH}^\circ \rightleftharpoons \text{Na}^+ + \text{HS}^-$	0.870	0.378	-0.286	-1.457	-6.574	d
$\text{HCl}^\circ \rightleftharpoons \text{H}^+ + \text{Cl}^-$	0.702	0.411	-0.422	-2.234	-9.868	e
Debye-Hückel Parameters						
A	0.5455	0.6975	0.9594	1.9108	3.1077	f
B	3.370E+07	3.570E+07	3.83E+07	4.08E+07	4.21E+07	f
Bdot	0.044	0.047	0.03	0	0	g

a. Marshall and Franck (1981)

b. Suleimenov and Seward (1997) and modified following Stefánsson and Seward (2004), see text

c. Ho and Palmer (1996)

d. Ho et al. (1994), by analogy with NaCl[°]

e. Ruaya and Seward (1987) up to 100°C and Ho et al. (2001) at higher temperatures

f. Helgeson and Kirkham (1974)

g. Helgeson (1969)

*log K are at 1 bar to 70°C, at swvp for 150 to 350°C, and at 200 bar for 400°C

K_w , $K_{\text{H}_2\text{S}}$, K_{NaOH° , and K_{NaHS° are defined by Equations (2.17) through (2.20).

The speciation and charge balance calculations were performed in two iterative loops within the non-linear least squares refinement of stibnite solubility constants. First, the fluid was speciated using an estimated pH and an initial estimate of the solution's ionic strength. The pH was then varied until the solution was charged balanced within the fitting constraints (10^{-9} to 10^{-10}) using the Solver add-in to Excel (Fylstra et al., 1998). The new ionic strength calculated from this balanced solution was used to adjust (or re-speciate) the solution model, and the refinement procedure was repeated until the ionic strength of consecutive iterations converged. Charged antimony complexes were included in the calculation of ionic strength, as in Chapter (2), with the addition of an additional term to Equation (2.24). The a_{H^+} and a_{HS^-} from this procedure were inputs to the non-linear least squares fitting.

The activity coefficients for charged species were calculated using an extended version of the Debye-Hückel equation (Equation 2.23). The activity coefficients of neutral species were set to unity. The temperature dependence of the ion-independent parameters A, B, and \tilde{B} (or B-dot) were calculated from polynomial best fits to tabulations of the values in Helgeson (1969) and Helgeson and Kirkham (1974). The pressure dependence of these parameters is small over the pressure range of this study and so was not considered. At and above 300°C, the \tilde{B} parameter was set to zero so that the B-dot extension reduced to the conventional, extended Debye-Hückel equation. The ion size parameter, \tilde{a} , was assumed to be independent of temperature, and thus the values used were the same as those listed in Chapter (2) for Na⁺, OH⁻, HS⁻, H⁺ and antimony species. A value of 3×10^{-8} was used for the ion size parameter of Cl⁻ (Kielland, 1937).

The sources for the equilibrium constants at the physical conditions of the experiments are summarised in Table (4.2), in which the values are listed for select temperatures. The sources are the same as in Chapter (2) for the ion product of water, the dissociation constant of NaHS° (taken as analogous to NaCl°), and the dissociation constant of NaOH° (Marshall and Franck, 1981; Ho et al., 1994; Ho and Palmer, 1996). The dissociation constant of HCl° was taken from Ruaya and Seward (1987) for temperatures up to 250°C. Above 250°C, a three term density equation from Ho et al. (2001) was used. For the first dissociation constant of H_2S° , the equation at swvp from Suleimenov and Seward (1997) was modified for increased pressure using the molar volume change of the reaction reported by Ellis and McFadden (1972) up to 250°C. Above 250°C, a four term density equation was used to extrapolate the dissociation constant to 350°C (Mesmer et al., 1988; Stefánsson and Seward, 2004). The density of the fluid was calculated from the measured temperatures and pressures according to the IAPWS-IF97 industrial standard (Wagner et al., 2000; Spang, 2002).

4.2.4. Fitting of heterogeneous solubility constants

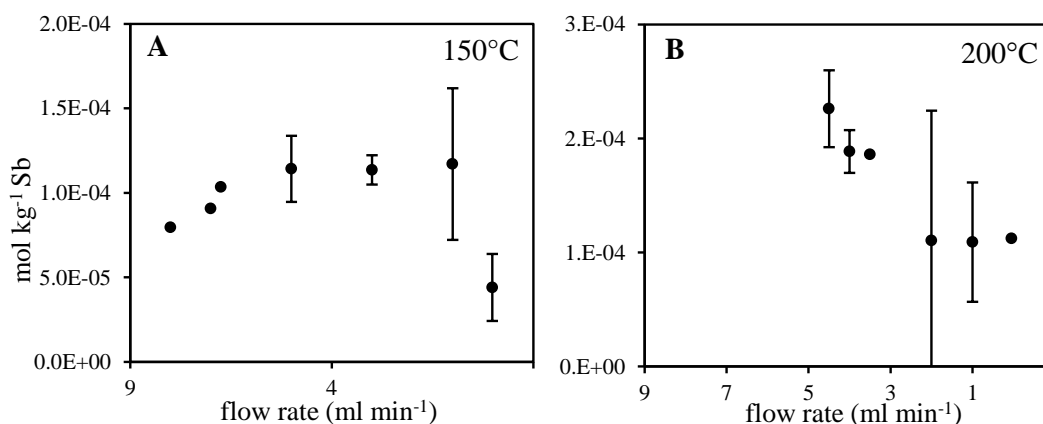
Determination of the values for heterogeneous solubility constants (K_{xyzw} , Equation 2.6) for different antimony speciation models was completed using a non-linear least squares fitting procedure as described in Chapter (2) in Section (2.2.3), with the exception that a_{H^+} was the pH calculated for experimental temperatures rather than the pH measured at ambient temperature. The inputs to the fitting procedure were a_{H^+} , a_{HS^-} , ionic strength (I), and the measured stibnite solubility ($\text{mol kg}^{-1} \text{Sb}_{\text{total}}$). Fits were conducted using data collected at constant temperature, and the values for K_{xyzw} determined from the non-linear least squares fitting were used to recalculate the distribution of aqueous species and the pH. This iterative process was repeated until K_{xyzw} converged and the calculated pH did not change between successive iterations.

4.3. Results

4.3.1. Attainment of equilibrium

In preliminary experiments, stibnite solubility was measured at various flow rates at 150 and 200°C to evaluate if the system was at equilibrium. A plateau in measured antimony concentration with decreasing flow rate between 3 and 7 ml min^{-1} flow rate was taken to indicate that the system was at equilibrium and is shown for both temperatures in Figure (4.3). A decrease in antimony concentration at flow rates $< \sim 1 \text{ ml min}^{-1}$ was due to antimony sulfide precipitation (both stibnite and amorphous antimony sulfide) during fluid cooling at the exit to the flow through system. A decrease in concentration at flow rates of $> 7 \text{ ml min}^{-1}$ may indicate that the system has not reached equilibrium during the fluid residence time at 150°C. At temperatures $> 150^\circ\text{C}$, reaction kinetics were faster and equilibrium was reached at faster flow rates. Flow rates of 4.5 to 5 ml min^{-1} were used during experiments from 70 to 200 and flow rates of 6 to 7 ml min^{-1} at higher temperatures, with 7 ml min^{-1}

Figure (4.3) Stibnite solubility at different flow rates at 150°C (A) and 200°C (B). Flow rate test were conducted using slightly alkaline solutions containing moderate sulfide (pH ~7.5 and 0.02 mol kg⁻¹ S²⁻_{total}; Sb94 and Sb97). Error bars are 2σ from the median solubility. Data points without error bars are individual measurements.



being the fastest flow rate that could be used at 350 to 400°C without flashing of the solution during collection into a syringe containing a weighed amount of chilled NaOH solution.

4.3.2. Pressure dependence of stibnite solubility from 100 to 350°C

Stibnite solubility experiments in this study were generally conducted at slightly above swvp. However, in five experiments, additional measurements of stibnite solubility were taken at higher pressures up to 250 bars to determine the effect of pressure on stibnite solubility in this temperature range. The results of these measurements are shown in Figure (4.4), in which are plotted the stibnite solubilities measured at constant temperature and various pressures for several solutions with different pH and sulfide concentrations. As can be seen from Figure (4.4), stibnite solubility is independent of pressure within the error of the solubility measurements from 110 to 350°C.

Figure (4.4) Variation in stibnite solubility with pressure at constant temperature and input fluid conditions for five experiments from 110 to 350°C. Pressure and antimony concentration error bars are 2σ.

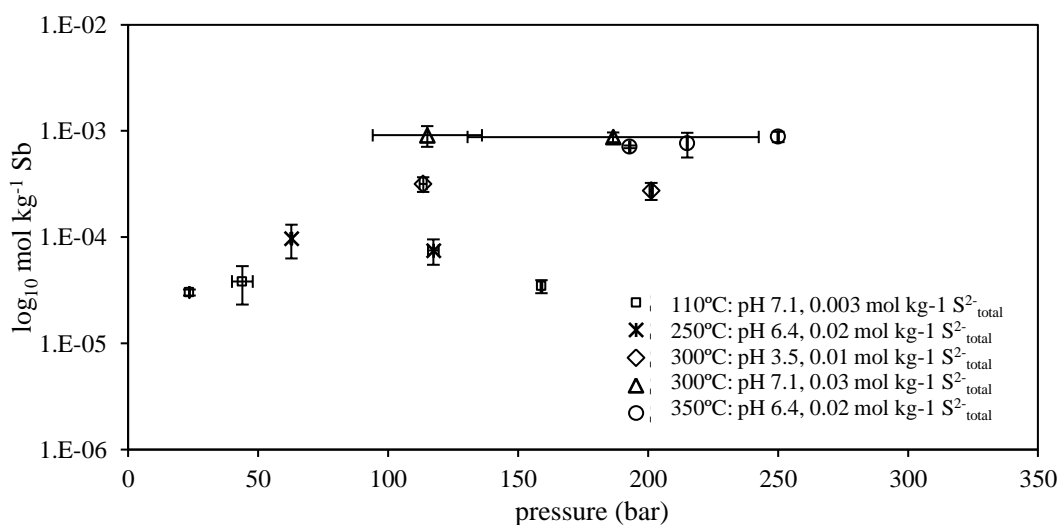
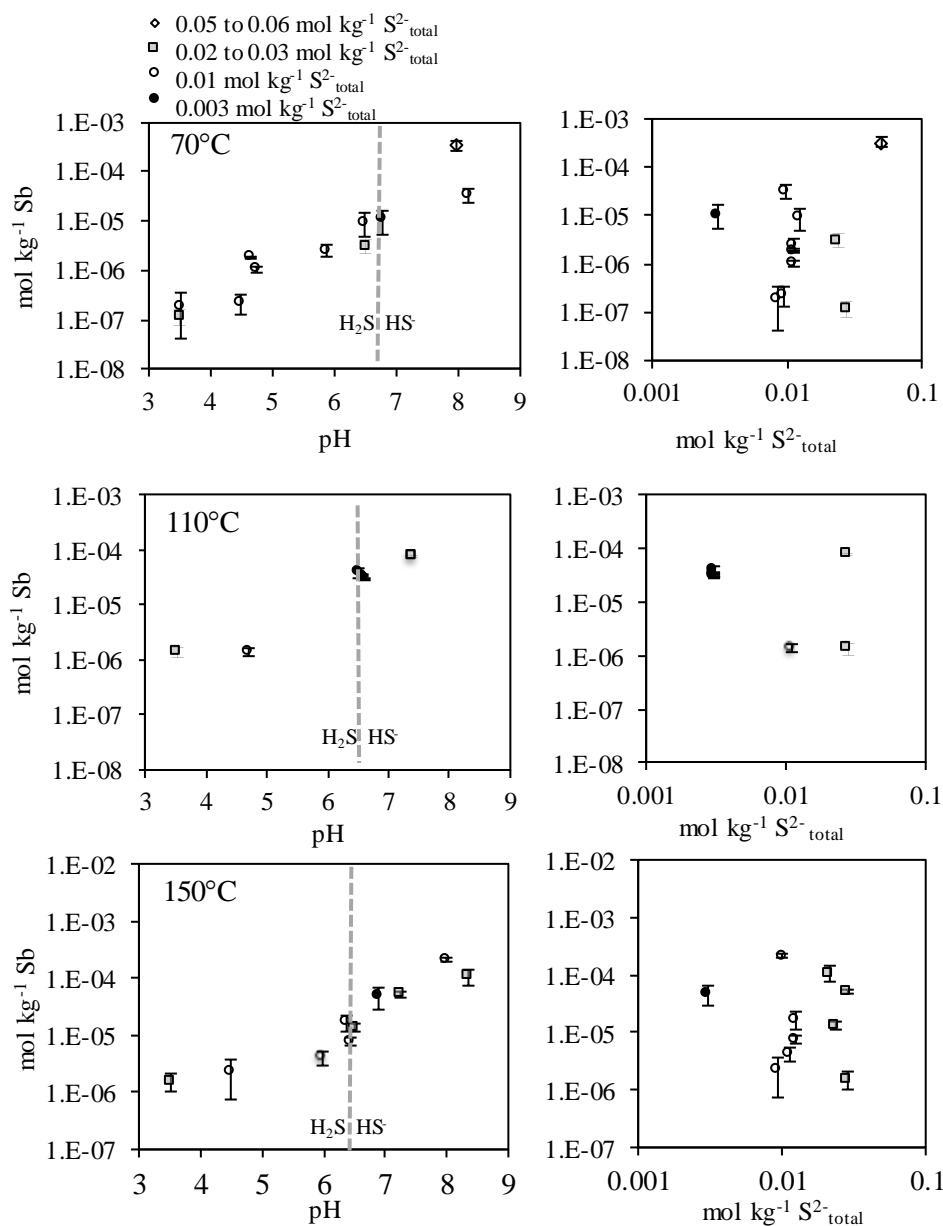


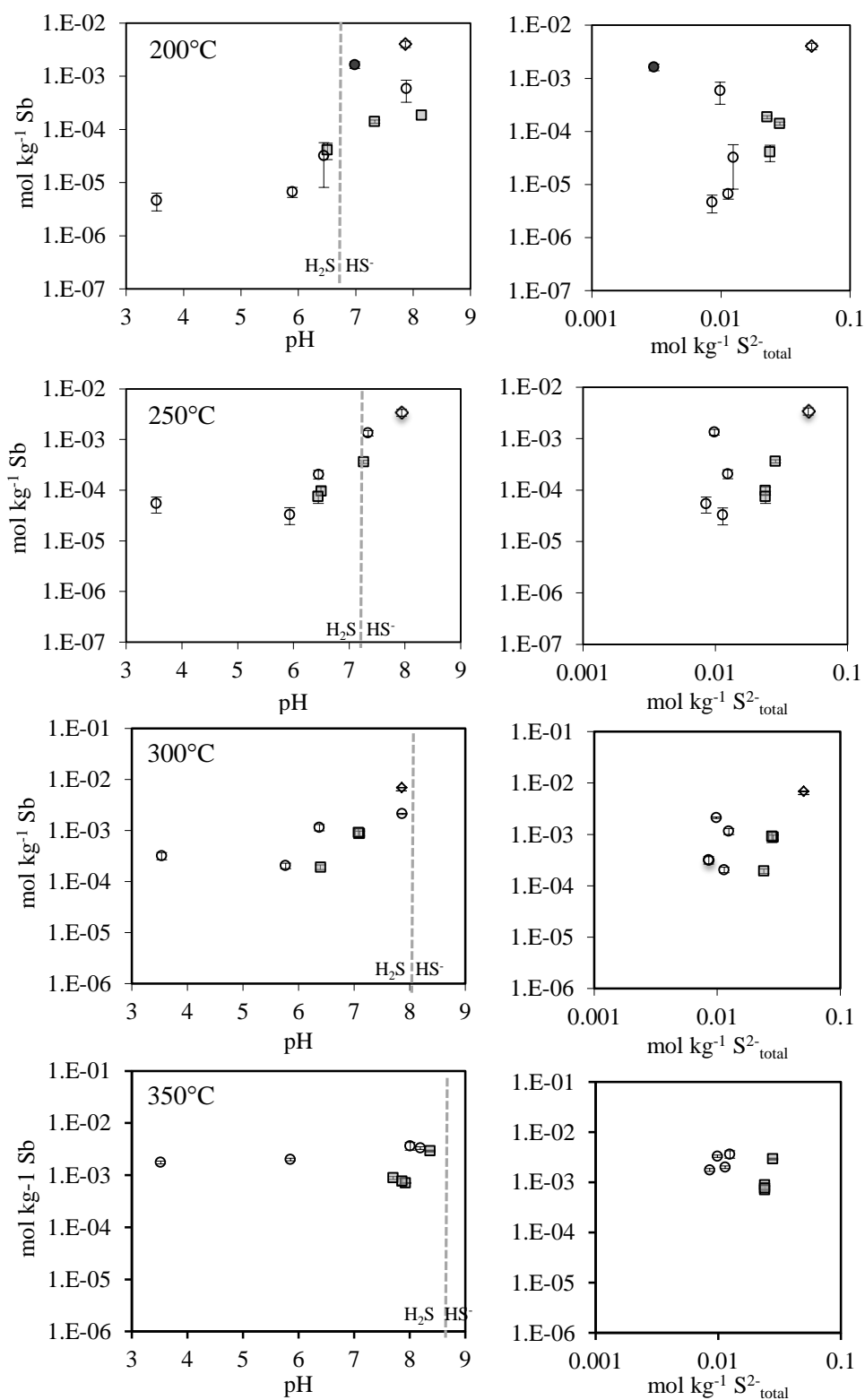
Figure (4.5) Measured stibnite solubility from 70 to 350°C plotted with respect to pH (left) and sulfide concentration (right). Range of sulfide concentrations are indicated by symbols: black circles $\sim 0.003 \text{ mol kg}^{-1} \text{ S}^{2-}_{\text{total}}$, open circles $\sim 0.01 \text{ mol kg}^{-1} \text{ S}^{2-}_{\text{total}}$, gray squares 0.02 to 0.03 $\text{mol kg}^{-1} \text{ S}^{2-}_{\text{total}}$, and open diamonds = 0.05 to 0.06 $\text{mol kg}^{-1} \text{ S}^{2-}_{\text{total}}$. Error bars are 2σ .



4.3.3. General changes in stibnite solubility with temperature

The results from stibnite solubility experiments from 70 to 350°C are shown in Figure (4.5), in which measured stibnite solubilities are plotted without projection to constant sulfide or pH. The complete stibnite solubility results are tabulated in Appendix (A). The shape of the stibnite solubility curve with respect to pH and the dependence of stibnite solubility on sulfide concentration changed as the temperature increased from 70 to 400°C. From 70 to 150°C, the general shape of the stibnite solubility curve was similar to that at 30°C. As at 30°C, stibnite solubility was independent of pH at

Figure (4.5) continued...



pH < 5 at 150°C, indicating the presence of a neutral complex. At pH > 5, stibnite solubility generally increased with increasing pH but was independent of pH for a small pH region around where pH = pKa of H₂S°. Fitting of this feature required partially protonated antimony-sulfide dimers as at 30°C. Above 150°C, the prominence of the plateau in stibnite solubility at pH near the pKa of H₂S° diminished, and at temperatures ≥ 250°C, it was no longer present. Over the same temperature range, stibnite solubility became negatively rather than positively related to the sulfide concentration across the entire pH range except for the most alkaline experiments (pH ~ 8.5). These general patterns suggest that antimony-sulfide dimers (i.e., HSb₂S₄⁻ and Sb₂S₄²⁻) were replaced by Sb(OH)₃, and possibly other mixed-ligand complexes, as the temperature increased above 150°C at the moderate sulfide concentrations (0.01 to 0.02 mol kg⁻¹ S²⁻_{total}). At 400°C, stibnite solubility was 0.015 to 0.016 mol kg⁻¹ Sb (nearly 2000 ppm) at 300 bars. Stibnite solubility in supercritical fluids decreased by approximately two orders of magnitude with a pressure decrease from 300 to 200 bars.

4.3.4. Fitting of stibnite solubility from 70 to 350°C

Stibnite solubility at 70 and 110°C

The heterogeneous stibnite solubility reactions relevant to the following discussion are presented in Table (4.3). A complete set of reactions considered in the interpretation of measured solubility curves was presented Table (2.2). Plots of the results for selected fits are shown with the results of fits in Tables (4.4) through (4.8). For the 70 and 110°C solubility data, the species HSb₂S₄⁻ was able to fit most of the experimental data (Table 4.4) except at the high and low pH ends of the data range. Fitting these pH extremes required a neutral species at pH < 4 and a species producing a Sb/pH slope ~ +1 (i.e., Sb₂S₄²⁻) at pH > 7.5 (Fit 70-A). The limited number of solubility experiments at low pH meant that the Sb-S-O stoichiometry of the neutral complex could not be determined for each

Table (4.3) Summary of heterogeneous stibnite solubility reactions. Reactions included in following tables of fit results (i.e., Tables (4.4) through (4.8)). See Chapter (2) for complete set of aqueous antimony species considered (Table 2.2).

K _{xyzw}	Aqueous antimony species	Reaction
antimony-hydroxide complexes		
K ₁₀₃₃	Sb(OH) ₃	0.5Sb ₂ S ₃ + 3H ₂ O = Sb(OH) ₃ + 1.5HS ⁻ + 1.5H ⁺
K ₁₀₃₂	H ₂ SbO ₃ ⁻	0.5Sb ₂ S ₃ + 3H ₂ O = H ₂ SbO ₃ ⁻ + 1.5HS ⁻ + 2.5H ⁺
antimony-sulfide complexes		
K ₂₄₀₀	Sb ₂ S ₄ ²⁻	Sb ₂ S ₃ + HS ⁻ = Sb ₂ S ₄ ²⁻ + H ⁺
K ₂₄₀₁	HSb ₂ S ₄ ⁻	Sb ₂ S ₃ + HS ⁻ = HSb ₂ S ₄ ²⁻
antimony-hydroxide-sulfide (mixed-ligand) complexes		
K ₁₂₁₁	HSbS ₂ O ²⁻	0.5Sb ₂ S ₃ + 0.5HS ⁻ + H ₂ O = HSbS ₂ O ²⁻ + 1.5H ⁺
K ₁₂₁₂	H ₂ SbS ₂ O ⁻	0.5Sb ₂ S ₃ + 0.5HS ⁻ + H ₂ O = H ₂ SbS ₂ O ⁻ + 0.5H ⁺
K ₁₂₁₃	H ₃ SbS ₂ O	0.5Sb ₂ S ₃ + 0.5HS ⁻ + H ₂ O + 0.5H ⁺ = H ₃ SbS ₂ O

Table (4.4) Fits of stibnite solubility at 70 and 110°C. Accompanying each fit are plots of the data and the fit at experimental sulfide concentrations (*left*), the relative residuals of the fit (*middle*), and the data and the distribution of species at 0.01 mol kg⁻¹ S²⁻_{total} (*right*). K is the equilibrium constant for the appropriate reaction from Table (4.3.), σ is one standard deviation, p and R^2 are fit statistics defined below, and N is the number of data points for each fit.

Fit	Reaction ^a	Aqueous antimony species	K	σ	p^b	R^2^c	pH range	N
70-A	K_{2400}	$\text{Sb}_2\text{S}_4^{2-}$	1.3E-11	2.2E-11	0.58	0.57	3.5 to 7.7	8
	K_{2401}	HSb_2S_4^-	6.6E-04	2.7E-04	0.06			
	K_{1213}	$\text{H}_3\text{SbS}_2\text{O}$	1.5E-03	1.9E-03	0.47			
110-A	K_{2401}	HSb_2S_4^-	2.4E-03	0.8E-03	0.04	0.66	3.5 to 6.7	6
	K_{1213}	$\text{H}_3\text{SbS}_2\text{O}$	1.2E-02	0.3E-02	0.02			

Relative residual is the difference between the fit and measured antimony concentrations normalized to the solubility, i.e. $(\text{mol kg}^{-1} \text{ Sb}_{\text{exp}} - \text{mol kg}^{-1} \text{ Sb}_{\text{fit}}) / \text{mol kg}^{-1} \text{ Sb}_{\text{exp}}$

^a K_{xyzw} as defined in Table (4.3)

^b The p value is $\text{Prob}(t)$ for the null hypothesis that $K=0$, i.e. values approaching 1 indicate that a species can be removed without changing the fit.

^c R^2 is the ratio of variation in the data explained by the fit to the total variation in the data, i.e. $R^2 = \frac{\sum_{i=1}^N (\hat{y}_i - \bar{y})^2}{\sum_{i=1}^N (y_i - \bar{y})^2}$, where y_i is the antimony concentration of the i^{th} data point, \bar{y} is the mean of N data points, and \hat{y}_i is the fit to the i^{th} data point.

temperature independently and the species used in the 30°C model have been used. Both species $\text{H}_2\text{Sb}_2\text{S}_4$ and H_3SbSO_2 could be used to fit the 70 to 150°C data, but the goodness of fit statistics of fits with $\text{H}_2\text{Sb}_2\text{S}_4$ or H_3SbSO_2 were not as good as those with $\text{H}_3\text{SbS}_2\text{O}$ (fits not shown). The experimental data at 70°C barely extended up to the alkaline pH where $\text{Sb}_2\text{S}_4^{2-}$ was present and so the fitted value for the equilibrium constant for $\text{Sb}_2\text{S}_4^{2-}$ (K_{2400}) has a larger uncertainty than at other temperatures.

Attempts to include $\text{H}_2\text{Sb}_2\text{S}_5^{2-}$ in fits of 70°C and higher temperature data failed because the solubility versus pH slope which the species produces at $\text{pH} < \text{pK}_a$ of H_2S° (i.e., a Sb/pH slope = +2) was not representative of the data. A solubility curve using $\text{H}_2\text{Sb}_2\text{S}_5^{2-}$ has a +2 slope at $\text{pH} < \text{pK}_a$ of H_2S , but the experimental curve was best fit by species with a +1 slope from $\text{pH} = 5$ to 7 (i.e., by a

singly charged negative species at $\text{pH} < \text{pK}_a$ of H_2S°). At 70°C , fits including singly charged complexes other than HSb_2S_4^- (i.e., $\text{H}_2\text{SbS}_2\text{O}^-$ and H_2SbS_3^-) did not improve the quality of the fit (i.e., $\text{H}_2\text{SbS}_3^- + \text{SbS}_3^{3-}$) or they were unable to fit the data in the alkaline region (i.e., $\text{H}_2\text{SbS}_2\text{O}^-$). Thus, $\text{Sb}_2\text{S}_4^{2-}$ and HSb_2S_4^- are considered to be the major aqueous antimony species at 70°C at moderate sulfide concentrations (0.01 to 0.02 mol kg^{-1}) and at $\text{pH} = 4$ to 8 .

For a limited number of experiments ($N = 6$), stibnite solubility was also measured at 110°C . The pH range of these experiments did not extend high enough to include $\text{Sb}_2\text{S}_4^{2-}$, and fits of these experiments were used to improve the interpolation of equilibrium constants for HSb_2S_4^- and $\text{H}_3\text{SbS}_2\text{O}$ between 70 and 150°C (Fit (110-A) in Table (4.4)).

Stibnite solubility from 150 to 250°C

At 150°C , the inclusion of HSb_2S_4^- in the model produced a good fit to the stibnite solubility data between $\text{pH} \approx 5$ to 7 and $\text{Sb}_2\text{S}_4^{2-}$ contributed significantly at $\text{pH} > 8$, but fitting of the data from experiments with mildly acidic and alkaline fluids required the addition of antimony species with a negative dependence on the sulfide concentration (i.e., $\text{Sb}(\text{OH})_3$, H_3SbSO_2 , or $\text{H}_2\text{SbSO}_2^-$). The preferred speciation model for stibnite solubility at 150°C is shown in Table (4.5). In this fit (Fit 150-A), four aqueous antimony species are responsible for stibnite solubility: $\text{Sb}_2\text{S}_4^{2-}$, HSb_2S_4^- , $\text{H}_3\text{SbS}_2\text{O}$, and $\text{Sb}(\text{OH})_3$. This speciation model is similar to the speciation model for 30 and 70°C (i.e., $\text{Sb}_2\text{S}_4^{2-} + \text{HSb}_2\text{S}_4^- + \text{H}_3\text{SbS}_2\text{O}$) with the addition of $\text{Sb}(\text{OH})_3$, which contributed significantly to stibnite solubility at $\text{pH} < 5$ and at $\text{pH} > 7$ when $\text{S}^{2-}_{\text{total}} \leq 0.02 \text{ mol kg}^{-1}$. Previously published values (Spycher and Reed, 1989; Akinifiyev et al., 1994; Shikina and Zotov, 1999) for stibnite solubility in terms of $\text{Sb}(\text{OH})_3$ (Reaction (4.2), K_{1033}) ranged from 3.16×10^{-21} to 1.7×10^{-20} at 150°C , as shown graphically in Figure (4.1). The value obtained in this study is $K_{1033} = 2.2 \times 10^{-19}$ (from Fit 150-A).

At 150°C , there was one experiment and only one sulfide concentration at strongly alkaline conditions. Thus, the Sb-S stoichiometry of the species present here could not be determined uniquely from the data. The species $\text{Sb}_2\text{S}_4^{2-}$ was selected at alkaline pH because HSb_2S_4^- produced the best fits to the circumneutral region and $\text{Sb}_2\text{S}_4^{2-}$ was necessary to reproduce stibnite solubility in the alkaline region at 200 and 250°C .

To confirm if HSb_2S_4^- is still the best species to reproduce the distinctive shape of the stibnite solubility curve at $\text{pH} \approx \text{pK}_a$ of H_2S , fits using other singly charged species (i.e., $\text{H}_2\text{SbS}_2\text{O}^-$ and H_2SbS_3^-) were completed at 150 , 200 , and 250°C . An example of such fits at 150°C follow Fit (150-A) in Table (4.5). A good fit could be obtained with the $\text{H}_x\text{SbS}_2\text{O}^{3-x}$ series (i.e., $\text{H}_3\text{SbS}_2\text{O}$, $\text{H}_2\text{SbS}_2\text{O}^-$, and $\text{HSbS}_2\text{O}^{2-}$; Fit 150-B), but fits using these species diverged from the measured solubility data at $\text{pH} > 7$ both at 150 and at 200°C . This is because species $\text{H}_2\text{SbS}_2\text{O}^-$ was unable to reproduce the change in the slope of stibnite solubility versus pH curve at neutral pH and consistently overestimated the stibnite solubility at $\text{pH} > 7$. As a result, the relative residuals from Fit (150-B) were all negatively biased at $\text{pH} > 6$ (see the middle plot accompanying Fit (150-B)). In contrast, the fit at 150°C using HSb_2S_4^- produced a random distribution of residuals across the experimental pH range. Combinations

Table (4.5) Preferred fit of stibnite solubility at 150°C (150-A) and fits demonstrating misfit of speciation models including $\text{H}_2\text{SbS}_2\text{O}^-$ (150-B) and H_2SbS_3^- (150-C). Accompanying each fit are plots of the data and the fit at experimental sulfide concentrations (*left*), the relative residuals of the fit (*middle*), and the data and the distribution of species at 0.01 mol kg⁻¹ $\text{S}^{2-}_{\text{total}}$ (*right*). K is the equilibrium constant for the appropriate reaction from Table (4.3.), σ is one standard deviation, p and R^2 are fit statistics defined in Table (4.4), and N is the number of data points for each fit.

Fit	Reaction ^a	Aqueous antimony species	K	σ	p	R ²	pH range	N
150-A	K_{2400}	$\text{Sb}_2\text{S}_4^{2-}$	2.3E-11	1.0E-11	0.07	0.99	3.5 to 7.8	9
	K_{2401}	HSb_2S_4^-	9.1E-04	1.0E-04	0.0002			
	K_{1213}	$\text{H}_3\text{SbS}_2\text{O}$	1.5E-02	0.6E-02	0.05			
	K_{1033}	$\text{Sb}(\text{OH})_3$	2.0E-19	0.3E-19	0.002			
150-B	K_{1211}	$\text{HSbS}_2\text{O}^{2-}$	7.0E-16	1.7E-16	0.007	0.98	3.5 to 7.8	9
	K_{1212}	$\text{H}_2\text{SbS}_2\text{O}^-$	1.2E-07	0.1E-07	5.E-05			
	K_{1213}	$\text{H}_3\text{SbS}_2\text{O}$	2.0E-02	0.7E-02	0.02			

Relative residual is the difference between the fit and measured antimony concentrations normalized to the solubility, i.e. (mol kg⁻¹ Sb_{exp} - mol kg⁻¹ Sb_{fit}) / mol kg⁻¹ Sb_{exp}

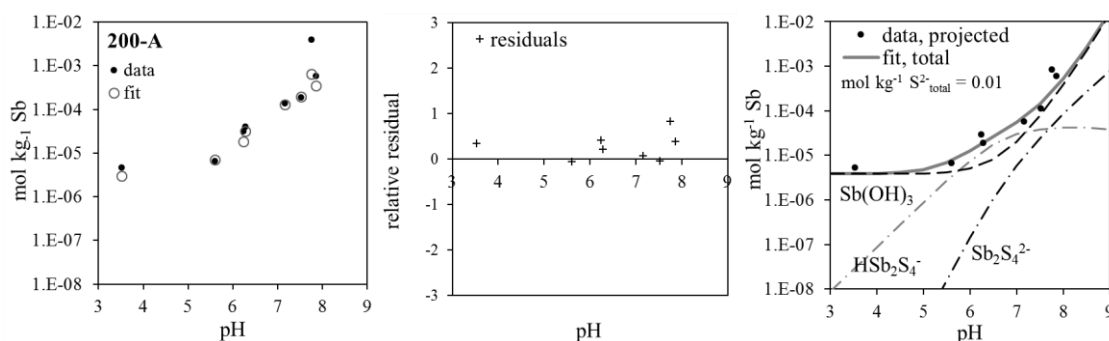
^a K_{xyzw} as defined in Table (4.3)

of partially Sb-S monomers ($\text{H}_3\text{SbS}_3^{x-3}$) produced fits with poor statistics relative to fits which included HSb_2S_4^- .

At 200°C, fits including $\text{Sb}(\text{OH})_3$ and HSb_2S_4^- were able to fit all of the data from pH = 3.5 to 8 except for in the most alkaline solutions containing the highest sulfide concentration (Table 4.6). This individual point at pH = 7.9 required the addition of a second antimony-sulfide complex, i.e., $\text{Sb}_2\text{S}_4^{2-}$ or SbS_3^{3-} which produced fits of very similar quality. The dimer $\text{Sb}_2\text{S}_4^{2-}$ was selected because it produced the best fits to stibnite solubility from 30 to 150°C and because the value for K_{2400} at 200°C was consistent with how the value for K_{2400} changed at lower and higher temperatures (Fit 200-A).

Table (4.6) Fit stibnite solubility at 200°C. Accompanying each fit are plots of the data and the fit at experimental sulfide concentrations (*left*), the relative residuals of the fit (*middle*), and the data and the distribution of species at 0.01 mol kg⁻¹ S²⁻_{total} (*right*). K is the equilibrium constant for the appropriate reaction from Table (4.3.), σ is one standard deviation, p and R^2 are fit statistics defined in Table (4.4), and N is the number of data points for each fit.

Fit	Reaction ^a	Aqueous antimony species	K	σ	p	R^2	pH range	N
200-A	K_{2400}	$\text{Sb}_2\text{S}_4^{2-}$	3.4E-11	2.6E-11	0.25	0.92	3.5 to 7.9	8
	K_{2401}	HSb_2S_4^-	2.3E-03	1.1E-03	0.09			
	K_{1033}	$\text{Sb}(\text{OH})_3$	2.9E-19	3.0E-19	0.37			



Relative residual is the difference between the fit and measured antimony concentrations normalized to the solubility, i.e. (mol kg⁻¹ Sb_{exp} - mol kg⁻¹ Sb_{fit}) / mol kg⁻¹ Sb_{exp}

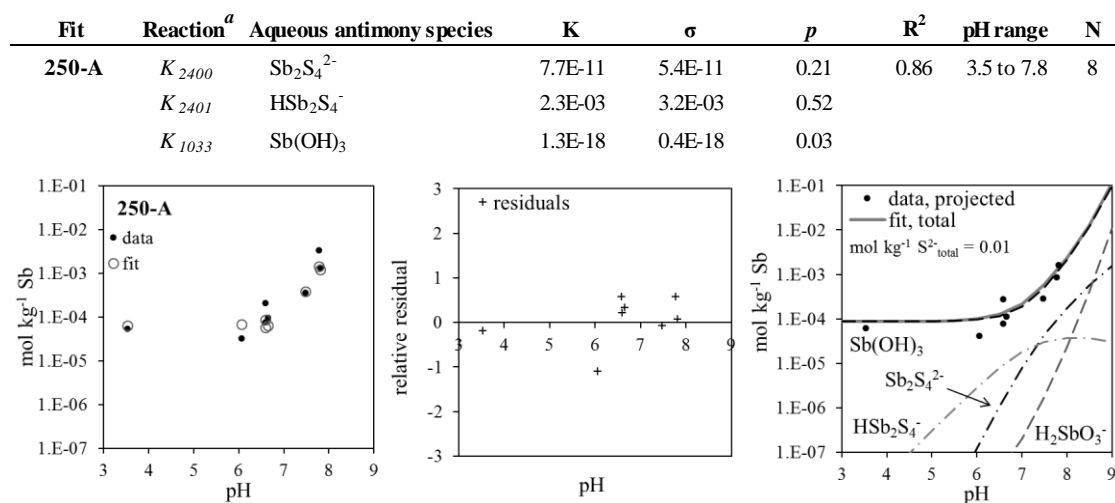
^a K_{xyzw} as defined in Table (4.3)

The value for $K_{1033, 200^\circ\text{C}} = 2.8 \times 10^{-19}$ from this study is very similar to the published value of $K_{1033} = 1.9 \times 10^{-19}$ of Akinifiev et al. (1994).

At 250°C, a speciation model considering $\text{Sb}(\text{OH})_3$ as the only species contributing to stibnite solubility produced a fit with $R^2 = 0.52$ (Fit not shown in Table (4.7)). The antimonous acid species, $\text{Sb}(\text{OH})_3$, can account for all of the dissolved antimony at pH < 7 and at pH = 7.8 in solutions with ~ 0.01 mol kg⁻¹ S²⁻_{total}. However, stibnite solubility at pH = 7.8 with a sulfide concentration of ~0.05 mol kg⁻¹ S²⁻_{total} and between pH = 6.5 to 7.5 could not be fit with $\text{Sb}(\text{OH})_3$ alone, and these experiments required a speciation model containing two partially deprotonated, dimeric antimony-sulfide complexes. A speciation model including $\text{Sb}(\text{OH})_3$, HSb_2S_4^- , and $\text{Sb}_2\text{S}_4^{2-}$ produced the best fit in terms of both R^2 and p values (Fit 250-A) and is the preferred fit.

Other combinations of antimony-sulfide dimers and monomers, including $\text{H}_2\text{SbSO}_2^-$ and $\text{H}_2\text{SbS}_2\text{O}^-$, did not improve fit statistics. The speciation models with mixed-ligand monomers were able to partially fit the data because, although HSb_2S_4^- was the predominate species pH = 5 to 7.5, $\text{Sb}(\text{OH})_3$ contributed up to ~ 30% to the total antimony concentration in this pH range at 200 and 250°C. As a result, intermediate species with lesser sulfide dependence than HSb_2S_4^- could produce moderately good fits to the data. However, these species did not produce the best fits to the data, as was demonstrated with Fit (150-B), in which $\text{H}_2\text{SbS}_2\text{O}^-$ consistently over-estimated stibnite solubility at higher pH values. The dimer HSb_2S_4^- fitted the circumneutral region more accurately. It was concluded that the good fit statistics which could be produced by a mixed-ligand monomer (e.g.,

Table (4.7) Fit of stibnite solubility at 250°C. Accompanying each fit are plots of the data and the fit at experimental sulfide concentrations (*left*), the relative residuals of the fit (*middle*), and the data and the distribution of species at 0.01 mol kg⁻¹ S₂²⁻_{total} (*right*). K is the equilibrium constant for the appropriate reaction from Table (4.3.), σ is one standard deviation, p and R^2 are fit statistics defined in Table (4.4), and N is the number of data points for each fit.



Relative residual is the difference between the fit and measured antimony concentrations normalized to the solubility, i.e. $(\text{mol kg}^{-1} \text{Sb}_{\text{exp}} - \text{mol kg}^{-1} \text{Sb}_{\text{fit}}) / \text{mol kg}^{-1} \text{Sb}_{\text{exp}}$

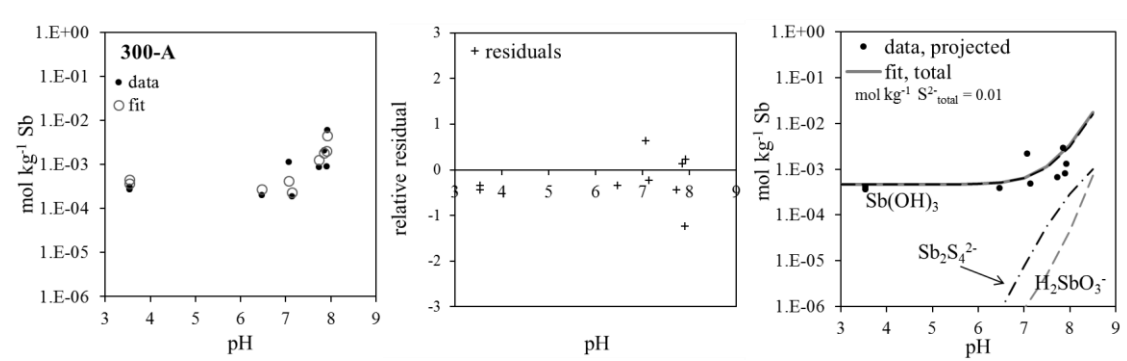
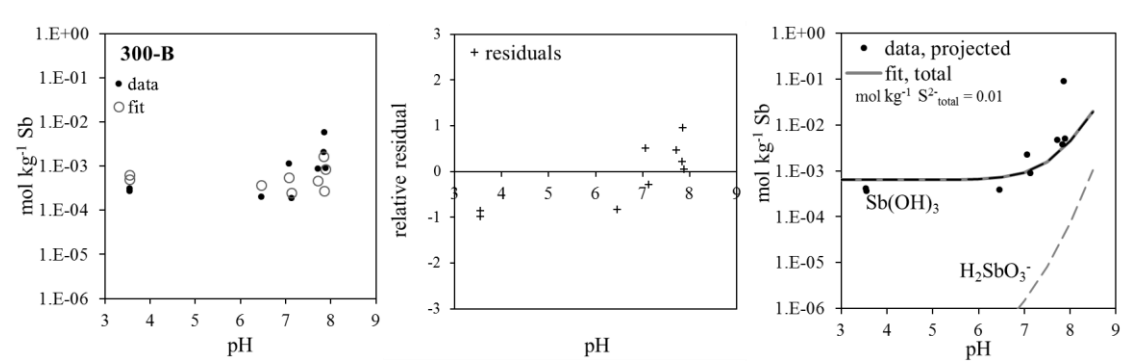
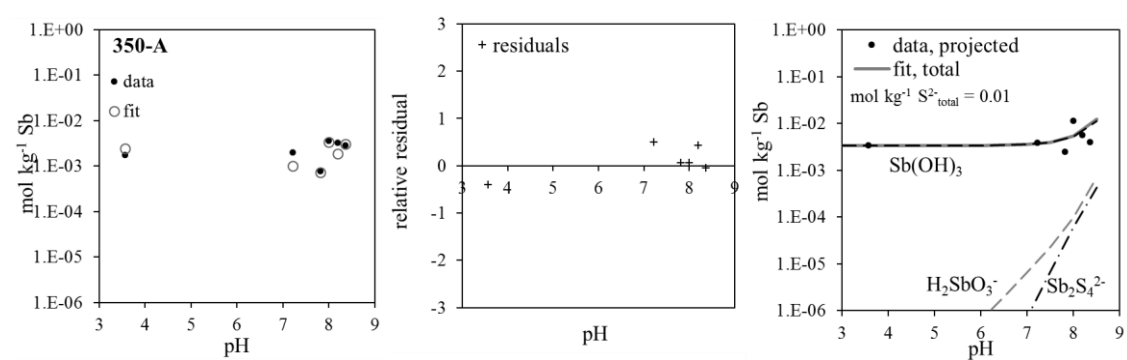
^a K_{xyzw} as defined in Table (4.3)

$\text{H}_2\text{SbS}_2\text{O}^-$) were the result of both $\text{Sb}(\text{OH})_3$ and HSb_2S_4^- being present in significant proportions rather than evidence for the predominance of a single intermediate species. The value of $K_{1033} = 1.3 \times 10^{-18}$ at 250°C from this study is in reasonable agreement with values for this equilibrium constant of $K_{1033} = 7.5 \times 10^{-19}$ and $K_{1033} = 1.2 \times 10^{-18}$ reported by Akinifiyev et al. (1994) and Shikina and Zotov (1999), respectively.

Stibnite solubility at 300 and 350°C

Stibnite solubility at 300 and 350°C continued the trend starting at 150°C of a diminishing importance of the antimony-sulfide complexes and an increasing predominance of $\text{Sb}(\text{OH})_3$. The preferred speciation model and plots of their fits are shown in Table (4.8). The preferred speciation model includes $\text{Sb}_2\text{S}_4^{2-}$, $\text{Sb}(\text{OH})_3$, and H_2SbO_3^- (Fits (300-A) and (350-A)). The pH at which $\text{Sb}(\text{OH})_3$ deprotonates to form H_2SbO_3^- decreases from 11.82 at 30°C to 9.88 at 350°C (Zakaznova-Herzog and Seward, 2006), and as a result, H_2SbO_3^- makes a larger contribution to the dissolved antimony in alkaline fluids at higher temperatures, and it was therefore included in the 300 and 350°C fits. As in the 30°C dionised water experiments, this was done by adding K_{1032} as a parameter dependent on K_{1033} . Thus, the addition of H_2SbO_3^- did not increase the number of independent variables in the fitting equation. The value for the pKa of $\text{Sb}(\text{OH})_3$ has not been determined at 350°C, but was estimated to be 9.85 based on Zakaznova-Herzog and Seward's (2006) spectroscopic measurements from 25 to 300°C. The deprotonated antimonous acid species, H_2SbO_3^- , contributed $\leq 1\%$ and $\leq 2\%$ of the total dissolved antimony in the experiments at 300 and 350°C, respectively.

Table (4.8) Fits of stibnite solubility at 300 and 350°C. Fits (300-A) and (350-A) are the preferred speciation models. Fit (300-B), which used antimonous acid species only, demonstrates that $\text{Sb}(\text{OH})_3$ is responsible for stibnite solubility. Accompanying each fit are plots of the data and the fit at experimental sulfide concentrations (*left*), the relative residuals of the fit (*middle*), and the data and the distribution of species at $0.01 \text{ mol kg}^{-1} \text{ S}^{2-}_{\text{total}}$ (*right*). K is the equilibrium constant for the appropriate reaction from Table (4.3.), σ is one standard deviation, p and R^2 are fit statistics defined in Table (4.4), and N is the number of data points for each fit.

Fit	Reaction ^a	Aqueous antimony species	K	σ	p	R ²	pH range	N
300-A	K ₂₄₀₀	Sb ₂ S ₄ ²⁻	1.7E-10	0.5E-11	0.01	0.91	3.5 to 8	9
	K ₁₀₃₃	Sb(OH) ₃	1.3E-18	0.2E-18	4.E-04			
	K ₁₀₃₂	H ₂ SbO ₃ ⁻	1.7E-28	dependent on K ₁₀₃₃				
								
300-B	K ₁₀₃₃	Sb(OH) ₃	1.8E-18	0.3E-18	4.E-04	0.70	3.5 to 7.9	9
	K ₁₀₃₂	H ₂ SbO ₃ ⁻	2.4E-28	dependent on K ₁₀₃₃				
								
350-A	K ₂₄₀₀	Sb ₂ S ₄ ²⁻	5.8E-11	3.1E-11	0.13	0.63	3.5 to 7.8	6
	K ₁₀₃₃	Sb(OH) ₃	3.3E-19	0.8E-19	0.02			
	K ₁₀₃₂	H ₂ SbO ₃ ⁻	4.6E-29	dependent on K ₁₀₃₃				
								

Relative residual is the difference between the fit and measured antimony concentrations normalized to the solubility, i.e. $(\text{mol kg}^{-1} \text{ Sb}_{\text{exp}} - \text{mol kg}^{-1} \text{ Sb}_{\text{fit}}) / \text{mol kg}^{-1} \text{ Sb}_{\text{exp}}$

^a K_{xyzw} as defined in Table (4.3)

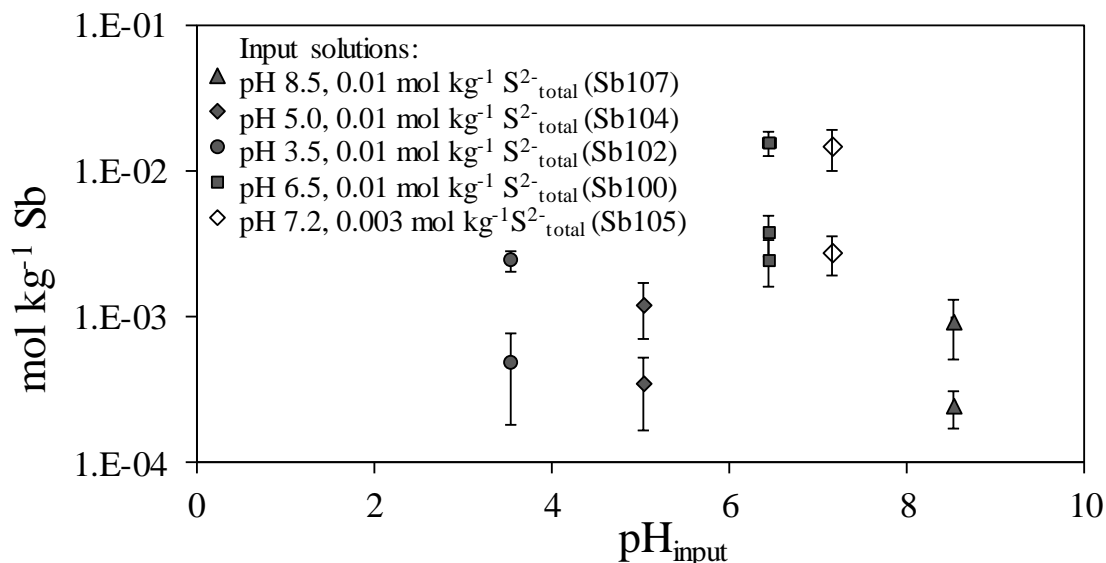
At 300 and 350°C, $\text{Sb}(\text{OH})_3$ was the major antimony species in all solutions containing $\leq 0.03 \text{ mol kg}^{-1} \text{ S}^{2-}_{\text{total}}$. However, at both 300 and 350°C, an antimony-sulfide complex was needed to fit the $\text{pH} \approx 8$ experiments with sulfide concentrations of 0.03 to 0.06 $\text{mol kg}^{-1} \text{ S}^{2-}_{\text{total}}$. An example of a fit using only antimony-hydroxide complexes is Fit (300-B), which used $\text{Sb}(\text{OH})_3$ and H_2SbO_3^- . Fit (300-B) had $R^2 = 0.70$, but the antimony concentrations predicted by this fit for the experiments at $\text{pH} \approx 8$ and $\text{S}^{2-}_{\text{total}} = 0.06 \text{ mol kg}^{-1}$ were $< 10\%$ of the measured stibnite antimony concentrations, suggesting that an antimony-sulfide complex is present at these higher sulfide concentrations.

The experimental solubilities were well fitted with a speciation model including $\text{Sb}(\text{OH})_3$, H_2SbO_3^- , and $\text{Sb}_2\text{S}_4^{2-}$. In addition, the values of K_{2400} at 300 and 350°C from fits using this speciation model were consistent the behavior of K_{2400} at lower temperatures. In contrast, when HSb_2S_4^- was included in the speciation model at these temperatures, the value of its equilibrium constant ($K_{2401} = 6 \times 10^{-2}$) was an order of magnitude too high based upon the behavior of K_{2401} at lower temperatures. At temperatures $> \sim 100^\circ\text{C}$, HSb_2S_4^- does not become more stable with increasing temperature because K_{2401} is effectively constant between 110 and 250°C (i.e., $K_{2401, 110^\circ\text{C}} = 2.5 \times 10^{-3}$ and $K_{2401, 250^\circ\text{C}} = 2.4 \times 10^{-3}$). It was judged that the contribution of HSb_2S_4^- at 300 and 350°C was too small to accurately estimate its equilibrium constant, and hence, this species was not included in the preferred speciation model. At 300°C, $\text{Sb}(\text{OH})_3$ was the major aqueous antimony species except when $\text{pH} \geq 7.3$ and $\text{S}^{2-}_{\text{total}} \geq 0.03$. At 350°C, $\text{Sb}_2\text{S}_4^{2-}$ is also the dominant species at $\text{pH} \geq \sim 8$ when $\text{S}^{2-}_{\text{total}} \geq 0.03$, where $\text{Sb}_2\text{S}_4^{2-}$ predominates. The values for the K_{1033} using the preferred speciation model overlap with previously published values at 300 and 350 °C (refer to Figure (4.8) in the Discussion).

4.3.5. Stibnite solubility at 400°C in supercritical fluids and in fluids with vapour-like densities

Stibnite solubility approached 2,000 ppm ($\sim 0.015 \text{ mol kg}^{-1} \text{ Sb}$) in fluids at 396 and 401°C when the pressure was $\sim 300 \text{ bar}$, which corresponded to fluid densities of 0.3 to 0.4 g cm^{-3} . With these extremely high concentrations of dissolved antimony, minor amounts of stibnite precipitation caused clogging of the exit tubing connected to the backpressure regulator and of the backpressure regulator itself after only a few samples had been taken. At lower pressures, particularly at $< 200 \text{ bar}$, stibnite solubility decreased rapidly, and conducting experiments at $\leq 250 \text{ bar}$ in fluids with vapour-like densities ($\rho_{\text{H}_2\text{O}} \leq 0.3 \text{ g cm}^{-3}$) enabled collection of more replicate samples. In Figure (4.6), the measured solubilities are plotted versus the input pH, which is the pH of initial solution as it enters the flow-through system at ambient temperature (Table 4.1). The pressure of individual data points and the input sulfide concentration are as indicated. The pressure had a strong influence on the stibnite solubility for all the experiments, and small increases in pressure produced large increases in stibnite solubility for the five different input pH's. The sulfide concentration in the output solution after reaction with stibnite was higher than the concentration in the input solution because of sulfide added by stibnite dissolution. The measured sulfide concentration in the output solution was used in estimating K_{1033} .

Figure (4.6) Stibnite solubility between 390 and 406°C versus input solution pH. The experimental pressure (in bars) is listed with each data point and the shade of the data points indicates the sulfide concentration of the input experimental solution (i.e., filled symbols contained sulfide concentrations of $\sim 0.01 \text{ mol kg}^{-1}$ and the open symbols $\sim 0.003 \text{ mol kg}^{-1}$).

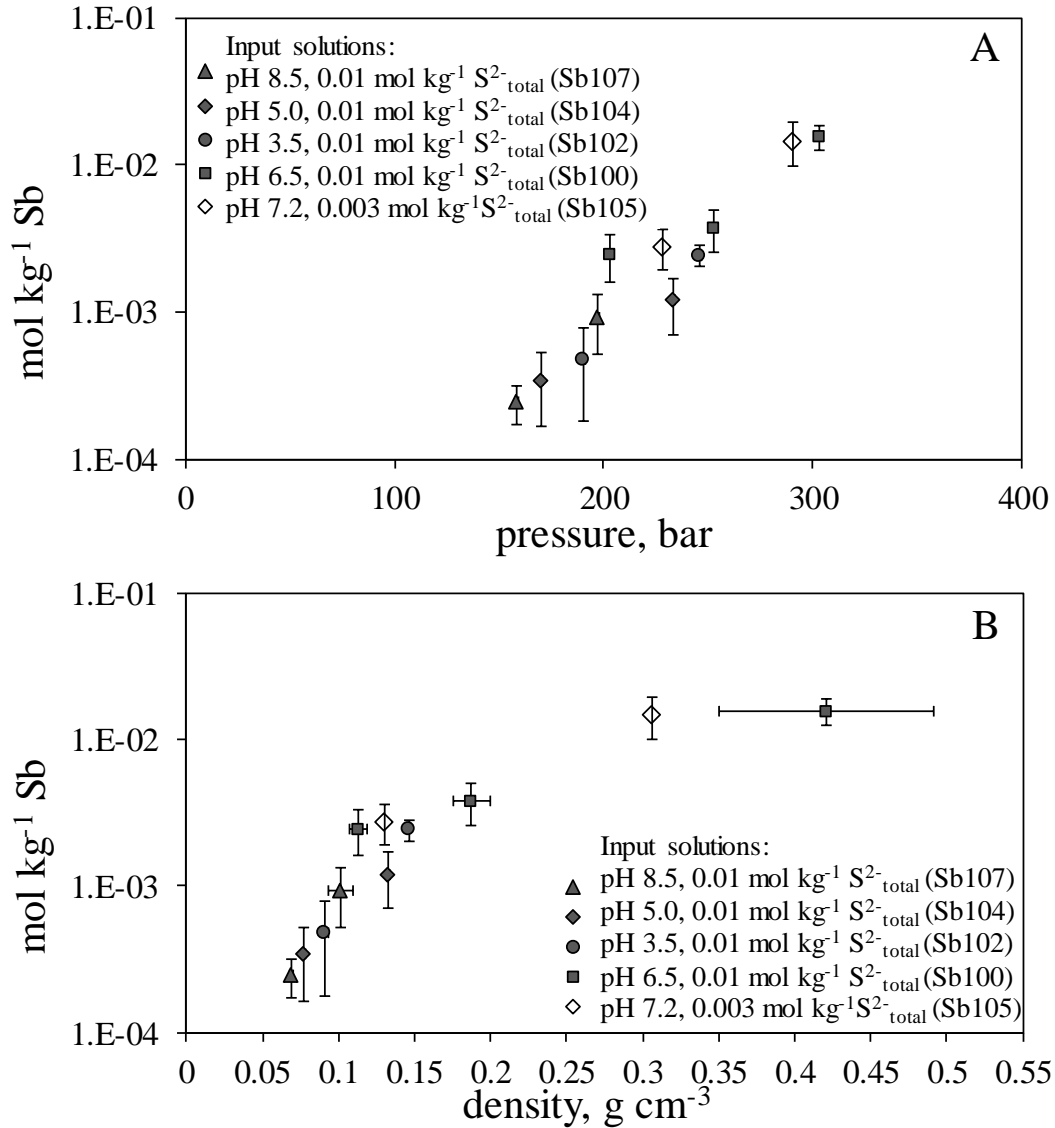


Experiments were completed at temperatures from 390 to 406°C and 159 to 304 bar, producing a variation in fluid density from 0.07 to 0.42 g cm^{-3} . Fluids with these characteristics can be involved in the formation of hydrothermal ore deposits, particularly in systems that involve a transition between high temperature ($> 400^\circ\text{C}$) porphyry environments to lower temperature, lower pressure epithermal environments (e.g., Heinrich et al., 2004; Williams-Jones and Heinrich, 2005; Hurtig and Williams-Jones, 2015). The relationship of stibnite solubility to experimental pressure and fluid density is shown in Figure (4.7). In contrast to the insignificant pressure dependence of stibnite solubility observed between 110 and 350°C (Figure 4.4), stibnite solubility decreased by 2.5 orders of magnitude in the supercritical fluids over the pressure range studied. However, the solubility of stibnite at 401°C and 159 bar, which corresponded to a fluid density of $\rho_{\text{H}_2\text{O}} \approx 0.07 \text{ g cm}^{-3}$, was still approximately the same as its solubility in the liquid phase at 300°C at swvp in a $\text{pH} < 6$ fluid (i.e., Fit (300-A) in Table (4.8)).

The temperature and pressure conditions for which the ion association constants given in Table (4.2) are well constrained by experimental data are limited to conditions in which $\rho_{\text{H}_2\text{O}} > 0.25 \text{ g cm}^{-3}$ for HCl° and NaOH° (Ho and Palmer, 1996; Ho et al., 2001) and $\rho_{\text{H}_2\text{O}} > 0.6 \text{ g cm}^{-3}$ for NaHS° (by analogy with NaCl ; Ho et al., 1994). However, the experimental data from the current study had a maximum density of $\rho_{\text{H}_2\text{O}} = 0.42 \text{ g cm}^{-3}$ and most were $< 0.2 \text{ g cm}^{-3}$. Therefore, the solution charge balance and the activities of aqueous species including Na^+ , HS^- , and Cl^- could only be estimated between 390 and 406°C and their values became increasingly uncertain at lower pressures.

Neutral antimonous acid, $\text{Sb}(\text{OH})_3$, is expected to be the main aqueous antimony species based upon the predominance of this species at 300 and 350°C and upon the increasing stability of neutral species given the low dielectric constant of water under these conditions. Assuming $\text{Sb}(\text{OH})_3$

Figure (4.7) Stibnite solubility at ~ 400°C versus pressure (A) and fluid density (B). The chemistry of the input solution is indicated. Below a fluid density of ~0.2 g cm⁻³, stibnite solubility decreases by nearly one and half orders of magnitude.



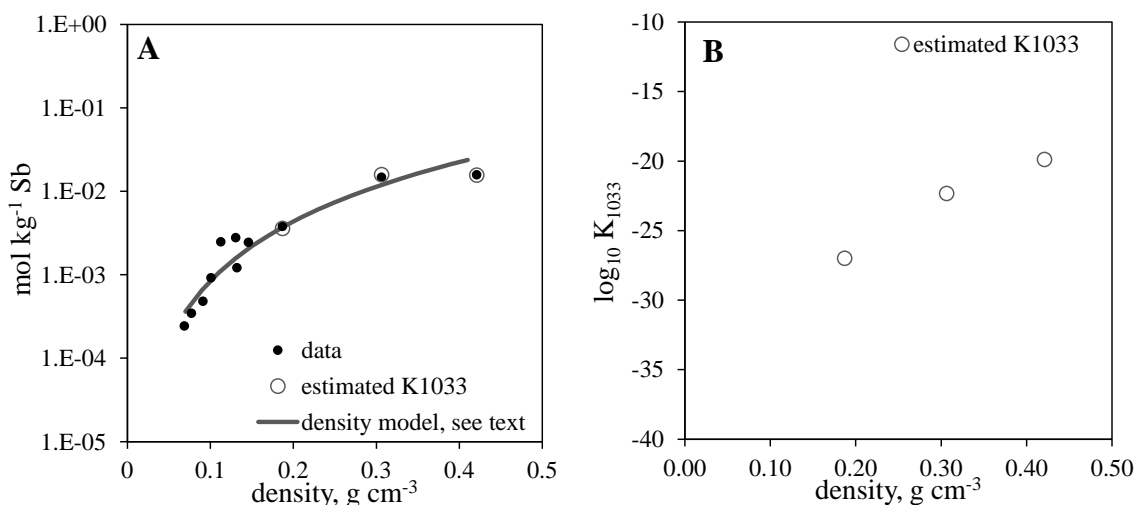
was the only species present, values for K_{1033} were estimated for the three highest density solutions with $\rho_{H_2O} = 0.19, 0.31,$ and 0.42 , resulting in $K_{1033} = 10^{-27.0}, 10^{-22.3},$ and $10^{-19.9}$, respectively. The predicted stibnite solubility is compared to the solubility data in Figure (4.8A) and K_{1033} is plotted versus ρ_{H_2O} in Figure (4.8B). These values are consistent with lower temperature data considering that K_{1033} reached a maximum of $10^{-17.9}$ at 250 and 300°C (Table 4.8) and then decreased to $10^{-18.5}$ at 350°C. Stibnite solubility across the entire experimental pressure range was also evaluated using a density equation of the form

$$\log Sb \text{ (mol kg}^{-1}\text{)} = a + b \cdot \log \rho_{H_2O} \quad (4.11)$$

where ρ_{H_2O} is the fluid density in g cm⁻³ and a and b are constants (Pokrovski et al., 2013). A fit with $a = -0.7052$ and $b = 2.3693$ had $R^2 = 91.3$ and is shown with the experimental data in Figure (4.8A).

Inclusion of a temperature-dependent factor did not improve the fit.

Figure (4.8) Stibnite solubility (A) and estimated K_{1033} (B) between 390 and 406°C as a function of fluid density. Fits of data using estimated K_{1033} and a density model (Equation 4.11) are also shown in (A).



4.4. Discussion

4.4.1. Temperature dependence of equilibrium constants for $Sb_2S_4^{2-}$, $HSb_2S_4^-$, and $Sb(OH)_3$

The logarithms of equilibrium constants derived from measurements of stibnite solubility in this study are summarised in Table (4.9). This table includes values for the equilibrium constants for $Sb_2S_4^{2-}$, $HSb_2S_4^-$, H_3SbS_2O , and $Sb(OH)_3$ determined from 70 to 350°C in this Chapter and those for the same reactions at 30°C from Chapter (2). The experimentally determined values for $\log K_{1033}$, $\log K_{2401}$, and $\log K_{2400}$ are compared to previously published values for these reactions in Figure (4.9). Also included in Figure (4.9) curves of $\log K_{xyzw}$ versus temperature (T , in Kelvin) that were derived from the form of the Van't Hoff isochore which best fitted the data, i.e.

$$\log K_{xyzw} = a + bT + cT^2 + dT^{-1} + e \log_{10}(T) \quad (4.12)$$

The constants for these fitted lines are found in Table (4.10). The heterogeneous equilibrium constants for the antimony-sulfide complexes (i.e., $Sb_2S_4^{2-}$, $HSb_2S_4^-$, and H_3SbS_2O) increased rapidly between 30 and 70°C and reached maximums at 150 to 300°C, depending on the complex. The value of K_{2400} was greatest ($K_{2400} = 10^{-9.6}$) at 300°C and then decreased slightly at 350°C. The equilibrium constant for the partially protonated dimer ($HSb_2S_4^-$, K_{2401}) increased rapidly between 30 and 70°C but then remained effectively constant between 110 and 250°C. The ambient temperature neutral species, H_3SbS_2O , did not contribute to the dissolved antimony concentration at $> 150^\circ\text{C}$ and its equilibrium constant could not be determined at higher temperatures.

At 150°C, $Sb(OH)_3$ began to be an important species, and K_{1033} reached a maximum value of $10^{-17.9}$ at 250 and 300°C. The equilibrium constant for stibnite solubility in terms of $H_2SbO_3^-$ was estimated using published values for the deprotonation reaction of $Sb(OH)_3$ (Zakaznova-Herzog and

Table (4.9) Experimentally derived logarithms of equilibrium constants for heterogeneous stibnite solubility reactions from 30 to 350°C at saturated water vapour pressure. The given uncertainties are one standard deviation (i.e., 1 σ); details of fits are shown in Table (2.4) for 30°C data and Tables (4.4) through (4.8) for higher temperatures.

Temperature (°C)	30	70	110	150	200	250	300	350
Reaction: $\text{Sb}_2\text{S}_3 + \text{HS}^- \rightleftharpoons \text{Sb}_2\text{S}_4^{2-} + \text{H}^+$								
logK₂₄₀₀								
	-13.33 \pm 0.04	-10.9 \pm 0.7	- \pm -	-10.6 \pm 0.2	-10.5 \pm 0.3	-10.1 \pm 0.3	-9.8 \pm 0.1	-10.2 \pm 0.2
Reaction: $\text{Sb}_2\text{S}_3 + \text{HS}^- \rightleftharpoons \text{HSb}_2\text{S}_4^-$								
logK₂₄₀₁								
	-5.4 \pm 0.2	-3.2 \pm 0.2	-2.6 \pm 0.1	-3.04 \pm 0.05	-2.6 \pm 0.2	-2.6 \pm 0.6	- \pm -	- \pm -
Reaction: $0.5\text{Sb}_2\text{S}_3 + 0.5\text{HS}^- + 0.5\text{H}^+ + \text{H}_2\text{O} \rightleftharpoons \text{H}_3\text{SbS}_2\text{O}$								
logK₁₂₁₃								
	-4.3 \pm 0.2	-2.8 \pm 0.6	-1.90 \pm 0.11	-1.8 \pm 0.2	- \pm -	- \pm -	- \pm -	- \pm -
Reaction: $0.5\text{Sb}_2\text{S}_3 + 3\text{H}_2\text{O} \rightleftharpoons \text{Sb}(\text{OH})_3 + 1.5\text{HS}^- + 1.5\text{H}^+$								
logK₁₀₃₃								
	-26.5 \pm 0.1	- \pm -	- \pm -	-18.70 \pm 0.07	-18.5 \pm 0.4	-17.9 \pm 0.1	-17.88 \pm 0.07	-18.5 \pm 0.1

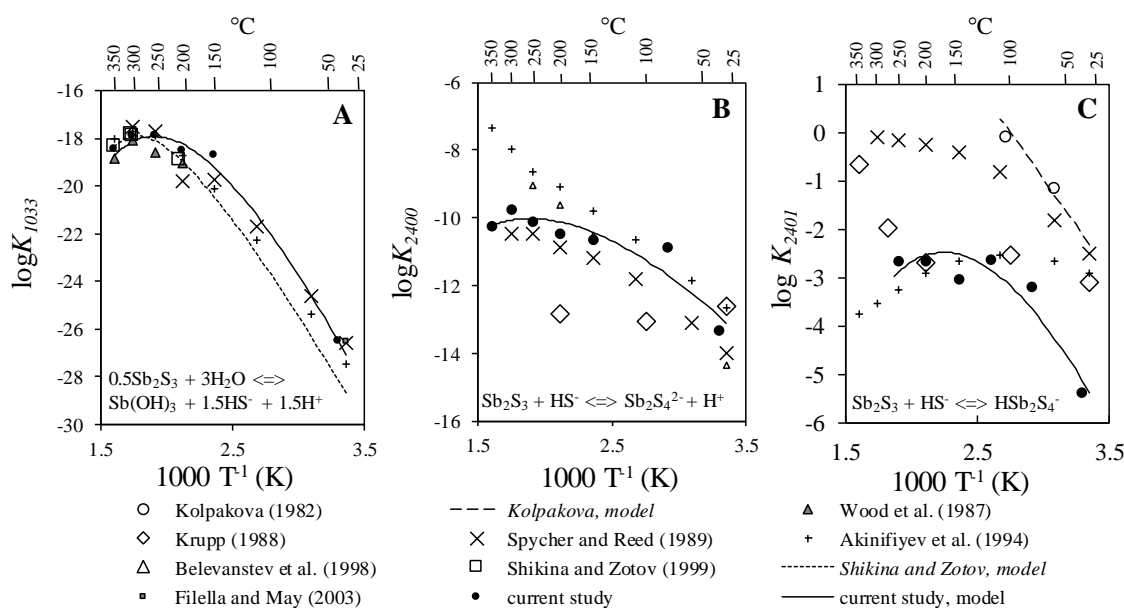
Seward, 2006). However, it did not contribute significantly to the total dissolved antimony concentration at 300 or 350°C (i.e., was \leq 2% of the total dissolved antimony) and so its equilibrium constant could not be independently determined and is not included in the Table (4.9).

The values for logK₁₀₃₃, logK₂₄₀₁, and logK₂₄₀₀ are compared to previously published values for these reactions in Figure (4.9). The estimated value for K₁₀₃₃ was in excellent agreement with the literature at 30°C, as were the values from 200 to 300°C (Figure 4.9A). The literature data includes values for K₁₀₃₃ derived from antimony (III)–oxide batch solubility studies (Spycher and Reed, 1989), stibnite batch solubility-based studies from 200 to 300°C (Shikina and Zotov, 1999) , and stibnite solubility in a system containing other additional sulfide minerals (Wood et al., 1987). The agreement between the new solubility data derived from flow-through solubility experiments with moderate to

Table (4.10) Coefficients for fits to Equation (4.12).

$\log K_{xyzw} = a + bT + cT^2 + dT^{-1} + e \log_{10}T$						
	<i>a</i>	<i>b</i>	<i>c</i>	<i>d</i>	<i>e</i>	Temperature range
logK₂₄₀₀	102	0	0	-8.13E+03	-35.4	30 to 350°C
logK₂₄₀₁	222	0	0	-1.41E+04	-72.9	30 to 250°C
logK₁₂₁₃	47.1	-5.86E-02	0	-1.02E+04	0	30 to 150°C
logK₁₀₃₃	37.2	-5.23E-02	0	-1.45E+04	0	30 to 350°C

Figure (4.9) Temperature dependence of logarithms of the equilibrium solubility constants for heterogeneous stibnite solubility reactions involving $\text{Sb}(\text{OH})_3$ (A), $\text{Sb}_2\text{S}_4^{2-}$ (B), and HSb_2S_4^- (C).



high sulfide concentrations (i.e., this study) and the previously published data derived from an array of experimental conditions suggests that the K_{1033} presented here is robust and confirms that $\text{Sb}(\text{OH})_3$ will be the primary aqueous antimony species in many hydrothermal environments, depending on the reduced sulfur activity.

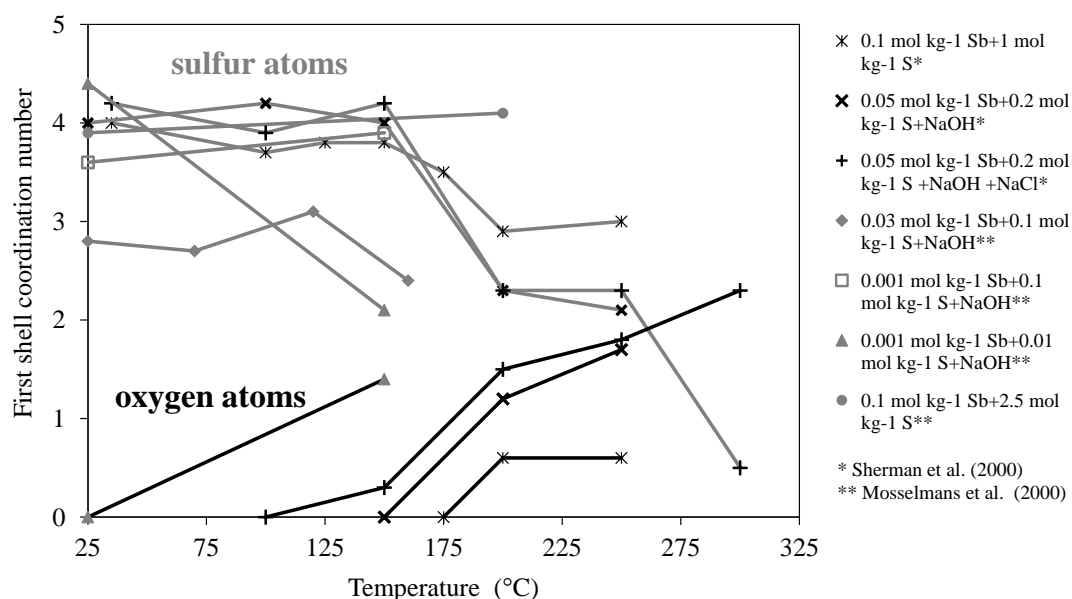
There was more scatter in the previously published thermodynamic data for the antimony-sulfide dimers (i.e., $\text{Sb}_2\text{S}_4^{2-}$ and HSb_2S_4^- , Figures 4.9B and 4.9C) than for $\text{Sb}(\text{OH})_3$ (Figure 4.9A). The equilibrium constant for the fully deprotonated antimony-sulfide dimer (K_{2400} , $\text{Sb}_2\text{S}_4^{2-}$) lay approximately in the middle of previously published values and was most similar to, although generally higher than, the data from Spycher and Reed (1989). The value for K_{2400} derived from that published by Krupp (1988) followed a different trend from the rest of the data at temperatures $> 100^\circ\text{C}$. The equilibrium constant for the partially protonated dimer (K_{2401} , HSb_2S_4^-) was in reasonable agreement with the data from Krupp (1988) and Akinifiyev et al. (1994) from 100 to 200°C . However, above 200°C , the values for K_{2401} from Krupp (1988) increased by nearly three orders of magnitude, while values from the current study and from Akinifiyev et al. (1994) remained constant or decreased slightly. The other literature data for K_{2401} are 1 to 3 orders of magnitude higher than the current study and Akinifiyev et al. (1994) at temperatures $> 50^\circ\text{C}$. In the current and previous studies, obtaining thermodynamic data for $\text{Sb}_2\text{S}_4^{2-}$ and HSb_2S_4^- often involved the interpretation of solubility results from experimental conditions where multiple antimony-sulfide species and $\text{Sb}(\text{OH})_3$ were present. Failure to accurately constrain the contribution of multiple species is likely behind some of the spurious equilibrium constants reported for $\text{Sb}_2\text{S}_4^{2-}$ and HSb_2S_4^- .

4.4.2. Evidence for changes in antimony speciation at elevated temperatures from previous spectroscopic studies

Three studies have used Raman or X-ray absorption spectroscopy (XAS) to study aqueous antimony-sulfide interactions up to 300°C, and both types of spectroscopic techniques found distinct changes in antimony spectra between 150 and 200°C. A Raman spectroscopy study by Gushchina et al. (2000) detected a major change in antimony speciation beginning at ~150°C, as was shown schematically in Figure (2.1) in Chapter (2). The authors did not identify the complex or complexes responsible for the change in the Raman spectrum at higher temperatures. However, it should be noted that one of the high temperature spectral features (a peak at 280 cm⁻¹) was only present at 25°C in solutions where the sulfide concentration was only slightly greater than the antimony concentration, i.e. a solution chemistry where the antimonous acid species might be expected.

The extended x-ray fine structure (EXAFS) portion of XAS spectra can identify and quantify the number of different coordinating atoms in an aqueous complex. EXAFS studies of antimony in sodium sulfide solutions find oxygen atoms and/or decrease in the number of sulfur atoms in antimony's first coordination shell beginning at 150°C for both Sb(III) and Sb(V) (Mosselmans et al., 2000; Sherman et al., 2000). The number of sulfur and oxygen atoms in the first coordination shell from these studies is plotted versus temperature in Figure (4.10). Unfortunately, only solutions containing Sb(V), have been studied at temperatures > 150°C (Sherman et al., 2000) and thus are not strictly comparable to this study.

Figure (4.10) Previously published EXAFS results for antimony in sodium sulfide solutions at elevated temperatures. Plot shows the number of coordinating sulfur and oxygen atoms reported by Mosselmans et al. (2000) and Sherman et al. (2000) for solutions from 25 to 350°C. Chemistries of the experimental solutions are listed in the legend.



4.4.3. Stibnite solubility and antimony speciation applied in natural hydrothermal fluids

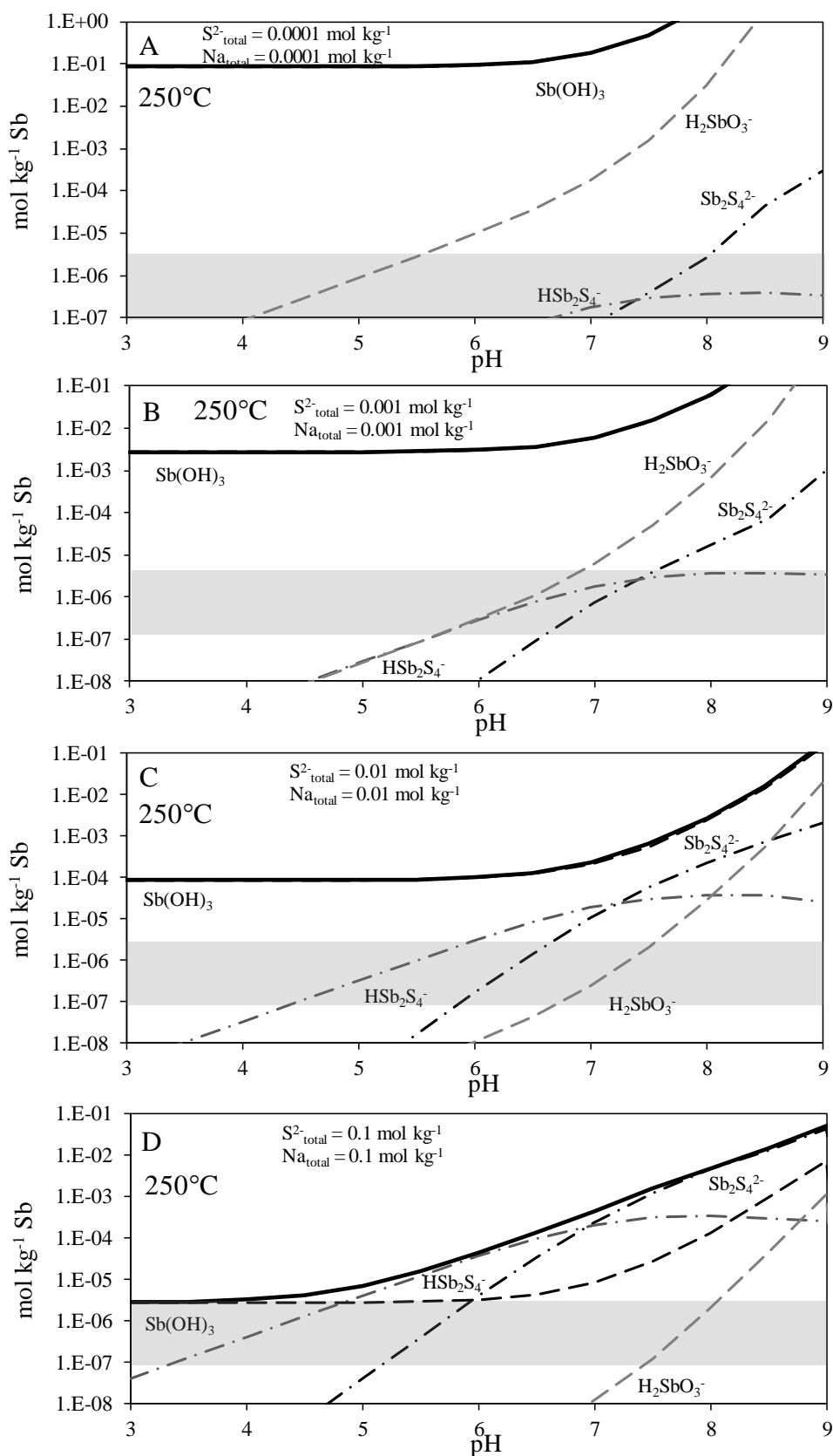
Stibnite solubility in geothermal reservoir fluids

The motivation for the current study was to provide thermodynamic data to assist in the interpretation of antimony behavior in natural, sulfide-containing hydrothermal fluids. Of particular interest are calculations of stibnite saturation in (a) the reservoir conditions of active hydrothermal systems (i.e., slightly alkaline, ~200 to 300°C) and (b) in the lower temperature, sometimes more acidic conditions present within geothermal power generation stations, where significant and problematic precipitation of stibnite from geothermal fluids has been documented in New Zealand (Dorrington and Brown, 2000; Ward et al., 2006; Wilson et al., 2007). Therefore, plots of stibnite solubility from pH = 3 to 9 and the distribution of antimony species at stibnite saturation have been constructed for a range of sulfide concentrations ($S^{2-}_{\text{total}} = 0.0001$ to 0.1 mol kg^{-1}). Such plots have been constructed at a temperature representative of reservoir conditions (250°C, Figure 4.11) and approximate operational temperatures within the Rotokawa and Ngawha geothermal stations (200 to 100°C, Figure 4.12).

The antimony concentration of deep hydrothermal fluids has been measured or estimated in the deep fluids of six hydrothermal systems in the Taupo Volcanic Zone (TVZ) in New Zealand currently utilized for geothermal power generation (Broadlands-Ohaaki, Kawerau, Rotokawa, Mokai, and Wairakei) and for a seventh TVZ system (Waiotapu) (Weissberg, 1969; Weissberg et al., 1979; Krupp and Seward, 1990; Simmons and Brown, 2007; Simmons et al., 2016). The antimony concentration in these deep fluids ranged from 5.7×10^{-8} to $9.8 \times 10^{-6} \text{ mol kg}^{-1}$ (7 to 1200 ppb) and the total sulfide concentration varied between 0.00026 and $0.0071 \text{ mol kg}^{-1}$ (median ~ $0.003 \text{ mol kg}^{-1}$). The pHs calculated at the reservoir temperatures are between pH ~ 5 and 7. The Ngawha hydrothermal system (Barnes and Seward, 1997), located outside of the TVZ, has the highest antimony concentrations of any active hydrothermal system in New Zealand (1.3×10^{-5} to $1.7 \times 10^{-5} \text{ mol kg}^{-1}$; Brown and Simmons, 2003; Wilson et al., 2007). The shaded area in Figure (4.11) shows the range of antimony concentrations reported in deep geothermal fluids sampled from New Zealand geothermal wells (1×10^{-7} to $1 \times 10^{-5} \text{ mol kg}^{-1}$).

At reservoir temperatures (200 to 250°C), Sb(OH)_3 is the dominant aqueous antimony species, although antimony-sulfide complexes contributed between 1 to 13 % of the total antimony between pH = 5.5 and 9 if $S^{2-}_{\text{total}} = 0.01 \text{ mol kg}^{-1}$. This is demonstrated in Figure (4.11), which shows the stibnite saturation curve and the distribution of antimony species at 250°C for four sulfide contents ($S^{2-}_{\text{total}} = 0.0001, 0.001, 0.01, \text{ and } 0.1 \text{ mol kg}^{-1}$). Antimony concentrations (1.3×10^{-4} to 8.1×10^{-3} or 16 to 988 ppm) reported in fluid inclusions from epithermal gold deposits in the Coromandel Peninsula, New Zealand (Simpson et al., 2015) approach stibnite solubility at 250°C for a sulfide concentration of 0.01 mol kg^{-1} (Figure 4.11C), as do the antimony concentrations in fluid inclusions from some of the magmatic-hydrothermal ore deposits included in Williams-Jones and Heinrich (2005).

Figure (4.11) Stibnite solubility at 250°C for $S^{2-}_{total} = 0.0001, 0.001, 0.01, \text{ and } 0.1 \text{ mol kg}^{-1}$. This range of sulfide concentrations covers the range of sulfide concentrations recorded for active hydrothermal systems from a variety of geologic settings. The gray region indicates the range of antimony concentrations measured in active New Zealand hydrothermal systems (Simmons and Brown, 2007; Wilson et al., 2007; Simmons et al. 2016).



However, fluids sampled directly from geothermal wells with temperatures between 200 and 300°C, represented by the shaded area in Figure (4.11), are understaturated with respect to stibnite. The undersaturation of stibnite is consistent with observations from active geothermal systems in the TVZ and in Nevada, U.S.A. that the enrichment of antimony in hydrothermally-altered rocks is most intense at shallow depths (i.e., < 500 m or even < 100 m depths) where temperatures are < 150°C (Weissberg, 1969; Chambefort and Dilles, 2015). As demonstrated in the following discussion of stibnite precipitation within two geothermal power stations, fluids with antimony concentrations $\sim 1 \times 10^{-5} \text{ mol kg}^{-1}$ can become over-saturated with respect to stibnite at 150°C if $\text{pH} < 7$.

Stibnite solubility in the Rotokawa and Ngawha geothermal power stations

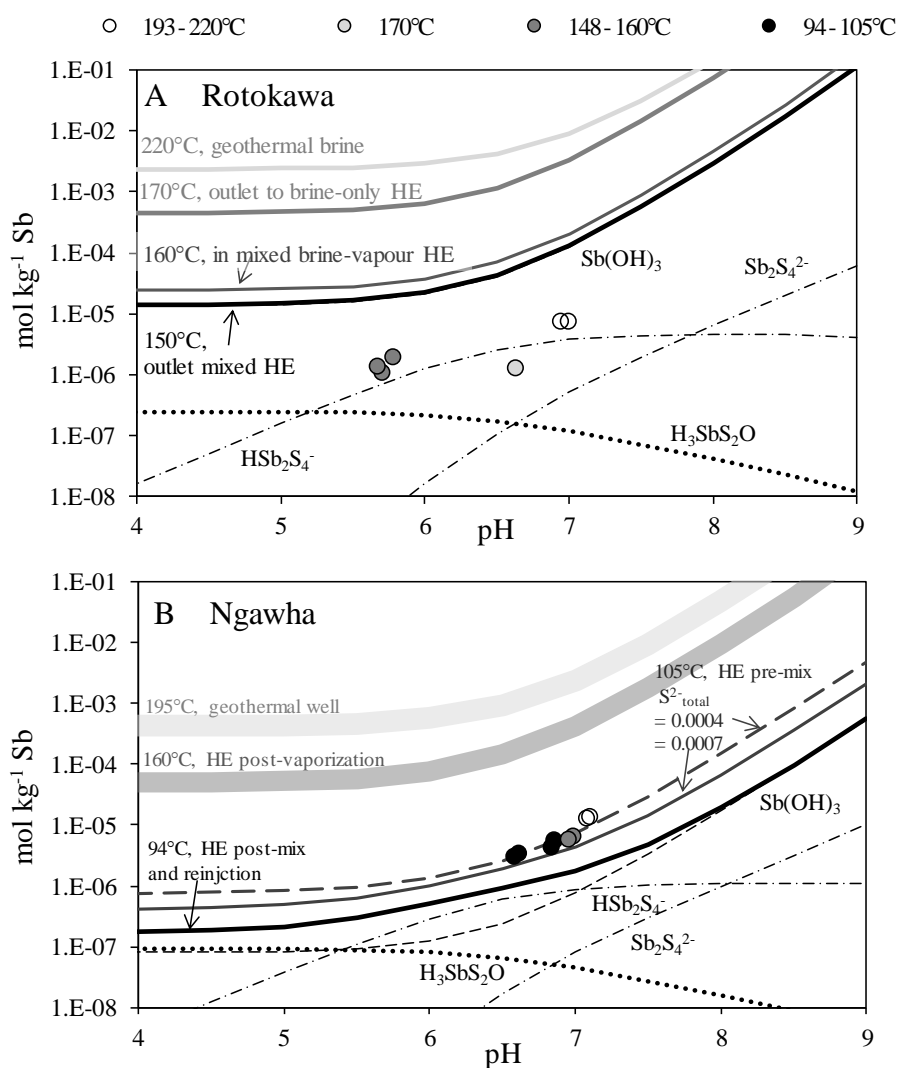
The precipitation of stibnite, or stibnite scaling, within two New Zealand geothermal power stations was studied in detail by Wilson et al. (2007). The Rotokawa and Ngawha power stations are binary facilities in which heat energy from geothermal fluid is transferred to a secondary working fluid (which drives the turbine) using a series of heat exchangers. The geothermal fluid is then reinjected to recharge the aquifer. During its transit through the power station, the geothermal fluid undergoes decreases in both temperature and pH. For Rotokawa, the temperature and pH decrease are from ~ 220 to $\sim 150^\circ\text{C}$ and from $\text{pH} = 7$ to 5.7, respectively, whereas for Ngawha, they vary from ~ 200 to $\sim 90^\circ\text{C}$ and from $\text{pH} = 7.1$ to 6.6. The largest temperature decrease occurs in the heat exchanger units, while the pH decrease occurs in response to mixing of acidic condensed vapour with the brine part way through the heat exchange process. Between the high temperature well and reinjection, the antimony concentration in the fluid decreases from 7.8×10^{-6} to 1.4×10^{-6} (960 to 170 ppb) at Rotokawa and from 1.3×10^{-5} to 3×10^{-6} (1600 to 375 ppb) at Ngawha. Most of the stibnite scaling (i.e., precipitation) is observed within the heat exchanger units. Wilson et al. (2007) concluded that stibnite deposition primarily occurred in response to a pH change at Rotokawa and due to temperature decrease at Ngawha. However, thermodynamic modeling of the system in this earlier study was limited by the available data, and antimony-sulfide complexes were not included in the stibnite saturation calculations.

Figures (4.12A) and (4.12B) show the solubility of stibnite as a function of pH for the temperatures and sulfide concentrations reported by Wilson et al. (2007) for the Rotokawa and Ngawha power stations, respectively, as calculated with the new thermodynamic data from the current study. Also plotted are antimony concentrations measured by Wilson et al. (2007) at different locations within the two power stations. The shade of these data points indicates the sample temperature. The sulfide concentration in these fluids varied from 0.0002 to 0.0009 mol kg^{-1} depending on the sampling location and the stibnite solubility curve at these different sulfide concentrations is included for Ngawha.

Stibnite solubility curves for Rotokawa fluids are shown in Figure (4.12A) at 220, 170, 160, and 150°C, which reflect the temperatures within the power station of separated brine (~ 220°C) prior to the heat exchangers (“HE”), of fluids within two heat exchangers (one using the brine only (170°C) and a second using a mixture of brine and condensed vapour (160 to 151°C)), and of reinjected fluid (148°C). This lower temperature brine-vapour heat exchanger unit is where stibnite deposition has been observed.

According to Figure (4.12A), the fluid remained undersaturated with respect to stibnite throughout the entire system but most closely approached stibnite saturation in the mixed brine-vapour heat exchanger and in the reinjection line. This was due to the large decrease in stibnite solubility

Figure (4.12) Stibnite solubility curves for fluids in the Rotokawa (A) and Ngawha (B) power stations. Stibnite solubilities (solid lines) have been calculated using equations from Table (4.10) for total sulfide concentrations and temperatures representative of fluid conditions based upon data reported in Wilson et al. (2007). Species distributions are for the lowest temperature. Also included are dissolved antimony concentrations (open and closed circles) measured by Wilson et al. (2007), with the sample temperature indicated by symbol shade. “HE” refers to heat exchanger. The sulfide concentration at Ngawha varied between $S^{2-}_{total} \sim 0.0004$ and $0.0007 \text{ mol kg}^{-1}$; and the influence of this variation on stibnite solubility is indicated at 195 and 160°C by the width of the solubility curves.



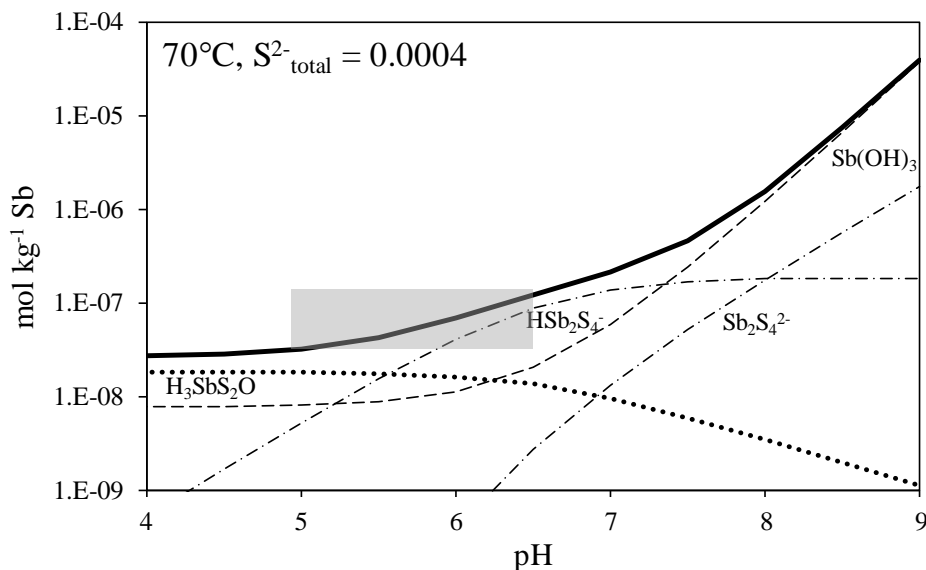
between 170 and 150°C as the stability of $\text{Sb}(\text{OH})_3$ begins to rapidly decrease with decreasing temperature (i.e., see the curve for K_{1033} in Figure (4.9)). However, antimony concentrations measured in the outlet fluids from both heat exchangers (1.3×10^{-6} to 2.0×10^{-6} mol kg⁻¹ or 160 to 250 ppb) were lower than concentrations in the input brine (7.9×10^{-6} mol kg⁻¹, ~ 960 ppb), which implies that precipitation of an antimony solid phase did occur, possibly within the system prior to the sampling location. It should be noted that the value for K_{1033} calculated between ~ 100 and 175°C using the equation in Table (4.10) is greater than previously published (Figure 4.9). This region of variability corresponds to the temperature range in which K_{1033} was not experimentally determined in this study because of the moderate to high sulfide concentrations used. If the value of K_{1033} decreases by about one order of magnitude at 160 and 170°C, which is within the variation observed in previous studies for K_{1033} at these temperatures, the fluids exiting the brine-vapour heat exchanger (at ~ 160°C) and in the reinjection line (at ~ 150°C) become saturated with respect to stibnite.

The antimony concentration in the input geothermal fluids at the Ngawha power station is higher than at Rotokawa (Figure 4.12B). The total sulfide concentration for fluids at Ngawha reported by Wilson et al. (2007) varied between ~ 0.0004 and 0.0007 mol kg⁻¹. This sulfide concentration variation resulted in slight changes to the stibnite solubility, which is indicated with line width at 195 and 160°C and with two separate lines at 105°C. Based upon total dissolved antimony concentrations measured by Wilson et al. (2007), the fluids in the Ngawha power station are undersaturated with respect to stibnite at the geothermal well head (at ~ 200°C) and after vapour-brine separation (at ~ 160°C). However, the temperature decreases within the heat exchanger, and fluids are at stibnite saturation when next sampled at ~ 105°C. The temperature of the fluid further decreases to ~ 93°C and the pH decreases to pH ≈ 5.7 with the addition of condensed vapour, making stibnite over saturated and contributing to additional stibnite precipitation as indicated by a decrease in antimony concentration before and after the addition of the condensed vapor (from ~ $5.6.1 \times 10^{-6}$ mol kg⁻¹ to ~ 4×10^{-6} mol kg⁻¹). At the Ngawha power station, HSb_2S_4^- becomes important when the fluid temperature decreases to 105°C. At 93°C, this antimony-sulfide dimer is the dominant aqueous antimony species at the near neutral pH of the fluids, and it causes stibnite solubility to be higher by approximately an order of magnitude from what it would be if modeled with $\text{Sb}(\text{OH})_3$ alone.

Antimony speciation in surface hot springs

The discussion above emphasizes the dramatic changes in stibnite solubility of between 10^{-2} to 10^{-6} mol kg⁻¹ that occur in natural hydrothermal systems as buoyantly ascending fluids rise through fracture permeability in the Earth's crust and undergo boiling, cooling, and mixing with near surface fluids. In the upper 500 to 100 m of hydrothermal systems, the mixing of hydrothermal fluids with acidic steam-heated waters and oxygenated meteoric waters, changes in redox environment, ligand (i.e., reduced sulfur) transfer to a volatile-rich steam phase, and changes in pH accompanying these processes will play important roles in the transport and deposition chemistry of antimony. At temperatures < 100°C in surface hot springs, stibnite solubility will decrease further. Such an

Figure (4.13) Stibnite solubility and antimony speciation from pH = 4 to 9 for a 70°C fluid with ~15 ppm sulfide. Gray shaded region indicates approximate pH range observed in Champagne Pool and associated range in stibnite solubility (~ 4 to 20 ppb Sb).



environment is represented in Figure (4.13) with a 70°C fluid containing 15 ppm sulfide. For these conditions, the dominant aqueous antimony species at stibnite saturation in slightly acidic fluids (indicated by gray shaded region) is HSb_2S_4^- . Stibnite solubility at $\text{pH} \approx 6.5$ is ~ 20 ppb (i.e., $\sim 1.5 \times 10^{-7} \text{ mol kg}^{-1}$) and then decreases with decreasing pH to 4 ppb at $\text{pH} = 5$, which is a similar antimony concentration range to that observed in studies of trace metals in surface fluids from active hydrothermal systems in New Zealand and elsewhere (Pope et al., 2004; Pope et al., 2005; Planer-Friedrich and Scheinost, 2011; Ullrich et al., 2013).

4.5. Conclusions

The main findings from the high temperature solubility experiments presented in here are:

- 1) Stibnite solubility from 70 to 350°C with total sulfide concentration (S^{2-}_{total}) from 0.003 to 0.06 mol kg^{-1} and between pH 3.5 to 9 requires a scheme of four species to account for the solubility curve. The four species were $\text{Sb}_2\text{S}_4^{2-}$, HSb_2S_4^- , $\text{H}_3\text{SbS}_2\text{O}$, and $\text{Sb}(\text{OH})_3$.
 - a. Between 70 to 110°C, stibnite solubility was due to $\text{Sb}_2\text{S}_4^{2-}$, HSb_2S_4^- , and $\text{H}_3\text{SbS}_2\text{O}$.
 - b. At 150°C, all four complexes were present, with $\text{Sb}(\text{OH})_3$ contributing significantly to stibnite solubility in acidic and alkaline solutions with $S^{2-}_{\text{total}} < 0.02 \text{ mol kg}^{-1}$.
 - c. From 200 to 250°C, $\text{Sb}_2\text{S}_4^{2-}$, HSb_2S_4^- , and $\text{Sb}(\text{OH})_3$ were the major complexes. The stability of $\text{Sb}(\text{OH})_3$ continued to increase such that $\text{Sb}_2\text{S}_4^{2-}$ and HSb_2S_4^- were limited to $S^{2-}_{\text{total}} \geq 0.03 \text{ mol kg}^{-1}$.
 - d. At 300 and 350°C, $\text{Sb}_2\text{S}_4^{2-}$ and $\text{Sb}(\text{OH})_3$ were the only species present.
 - e. At $\sim 400^\circ\text{C}$, stibnite solubility in supercritical fluids was extremely sensitive to pressure and solubilities are consistent with the presence of $\text{Sb}(\text{OH})_3$ at pressures < 350 bar.

The experimentally determined equilibrium constants up to 350°C are summarised in Table (4.9). The best fits to various forms of the Van't Hoff isochore, $\log K_{xyzw} = a + bT + cT^2 + dT^{-1} + e\log_{10}(T)$, are given in Table (4.10).

- 2) Stibnite solubility is independent of pressure from 70 to 350°C up to 250 bar. In supercritical solutions, stibnite solubility is strongly dependent on pressure and this temperature dependence can be described using $\log Sb = a + b\log(\rho_{H_2O})$ with $a = -0.7052$ and $b = 2.3693$ and the concentration of antimony in mol kg^{-1} .
- 3) High temperature fluids in active hydrothermal systems containing $\sim 1 \times 10^{-5} \text{ mol kg}^{-1} \text{ Sb}$ are undersaturated with respect to stibnite at $\geq 200^\circ\text{C}$. At temperatures $< 150^\circ\text{C}$, these solutions may become oversaturated with respect to stibnite depending on the sulfide content and fluid pH. In the slightly acidic and low sulfide concentrations of a hot spring such as Champagne Pool (Waiotapu), stibnite solubility is $\leq 4 \times 10^{-7} \text{ mol kg}^{-1}$ (i.e., $< \sim 50 \text{ ppb}$).

The stibnite solubility experiments in this study confirmed that antimony speciation in reducing, sulfide-containing fluids changes from antimony-sulfide complexes to $\text{Sb}(\text{OH})_3$ with increasing temperature. The temperature at which this change occurs will vary depending on the sulfide concentration in the hydrothermal fluid. As shown in Figure (4.10), $\text{Sb}(\text{OH})_3$ controls stibnite solubility for a wide range of sulfide concentrations at 250°C. In contrast, for lower temperature fluids within power stations (Figure 4.11), antimony-sulfide complexes started to contribute significantly to the total dissolved antimony, and at 150°C, 10% of the total dissolved antimony in a near neutral fluid was comprised of antimony-sulfide moieties. For hydrothermal fluids with typical sulfide concentrations (i.e., 10^{-4} to $10^{-2} \text{ mol kg}^{-1} \text{ S}^{2-}_{\text{total}}$), $\text{Sb}(\text{OH})_3$ alone can be used to model antimony behavior at temperatures $> 150^\circ\text{C}$, but at temperatures $\leq 150^\circ\text{C}$ antimony sulfide complexes must be included in geochemical modeling. In addition, at sulfide concentrations $\geq 0.01 \text{ mol kg}^{-1}$, the two dimers HSb_2S_4^- and $\text{Sb}_2\text{S}_4^{2-}$ will be the species defining stibnite solubility at near neutral to alkaline pH's.

4.6. References

- Akinifiyev, N.N., Zotov, A.V., Shikina, N.D., 1994. Experimental studies and self-consistent thermodynamic data in the Sb(III)-S(II)-O-H system. *Geochem. Internat.* **31**, 27-40.
- Barnes, H.L., Seward, T.M., 1997. Geothermal systems and mercury deposits, in: Barnes, H.L. (Ed.), *Geochemistry of Hydrothermal Ore Deposits*, 3rd ed. Wiley Interscience, New York, pp. 699-736.
- Belevantsev, V.I., Gushchina, L.I., Obolenskii, A.A., 1998. Solubility of stibnite, $\text{Sb}_2\text{S}_3(\text{cr})$: A revision of proposed interpretations and refinements. *Geochem. Internat.* **36**, 58-64.
- Brown, K.L., Simmons, S.F., 2003. Precious metals in high-temperature geothermal systems in New Zealand. *Geothermics* **32**, 619-625.
- Chambefore, I., Dilles, J.H., 2015. Trace metals and volatiles zoning in active geothermal systems, Proceedings of the 37th New Zealand Geothermal Workshop, Taupo, New Zealand.
- Dorrington, P., Brown, K., 2000. Management of stibnite deposition at Ngawha, Proceedings of the 22nd New Zealand Geothermal Workshop, Auckland, New Zealand.

- Ellis, A.J., McFadden, I.M., 1972. Partial molal volumes of ions in hydrothermal solutions. *Geochim. Cosmochim. Acta* **36**, 413-426.
- Fylstra, D., Lasdon, L., Watson, J., Warren, A., 1998. Design and use of the Microsoft Excel Solver. *Interfaces* **28**, 29-55.
- Gushchina, L.V., Borovikov, A.A., Shebanin, A.P., 2000. Formation of antimony(III) complexes in alkali sulfide solutions at high temperatures: An experimental Raman spectroscopic study. *Geochem. Internat.* **38**, 510-513.
- Hannington, M.D., Harðardóttir, V., Garbe-Schönberg, D., Brown, K.L., 2016. Gold enrichment in active geothermal systems by acculating colloidal suspensions. *Nature Geoscience*.
- Hardardottir, V., Brown, K.L., Fridriksson, T., Hedenquist, J.W., Hannington, M.D., Thorhallsson, S., 2009. Metals in deep liquid of the Reykjanes geothermal system, southwest Iceland: Implications for the composition of seafloor black smoker fluids. *Geology* **37**, 1103-1106.
- Heinrich, C.A., Driesner, T., Stefánsson, A., Seward, T.M., 2004. Magmatic vapor contraction and the transport of gold from the porphyry environment to epithermal ore deposits. *Geology* **32**, 761.
- Helgeson, H.C., 1969. Thermodynamics of hydrothermal systems at elevated temperatures and pressures. *American Journal of Science* **267**, 729-804.
- Helgeson, H.C., Kirkham, D.H., 1974. Theoretical prediction of the thermodynamic behavior of aqueous electrolytes at high pressures and temperatures: II. Debye-Huckel parameters for activity coefficients and relative partial molal properties. *American Journal of Science* **274**, 1199-1261.
- Ho, P.C., Palmer, D.A., 1996. Ion association of dilute aqueous sodium hydroxide solutions to 600°C and 300 MPa by conductance measurements. *Journal of Solution Chemistry* **25**, 711-729.
- Ho, P.C., Palmer, D.A., Gruszkiewicz, M.S., 2001. Conductivity measurements of dilute aqueous HCl solutions to high temperatures and pressures using a flow-through cell. *Journal of Physical Chemistry B* **105**, 1260-1266.
- Ho, P.C., Palmer, D.A., Mesmer, R.E., 1994. Electrical conductivity measurements of aqueous sodium chloride solutions to 600°C and 300 MPa. *Journal of Solution Chemistry* **23**, 997-1018.
- Hurtig, N.C., Williams-Jones, A.E., 2015. Porphyry-epithermal Au-Ag-Mo ore formation by vapor-like fluids: New insights from geochemical modeling. *Geology* **43**, 587-590.
- Kielland, J., 1937. Individual activity coefficients of ions in aqueous solutions. *J. Am. Chem. Soc.* **59**, 1675-1678.
- Kolpakova, N.N., 1971. On the speciation of antimony (III) in sulfide solutions (in Russian), *Geochemistry of Hydrothermal Ore Deposition*, Nauka, Moscow, pp. 197-209.
- Kolpakova, N.N., 1982. Laboratory and field studies of ionic equilibria in the $\text{Sb}_2\text{S}_3\text{-H}_2\text{O-H}_2\text{S}$ system. *Geochem. Internat.* **19**, 46-54.
- Krupp, R.E., 1988. Solubility of stibnite in hydrogen sulfide solutions, speciation, and equilibrium constants, from 25 to 350°C. *Geochim. Cosmochim. Acta* **52**, 3005-3015.
- Krupp, R.E., Seward, T.M., 1990. Transport and deposition of metals in the Rotokawa geothermal system, New Zealand. *Min. Dep.* **25**, 73-81.
- Landrum, J.T., Bennett, P.C., Engel, A.S., Alsina, M.A., Pastén, P.A., Milliken, K., 2009. Partitioning geochemistry of arsenic and antimony, El Tatio Geyser Field, Chile. *Appl. Geochem.* **24**, 664-676.
- Learned, R.E., 1966. The solubilities of quartz, quartz-cinnabar and cinnabar-stibnite in sodium sulfide solutions and their implications for ore genesis, Department of Geology, University of California, Riverside, Riverside, California.
- Marshall, W.L., Franck, E.U., 1981. Ion product of water substance, 0-1000°C, 1-10,000 bars. New international formulation and its background. *Journal of Physical Reference Data* **10**, 295-304.
- Mesmer, R.E., Marshall, W.L., Palmer, D.A., Simonson, J.M., Holmes, H.F., 1988. Thermodynamics of aqueous association and ionization reactions at high temperatures and pressures. *Journal of Solution Chemistry* **17**, 699-718.
- Migdisov, A.A., Bychkov, A.Y., 1998. The behaviour of metals and sulphur during the formation of hydrothermal mercury-antimony-arsenic mineralization, Uzon caldera, Kamchatka, Russia. *J. Volcanol. Geotherm. Res.* **84**, 152-171.
- Morteani, G., Ruggieri, G., Möller, P., Preinfalk, C., 2010. Geothermal mineralized scales in the pipe system of the geothermal Piancastagnaio power plant (Mt. Amiata geothermal area): a key to

- understand the stibnite, cinnabarite and gold mineralization of Tuscany (central Italy). *Min. Dep.* **46**, 197-210.
- Mosselmans, J.F.W., Helz, G.R., Patrick, R.A.D., Charnock, J.M., Vaughan, D.J., 2000. A study of speciation of Sb in bisulfide solutions by X-ray absorption spectroscopy. *Appl. Geochem.* **15**, 879-889.
- Planer-Friedrich, B., Scheinost, A.C., 2011. Formation and structural characterization of thioantimony species and their natural occurrence in geothermal waters. *Environ. Sci. Technol.* **45**, 6855-6863.
- Pokrovski, G.S., Borisova, A.Y., Bychkov, A.Y., 2013. Speciation and transport of metals and metalloids in geological vapors. *Reviews in Mineralogy and Geochemistry* **76**, 165-218.
- Pope, J.G., Brown, K.L., McConchie, D.M., 2005. Gold Concentrations in Springs at Waiotapu, New Zealand: Implications for Precious Metal Deposition in Geothermal Systems. *Econ. Geol.* **100**, 677-687.
- Pope, J.G., McConchie, D.M., Clark, M.D., Brown, K.L., 2004. Diurnal variations in the chemistry of geothermal fluids after discharge, Champagne Pool, Waiotapu, New Zealand. *Chem. Geol.* **203**, 253-272.
- Raymond, J., Williams-Jones, A., Clark, J., 2005. Mineralization associated with scale and altered rock and pipe fragments from the Berlín geothermal field, El Salvador; implications for metal transport in natural systems. *J. Volcanol. Geotherm. Res.* **145**, 81-96.
- Ruaya, J.R., Seward, T.M., 1987. The ion-pair constant and other thermodynamic properties of HCl up to 350°C. *Geochim. Cosmochim. Acta* **51**, 121-130.
- Sherman, D.M., Ragnarsdottir, K.V., Oelkers, E.H., 2000. Antimony transport in hydrothermal solutions: an EXAFS study of antimony(V) complexation in alkaline sulfide and sulfide-chloride brines at temperatures from 25°C to 300°C at P_{sat} . *Chem. Geol.* **167**, 161-167.
- Shikina, N.D., Zotov, A.V., 1999. Solubility of stibnite (Sb_2S_3) in water and hydrogen sulfide solutions at temperature of 200-300°C under-vapor saturated conditions and a pressure of 500 bars. *Geochem. Internat.* **37**, 82-86.
- Simmons, S.F., Brown, K.L., 2007. The flux of gold and related metals through a volcanic arc, Taupo Volcanic Zone, New Zealand. *Geology* **35**, 1099-1102.
- Simmons, S.F., Brown, K.L., Tutolo, B.M., 2016. Hydrothermal transport of Ag, Au, Cu, Pb, Te, Zn and other metals and metalloids in New Zealand geothermal systems: Spatial patterns, fluid-mineral equilibria, and implications for epithermal mineralization. *Econ. Geol.* **111**, 589-618.
- Simmons, S.F., Browne, P.R.L., 2000. Hydrothermal minerals and precious metals in the Broadlands-Ohaaki geothermal system: Implications for understanding low-sulfidation epithermal environments. *Econ. Geol.* **95**, 971-999.
- Simpson, M.P., Palinkas, S.S., Mauk, J.L., Bodnar, R.J., 2015. Fluid inclusion chemistry of adularia-sericite epithermal Au-Ag deposits of the Southern Hauraki Goldfield, New Zealand. *Econ. Geol.* **110**, 763-786.
- Sonney, R., Mountain, B.W., 2013. Experimental simulation of greywacke–fluid interaction under geothermal conditions. *Geothermics* **47**, 27-39.
- Spang, B., 2002. Water97_v13.xla, <http://www.cheresources.com/staff.shtml>.
- Spycher, N.F., Reed, M.H., 1989. As(III) and Sb(III) sulfide complexes: An evaluation of stoichiometry and stability from existing experimental data. *Geochim. Cosmochim. Acta* **53**, 2185-2194.
- Stauffer, R.E., Thompson, J.M., 1984. Arsenic and antimony in geothermal waters of Yellowstone National Park, Wyoming, USA. *Geochim. Cosmochim. Acta* **48**, 2547-2561.
- Stefánsson, A., Seward, T.M., 2004. Gold(I) complexing in aqueous sulphide solutions to 500°C at 500 bar. *Geochim. Cosmochim. Acta* **68**, 4121-4143.
- Suleimenov, O.M., Seward, T.M., 1997. A spectrophotometric study of hydrogen sulphide ionisation in aqueous solutions to 350°C. *Geochim. Cosmochim. Acta* **61**, 5187-5198.
- Tagirov, B.R., Suleimenov, O.M., Seward, T.M., 2007. Zinc complexation in aqueous sulfide solutions: Determination of the stoichiometry and stability of complexes via $\text{ZnS}_{(\text{cr})}$ solubility measurements at 100C and 150 bars. *Geochim. Cosmochim. Acta* **71**, 4942-4953.
- Tanger, J.C.I., Helgeson, H.C., 1988. Calculation of the thermodynamic and transport properties of aqueous species at high pressures and temperatures: Revised equations of state for the

- standard partial molal properties of ions and electrolytes. *American Journal of Science* **288**, 19-98.
- Ullrich, M.K., Pope, J.G., Seward, T.M., Wilson, N., Planer-Friedrich, B., 2013. Sulfur redox chemistry governs diurnal antimony and arsenic cycles at Champagne Pool, Waiotapu, New Zealand. *J. Volcanol. Geotherm. Res.* **262**, 164-177.
- Wagner, W., Cooper, J.R., Dittman, A., Kijima, J., Kretzschmar, H.-J., Kruse, A., Mareš, R., Oguchi, K., Sato, H., Stöcker, I., Šifner, O., Takaishi, Y., Trübenbach, J., Wilkommen, T., 2000. The IAPWS industrial formulation 1997 for the thermodynamic properties of water and steam. *ASME Journal of Engineering for Gas Turbines and Power* **122**, 150-182.
- Ward, K.T., Brown, K.L., Webster-Brown, J., 2006. Mineral precipitation in the Rotokawa geothermal power station, New Zealand. *Proceedings 28th New Zealand Geothermal Workshop*.
- Weissberg, B.G., 1969. Gold-silver ore-grade precipitates from New Zealand thermal waters. *Econ. Geol.* **64**, 95-108.
- Weissberg, B.G., Browne, P.R.L., Seward, T.M., 1979. Ore metals in active geothermal systems, in: Barnes, H.L. (Ed.), *Geochemistry of Hydrothermal Ore Deposits*, 2nd ed. Wiley Interscience, New York, pp. 738-780.
- Williams-Jones, A.E., Heinrich, C.A., 2005. Vapor transport of metals and the formation of magmatic-hydrothermal ore deposits. *Econ. Geol.* **100**, 1287-1312.
- Williams-Jones, A.E., Normand, C., 1997. Controls of mineral parageneses in the system Fe-Sb-S-O. *Econ. Geol.* **92**, 308-324.
- Wilson, N., Webster-Brown, J., Brown, K., 2007. Controls on stibnite precipitation at two New Zealand geothermal power stations. *Geothermics* **36**, 330-347.
- Wood, S.A., Crerar, D.A., Borcsik, M.P., 1987. Solubility of the assemblage pyrite-pyrrhotite-magnetite-sphalerite-galena-gold-stibnite-bismuthinite-argenitite-molybdenite in H₂O-NaCl-CO₂ solutions from 200 to 350°C. *Econ. Geol.* **82**, 1864-1887.
- Zakaznova-Herzog, V.P., Seward, T., 2006. Antimonous acid protonation/deprotonation equilibria in hydrothermal solutions to 300°C. *Geochim. Cosmochim. Acta* **70**, 2298-2310.
- Zotov, A.V., Shikina, N.D., Akinfiev, N.N., 2003. Thermodynamic properties of the Sb(III) hydroxide complex Sb(OH)_{3(aq)} at hydrothermal conditions. *Geochim. Cosmochim. Acta* **67**, 1821-1836.

Chapter (5):

Antimony geochemistry in hydrothermal solutions: Concluding remarks

5.1. Summary of results

The aim of this study was to determine the aqueous antimony species present at stibnite saturation in reducing solutions containing moderate to high concentrations of dissolved sulfide ($S^{2-}_{\text{total}} = 0.001$ to 0.1 mol kg^{-1}) from ambient to supercritical conditions and to obtain the heterogeneous equilibrium constants for stibnite dissolution in equilibrium with these antimony species. This was undertaken because these constants are needed to accurately predict antimony solubility in sulfidic fluids in natural hydrothermal systems. In addition, there is disagreement amongst previously published studies using various techniques (e.g., solubility, Raman spectroscopy, and X-ray absorption spectroscopy), and it was of interest to try to resolve these discrepancies. Thus, an additional aim of this study was to investigate the utility of using both solubility and spectroscopic experimental approaches to study complementary solutions. These objectives were accomplished by combining 30°C flow-through stibnite solubility experiments (Chapter 2), ambient temperature X-ray absorption spectroscopy measurements (Chapter 3), and high-temperature flow-through stibnite solubility experiments (Chapter 4). The main findings from these Chapters are:

Chapter (2): Stibnite solubility and antimony speciation in aqueous sulfide solutions at 30°C

The aqueous antimony species present at ambient temperatures are $\text{Sb}_2\text{S}_4^{2-}$, $\text{H}_2\text{Sb}_2\text{S}_5^{2-}$, HSb_2S_4^- , $\text{H}_3\text{SbS}_2\text{O}$, $\text{Sb}(\text{OH})_3$, and H_2SbO_3^- . Stibnite solubility in moderately to strongly alkaline solutions is solely due to $\text{Sb}_2\text{S}_4^{2-}$ over a wide range of sulfide concentrations from 0.1 to $\sim 0.0005 \text{ mol kg}^{-1}$. Between $\text{pH} \sim 9$ and ~ 5 , partially protonated antimony-sulfide dimers ($\text{H}_2\text{Sb}_2\text{S}_5^{2-}$ and/or HSb_2S_4^- depending on sulfide concentrations) are the stable antimony species at sulfide concentrations from 0.001 to 0.01 mol kg^{-1} . Neutral monomers ($\text{H}_3\text{SbS}_2\text{O}$ and/or $\text{Sb}(\text{OH})_3$ depending on sulfide concentration) make stibnite solubility independent of pH in moderately acidic solutions (i.e., at $\text{pH} < \sim 5$). At sulfide concentrations $\leq 0.0001 \text{ mol kg}^{-1}$, $\text{Sb}(\text{OH})_3$ is a major species at $\text{pH} < 7$ and the predominant species at $\text{pH} > 8$. Equilibrium constants for the heterogeneous solubility reactions at 30°C were summarised in Table (2.8).

Chapter (3): X-ray absorption spectroscopy measurements of antimony- sulfide and- hydroxide complexes at stibnite saturation

Average first coordination shells in alkaline solutions are consistent with $\text{Sb}_2\text{S}_4^{2-}$ at moderate to high sulfide concentrations. At low sulfide concentrations, EXAFS are consistent with mixture of $\text{Sb}_2\text{S}_4^{2-}$, $\text{Sb}(\text{OH})_3$, and H_2SbO_3^- . The quality of the XAS spectra produced by millimolar antimony concentrations ($\leq 0.005 \text{ mol kg}^{-1}$) in aqueous samples is too poor to enable detection of the first shell antimony atoms. However, the combination of XAS average coordination shells with the alkaline solubility curve enabled the elimination of the speciation model including antimony-sulfide monomers (i.e., SbS_3^{3-} and $\text{HSbS}_2\text{O}^{2-}$) at high pH.

Chapter (4): Stibnite solubility and antimony speciation in hydrosulfide solutions from 70 to 400°C

The antimony species in aqueous sulfide solutions in equilibrium with stibnite at temperatures $> 70^\circ\text{C}$ are $\text{Sb}_2\text{S}_4^{2-}$, HSb_2S_4^- , $\text{H}_3\text{SbS}_2\text{O}$, and $\text{Sb}(\text{OH})_3$. With increasing temperature, the stability of neutral antimonous acid, $\text{Sb}(\text{OH})_3$, increases relative to the stability of the antimony-sulfide species. At temperatures $> 300^\circ\text{C}$, $\text{Sb}(\text{OH})_3$ is the only important species except at elevated sulfide concentrations (i.e., $\geq 0.05 \text{ mol kg}^{-1}$). As a result, the relationship of stibnite solubility to changes in sulfide concentration changes with temperature. At $t < \sim 150^\circ\text{C}$ when antimony-sulfide complexes are stable, stibnite solubility increases with increasing sulfide concentration in near neutral fluids for the range of sulfide concentrations found in deep New Zealand geothermal fluids (~ 0.0003 to $\sim 0.007 \text{ mol kg}^{-1}$). In contrast, the relationship is reversed and stibnite solubility decreases with increasing sulfide concentration at $t > 200^\circ\text{C}$. In supercritical fluids with vapour-like density between 390 and 406°C , stibnite solubility was strongly dependent on fluid density, but the relationship to input pH, Cl^- , and sulfide concentration was consistent with the presence of $\text{Sb}(\text{OH})_3$. Equilibrium constants for the heterogeneous solubility reactions up to 350°C are summarised in Tables (4.9).

The thermodynamic data presented in this chapter were used to predict antimony saturation for conditions within the Rotokawa and Ngawha geothermal power stations in New Zealand (Figure 4.12) and highlighted the need for better thermodynamic data the heterogeneous stibnite- $\text{Sb}(\text{OH})_3$ equilibrium between 90 and 150°C . This, however, was not the focus of the current study which was targeted at $\text{Sb}(\text{III})$ -sulfide complexes. The formation of stibnite scaling within these two stations was largely due to a temperature decrease from the geothermal well (temperatures 200 to 220°C) to the exit of the heat-exchangers ($\sim 90^\circ\text{C}$ at Ngawha and $\sim 150^\circ\text{C}$ at Rotokawa). In addition, a pH decrease from $\text{pH} = 7$ to ~ 6 , resulting from the addition of condensed vapour, has the potential to decrease stibnite stability by $\sim 1 \text{ ppm}$ at 150°C or several hundred ppb at 100°C .

5.2. Scope of current study and avenues for future research

Stability of $\text{Sb}(\text{OH})_3$ at temperatures $< 200^\circ\text{C}$

This study was focused on the stoichiometry and stability of antimony-sulfide complexes in the $\text{Sb}(\text{III})$ - $\text{S}(\text{II})$ - H_2O system and most experiments were conducted at sulfide concentrations between 0.01 and 0.1 mol kg^{-1} , from pH 4 to 12, and from 30 to 350°C. The thermodynamic equilibrium constants derived from these experiments can be applied to natural systems to gain insight into antimony transport chemistry and stibnite deposition. However, many reducing fluids in natural settings contain total reduced sulfur concentrations < 0.01 mol kg^{-1} . This study has confirmed that $\text{Sb}(\text{OH})_3$ is major species at moderate to low sulfide concentrations and at elevated temperatures, particularly at $t > 200^\circ\text{C}$. Thus, thermodynamic modeling of antimony geochemistry will still benefit from additional experimental data in the $\text{Sb}(\text{III})$ - $\text{S}(\text{II})$ - O-H system at sulfide concentrations ≤ 0.005 mol kg^{-1} . As noted in the introduction to Chapter (4), published values for heterogeneous equilibrium constant for $\text{Sb}(\text{OH})_3$ are based on antimony-oxide ($\text{Sb}(\text{III})_2\text{O}_{3(\text{s})}$) solubility experiments in the $\text{Sb}(\text{III})$ - O-H system at temperatures $< 200^\circ\text{C}$ and on stibnite solubility experiments at low sulfide concentrations and in pure water at temperatures $\geq 200^\circ\text{C}$. The agreement between these high temperature stibnite solubility experiments is excellent (Figure 4.1). The current study has added to the available experimental data for K_{1033} at 30°C and at 150 through 400°C. However, the variation in reported values within the current and previous studies suggests that more experimental solubility studies are needed from ambient temperature and up to at least 150°C.

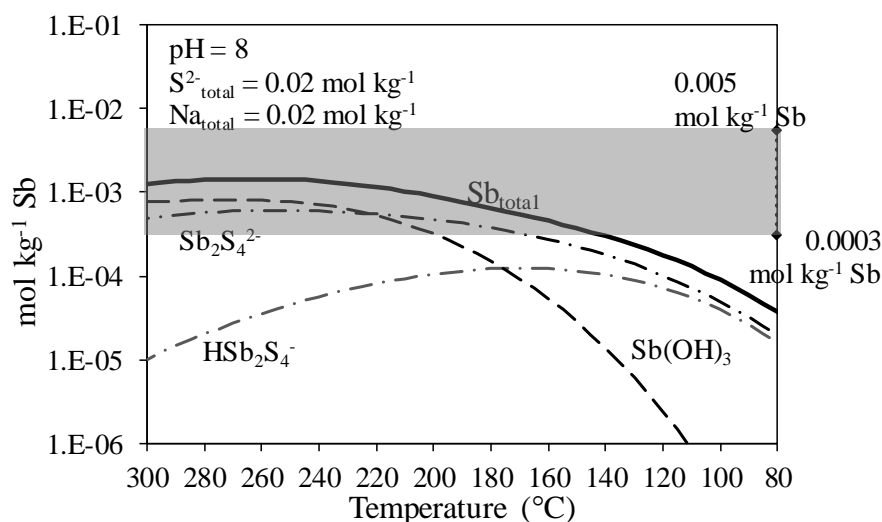
XAS measurements in alkaline solutions at low sulfide concentrations

X-ray absorption spectroscopic measurements were completed on alkaline solutions containing 0.0003 to 0.005 mol kg^{-1} Sb. These experiments presented in Chapter (3) were able to quantify the average coordination environment of antimony, and partially delineate the change from sulfide to hydroxide ligands in decreasing sulfide concentration. The selection of solutions in the current study did not include enough solutions with S:Sb ratios between approximately 1:3 and 6:1 in order to distinguished between various speciation models containing different antimony(III)-sulfide-hydroxide complexes, such as $\text{HSbS}_2\text{O}^{2-}$ or $\text{H}_2\text{SbSO}_2^-$. Combining XAS measurements of $\text{Sb}(\text{III})$ in strongly alkaline solutions with sulfide concentrations ≤ 0.001 mol kg^{-1} and stibnite solubility experiments in similar solutions could be used to investigate the transition between a strongly charged antimony-sulfide dimer (i.e., $\text{Sb}_2\text{S}_4^{2-}$) and a neutral antimony-hydroxide monomer (i.e., $\text{Sb}(\text{OH})_3$). The interpretation of the EXAFS results from such experiments could be assisted by including complementary suites of solutions with similar S:Sb ratios buffered above and below the pK_a of $\text{Sb}(\text{OH})_3$ (i.e., at pH = 11.5 and 12.5), so that the relative magnitude of the contributions of $\text{Sb}(\text{OH})_3$ and H_2SbO_3^- could be constrained.

XAS measurements at stibnite saturation at temperatures $\geq 150^\circ\text{C}$

Previous high temperature XAS are summarised in Figure (4.10) and were able to detect the change in predominate ligand complexing antimony beginning at $\sim 150^\circ\text{C}$. The strongly alkaline pH conditions for most of these experiments make them difficult to quantitatively compare to the current study or to natural systems. The stibnite solubilities measured in this study indicate that in a solution with $\text{pH} = 8$ and a sulfide concentration of 0.02 mol kg^{-1} , the antimony concentration would be at millimolar levels ($0.001 \text{ mol kg}^{-1}$) by $\sim 200^\circ\text{C}$ and have comparable concentrations of $\text{Sb}(\text{OH})_3$ and HSb_2S_4^- between ~ 230 and 250°C (Figure 5.1). Measurements of antimony speciation in a high-temperature XAS cell might provide independent verification of the speciation model presented here or identify a transitional species present that was not identified in the current study due to the limited number of different input sulfide concentrations used.

Figure (5.1) Stibnite solubility and antimony species distribution from 300 to 80°C at $\text{pH} = 8$ and a sulfide concentration of 0.02 mol kg^{-1} at swvp. The range of antimony concentrations used in this study for XAS analysis (Chapter 3) is indicated by gray shaded area (0.0003 to $0.005 \text{ mol kg}^{-1}$). Future XAS experiments could target total antimony concentrations $\sim 0.001 \text{ mol kg}^{-1}$ where both $\text{Sb}(\text{OH})_3$ and antimony-sulfide species constitute a large proportion of the total dissolved antimony.



Stibnite solubility in supercritical aqueous fluids

Experiments were undertaken in this study which measured stibnite solubility in supercritical fluids at $t \sim 400^\circ\text{C}$. The pH and sulfide concentration of these solutions covered a limited range and the fluids were limited to fluids with vapour-like densities. The experiments were made challenging by the cooling of solutions between the back-pressure regulator (near 400°C) and the sampling syringe, which is part of the basic setup of a continuous flow through system. In addition, there has been evidence that in aqueous vapor, antimony solubility is enhanced by the formation of volatile chloride complexes. The high stibnite solubilities measured in the few experiments in this study conducted in supercritical conditions indicated that antimony can be effectively transported in low salinity fluids (the chloride concentration in this study was $3 \times 10^{-4} \text{ mol kg}^{-1}$) with vapour-like densities. Metal and

metalloid transport in such fluids has been invoked in models for the formation of porphyry copper deposits (e.g., Pokrovski et al., 2013 and references therein). The extremely high stibnite solubilities in fluids approaching fluid-like densities make solubility experiments difficult to measure in a flow through experimental apparatus.

Antimony(V)-sulfide complexation

The current study was focused on Sb(III)-S(II) interactions and atmospheric oxygen was eliminated from experimental solutions to prevent the formation of Sb(V) or more oxidized forms of sulfur. Evidence for Sb(V)-sulfide interactions has been found by UV-vis and X-ray absorption spectroscopy (Kunkely and Vogler, 1995; Sherman et al., 2000), by stibnite solubility measurements in a system containing sulfide and elemental (i.e., zero valent) sulfur (Helz, 2002), and by LC-ICP-MS analysis of 20 to 90°C fluids from natural hot springs and their outflows (Planer-Friedrich and Scheinost, 2011; Ullrich et al., 2013).

Helz et al. (2002) measured stibnite solubility from pH = 7.6 to 10.1 in the presence of both sulfide and elemental sulfur and interpreted the results in terms a mixed-valence Sb(III,V) dimer and a Sb(V) dimer, specifically $\text{HSb(III,V)}_2\text{S}_5^-$ and $\text{Sb(V)}_2\text{S}_6^{2-}$. The Sb-S stoichiometry of the mixed-valence complex ($\text{HSb(III,V)}_2\text{S}_5^-$) proposed by Helz et al. (2002) was the same as for the Sb(III) dimer proposed in this study (i.e., $\text{H}_2\text{Sb}_2\text{S}_5^{2-}$). However, the solubility measured by Helz et al. (2002) was generally ~2 orders of magnitude higher than the current study for comparable sulfide concentrations and pH. In addition, the solubility curve measured by Helz et al. (2002) was not independent of pH between pH = 7.5 and 9.5, as it measured in the current study (Figure 2.5). Instead, stibnite solubility increased with decreasing pH when pH < 9.5. These findings and the later LC-ICP-MS studies suggest that Sb(V)-S(II) interactions are an important part of antimony geochemistry at the interface between hydrothermal and surface environments.

Although reduced geothermal fluids can be modeled with the thermodynamic data presented in this study, accurate modeling of antimony geochemistry in environmental settings or in the outflow of hot springs will require thermodynamic data for antimony(V)-sulfide complexes, which is currently extremely limited (i.e., only available for $\text{Sb}_2\text{S}_6^{2-}$ (Helz, 2002) and for SbS_4^{3-} (Akeret, 1953; see compilation in Filella and May, 2003)). X-ray absorption spectroscopy (Sherman et al., 2000) and LC-ICP-MS studies (Planer-Friedrich and Scheinost, 2011; Ullrich et al., 2013) appear to confirm the SbS_4 stoichiometry, but LC-ICP-MS also suggests the presence of an antimony(V) species with SbS_3 stoichiometry (possibly $\text{Sb}_2\text{S}_6^{2-}$?). The UV-vis spectra of $\text{Na}_3[\text{SbS}_4] \cdot 9\text{H}_2\text{O}$ (Schlippe's Salt) dissolved in a 0.001 M NaOH solution was consistent with SbS_4^{3-} (Kunkely and Vogler, 1995). This experiment and the quantum chemical calculations of Tossell (2003a, b) who obtained the UV-vis spectra of Sb(V)-sulfide complexes and their oxidation energetics and deprotonation energies could provide the starting point for UV-vis measurements of Sb(V) in solutions with a wide range of pH and sulfide concentrations.

5.2.2. Ruminations on the value of combining solubility and spectroscopic experimental techniques

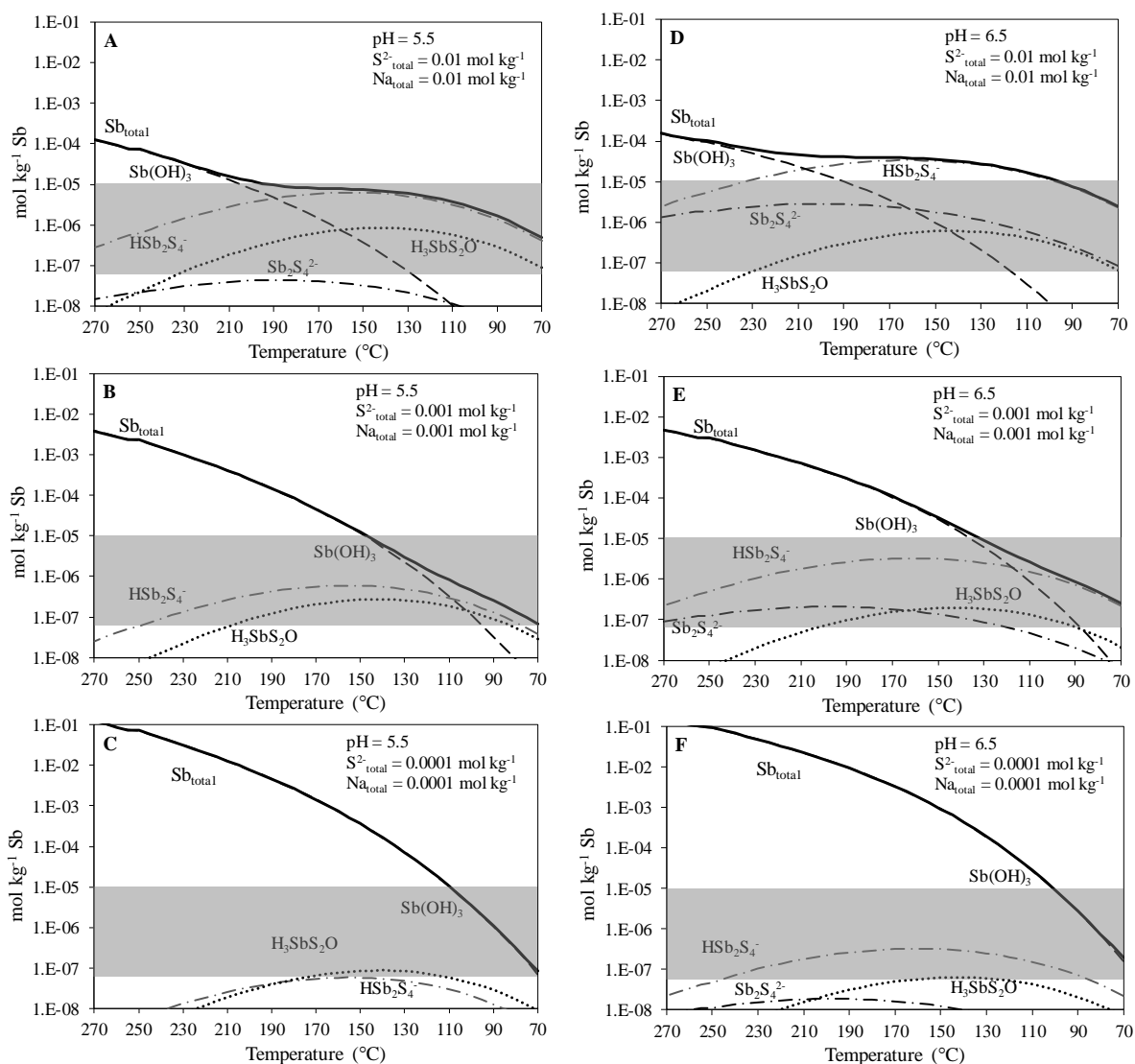
The use of complementary solubility and XAS studies in this work demonstrated that XAS spectroscopy on its own did not identify the thermodynamically stable complex dimer, i.e., $\text{Sb}_2\text{S}_4^{2-}$, by detection of an Sb-Sb interaction at the appropriate distance. Nevertheless, some speciation models (specifically $\text{SbS}_3^{3-} + \text{HSbS}_2\text{O}^{2-}$) could be eliminated when the average first shell coordination numbers derived from EXAFS were combined with the results from solubility experiments. This demonstrates that XAS results may be interpreted erroneously in this system if considered in isolation and that the interpretation of the solubility data can be enhanced by the inclusion of complimentary spectroscopic measurements. As only the fourth study to attempt to use XAS to study Sb(III)-S(II) interactions in solution, the current work emphasizes the importance of different techniques, in this case solubility and XAS, in elucidating reliable stoichiometries and stabilities of aqueous species in redox sensitive, heterogeneous systems involving sparingly soluble compounds (e.g., sulfides).

5.3. Implications for antimony transport by hydrothermal fluids in the Earth's crust

Multiple studies of antimony concentrations in hydrothermal fluids (Simmons et al., 2016), hydrothermally altered rocks (Simmons and Browne, 2000; Chambefort and Dilles, 2015), and ore deposits (Goldfarb et al., 2005) have demonstrated that antimony (along with arsenic and mercury) is an element that can be readily transported to the Earth's surface or the distal parts of a hydrothermal system. In light of the results from the current study, this occurs because appreciable concentrations of antimony (100 to 1000 ppb) can be dissolved in near neutral fluids at temperatures $> 100^\circ\text{C}$ due to the stability of $\text{Sb}(\text{OH})_3$ at higher temperatures (at $t > \sim 120^\circ\text{C}$ for $\text{S}^{2-}_{\text{total}} = 0.001 \text{ mol kg}^{-1}$) and due to the stability of HSb_2S_4^- at lower temperatures (at $t < \sim 120^\circ\text{C}$ for $\text{S}^{2-}_{\text{total}} = 0.001 \text{ mol kg}^{-1}$) for sulfide concentrations typical in crustal hydrothermal systems.

The stability of the $\text{Sb}(\text{OH})_3$ complex at higher temperatures means that, if boiling occurs at reservoir conditions with temperatures between 200 and 300°C , the predominant aqueous antimony complex is not destabilized by the loss of $\text{H}_2\text{S}_{(\text{aq})}$ to the vapor phase (and resulting decrease of HS^- ligands). This is the case in most developed New Zealand geothermal systems where the reservoirs are generally two-phase. Antimony's behavior during boiling is in contrast to gold (Au) and other "softer" metals that are transported as sulfide complexes at these temperatures (Seward, 1989; Stefánsson and Seward, 2004) and thus are sensitive to decreases in the activity of reduced sulfur. In addition, when $\text{Sb}(\text{OH})_3$ is the major aqueous species, stibnite solubility in slightly acidic fluids does not change if the pH is decreased during boiling, oxidation, fluid mixing, or reaction with wallrock because the stability of the $\text{Sb}(\text{OH})_3$ complex is independent of pH at $\text{pH} < \text{pK}_a$ of H_2S . This can be seen by comparing the left and right hand panels of Figure (5.2), which show the decrease in stibnite solubility from 270 to 70°C for two pH's ($\text{pH} = 5.5$ and 6.5) and three sulfide contents (0.01, 0.001, and 0.0001

Figure (5.2) Stibnite solubility and antimony species distribution from 270 to 70°C at pH = 5.5 (A, B, and C) and pH = 6.5 (D, E, and F) for sulfide concentrations of 0.01, 0.001, and 0.0001 mol kg⁻¹. Plots are at swvp. The range of antimony concentrations reported by Simmons et al. (2016) in reservoir fluids sampled from seven New Zealand geothermal systems is indicated by the gray region (i.e., 7 to 1230 µg kg⁻¹ or ~6x10⁻⁸ to 1x10⁻⁵ mol kg⁻¹).



mol kg⁻¹). The Sb(OH)₃ curve, which defines stibnite solubility in all plots at temperatures > ~240°C, is the same at pH = 5.5 (left panels) and at pH = 6.5 (right panels). The difference between the left and right plots is produced by antimony-sulfide species.

When antimony-sulfide complexes are predominant, specifically HSb₂S₄⁻ at the near neutral conditions used in Figure (5.2), stibnite solubility will decrease with decreases in temperature, pH, and sulfide concentration. Such conditions might be encountered the lower-temperature peripheries of hydrothermal systems, particularly for systems with pH and sulfide concentrations at the, respectively, low and high ranges of what is observed in natural systems (i.e., Figure 5.2A). The gray shaded region (Figure 5.2) shows the range of antimony concentrations (~10 ppb to ~1 ppm) reported by Simmons et al. (2016) in reservoir fluids sampled at depth from seven New Zealand geothermal systems and suggests that under certain conditions, namely pH ≤ 5.5, sulfide concentrations ~ 0.01 mol kg⁻¹, and antimony concentrations ~ 1ppm (Figure 5.2A), geothermal fluids may reach saturation with stibnite

at temperatures as high as $\sim 200^{\circ}\text{C}$. However more commonly, stibnite will not become saturated until temperatures $< 150^{\circ}\text{C}$, especially considering that antimony concentrations are often < 500 ppb ($\sim 4 \times 10^{-6} \text{ mol kg}^{-1}$). The most rapid decrease in stibnite solubility represented in Figure (5.2) occurs in fluids with the lowest sulfide concentration ($0.0001 \text{ mol kg}^{-1}$, Figures 5.2C and 5.2F) in response to a temperature decrease. For these conditions, stibnite solubility decreases by two orders of magnitude from $\sim 1 \times 10^{-5}$ to $\sim 1 \times 10^{-7} \text{ mol kg}^{-1}$ (~ 1 ppm to ~ 10 ppb) over a temperature decrease of 40°C from 110 to 70°C (Figures 5.1C and 5.1F). In natural hydrothermal systems, changes in pH and sulfide concentration will accompany temperature decreases, and thus the path of stibnite solubility will be more complicated than the curves represented in Figure (5.2).

Over the temperature range from ambient to hydrothermal, antimony-ligand interactions change from interactions that produce charged complexes with softer, more covalent bonding (i.e., with HS^{-} and S^{2-}) at lower temperatures to neutral complexes with harder, more ionic bonding at higher temperatures (i.e., OH^{-}). This behavior means that the way in which stibnite solubility responds to changes in pH and sulfide ligand availability will vary with temperature. From a geothermal geochemistry perspective, the stability of $\text{Sb}(\text{OH})_3$ will link antimony behavior strongly to temperature, isolate it from changes in pH, salinity, and sulfide concentration, and enable antimony to remain in solution (i.e., act conservatively) until the low temperature regions of a hydrothermal system. From an environmental perspective, the formation of antimony-sulfide complexes allows higher concentrations of antimony to remain in solution at temperatures $< 90^{\circ}\text{C}$ (i.e., Figure 5.2A and 5.2D) and therefore facilitates the aqueous transport of antimony to the Earth's surface.

5.5. References

- Akeret, R., 1953. Ueber die Löslichkeit von Antimon(3)sulfid. Dissertation (PhD thesis) ETH, Zurich, p. 77.
- Chambefort, I., Dilles, J.H., 2015. Trace metals and volatiles zoning in active geothermal systems, Proceedings of the 37th New Zealand Geothermal Workshop, Taupo, New Zealand.
- Filella, M., May, P.M., 2003. Computer simulation of the low-molecular-weight inorganic species distribution of antimony(III) and antimony(V) in natural waters. *Geochim. Cosmochim. Acta* **67**, 4013-4031.
- Goldfarb, R.J., Baker, T., Dubé, B., Groves, D.I., Hart, C.J.R., Gosselin, P., 2005. Distribution, character, and genesis of gold deposits in metamorphic terranes. *Econ. Geol.* **100**, 407-450.
- Helz, G.R., Valerio, Melissa S., Capps, Nathan E., 2002. Antimony speciation in alkaline sulfide solutions: Role of zerovalent sulfur. *Environ. Sci. Technol.* **36**, 943-948.
- Kunkely, H., Vogler, A., 1995. Photochemistry of Aqueous Tetrathioantimonate(V). *Verlag der Zeitschrift für Naturforschung* **50B**, 1155-1157.
- Planer-Friedrich, B., Scheinost, A.C., 2011. Formation and structural characterization of thioantimony species and their natural occurrence in geothermal waters. *Environ. Sci. Technol.* **45**, 6855-6863.
- Pokrovski, G.S., Borisova, A.Y., Bychkov, A.Y., 2013. Speciation and transport of metals and metalloids in geological vapors. *Reviews in Mineralogy and Geochemistry* **76**, 165-218.
- Seward, T.M., 1989. The hydrothermal chemistry of gold and its implication for ore formation: boiling and conductive cooling as examples. *Economic Geology Monograph* **6**, 390-396.
- Sherman, D.M., Ragnarsdottir, K.V., Oelkers, E.H., 2000. Antimony transport in hydrothermal solutions: an EXAFS study of antimony(V) complexation in alkaline sulfide and sulfide-chloride brines at temperatures from 25°C to 300°C at P_{sat} . *Chem. Geol.* **167**, 161-167.

- Simmons, S.F., Brown, K.L., Tutolo, B.M., 2016. Hydrothermal transport of Ag, Au, Cu, Pb, Te, Zn and other metals and metalloids in New Zealand geothermal systems: Spatial patterns, fluid-mineral equilibria, and implications for epithermal mineralization. *Econ. Geol.* **111**, 589-618.
- Simmons, S.F., Browne, P.R.L., 2000. Hydrothermal minerals and precious metals in the Broadlands-Ohaaki geothermal system: Implications for understanding low-sulfidation epithermal environments. *Econ. Geol.* **95**, 971-999.
- Stefánsson, A., Seward, T.M., 2004. Gold(I) complexing in aqueous sulphide solutions to 500°C at 500 bar. *Geochim. Cosmochim. Acta* **68**, 4121-4143.
- Tossell, J.A., 2003a. Calculation of the energetics for the oxidation of Sb(III) sulfides by elemental S and polysulfides in aqueous solution. *Geochim. Cosmochim. Acta* **67**, 3347-3354.
- Tossell, J.A., 2003b. Calculation of the visible-UV absorption spectra of hydrogen sulfide, bisulfide, polysulfides, and As and Sb sulfides, in aqueous solution. *Geochem. Trans.* **4**, 28-33.
- Ullrich, M.K., Pope, J.G., Seward, T.M., Wilson, N., Planer-Friedrich, B., 2013. Sulfur redox chemistry governs diurnal antimony and arsenic cycles at Champagne Pool, Waiotapu, New Zealand. *J. Volcanol. Geotherm. Res.* **262**, 164-177.

Appendix (A)

Figure (A.1) XRD of Chinese stibnite used in experiments.

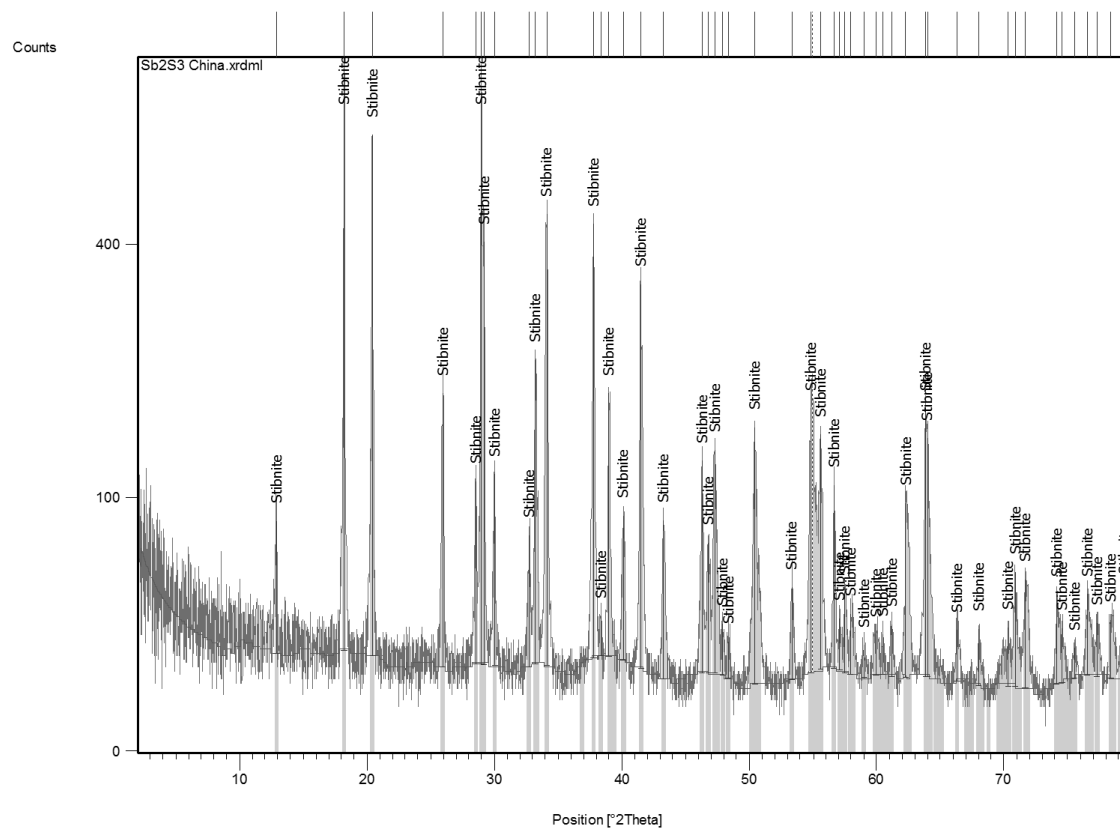


Table (A.1) Calculation of detection limits for antimony analyses by inductively-coupled plasma-optical spectroscopy (ICP-OES) and hydride-generation atomic absorption spectroscopy (HG-AAS).
Reference: Section 1030C of Standard Methods for the Examination of Water and Wastewater (20th Ed.).

ICP-OES		Sb (ppm)		HG-AAS		Sb (ppb)	
QC = 0.05 ppm		Wavelength		QC = 1 ppb		Wavelength	
Date (year-month-day)		206.8	217.5	Date (year-month-day)		206.8	
20150401		0.056296	0.056296	2013		1.1139	
20150401		0.060531	0.057411	20121214		1.2740	
20150401		0.058499	0.06082	20131214		1.0080	
20150401		0.059872	0.060033	20131220		1.0020	
20150401		0.058574	0.060076	20140525		1.0510	
20150401		0.06056	0.061021	20140425		1.0710	
20150401		0.057317	0.060496				
20150303		0.047998	0.051248				
20150303		0.049516	0.050458				
20150303		0.047842	0.050087				
20150319		0.051998	0.049988				
20150319		0.049785	0.04883				
20150319		0.050705	0.052451				
20150319		0.047968	0.047681				
20150309		0.050384	0.050901				
20150309		0.054772	0.05253				
20150309		0.050432	0.051506				
20150309		0.049748	0.048732				
20150319		0.048839	0.046409				
20150319		0.053555	0.054863				
20150319		0.04864	0.051843				
20150323		0.046297	0.04834				
20150324		0.045532	0.053087				
20150324		0.050885	0.054591				
20150324		0.046013	0.051498				
20150324		0.051218	0.053207				
20150324		0.048326	0.055029				
20150216		0.050467	0.052708				
20150216		0.049373	0.048922				
20150216		0.048109	0.051894				
20150216		0.049419	0.054595				
20150218		0.050447	0.052297				
20150225		0.052522	0.054516				
20150225		0.049906	0.051036				
20150225		0.053588	0.052031				
20150227		0.049071	0.048591				
20150227		0.046275	0.049557				
20150227		0.049165	0.047507				
20150227		0.057508	0.054068				
20150227		0.051789	0.0468				
20150227		0.051801	0.047682				
20150227		0.04951	0.049474				
20150227		0.049386	0.052828				
20150209		0.053088	0.054131				
20150209		0.058295	0.060538				
20150216		0.048694	0.05083				
20150216		0.050969	0.051425				
20150216		0.048127	0.052966				
Average (ppm)		0.05145	0.0525798	Average (ppb)		1.086651528	
Stdev (ppm)		0.004012	0.0039011	Stdev (ppb)		0.100707869	
Detection limit (ppm)		0.0132	0.012835	Detection limit (ppb)		0.3313289	
(defined as 3.29*stdev of a low standard)							
% Uncertainty		15.6	14.8			18.5	

Table (A.2) Stibnite solubility data at 30°C. Experiment number, pH, antimony concentration, sulfide concentration, oven temperature, and sodium concentration for stibnite solubility experiments. Data is listed by increasing pH. Concentrations, pH, and temperatures are median values.

Exp.	pH	2* σ	Sb (mol kg ⁻¹)	2* σ	S _{tot} (mol kg ⁻¹)	2* σ	T _{oven} (°C)	2* σ	Na (mol kg ⁻¹)
Sb85	4.56	0.002	4.34x10 ⁻⁹	7.9x10 ⁻⁹	0.020	0.0012	31.9	0.1	0
Sb62	4.66	0.23	3.21x10 ⁻⁹	1.1x10 ⁻⁹	0.021	0.0023	32.3	2.1	0.0001
Sb63	4.70	0.03	1.12x10 ⁻⁸	1.7x10 ⁻⁹	0.093	0.0077	32.8	0.5	0.0006
Sb61	4.92	0.03	4.23x10 ⁻⁹	1.4x10 ⁻⁹	0.021	0.0018	32.0	0.1	0.0001
Sb60	5.07	0.14	4.81x10 ⁻⁹	1.3x10 ⁻⁹	0.019	0.0011	31.9	0.6	0.0002
Sb58	5.59	0.11	1.74x10 ⁻⁸	2.9x10 ⁻⁹	0.020	0.0004	32.5	0.7	0.0009
Sb64	5.99	0.06	2.89x10 ⁻⁸	6.0x10 ⁻⁹	0.012	0.0027	31.8	0.4	0.0014
Sb57	6.06	0.06	1.58x10 ⁻⁷	4.1x10 ⁻⁸	0.020	0.0012	31.9	0.4	0.0026
Sb96	6.36	0.05	2.26x10 ⁻⁶	1.2x10 ⁻⁷	0.070	0.0013	30.4	0.2	0.0201
Sb96	6.43	0.05	2.20x10 ⁻⁶	1.3x10 ⁻⁷	0.063	0.0026	30.7	0.2	0.0201
Sb96	6.46	0.06	2.49x10 ⁻⁶	2.1x10 ⁻⁷	0.060	0.0017	31.3	0.3	0.0201
Sb84	6.47	na	2.31x10 ⁻⁷	5.1x10 ⁻⁸	0.024	0.0014	31.2	0.3	0.0065
Sb83	6.48	0.02	8.92x10 ⁻⁸	8.8x10 ⁻⁹	0.012	0.0004	32.4	0.4	0.0031
Sb82	6.84	0.02	4.47x10 ⁻⁷	5.5x10 ⁻⁸	0.015	0.0008	32.5	0.4	0.0068
Sb56	6.91	0.04	1.74x10 ⁻⁶	5.6x10 ⁻⁷	0.021	0.0026	32.0	0.8	0.0112
Sb55	7.10	0.02	2.74x10 ⁻⁶	6.9x10 ⁻⁷	0.026	0.0009	32.5	0.2	0
Sb54	7.11	0.04	1.12x10 ⁻⁵	1.0x10 ⁻⁶	0.053	0.0018	32.3	1.8	0.0352
Sb66	7.28	0.03	2.00x10 ⁻⁶	3.6x10 ⁻⁷	0.028	0.0010	31.8	0.5	0.0206
Sb95	7.40	0.02	1.68x10 ⁻⁶	3.0x10 ⁻⁷	0.013	0.0012	30.8	0.2	0.0104
Sb68	7.45	0.05	1.77x10 ⁻⁵	3.2x10 ⁻⁷	0.049	0.0018	31.9	0.6	0.0206
Sb67	7.56	0.04	1.84x10 ⁻⁵	1.1x10 ⁻⁶	0.051	0.0015	31.5	0.4	0.0429
Sb95	7.97	0.02	1.10x10 ⁻⁶	3.3x10 ⁻⁸	0.010	0.0003	31.6	na	0.0104
Sb74	8.06	0.00	1.21x10 ⁻⁶	1.7x10 ⁻⁷	0.010	0.0002	32.1	0.0	0.0100
Sb73	8.09	0.02	9.24x10 ⁻⁷	1.3x10 ⁻⁸	0.010	0.0004	31.5	0.2	0.0101
Sb72	8.11	0.16	1.76x10 ⁻⁶	1.4x10 ⁻⁷	0.010	0.0001	32.3	0.1	0.0099
Sb65	8.19	na	2.28x10 ⁻⁶	2.2x10 ⁻⁷	0.021	0.0005	31.6	0.7	0.0204
Sb69	8.25	0.01	3.05x10 ⁻⁵	2.2x10 ⁻⁶	0.049	0.0033	31.5	0.9	0.0514
Sb95	8.27	0.01	1.11x10 ⁻⁶	2.7x10 ⁻⁸	0.010	0.0004	31.3	0.5	0.0104
Sb40	8.57	0.11	3.57x10 ⁻⁵	2.5x10 ⁻⁶	0.050	0.0045	30.0	na	0.0520
Sb42	8.78	0.03	3.57x10 ⁻⁵	2.9x10 ⁻⁶	0.051	0.0045	27.6	1.2	0.0520
Sb44	9.05	0.04	3.65x10 ⁻⁵	3.1x10 ⁻⁷	0.054	0.0031	30.1	3.4	0.0534
Sb71	9.53	0.08	1.64x10 ⁻⁵	8.6x10 ⁻⁷	0.019	0.0001	31.8	na	0.0201
Sb45	9.57	0.02	4.96x10 ⁻⁵	6.2x10 ⁻⁷	0.053	0.0036	30.0	0.1	0.0533
Sb78	9.59	0.01	1.42x10 ⁻⁵	5.2x10 ⁻⁷	0.022	0.0005	31.9	0.0	0.0233
Sb47	9.79	0.06	6.91x10 ⁻⁵	2.7x10 ⁻⁶	0.051	0.0007	30.5	0.5	0.0531
Sb78	9.79	0.05	1.84x10 ⁻⁵	2.7x10 ⁻⁶	0.022	0.0005	32.0	0.8	0.0233
Sb46	9.83	0.11	6.62x10 ⁻⁵	1.1x10 ⁻⁶	0.051	0.0020	29.7	0.5	0.0535
Sb46	9.88	0.05	7.16x10 ⁻⁵	2.3x10 ⁻⁶	0.051	0.0020	30.2	0.5	0.0535

Table (A.1) Stibnite solubility data at 30°C. Continued

Exp.	pH	2* σ	Sb (mol kg ⁻¹)	2* σ	S _{tot} (mol kg ⁻¹)	2* σ	T _{oven} (°C)	2* σ	Na (mol kg ⁻¹)
Sb50	10.10	0.08	2.85x10 ⁻⁴	2.4x10 ⁻⁶	0.099	0.0058	30.7	0.1	0.0999
Sb48	10.25	0.05	1.21x10 ⁻⁴	1.2x10 ⁻⁵	0.052	0.0042	30.5	1.4	0.0530
Sb49	10.43	0.01	1.89x10 ⁻⁴	2.4x10 ⁻⁶	0.053	0.0043	30.7	0.5	0.0532
Sb90	10.57	0.03	1.47x10 ⁻⁵	3.1x10 ⁻⁷	2.2E-05	4.8E-07	31.7	0.3	0.0005
Sb51	11.09	0.03	4.33x10 ⁻³	3.8x10 ⁻⁴	0.097	0.0059	30.7	0.4	0.1001
Sb51	11.17	0.05	3.98x10 ⁻³	5.9x10 ⁻⁵	0.097	0.0083	30.7	2.5	0.1001
Sb77	11.20	0.03	1.48x10 ⁻³	1.8x10 ⁻⁴	0.057	0.0009	31.7	0.2	0.0599
Sb77	11.29	0.07	1.73x10 ⁻³	2.1x10 ⁻⁵	0.057	0.0085	31.8	na	0.0599
Sb77	11.35	0.06	2.13x10 ⁻³	1.9x10 ⁻⁴	0.056	0.0008	31.8	na	0.0599
Sb75	11.38	0.06	3.70x10 ⁻⁴	1.0x10 ⁻⁵	0.009	0.0003	31.7	0.1	0.0116
Sb75	11.40	0.06	3.97x10 ⁻⁴	1.1x10 ⁻⁵	0.009	5.1E-05	31.7	0.3	0.0116
Sb75	11.42	0.03	4.15x10 ⁻⁴	5.6x10 ⁻⁶	0.008	0.0003	32.0	0.3	0.0116
Sb80	11.81	na	1.75x10 ⁻³	1.3x10 ⁻⁴	0.018	0.0004	31.0	0.2	0.0237
Sb80	11.87	0.01	2.00x10 ⁻³	5.6x10 ⁻⁵	0.018	0.0003	31.3	0.2	0.0237
Sb91	11.98	0.02	9.27x10 ⁻⁴	1.3x10 ⁻⁴	0.001	0.0002	31.6	0.2	0.0102

VisualBasic code to use DataFitX to run non-linear regression fits on solubility data in an Excel spreadsheet. Fits could be weighted or non-weighted and regression tolerances could be set in the "Fitting_Setup" sheet. Inputs were (a) antimony concentration, (b) activity of H⁺ (aH⁺), (c) activity of HS⁻, and (d) ionic strength. Variables were heterogeneous solubility constants that could be set to a constant value if desired. The parameters A, B, and B_Dot reference named ranges in "Fitting_Setup" spreadsheet. The equations used for these constants are the following:

$$A = 0.00000000041775 * ((Temp + 273.15)^4) - 0.00000069009 * ((Temp + 273.15)^3) + 0.00042737 * ((Temp + 273.15)^2) - 0.11558 * (Temp + 273.15) + 11.975$$

$$B = (0.00025587 * (Temp + 273.15) + 0.2487) * 10^8$$

$$Bdot = IF(Temp > 299, 0, IF(Temp < 200, -0.00000030611 * Temp * Temp + 0.0001027 * Temp + 0.038646, -0.0000028612 * Temp * Temp + 0.00094299 * Temp - 0.026621))$$

*******Debye-Huckel Equation for activity coefficient*******

Function G(I As Double, z As Double, Optional Size As Variant) As Double
Dim A As Double, B As Double, B_Dot As Double

A = Worksheets("Fitting_Setup").Range("A").Value
B = Worksheets("Fitting_Setup").Range("B").Value
B_Dot = Worksheets("Fitting_Setup").Range("Bdot").Value

'A = 0.00000000041775 * ((Temp + 273.15)^4) - 0.00000069009 * ((Temp + 273.15)^3) +
0.00042737 * ((Temp + 273.15)^2) - 0.11558 * (Temp + 273.15) + 11.975
'B = (0.00025587 * (Temp + 273.15) + 0.2487) * 10^8
'Bdot = IF(Temp > 299, 0, IF(Temp < 200, -0.00000030611 * Temp * Temp + 0.0001027 *
Temp + 0.038646, -0.0000028612 * Temp * Temp + 0.00094299 * Temp - 0.026621))

If z = 0 Then

G = 1#

Else

If IsMissing(Size) Then

Select Case Abs(z)

Case 1

Size = 0.00000004

Case 2

Size = 0.00000005

Case 3

Size = 0.00000004

Case Else

Size = 0.00000004

End Select

End If

G = 10 ^ (-A * z * z * Sqr(I) / (1 + B * Size * Sqr(I)) + B_Dot * I)

End If

End Function

*******Fitting Function*******

Sub Fit_Solubility_Data()

Dim Found As Boolean, WeightedFit As Boolean

Dim OutputSheet As String, InputSheet As String, ExptSheetS As String, TheoreticalSheet As String

Dim InputArray As Variant, Param_Array As Variant, Series As Variant, PredictArrayIn() As Double, PredictArrayOut() As Double, Deviation() As Double

Dim DataArray() As Double

```

Dim NumParams As Integer, NumDataRows As Integer, NumDataColumns As Integer,
NumSeries As Integer, TotNumSeries As Integer
Dim SeriesNames() As String, Param_Names() As String, Param_Estimate() As Double
Dim I As Integer, J As Integer, K As Integer, Lb As Integer, Lb_2 As Integer, Ub_2 As
Integer, Ub As Integer, YSeriesColNum As Integer
Dim Rw As Integer, Cl As Integer, Failed As Boolean
Dim Cl As Double
Dim OutArray As Variant
Dim ModelString As String, Title As String, CurrentDir As String, LogDir As String,
ResultsFile As String, TimeStamp As String
Dim ResultsTable As Variant
'*** DataFitX declarations
Dim Model As MultipleNonlinearRegression
Dim Parameter As RegressionParameter
Dim SolubilityData As DataCollection
Dim ConstantArray As Variant
Dim ConstantKs As Variant
Application.ScreenUpdating = False
'***
**** Setup output sheet
OutputSheet = Worksheets("Fitting_Setup").Range("OutputSheetName").Value
InputSheet = Worksheets("Fitting_Setup").Range("InputsheetName").Value
For Each sht In Worksheets
    If sht.Name = OutputSheet Then
        Worksheets(sht.Name).Cells.Delete
        Found = True
        Exit For
    End If
Next sht
If Not Found Then
    Worksheets.Add
    ActiveSheet.Name = OutputSheet
End If
'***
***** Read in fit parameters from setup sheet
Title = Worksheets("Fitting_Setup").Range("Title").Value
Param_Array = Worksheets("Fitting_Setup").Range("Complex_Estimates").Value
ConstantArray = Worksheets("Fitting_Setup").Range("ConstantKs").Value
Lb = LBound(Param_Array, 1)
Ub = UBound(Param_Array, 1)
ReDim Param_Names(Lb To Ub)
ReDim Param_Estimate(Lb To Ub)
NumParams = Ub - Lb + 1
For J = Lb To Ub
    If Len(Param_Array(J, 1)) = 0 Then
        NumParams = J - 1
        Exit For
    End If
    Param_Names(J) = Param_Array(J, 1)
    Param_Estimate(J) = Param_Array(J, 2)
Next
'***
**** Read in independent variables from the fit set up sheet and input data sheet
Series = Worksheets("Fitting_Setup").Range("Series").Value
Lb = LBound(Series, 1)
Ub = UBound(Series, 1)
NumSeries = Ub - Lb + 1

```

```

For J = Lb To Ub
    If Len(Series(J, 1)) = 0 Then
        NumSeries = J - 1
        Exit For
    End If
Next
ReDim SeriesNames(0 To NumSeries)
For J = 0 To NumSeries - 1
    SeriesNames(J) = Series(J + Lb, 1)
Next
NumDataRows = Worksheets(InputSheet).Range("A1").CurrentRegion.Rows.Count
NumDataColumns = Worksheets(InputSheet).Range("A1").CurrentRegion.Columns.Count
InputArray = Worksheets(InputSheet).Range("A1").CurrentRegion.Value
ReDim DataArray(0 To NumDataRows - 2, 0 To NumSeries)
On Error Resume Next
For I = 1 To NumSeries
    J = 0
    J = Application.WorksheetFunction.Match(SeriesNames(I - 1),
Worksheets(InputSheet).Rows(1), 0)
    If (J = 0) Then
        MsgBox ("Can't find series name '" & SeriesNames(I - 1) & "' in first row of sheet '" &
InputSheet)
    End
End If
    For K = 0 To NumDataRows - 1
        DataArray(K, I - 1) = Worksheets(InputSheet).Cells(K + 2, J).Value
    Next
Next
'***
*** Read in the dependent variable name from fit setup sheet and values from input
'sheet
YSeriesColNum = 0
SeriesNames(NumSeries) = Worksheets("Fitting_Setup").Range("Y").Value ' add onto the
end of the series names; recall 0 is the first index
YSeriesColNum = Application.WorksheetFunction.Match(SeriesNames(NumSeries),
Worksheets(InputSheet).Rows(1), 0)
If YSeriesColNum = 0 Then
    MsgBox ("Can't find Yseries name '" & SeriesNames(NumSeries) & "' in first row of
sheet '" & InputSheet)
End
End If
For K = 0 To NumDataRows - 1
    DataArray(K, NumSeries) = Worksheets(InputSheet).Cells(K + 2, YSeriesColNum).Value
Next
*** Now read in the weights (if any)
If Len(Worksheets("Fitting_Setup").Range("Weights").Value) > 0 Then
    WeightedFit = True
    YSeriesColNum = 0
    TotNumSeries = NumSeries + 1
    ReDim Preserve SeriesNames(0 To TotNumSeries)
    SeriesNames(TotNumSeries) = Worksheets("Fitting_Setup").Range("Weights").Value '
add onto the end of the series names +1 for weight; recall 0 is the first index
    YSeriesColNum = Application.WorksheetFunction.Match(SeriesNames(TotNumSeries),
Worksheets(InputSheet).Rows(1), 0)
    If YSeriesColNum = 0 Then
        MsgBox ("Can't find Weights name '" & SeriesNames(TotNumSeries) & "' in first row of
sheet '" & InputSheet)
    End
End If

```

```

End
End If
ReDim Preserve DataArray(0 To NumDataRows - 2, 0 To TotNumSeries)
For K = 0 To NumDataRows - 1
    DataArray(K, TotNumSeries) = Worksheets(InputSheet).Cells(K + 2,
YSeriesColNum).Value ' Add Weights series to end of the data array
Next
Else
    WeightedFit = False
    TotNumSeries = NumSeries
End If
On Error GoTo 0
****

**** Set up regression model from settings in fit setup sheet
Set Model = New MultipleNonlinearRegression
Set SolubilityData = New DataCollection
Model.RegressionTolerance = Worksheets("Fitting_Setup").Range("RegTolerance").Value
Model.MaxIterations = Worksheets("Fitting_Setup").Range("MaxIterations").Value
Model.MaxUnchangedIterations =
Worksheets("Fitting_Setup").Range("MaxUnchangedIterations").Value
SolubilityData.ImportSeriesFromArray DataArray, SeriesNames
ModelString = Worksheets("Fitting_Setup").Range("Model").Value
For I = 0 To NumSeries - 1
    SolubilityData(SeriesNames(I)).RegressionKey = "X" & (I + 1)
    ModelString = Replace(ModelString, SeriesNames(I), "X" & (I + 1))
Next
SolubilityData(SeriesNames(NumSeries)).RegressionKey = "Y" ' this is the Y series
If WeightedFit Then
    SolubilityData(SeriesNames(TotNumSeries)).RegressionKey = "SD" ' this is the Weights
series
End If
****

Model.DefineUserModel ModelString, dfxLocaleEnglish, Title
Lb = LBound(Param_Names)
For J = Lb To NumParams - Lb + 1
    If Not (IsNumeric(ConstantArray(J, 1))) Then
        Model.RegressionParameters.Item(Param_Names(J)).InitialEstimate = Param_Estimate(J)
    End If
Next
****

**** Fit data with model and write out results to text file and sheet if solution found
Model.FitCollection SolubilityData
Rw = 1
Worksheets(OutputSheet).Activate
LogDir = Worksheets("Fitting_Setup").Range("LogDir").Value
If Model.IsSolved Then
    If WeightedFit And Not (Model.IsWeighted) Then
        MsgBox ("Check SD column data; have been ignored in model fitting")
    End If
    ResultsFile = Worksheets("Fitting_Setup").Range("ResultsFile").Value
    TimeStamp = "_" & Year(Now) & Month(Now) & Hour(Now) & Minute(Now) &
Second(Now)
    Open LogDir & ResultsFile & TimeStamp & ".txt" For Output As #1
    Cells(Rw, 1).Offset(0, TotNumSeries + 4) = Title
    Print #1, DateTime.Now
    Print #1, Title
    Rw = Rw + 1

```



```

CI = Worksheets("Fitting_Setup").Range("CI").Value
Cells(Rw, 1).Offset(0, TotNumSeries + 4) = "Parameter"
Cells(Rw, 1).Offset(0, TotNumSeries + 5) = "Value"
Cells(Rw, 1).Offset(0, TotNumSeries + 6) = "Standard Error"
Cells(Rw, 1).Offset(0, TotNumSeries + 7) = "p Value"
Cells(Rw, 1).Offset(0, TotNumSeries + 8) = "CI (" & CI & "%)"
Rw = Rw + 1
For Each Parameter In Model.RegressionParameters
    Cells(Rw, 1).Offset(0, TotNumSeries + 4) = Parameter.Name
    Cells(Rw, 1).Offset(0, TotNumSeries + 5) = Parameter.Value
    Cells(Rw, 1).Offset(0, TotNumSeries + 6) = Parameter.StandardError
    Cells(Rw, 1).Offset(0, TotNumSeries + 7) = Parameter.ProbT
    Cells(Rw, 1).Offset(0, TotNumSeries + 8) = Parameter.CalculateCIDelta(CI)
    Print #1, "Parameter"; Tab(20); Parameter.Name
    Print #1, "Value"; Tab(20); Parameter.Value
    Print #1, "Standard Error"; Tab(20); Parameter.StandardError
    Print #1, "p Value"; Tab(20); Parameter.ProbT
    Print #1, "CI (" & CI & "%)"; Tab(20); Parameter.CalculateCIDelta(CI)
    Rw = Rw + 1
Next Parameter
Cells(Rw, 1).Offset(0, TotNumSeries + 4) = "Error Sum of squares = "
Cells(Rw, 1).Offset(0, TotNumSeries + 5) = Model.SST
Cells(Rw + 1, 1).Offset(0, TotNumSeries + 4) = "Regression sum of squares = "
Cells(Rw + 1, 1).Offset(0, TotNumSeries + 5) = Model.SSR
Cells(Rw + 2, 1).Offset(0, TotNumSeries + 4) = "Total Sum of Squares = "
Cells(Rw + 2, 1).Offset(0, TotNumSeries + 5) = Model.SST
Cells(Rw + 3, 1).Offset(0, TotNumSeries + 4) = "R^2 ="
Cells(Rw + 3, 1).Offset(0, TotNumSeries + 5) = Model.R2
Cells(Rw + 4, 1).Offset(0, TotNumSeries + 4) = "Standard Error ="
Cells(Rw + 4, 1).Offset(0, TotNumSeries + 5) = Model.StandardError
Cells(Rw + 5, 1).Offset(0, TotNumSeries + 4) = "ProbF ="
Cells(Rw + 5, 1).Offset(0, TotNumSeries + 5) = Model.ProbF
Cells(Rw + 6, 1).Offset(0, TotNumSeries + 4) = "Y ="
Cells(Rw + 6, 1).Offset(0, TotNumSeries + 9) =
Worksheets("Fitting_Setup").Range("Model").Value
Cells(Rw + 7, 1).Offset(0, TotNumSeries + 4) = "Model passed to DataFitX ="
Cells(Rw + 7, 1).Offset(0, TotNumSeries + 9) = ModelString
Print #1, "Error Sum of squares = "; Tab(30); Model.SST
Print #1, "Regression sum of squares = "; Tab(30); Model.SSR;
Print #1, "Total Sum of Squares = "; Tab(30); Model.SST
Print #1, "R^2 ="; Tab(30); Model.R2
Print #1, "Standard Error = "; Tab(30); Model.StandardError
Print #1, "ProbF = "; Tab(30); Model.ProbF
Print #1, "Y ="; Tab(30); Worksheets("Fitting_Setup").Range("Model").Value
Print #1, "Model passed to DataFitX ="; Tab(30); ModelString
Close #1
ResultsTable = Model.ResultTables.ExportSeriesToArrayAlt
Lb = LBound(ResultsTable, 1)
Lb_2 = LBound(ResultsTable, 2)
Ub = UBound(ResultsTable, 1)
Ub_2 = UBound(ResultsTable, 2)
Range(Cells(1, 1), Cells(Ub - Lb + 1, Ub_2 - Lb_2 + 1)).Offset(1, 0) = ResultsTable
For I = 0 To TotNumSeries
    Range("A1").Offset(0, I).Value = SeriesNames(I)
Next
' more headings
Range("A1").Offset(0, TotNumSeries + 1).Value = "Predicted"

```

```

Range("A1").Offset(0, TotNumSeries + 2).Value = "Residual"
Range("A1").CurrentRegion.Columns.AutoFit
Cells(1, TotNumSeries + 5).CurrentRegion.Columns.AutoFit
Columns(TotNumSeries + 5).Font.Bold = True
Range(Cells(2, TotNumSeries + 5), Cells(2, TotNumSeries + 9)).Font.Bold = True
Else
    MsgBox Model.LastSolveError
    MsgBox "Fit failed. See log file"
End If
Model.SaveLog LogDir & Trim(Title) & "_LOG.txt"
MsgBox Model.LastSolveError
MsgBox "log file written to " & LogDir & Trim(Title) & "_LOG.txt"
****
If Model.IsSolved Then
    ExptSheetS = Worksheets("Fitting_Setup").Range("ExptConstantS").Value
    TheoreticalSheet = Worksheets("Fitting_Setup").Range("Theoretical").Value
    If Not Prediction(TheoreticalSheet, NumSeries, SeriesNames, Model) Then End
    If Not Prediction(ExptSheetS, NumSeries, SeriesNames, Model) Then
        For J = 1 To Ub - Lb + 1
            Worksheets(ExptSheetS).Cells(J + 1, 20).Value = ResultsTable(Lb + J - 1, Ub_2) /
ResultsTable(Lb + J - 1, Ub_2 - 1) + 1
            Worksheets(ExptSheetS).Cells(J + 1, 24).Value = ResultsTable(Lb + J - 1, Ub_2)
        Next
        Worksheets(ExptSheetS).Cells(1, 20).Value = "Deviation"
        Worksheets(ExptSheetS).Cells(1, 24).Value = "Residuals"
        Worksheets(ExptSheetS).ChartObjects("DataPlot1").Activate
        ActiveChart.ChartArea.Copy
        Worksheets(ExptSheetS).ChartObjects("DataPlot1").Copy
        Sheets(OutputSheet).Select
        Range("M20").Select
        ActiveSheet.Paste
    End If
End Sub

```

Table (A.3) Stibnite solubility data from 70 to 400°C. Data listed by temperature. Two pH values are included: the pH measured at room temperature (pH_{exit}) and pH calculated by charge balance without antimony-sulfide species is included (pH_{calc}).

Exp.	T (°C)	2*σ	P (bar)	2*σ	pH _{exit}	2*σ	pH _{calc} with Sb(OH) ₃	Sb (mol kg ⁻¹)	2*σ	S _{tot} (mol kg ⁻¹)	2*σ
Sb107	66.6	0.4	25.9	1.3	8.51	0.01	8.19	3.31x10 ⁻⁵	1.01x10 ⁻⁵	0.011	0.0007
Sb108	68.8	0.3	23.0	0.3	8.44	0.10	7.97	3.38x10 ⁻⁴	7.86x10 ⁻⁵	0.055	0.005
Sb109	69.0	0.2	23.7	1.4	6.38	0.00	6.53	3.12x10 ⁻⁶	1.01x10 ⁻⁶	0.025	0.001
Sb103	70.4	0.0	23.4	0.0	3.59	-	3.52	1.20x10 ⁻⁷	4.18x10 ⁻⁸	0.032	0.000
Sb102	70.7	0.2	26.3	5.2	3.53	0.06	3.52	1.92x10 ⁻⁷	1.54x10 ⁻⁷	0.010	0.003
Sb100	71.1	0.3	38.0	5.7	6.49	0.01	6.51	9.35x10 ⁻⁶	4.69x10 ⁻⁶	0.012	0.001
Sb101	74.0	0.0	26.5	0.0	4.58	0.21	4.48	2.24x10 ⁻⁷	1.10x10 ⁻⁷	0.011	0.0003
Sb106	75.4	0.5	25.2	0.8	5.89	0.03	5.87	2.58x10 ⁻⁶	6.21x10 ⁻⁷	0.013	0.003
Sb103	98.0	0.0	27.6	0.0	-	-	3.52	1.41x10 ⁻⁶	6.83x10 ⁻⁷	-	-
Sb105	107.4	0.5	23.6	0.1	7.12	0.01	6.60	3.02x10 ⁻⁵	2.15x10 ⁻⁶	0.007	0.002
Sb99	108.7	0.4	63.1	17.5	7.22	0.03	7.38	7.74x10 ⁻⁵	6.33x10 ⁻⁶	0.028	0.001
Sb105	110.5	0.3	159.0	0.3	-	-	6.58	3.46x10 ⁻⁵	4.76x10 ⁻⁶	0.007	0.001
Sb105	111.2	0.8	43.9	4.0	7.28	0.01	6.52	3.82x10 ⁻⁵	1.55x10 ⁻⁵	0.008	0.003
Sb104	117.9	1.5	26.2	0.2	4.93	0.08	4.69	1.40x10 ⁻⁶	5.06x10 ⁻⁷	0.014	0.003
Sb101	146.0	0.0	20.7	0.0	4.73	-	4.50	2.23x10 ⁻⁶	1.51x10 ⁻⁶	0.010	-
Sb106	146.9	1.9	28.0	0.8	5.83	0.08	5.99	4.17x10 ⁻⁶	1.14x10 ⁻⁶	0.010	0.001
Sb109	148.5	1.2	32.2	1.1	6.38	0.00	6.51	1.33x10 ⁻⁵	1.95x10 ⁻⁶	0.025	0.002
Sb100	149.8	0.1	64.1	1.0	-	-	6.45	7.77x10 ⁻⁶	1.09x10 ⁻⁶	0.013	6.2E-05
Sb100	150.1	0.9	29.6	0.8	6.52	-	6.37	1.68x10 ⁻⁵	5.38x10 ⁻⁶	0.015	0.003
Sb103	150.3	0.0	0.0	0.0	-	-	3.52	1.56x10 ⁻⁶	5.56x10 ⁻⁷	-	-
Sb98	152.5	10.3	82.6	51.8	7.02	0.05	7.25	5.16x10 ⁻⁵	5.66x10 ⁻⁶	0.030	0.004
Sb107	153.2	1.1	30.4	0.2	8.47	0.11	7.99	2.16x10 ⁻⁴	1.82x10 ⁻⁵	0.011	0.0004
Sb97	154.5	4.9	63.4	3.7	7.49	0.05	8.35	1.08x10 ⁻⁴	2.90x10 ⁻⁵	0.022	0.004
Sb107	193.1	0.4	39.1	0.7	8.41	0.07	7.88	5.84x10 ⁻⁴	2.64x10 ⁻⁴	0.011	0.0009
Sb106	193.4	1.0	31.0	0.9	-	-	5.90	6.69x10 ⁻⁶	1.37x10 ⁻⁶	0.012	6.8E-05
Sb108	193.5	0.6	39.4	18.5	10.80	0.01	7.87	4.02x10 ⁻³	5.56x10 ⁻⁴	0.053	0.003
Sb102	195.9	0.4	26.3	0.2	-	-	3.53	4.63x10 ⁻⁶	1.74x10 ⁻⁶	0.011	0.001
Sb109	201.4	1.4	38.0	0.2	6.43	-	6.50	4.10x10 ⁻⁵	1.38x10 ⁻⁵	0.025	0.003
Sb94	203.0	2.0	45.1	3.8	7.54	0.17	8.14	1.87x10 ⁻⁴	1.19x10 ⁻⁵	0.020	0.001
Sb98	204.9	9.8	108.8	63.6	7.12	0.03	7.33	1.40x10 ⁻⁴	9.70x10 ⁻⁶	0.028	0.003
Sb100	205.1	2.7	30.0	0.7	6.57	0.14	6.44	3.22x10 ⁻⁵	2.36x10 ⁻⁵	0.013	0.0001
Sb106	246.8	0.4	61.9	0.7	-	-	5.93	3.30x10 ⁻⁵	2.32x10 ⁻⁵	0.011	0.011
Sb107	248.2	1.9	85.2	0.3	8.94	-	7.34	1.34x10 ⁻³	1.72x10 ⁻⁴	0.015	0.001
Sb98	248.3	10.2	161.9	29.8	-	-	7.26	3.62x10 ⁻⁴	2.71x10 ⁻⁵	0.029	0.005
Sb100	251.5	2.2	55.4	0.7	-	-	6.45	2.07x10 ⁻⁴	3.96x10 ⁻⁵	0.013	0.0005
Sb108	251.6	0.8	84.0	0.3	-	-	7.94	3.43x10 ⁻³	5.46x10 ⁻⁴	0.056	0.013
Sb109	252.7	0.5	62.8	0.4	-	-	6.49	9.73x10 ⁻⁵	3.45x10 ⁻⁵	0.025	0.001
Sb102	252.7	1.5	52.2	0.2	-	-	3.54	5.44x10 ⁻⁵	1.91x10 ⁻⁵	0.011	0.0004
Sb109	253.0	0.5	117.4	2.0	-	-	6.45	7.50x10 ⁻⁵	2.02x10 ⁻⁵	0.027	0.001
Sb107	300.2	0.6	155.0	1.6	-	-	7.87	2.12x10 ⁻³	5.97x10 ⁻⁵	0.015	0.0005
Sb106	301.1	0.8	131.3	5.3	-	-	5.77	2.04x10 ⁻⁴	2.47x10 ⁻⁵	0.016	0.003
Sb100	302.8	3.0	111.3	4.7	-	-	6.38	1.15x10 ⁻³	1.65x10 ⁻⁴	0.016	0.001
Sb102	303.1	1.4	113.5	1.4	-	-	3.54	3.17x10 ⁻⁴	5.09x10 ⁻⁵	0.012	0.004
Sb98	303.7	8.8	186.5	56.1	-	-	7.10	8.76x10 ⁻⁴	9.53x10 ⁻⁵	0.031	0.001
Sb109	304.1	0.8	137.7	0.2	-	-	6.39	1.92x10 ⁻⁴	2.12x10 ⁻⁵	0.028	0.002
Sb108	304.5	1.0	178.1	1.3	-	-	7.85	5.98x10 ⁻³	4.79x10 ⁻⁴	0.062	0.003
Sb102	307.7	1.1	201.2	0.6	-	-	3.55	2.74x10 ⁻⁴	4.90x10 ⁻⁵	0.012	0.002
Sb99	308.6	2.5	115.1	21.4	-	-	7.08	9.10x10 ⁻⁴	2.16x10 ⁻⁴	0.031	0.003

Table (A.3) Stibnite solubility data from 70 to 400°C. *Continued*

Exp.	T (°C)	2*σ	P (bar)	2*σ	pH _{exit}	2*σ	pH _{calc} with Sb(OH) ₃	Sb (mol kg ⁻¹)	2*σ	S _{tot} (mol kg ⁻¹)	2*σ
Sb106	343.2	1.8	192.2	57.6	-	-	5.85	2.01x10 ⁻³	2.33x10 ⁻⁴	0.016	0.0004
Sb107	344.6	1.0	249.1	0.4	-	-	8.19	3.31x10 ⁻³	3.61x10 ⁻⁴	0.018	0.002
Sb109	347.0	0.7	250.0	0.2	-	-	6.33	8.84x10 ⁻⁴	1.13x10 ⁻⁴	0.028	0.003
Sb109	347.1	0.5	192.9	0.2	-	-	6.33	7.09x10 ⁻⁴	2.33x10 ⁻⁵	0.027	0.0004
Sb109	348.1	1.5	215.1	0.2	-	-	6.33	7.63x10 ⁻⁴	1.95x10 ⁻⁴	0.027	0.003
Sb99	350.2	1.5	203.6	0.6	-	-	6.81	2.91x10 ⁻³	7.04x10 ⁻⁵	0.036	0.0002
Sb100	351.1	3.5	168.3	1.3	-	-	6.14	3.63x10 ⁻³	1.22x10 ⁻³	0.022	0.006
Sb102	352.7	1.7	201.0	0.7	-	-	3.55	1.76x10 ⁻³	2.23x10 ⁻⁴	0.016	0.001
Sb100	389.7	7.5	203.1	9.9	-	-	14.45	2.46x10 ⁻³	8.57x10 ⁻⁴	0.042	0.026
Sb107	395.8	7.9	197.2	15.5	-	-	13.83	9.16x10 ⁻⁴	3.80x10 ⁻⁴	0.038	0.007
Sb100	395.9	1.4	303.6	51.1	-	-	9.21	1.57x10 ⁻²	3.08x10 ⁻³	0.035	0.073
Sb100	396.0	3.0	252.7	16.5	-	-	12.65	3.78x10 ⁻³	1.21x10 ⁻³	0.029	0.009
Sb104	398.4	0.2	170.2	1.4	-	-	12.99	3.45x10 ⁻⁴	1.77x10 ⁻⁴	-	-
Sb105	400.5	0.0	228.2	0.0	-	-	12.65	2.77x10 ⁻³	8.50x10 ⁻⁴	0.039	0.030
Sb105	400.6	0.0	291.0	0.0	-	-	10.44	1.46x10 ⁻²	4.69x10 ⁻³	0.035	0.009
Sb107	401.1	0.4	158.8	3.8	-	-	14.60	2.43x10 ⁻⁴	7.08x10 ⁻⁵	0.036	0.008
Sb102	401.4	2.6	190.3	5.0	-	-	6.05	4.79x10 ⁻⁴	2.94x10 ⁻⁴	0.025	0.005
Sb104	404.3	0.9	233.6	1.2	-	-	11.59	1.21x10 ⁻³	4.65x10 ⁻⁴	-	-
Sb102	405.9	0.2	245.6	0.7	-	-	5.80	2.43x10 ⁻³	4.30x10 ⁻⁴	0.027	0.013

Speciation above 25°C involved two loops:

1. Speciation of solution using guessed pH and ionic strength using the following equations and the iterative capacity of Excel.
2. pH iterative calculated from the solution charge balance using the Solver add-in to Excel, including iteration of ionic strength in macro. Iterated until ionic strength and pH no longer changed.

Activity coefficients (γ) were defined in Equation (2.23) and ionic strength in Equation (2.24). K_{NaOH} , K_{NaHS} , and K_{H_2S} were defined in Equations (2.18) through (2.20).

pH balance equation:

Fit equation:

$$0 = m_{H^+} + m_{Na^+} - m_{HS^-} - m_{OH^-} + \sum_i^{xyzw} mSb_{xyzw} * (3x - 2y - 2z + w)$$

“3x-2y-2z+w” is the charge of the antimony complex (see Equation (2.3))

Components of fit equation:

$$\begin{aligned} m_{H^+} &= \frac{m_{H^+}}{\gamma_{H^+}} \\ m_{OH^-} &= \frac{K_w}{a_{H^+} \gamma_{OH^-}} \\ m_{Na^+} &= m_{Na_{total}} * fraction_{Na^+} \\ m_{HS^-} &= m_{S_{total}} * fraction_{HS^-} \end{aligned}$$

Derivation of $fraction_{Na^+}$ and $fraction_{HS^-}$:

Sulfide species:

$$fraction_{HS^-} = \frac{m_{HS^-}}{m_{S_{total}}} = \frac{m_{HS^-}}{m_{H_2S} + m_{NaHS^0} + m_{HS^-}}$$

Concentration of HS- combining H₂S disassociation reaction and sulfide balance:

$$m_{HS^-} = \frac{K_{H_2S} * m_{H_2S}}{\gamma_{HS^-} * a_{H^+}} = \frac{K_{H_2S}(m_{S_{total}} - m_{HS^-} - m_{NaSH^0})}{\gamma_{HS^-} * a_{H^+}}$$

Expanded and with mNaSH⁰ in terms of the association reaction:

$$m_{HS^-} = \frac{K_{H_2S} * m_{S_{total}} - K_{H_2S} * m_{HS^-} - K_{H_2S} \frac{\gamma_{Na^+} m_{Na^+} m_{HS^-} \gamma_{HS^-}}{K_{NaHS^0}}}{\gamma_{HS^-} * a_{H^+}}$$

Write as individual quotients

$$m_{HS^-} = \frac{K_{H_2S} * m_{S_{total}}}{\gamma_{HS^-} * a_{H^+}} - \frac{K_{H_2S} * m_{HS^-}}{\gamma_{HS^-} * a_{H^+}} - \frac{K_{H_2S} * \gamma_{Na^+} * m_{Na^+} * m_{HS^-}}{a_{H^+} * K_{NaSH^0}}$$

and divide through by 1/mHS- so that mHS- is only in one term:

$$1 = \frac{K_{H_2S} * m_{S_{total}}}{\gamma_{HS^-} * a_{H^+} * m_{HS^-}} - \frac{K_{H_2S}}{\gamma_{HS^-} * a_{H^+}} - \frac{K_{H_2S} * \gamma_{Na^+} * m_{Na^+}}{a_{H^+} * K_{NaSH^{\circ}}}$$

Rearrange to isolate term including mHS- on one side of the equation:

$$\frac{K_{H_2S} * m_{S_{total}}}{\gamma_{HS^-} * a_{H^+} * m_{HS^-}} = 1 + \frac{K_{H_2S}}{\gamma_{HS^-} * a_{H^+}} + \frac{K_{H_2S} * \gamma_{Na^+} * m_{Na^+}}{a_{H^+} * K_{NaSH^{\circ}}}$$

Divide through by quotient to isolate mHS-:

$$\frac{1}{m_{HS^-}} = \frac{\gamma_{HS^-} * a_{H^+}}{K_{H_2S} * m_{S_{total}}} + \frac{1}{m_{S_{total}}} + \frac{\gamma_{Na^+} * m_{Na^+} * \gamma_{HS^-}}{K_{NaSH^{\circ}} * m_{S_{total}}}$$

Invert above and divide through by 1/mS_{total} to obtain equation for fraction of HS- to get final equation:

$$fraction_{HS^-} = \frac{1}{\frac{a_{H^+} \gamma_{HS^-}}{K_{H_2S}} + 1 + \frac{\gamma_{HS^-} \gamma_{Na^+} m_{Na^+}}{K_{NaSH^{\circ}}}}$$

Note that $m_{S_{total}}$ was replaced with $m_{S_{free}}$ when antimony-sulfide complexes were present, as developed with Equations (2.22) and (4.9).

Sodium species:

$$fraction_{Na^+} = \frac{m_{Na^+}}{m_{Na_{total}}} = \frac{m_{Na^+}}{m_{Na^+} + m_{NaHS^{\circ}} + m_{NaOH^{\circ}}}$$

Divide left side by mNa+/mNa+

$$fraction_{Na^+} = \frac{1}{1 + \frac{m_{NaHS^{\circ}}}{m_{Na^+}} + \frac{m_{NaOH^{\circ}}}{m_{Na^+}}}$$

Write m_{NaOH[°]} in terms of NaOH dissociation reaction and water reaction. Similar treatment for NaHS

$$fraction_{Na^+} = \frac{1}{1 + \frac{\gamma_{Na^+} \gamma_{HS^-} m_{HS^-}}{K_{NaSH^{\circ}}}} + \frac{\gamma_{Na^+} K_w}{K_{NaOH} a_{H^+}}$$

VisualBasic Charge Balance Macro

Macro uses the generalized reduced gradient (GRG) method to minimize the charge balance equation by adjusting the pH. Then the new ionic strength is used and the optimization is repeated.

```
Sub balance_pH()  
For Each C In Selection  
    SolverReset  
    SolverOptions Iterations:=1000, _  
        Precision:=0.00000001, _  
        MaxTime:=1000  
  
    SolverOk SetCell:=C.Offset(0, 0), _  
        MaxMinVal:=3, _  
        ValueOf:=0, _  
        ByChange:=C.Offset(0, -2), _  
        Engine:=1  
    SolverSolve UserFinish:=True  
  
    C.Offset(0, 1).Copy  
    C.Offset(0, -3).PasteSpecial Paste:=xlPasteValues  
  
    SolverOk SetCell:=C.Offset(0, 0), _  
        MaxMinVal:=3, _  
        ValueOf:=0, _  
        ByChange:=C.Offset(0, -2), _  
        Engine:=1  
  
    SolverSolve UserFinish:=True  
  
    C.Offset(0, 1).Copy  
    C.Offset(0, -3).PasteSpecial Paste:=xlPasteValues  
  
Next  
End Sub
```

Figure (A.2) SEM images of reacted stibnite from high temperature experiments. Images demonstrate grain-size distribution and embayed surfaces of reacted grains, including preferential dissolution parallel to the c-axis.



